Investigating the role of continental blocks and their interplay with the Iberia, Newfoundland and Irish offshore margins using plate tectonic reconstructions

by

© Michael King

A Thesis submitted to the School of Graduate Studies in partial fulfillment of the requirements for the degree of Doctor of Philosophy.

Department of Earth Sciences

Memorial University of Newfoundland and Labrador

May 2023

St. John's, Newfoundland and Labrador

Abstract

Rifted margins encompass significant architectural variabilities and represent a transition zone between Earth's continents and oceans. Due to the abundance of natural resources that are hosted within their overlying sedimentary basins (e.g., hydrocarbons, carbon-capture targets, geothermal reservoirs, mineral deposits, and natural hydrogen), rifted margins are also highly influential regions for meeting our planet's energy needs. Furthermore, the structure and morphology of rifted margins during compressional re-activation can have a significant impact on the closure of oceans and the creation of continental landmasses. As a result, investigations that aim to explore their present-day architecture and the processes responsible for their formation are significantly important.

The Newfoundland, Irish, and Iberian rifted margins represent some of the best studied examples of rifted margins in the world. However, despite being relatively well-studied, their complex present-day crustal structure has made it difficult to unravel their plate kinematic history and crustal evolution. As well, the majority of previously published plate reconstruction studies within these regions have primarily focused on the kinematics of large, rigid tectonic plates, ignoring the fact that tectonic plates are often significantly deformed and partitioned into micro-plates and smaller continental blocks over geological time.

In this thesis, deformable plate tectonic reconstructions that account for 3-D kinematics and deformation are used to investigate the plate kinematic role of continental blocks (e.g., Flemish Cap and Galicia Bank) and their interplay with the Iberian micro-plate during the opening of the southern North Atlantic Ocean. A collection of deformable plate modelling investigations focussed

on Iberia's present-day offshore continental margins (West Iberian margin and Bay of Biscay), and former margins that have been re-activated by compressional deformation (e.g., Pyrenees and Iberian Ranges) provide a comprehensive assessment of Iberia's plate kinematic history and the influential role of continental block kinematics.

In addition, this thesis introduces new deformable plate tectonic modelling workflows that can be used to reduce their geologically unsatisfying assumptions and make quantitative comparisons between their results (e.g., crustal thickness and extension estimates) and similar, but independently obtained, estimates calculated using methods such as 2-D structural restorations of seismic interpretations. The application of these newly presented workflows to study the formation of the Newfoundland, Irish, and West Iberian margins provides new insights into the partitioning of deformation within continental blocks, their potential origin, and their interplay with inherited structures during rift-related deformation experienced within neighbouring sedimentary basins.

General Summary

This thesis is primarily focused on developing a better understanding of how the kinematics of large and small tectonic plates influenced the development of the Iberia, Newfoundland, and Irish rifted margins during the opening of the modern North Atlantic Ocean. To accomplish this, a combination of geophysical and geological data interpretation (e.g., seismic and potential field data) and modelling techniques such as deformable plate tectonic reconstructions have been used. New open-source workflows have been developed and applied to demonstrate how deformable plate tectonic models can be used to reconstruct present-day crustal thicknesses and seismic line locations back through time to assess the evolution of overlying sedimentary basins and surrounding continental blocks. These new methods for reconstructing and deforming tectonic plates/blocks of all sizes, seismic line locations, and present-day geophysical datasets back through time are allowing the impact of smaller tectonic plates (e.g., offshore continental blocks), and their interplay with ancient geological structures, to be assessed. Following an investigation of numerous previously published and newly presented model parameters and plate reconstructions, I have been able to demonstrate and conclude that the deformation experienced throughout Iberia, and the offshore Newfoundland, and Irish margins during rifting was largely influenced by the kinematics of smaller continental blocks situated between larger tectonic plates, as well as ancient pre-rift structures. Finally, my research results have shown strong correlations between across strike variations in pre-rift crustal thickness estimates calculated by deformable plate models and the offshore extensions of ancient pre-rift orogenic boundaries. These correlations suggest that orogenic inheritance significantly influenced the onset and progression of rifting throughout the North Atlantic Ocean, more so than previously thought.

Acknowledgments

I am incredibly fortunate and grateful for all of the love, support, and kindness I have received from so many people throughout my Ph.D. studies. First, I would like thank my supervisor, Kim Welford, for all of her support, guidance, and encouragement since my days as an undergraduate student. The progression of my Ph.D. research has always been mainly driven by my curiosity, and Kim has always been incredibly supportive of that. Her passion for teaching and mentoring students, and conducting impactful research is incredibly motivating. I would not be the geoscientist I am today without her everlasting guidance and support.

I am also thankful for the advice, feedback, and support I have received from other faculty members at MUN (Alison Malcolm and Colin Farquharson), my Ph.D. committee members (Alison Malcolm and Luke Beranek), the current and previous members of the MAGRIT research group, and the co-authors of my published papers (Alex Peace, Julie Tugend, and Patricia Cadenas). The pursuit of my undergraduate and graduate degrees within the Earth Sciences department at MUN has been an incredible journey, and the people within our department are largely responsible for the wonderful memories and experiences that I will forever cherish. Furthermore, I would like thank the Earthbyte Group from the University of Sydney, Australia, for developing and maintaining the GPlates software and the open-access databases that made my thesis possible. In addition, I would like to thank NSERC for awarding me an Alexander Graham-Bell Canada Graduate Scholarship that funded my Ph.D. studies.

Last but not least, I would like to thank my wife, Robyn, my Mom, Dad, brother, and the rest of my family and friends for their continuous love and support.

Table of Contents

List of Tables

List of Figures

Co-authorship Statement

The main scientific problems and research topics in this thesis were originally proposed via discussions between my supervisor, Dr. Kim Welford, myself, and Dr. Iain Sinclair. Kim Welford supervised the research. I conducted all of the research, modelling, preliminary data analysis and interpretation, and writing of the original manuscripts.

Chapter 3 is published in *Tectonophysics* (https://doi.org/10.1016/j.tecto.2020.228537) and co-authored by Kim Welford and Alex Peace. I was responsible for the design of deformable plate models, data analysis, map creation, preliminary interpretations, and writing the original draft. My co-authors (Kim Welford and Alex Peace) provided reviews and edits of the original manuscript draft. Tiago Alves and an anonymous reviewer provided constructive peer-review comments.

Chapter 4 is published in *Tectonics* (https://doi.org/10.1029/2020TC006467) and co-authored by Kim Welford, Patricia Cadenas, and Julie Tugend. Kim Welford supervised the research. All co-authors assisted in the review and editing of the original manuscript. Patricia Cadenas and Julie Tugend provided guidance and constructive comments pertaining to the Bay of Biscay plate kinematics and previously published geological and geophysical studies within the region. Valuable peer-review comments were received by Gabriela Fernandez-Viejo and two anonymous reviewers.

Chapter 5 is published in the *Journal of Geodynamics* (https://doi.org/10.1016/j.jog.2023.101962) and is co-authored by Kim Welford and Julie Tugend.

Both co-authors provided reviews and edits for the original draft. Julie Tugend provided additional thoughts and guidance surrounding the geology of the Pyrenees.

Chapter 6 (https://doi.org/10.1029/2022GC010372) and chapter 7 (https://doi.org/10.1029/2022GC010373) are companion contributions that are both published in *Geochemistry, Geophysics, Geosystems*. Both manuscripts were co-authored by Kim Welford. Constructive peer-review comments were received from Dietmar Müller and Gwenn Peron-Pinvidic.

Chapter 8 is currently being prepared for submission. This manuscript is co-authored by Kim Welford. Supervision of this research and editing of the original draft were also performed by Kim Welford. Peer-review comments on an earlier version of the manuscript were received by Frank Zwaan and Mohamed Gouiza.

Preamble

This thesis is written in a manuscript format and contains six manuscripts within its body that are either published or currently under review. Chapters 3-5 are published and present deformable plate modelling studies focused on the West Iberian margin (Chapter 3), Bay of Biscay (Chapter 4), and Pyrenean realm (Chapter 5). However, the comprehensive aim of investigating the plate kinematics of Iberia using a deformable plate modeling approach within Chapters 3-5 causes overlap and repetition between the methodology and geological background sections discussed in each of their published versions. To avoid said overlap and repetition within this thesis, the details pertaining to the geological background and methodology sections within the published versions of Chapters 3-5 are provided within Chapter 1 (introduction/geological background) and Chapter 2 (methodology). Thus, Chapters 3-5 in this thesis and their published versions are not identical in order to minimize the amount of redundant information/figures within each chapter. Chapters 6 and 7 are published papers that present new deformable plate modelling workflows (Chapter 6) and their detailed application to study the crustal evolution of the southern North Atlantic Ocean (Chapter 7). Similar to what was done for Chapters 3-5, the geological background sections within the published versions of Chapters 6 and 7 are also summarized in Chapter 1 to reduce repetition. As a result, Chapters 6-7 are also not identical to their published versions. Chapter 8 is currently being prepared for submission and presents a new approach for validating the results of 2-D structural restorations of seismic interpretations using deformable plate tectonic models.

Chapter 1

1 Introduction

Over the past century, our knowledge of plate tectonic theory and the methodologies used to explore plate tectonic processes and mechanisms have evolved substantially. A fundamental plate tectonic model used to describe the cyclic opening and closing of oceans along pre-existing plate boundaries is the Wilson Cycle (Wilson, 1966). An important stage of the Wilson Cycle encompasses the onset of continental margin development via continental extension, which can subsequently lead to the opening of an ocean, and sea-floor spreading. However, considering the extensive collection of literature focussed on the development of continental margins and their overlying sedimentary basins, geological and geophysical investigations often indicate significant architectural variations that are not easily described by the Wilson Cycle alone. These variations in crustal architecture are often attributed to their development within irregular terranes that resulted from preceding tectonic events, contrasting magmatic supplies, and temporal variations in the magnitude and orientation of regional stress directions during rifting, breakup, and oceanic spreading.

1.1 Rifted margins

Rifted margins are often classified into two end members: magma-poor (Figure 1.1) or magma-rich (Figure 1.2). Using previously published geological and geophysical investigations, the classification of magma-poor versus magma-rich rifted margins can be distinguished using observations related to their crustal structure and magmatic budget.

Magma-poor rifted margins (Figure 1.1) are classified as having a very limited magmatic supply and slow extension rates relative to magma-rich margins (Figure 1.2) (Peron-Pinvidic et al., 2013; Lundin et al., 2018). It is generally accepted that rifting during the formation of magma-poor margins is a poly-phase process that involves pure (McKenzie, 1978) and simple shear processes (Wernicke and Burchfiel, 1982). This led to the identification of three main deformation phases that consist of distributed stretching, localized thinning and exhumation (Lavier and Manatschal, 2006). In addition, the crustal architecture of magma-poor rifted margins can be grouped into morphological domains as described in detail by Péron-Pinvidic et al. (2013).

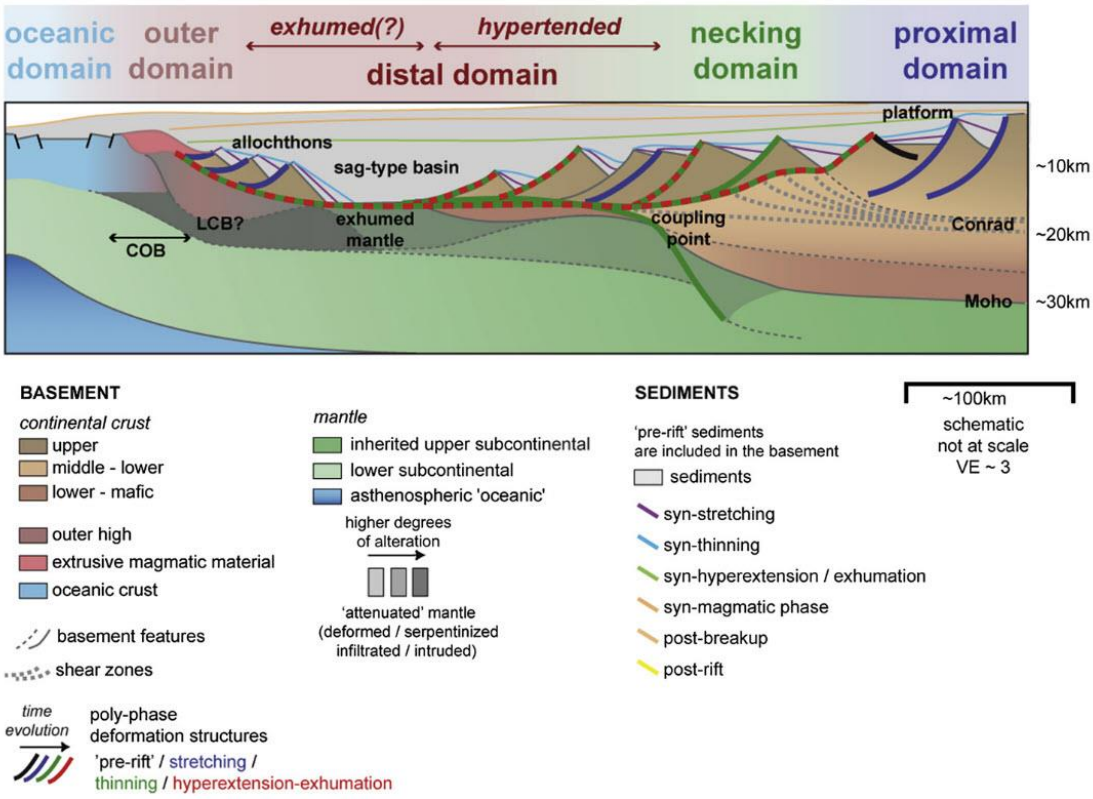

Figure 1.1 Schematic of a magma-poor rifted margin from Péron-Pinvidic et al. (2013).

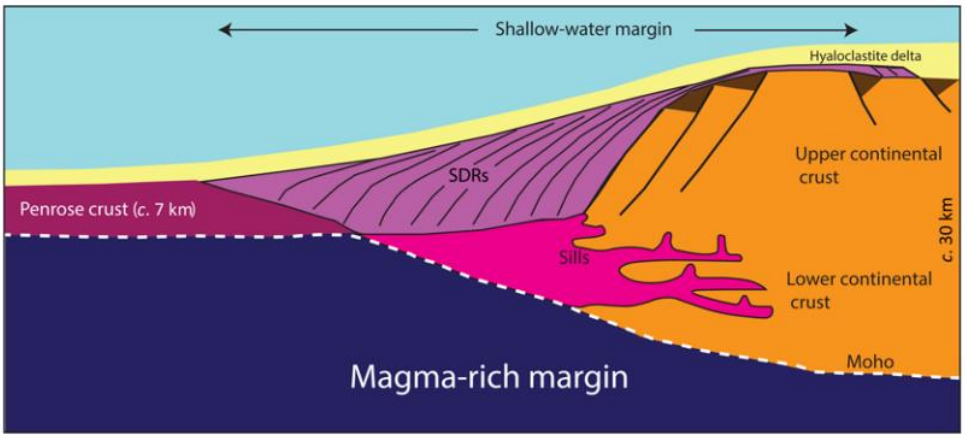

Figure 1.2 Schematic of magma-rich rifted margin from Lundin et al. (2018).

The proximal domain corresponds to the furthest inboard continental domain that has undergone little to no crustal thinning and hosts wedge shaped syn-tectonic sedimentary units deposited within graben and half-graben sedimentary basins. Normal faulting is observed within the brittle upper crust and major faults typically sole out at mid-crustal levels. At the lithospheric scale, deformation within the proximal domain is decoupled, and the sedimentary basement and Moho topographies are parallel and flat.

The necking domain, ocean-ward of the proximal domain, is characterized by intermediate thinning of the continental crust (from ~ 35 km to as low as ~ 10 km) and deepening of the sedimentary basement. This causes the continental crust to be wedge shaped, which continues until a so-called taper break that defines the point where the crust is thinned down to 10 km. This taper break also coincides with the coupling point, where brittle faults begin to cross-cut the entire crust and penetrate mantle. Thus, the coupling point corresponds to the continent-ward limit of the necking domain where deformation between the crust and mantle is decoupled, and the ocean-ward limit where deformation is coupled, resulting in the absence of ductile layers within the crust.

The distal domain, also referred to as the hyperextended domain in previous literature, corresponds to a region situated ocean-ward of the necking domain where the crust has been thinned to less than 10 km. A key characteristic of this domain is the absence of ductile layers within the crust, which allows brittle faults to penetrate the mantle. Within the distal domain, the morphology of the basement is considered to be variable, but it can broadly encompass lower and/or upper crust, exhumed and/or serpentinized mantle or embryonic oceanic crust.

Although the basic mechanisms associated with rift mechanics are generally agreed upon, the mechanisms responsible for extreme crustal thinning within the necking and distal domains prior to the exhumation phase have been extensively debated. Summarizing a compilation of multi-disciplinary studies focused on the tectonic evolution of rifted margins, two competing models can be defined. One model emphasizes the role of sequential faulting in order to achieve extreme crustal thinning (Pérez-Gussinyé et al., 2003; Reston, 2005, 2009; Ranero and Pérez-Gussinyé, 2010), while others propose extreme crustal thinning to occur via detachment faulting (Whitmarsh et al., 2001; Lavier and Manatschal, 2006; Manatschal et al., 2009). However, these two models are not considered to be mutually exclusive. This is because aspects from both of these models (e.g., detachment and sequential faulting) are often observed within proximal, necking, and distal domains along rifted margins globally, emphasizing their variable crustal architecture and symmetry.

The crustal structure of the outer domain, ocean-ward of the distal domain, is often poorly constrained but is a region that demonstrates some of the key differences between magma-poor and magma-rich rifted margins. At magma-rich margins, this domain is commonly referred to as the outer high. The outer high is characterized by magmatic sequences such as Seaward Dipping

Reflector (SDR) sequences made up of extrusive basalts and igneous underplating during breakup. At magma-poor rifted margins, the morphology of the outer domain can be highly variable and can encompass exhumed and/or serpentinized mantle, continental allochthons or embryonic oceanic crust. Previous seismic observations suggest the onset of the outer domain corresponds to ocean-ward termination of sag-type basins following a shallowing in seismic basement (Peron-Pinvidic et al., 2013 and references therein). However, alternative models of rifted margins have also been proposed that exclude sag-type basins in the distal to outer domain and emphasize the role of active detachment faulting (Perez-Gussinye and Reston, 2001; Pérez-Gussinyé et al., 2006).

The beginning of the oceanic domain is often characterized as comprising a continent-ocean boundary (COB), however, this boundary is highly ambiguous. The ambiguity of this boundary is primarily associated with the slow onset of sea-floor spreading and the resultant heterogeneous nature of embryonic oceanic crust. This leads to considerable uncertainty when defining continent-ocean boundaries using geophysical signals. Outboard of the COB vicinity, classic oceanic domains consist of homogenous oceanic crust that is ~ 6-10 km thick. For example, along the Newfoundland, Iberia and Irish offshore rifted margins, undisputed oceanic crust is commonly associated with the chron 34 magnetic anomaly (~ 83 Ma). However, the onset of oceanic crust generation within the North Atlantic Ocean continues to be debated as recent studies have suggested an earlier and asymmetric onset of oceanic crust along the West Iberian margin (Grevemeyer et al., 2022).

1.2 Rifted margins of the southern North Atlantic Ocean

For several decades, the southern North Atlantic Ocean (Figure 1.3) has been of interest to many for independent geological (Brunet, 1984; Boillot and Winterer, 1988; Sinclair, 1995; Mata et al., 2015; Leleu et al., 2016; Peace et al., 2018; Spooner et al., 2019), geophysical (Sibuet et al., 2007; Welford et al., 2010, 2012; Brune et al., 2017; Sandoval et al., 2019), and plate tectonic reconstruction studies (Srivastava et al., 2000; Sibuet et al., 2004, 2012; Vissers and Meijer, 2012; Barnett-Moore et al., 2018; Nirrengarten et al., 2018; Peace et al., 2019b). In this thesis, the southern North Atlantic Ocean is interpreted to encompass the Newfoundland (magma-poor), Iberia (magma-poor), and Irish (magma-poor and magma-rich) offshore margins (Figure 1.3).

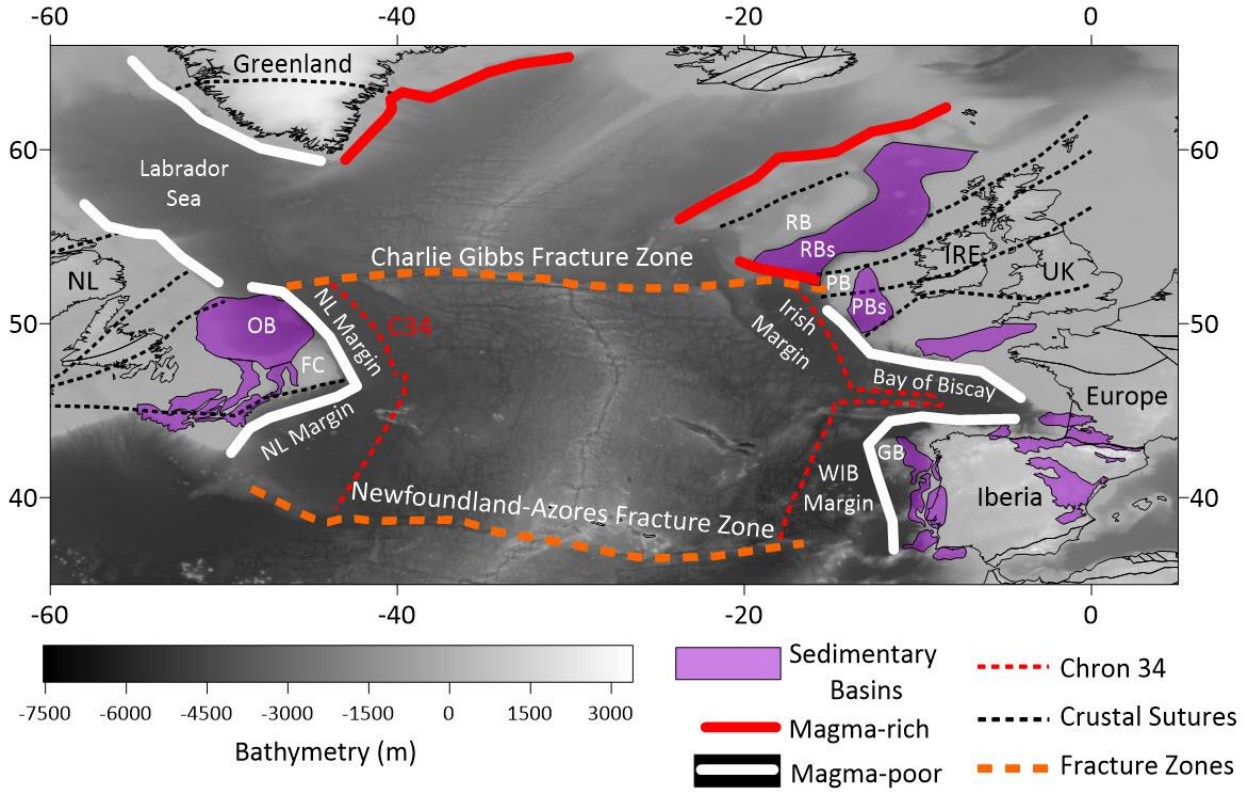

Figure 1.3 Bathymetric map (WGS 1984 coordinate system) of the southern North Atlantic Ocean. Crustal sutures, fracture zones, and chron 34 (C34) magnetic anomaly locations extracted from Welford et al. (2012), and sedimentary basin outlines extracted from Nirrengarten et al. (2018). FC = Flemish Cap, GB = Galicia Bank, IRE = Ireland, NL = Newfoundland and Labrador, OB = Orphan Basin, PB = Porcupine Bank, PBs = Porcupine Basin, RB = Rockall Bank, RBs = Rockall Basin, UK = United Kingdom, WIB = West Iberian Margin.

The rifted margins of the southern North Atlantic host numerous sedimentary basins such as the Orphan, Galicia Interior, and Porcupine basins (Figure 1.4), which continue to be of significant interest for frontier hydrocarbon exploration and carbon-capture storage (Brunet, 1984; Sinclair, 1995; Shannon et al., 2001; Pimentel and Pena Dos Reis, 2016; Sandoval et al., 2019).

These sedimentary basins are bordered by continental blocks/ribbons such as the Flemish Cap, Galicia Bank, and Porcupine Bank (Péron-Pinvidic and Manatschal, 2010) (Figure 1.4). Continental blocks/ribbons are blocks of relatively undeformed continental crust (> 20 km thick) that are separated from interior continental domains by sedimentary basins underlain by crust that underwent varying amounts of thinning (Péron-Pinvidic and Manatschal, 2010). In addition, the Newfoundland, Iberia, and Irish margins are intersected and segmented by older crustal terrane boundaries that divide ancient Archean and Proterozoic terranes (Figures 1.4 and 1.5), and fracture zones such as the Charlie Gibbs and Newfoundland-Azores fracture zones (Catalán et al., 2007; Stampfli et al., 2013; Arenas et al., 2014; Frizon De Lamotte et al., 2015; Peace et al., 2019a).

The present-day crustal structure of the southern North Atlantic offshore rifted margins (Figures 1.4 and 1.5) is a product of poly-phased and multi-stage rifting that initiated within a structurally complex Pangaean supercontinent ~ 200 Ma. The main phases of rifting causing deformation and subsequent opening of the southern North Atlantic include: 1) a NW-SE oriented Late Triassic-Early Jurassic phase, 2) an E-W Late Jurassic-Early Cretaceous phase, and 3) a NE-SW oriented break-up related rift phase during the Mid Cretaceous (Lundin, 2002; Barnett-Moore et al., 2018; Nirrengarten et al., 2018).

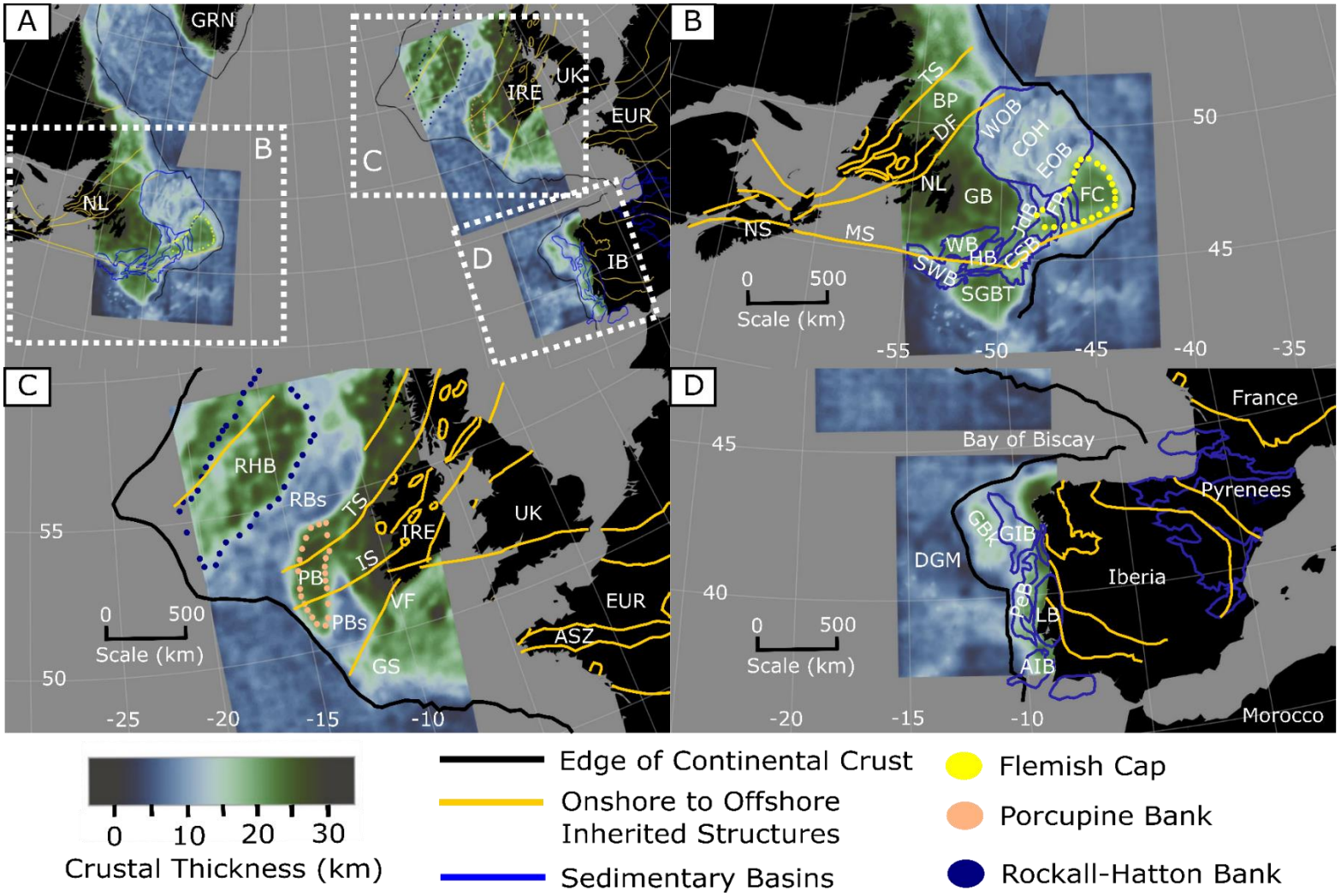
A
GRN
NL
B
C
IRE
UK
EUR
D
IB
B
TS
BP
DF
WOB
COH
EOB
NL
GB
FC
NS
MS
WB
HB
CSB
SWB
SGBT
0
500
Scale (km)
50
45
-55
-50
-45
-40
-35
C
RHB
RBs
TS
IRE
UK
IS
PB
PBs
VF
EUR
ASZ
GS
55
50
0
500
Scale (km)
-25
-20
-15
-10
D
France
Bay of Biscay
45
Pyrenees
GIB
DGM
Iberia
40
LB
AIB
0
500
Scale (km)
-20
-15
-10
Morocco
0
10
20
30
Crustal Thickness (km)
Edge of Continental Crust
Onshore to Offshore Inherited Structures
Sedimentary Basins
Flemish Cap
Porcupine Bank
Rockall-Hatton Bank

Figure 1.4 Southern North Atlantic crustal thickness estimates calculated by gravity inversion with onshore to offshore inherited basement terranes extracted from Welford et al., (2012) and Nirrengarten et al., (2018). The geometries of continental blocks are extracted from Peace et al., (2019). The dashed white boxes in panel (A) correspond to the enlarged panels (B), (C), and (D). AIB = Alentejo Basin, ASZ = Armorican Shear Zone, BP = Bonavista Platform, EUR = Europe, COH = Central Orphan High, CSB = Carson-Salar Basins, DF = Dover Fault, DGM = Deep Galicia Margin, EOB = East Orphan Basin, FC = Flemish Cap, FP = Flemish Pass, GB = Grand Banks, GBk = Galicia Bank, GIB = Galicia Interior Basin, GS = Goban Spur, HB = Horseshoe Basin, IRE = Ireland, IS = Iapetus Suture, JdB = Jeanne d'Arc Basin, LB = Lusitanian Basin, MS = Meguma Suture, NL = Newfoundland and Labrador, NS = Nova Scotia, PB = Porcupine Bank, PBs = Porcupine Basin, PeB = Peniche Basin, RBs = Rockall Basin, RHB = Rockall-Hatton Bank, SGBT = Southern Grand Banks Tail, SWB = South Whale Basin, TS = Taconian Suture, UK = United Kingdom, VF = Variscan Front, WOB = West Orphan Basin.

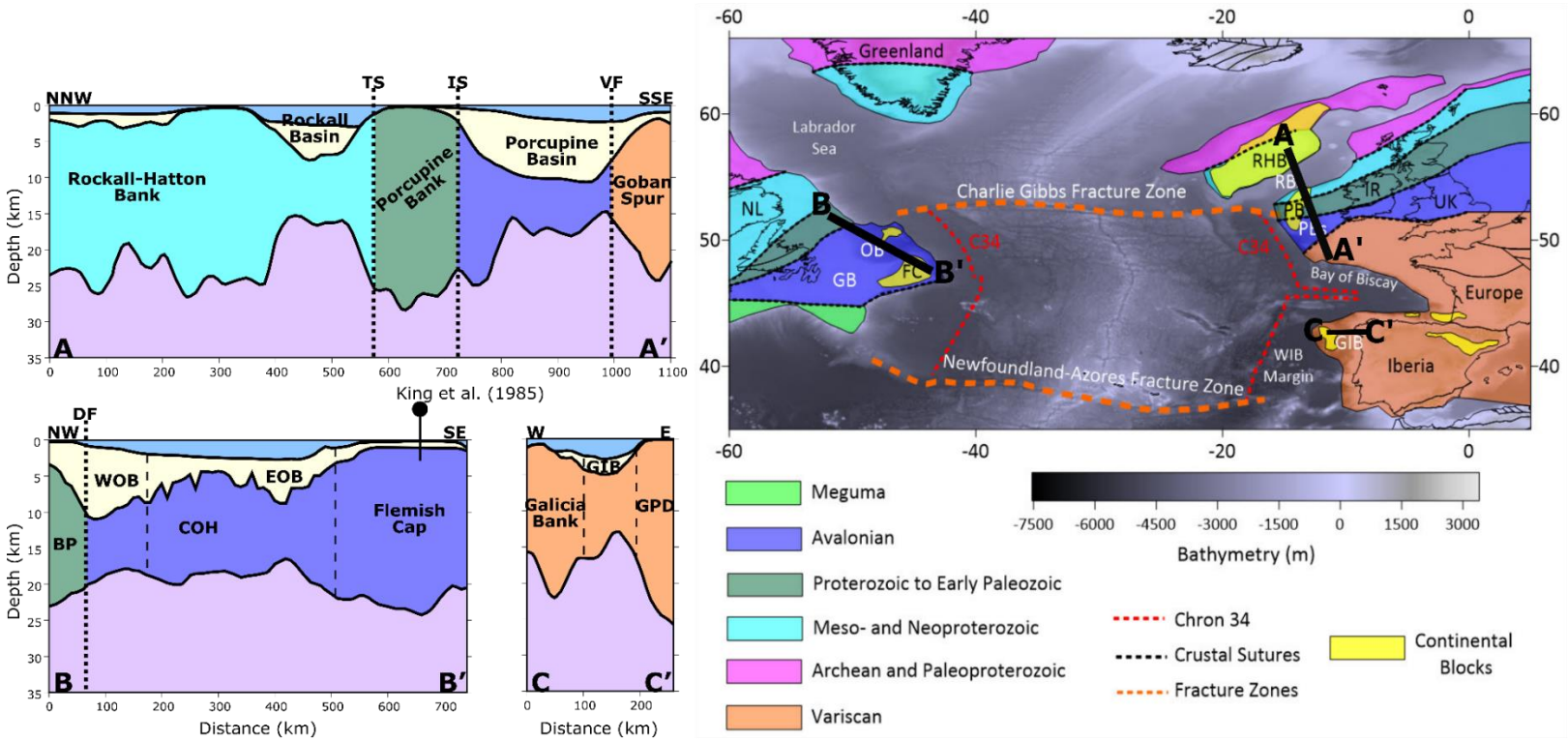

Figure 1.5 Cross-sections derived from extracted slices of inverted 3-D density models (used to obtain the crustal thickness estimates shown in Figure 1.4) and sedimentary basement affinities along the Irish (A-A'), Newfoundland (B-B'), and West Iberian margins (C-C') outlined from Welford et al. (2012). BP = Bonavista Platform, COH = Central Orphan High, DF = Dover Fault, EOB = East Orphan Basin, GIB = Galicia Interior Basin, GPD = Galicia Proximal Domain, IS = Iapetus Suture, RHB = Rockall-Hatton Bank, TS= Taconian Suture, VF = Variscan Front, WOB = West Orphan Basin.

1.2.1 Tectonic history of Iberia

In this thesis, detailed emphasis will be given to understanding the tectonic evolution of Iberia and its interplay with the Newfoundland and Irish offshore rifted margins. The main regions of interest throughout Iberia include the West Iberian margin, Bay of Biscay (e.g., North Iberian margin, Parentis Basin, Armorican margin, and Western Approaches margin), the Pyrenees Mountains, and the Central Iberian Ranges (Figure 1.6).

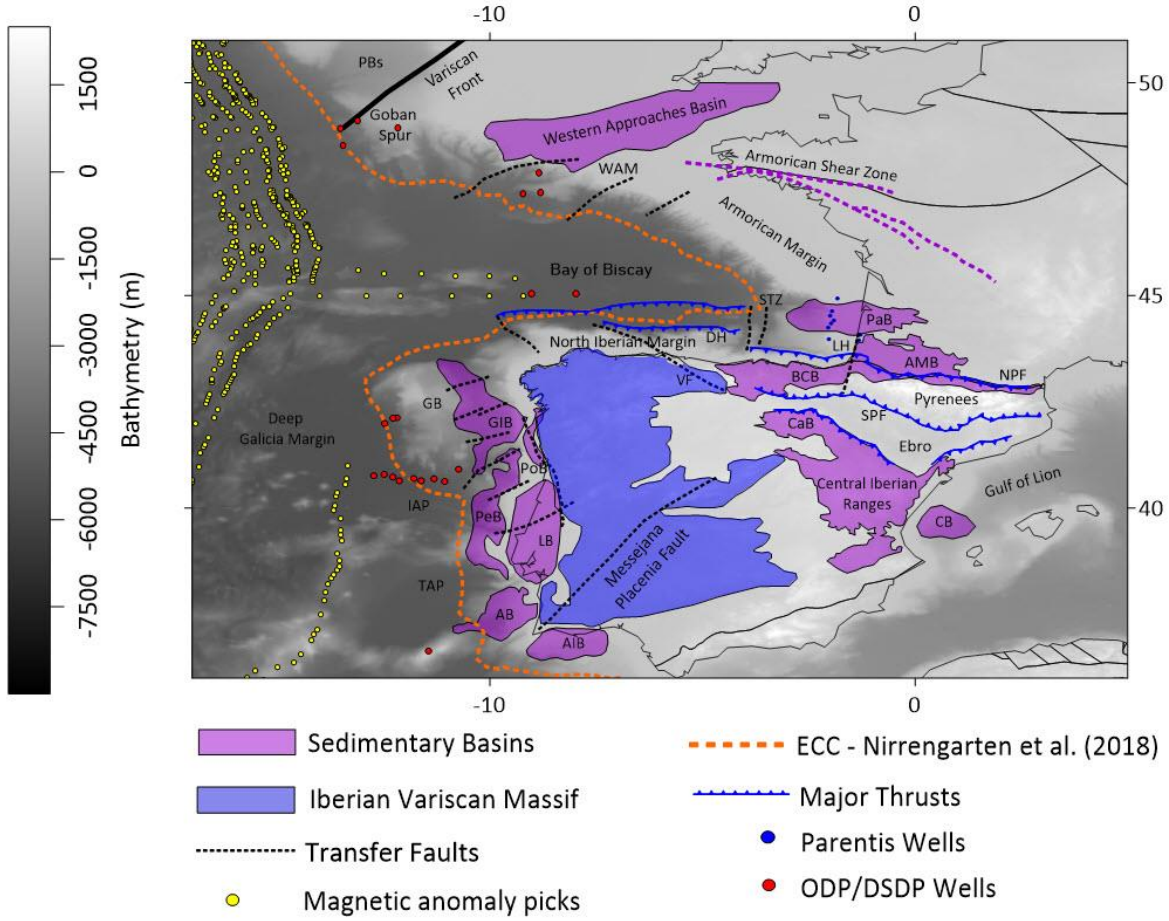

Figure 1.6 Bathymetric map (WGS 1984 coordinate system) of Iberia overlain with previously defined crustal structures, sedimentary basins, and crustal terranes. Crustal sutures, fracture zones,

and chron 34 (C34) magnetic anomaly locations extracted from Welford et al. (2012), and sedimentary basin and crustal terrane outlines extracted from Nirrengarten et al. (2018) and Tugend et al. (2014). AB = Alentejo Basin, AIB = Algarve Interior Basin, AMB = Arzacq-Mauleon Basin, ASZ = Armorican Shear Zone, BCB = Basque-Cantabrian Basin, CB = Cameros Basin, CIRB = Central Iberian Rift Basin, DGM = Deep Galicia Margin, DH = Le Danois High, EB = Ebro Block, ECC = Edge of Continental Crust, GIB = Galicia Interior Basin, GS = Goban Spur, IAP = Iberia Abyssal Plain, LaLOC = Landward Limit of Oceanic Crust, LB = Lusitanian Basin, MP = Messejana-Placencia fault, NPF = Northern Pyrenean Fault, PaB = Parentis Basin, PeB = Peniche Basin, PBs = Porcupine Basin, PoB = Porto Basin, SPF = Southern Pyrenean Fault, STZ = Santander Transfer Zone, TAP = Tagus Abyssal Plain, VF = Ventaniella Fault, WAB = Western Approaches Basin, WAM = Western Approaches Margin.

1.2.1.1 West Iberian Margin

Despite the regional rift and breakup related magmatism documented along the margin and within Iberia's interior (Martins et al., 2008; Miranda et al., 2009; Mata et al., 2015), the West Iberian margin is classified as a magma-poor rifted margin that hosts several sedimentary basins (Murillas et al., 1990; Alves et al., 2003). Along various parts of the West Iberian margin, these sedimentary basins are segmented by SW-NE trending Variscan/Hercynian transfer faults (Figure 1.6) (Murillas et al., 1990; Alves et al., 2003). The main crustal domains along the margin (Figure 1.6) are inferred from interpretations from various geophysical studies and well data from ocean drilling programs (Srivastava et al., 2000; Whitmarsh et al., 2001; Bronner et al., 2011; Szameitat et al., 2018b). From east to west, the transition across the margin generally consists of an area of continental crust with sedimentary basins overlying basement rocks deposited and accreted during

the Variscan orogeny, a zone of exhumed mantle primarily inferred from Ocean Drilling Program wells and seismic studies, a zone of embryonic oceanic crust approximately corresponding to the landward limit of oceanic crust (LaLOC) (Nirrengarten et al., 2018), and a zone of undisputed oceanic crust delimited by the C34 (~ 83 Ma) magnetic anomaly (Stanton et al., 2016; Szameitat et al., 2018b). In terms of north-south variations, the northern regions of the margin are comprised of the Porto and Galicia Interior basins situated within the proximal and distal domains of the margin, respectively. Along the western edge of the Galicia Interior Basin lies the Galicia Bank, a continental block separating the Galicia Interior Basin from the deep Galicia margin to the west (Sibuet et al., 2007; Péron-Pinvidic and Manatschal, 2010). Based on previous rigid plate models of the kinematics of the Galicia Bank, the Galicia Bank and Flemish Cap are commonly depicted as being connected until the debated timing of breakup between the Newfoundland and West Iberian margins (Srivastava et al., 2000; Sibuet et al., 2007). From the southern regions of the Galicia Interior Basin to the southern limit of the West Iberian margin lie the Peniche, Lusitanian, Alentejo, and Algarve Interior basins, all situated within the proximal and distal domains of the margin (Figure 1.6).

The present day crustal architecture of the West Iberian margin (Figure 1.4D) resulted from several stages of rifting followed by breakup, which propagated from south to north during the Mesozoic (Murillas et al., 1990; Srivastava et al., 2000; Alves et al., 2003; Alves and Cunha, 2018; Walker et al., 2021). The southwest Iberian margin crustal architecture is primarily a result of two rift phases. The first rift phase took place from the Late Triassic to the earliest Jurassic (early Pliensbachian) (Walker et al., 2021), and the second phase of extension prior to initiation of seafloor spreading occurred from late Oxfordian time to the earliest Cretaceous (Alves and Cunha,

2018). The most significant rift phase driving deformation within the Porto Basin, Galicia Interior Basin on the northern Iberian margin, and distal continental domains was initiated during Berriasian and Valanginian times (Murillas et al., 1990). This final stage of extension within the northern regions of the margin continued into the mid-Cretaceous, particularly within the distal Galicia margin (Druet et al., 2018; Lymer et al., 2019), and led to the continental breakup between the Newfoundland and Iberian margins, initiating during Late Aptian time (Nirrengarten et al., 2018).

During the Late Cretaceous and Cenozoic, compressional deformation impacted the West Iberian margin during the Pyrenean (in the north) and Betic (in the south) orogenies (Murillas et al., 1990; Cadenas et al., 2018). This resulted in thrust faulting, tectonic inversion of extensional structures, uplift and exhumation of seamounts, and subsidence of the West Iberian margin relative to the Iberian interior (Murillas et al., 1990; Alves et al., 2009; Druet et al., 2018).

1.2.1.2 Bay of Biscay

The Bay of Biscay is a V-shaped oceanic basin situated between Spain and France along the eastern side of the southern North Atlantic Ocean (Figure 1.3). The present-day crustal architecture of the Bay of Biscay is a result of southern North Atlantic and Western Tethys related deformation dating back to the Permian (Williams, 1975; Leleu et al., 2016; Angrand et al., 2020). Following Late Permian-Early Triassic rifting and the subsequent breakup of Pangaea initiating ~ 200 Ma, the future Bay of Biscay was subjected to two of the three main rift phases acknowledged within the southern North Atlantic: 1) Late Triassic to Early Jurassic and 2) Late Jurassic to Early Cretaceous (Boillot et al., 1979; Ziegler, 1988; Lundin, 2002; Tugend et al., 2015a; Barnett-Moore et al., 2018; Cadenas et al., 2018; Peace et al., 2019a). These two main phases of rifting between

Iberia and Europe led to significant crustal thinning along its offshore regions during the Early Cretaceous prior to a short lived period of sea-floor spreading initiating during Aptian-Albian time (Montadert et al., 1979; Thinon et al., 2003; Sibuet et al., 2004; Vissers and Meijer, 2012; Tugend et al., 2015a; Nirrengarten et al., 2018). Extensional deformation migrated into the Pyrenean realm during the Early to mid-Cretaceous (Jammes et al., 2009; Tugend et al., 2015a; Tavani et al., 2018). The southern Bay of Biscay experienced re-activation from the Late Cretaceous to Cenozoic caused by compressional deformation induced from the Alpine Orogeny (Boillot et al., 1979; Deregnaucourt and Boillot, 1982; Alvarez-Marrón et al., 1996, 1997; Gallastegui et al., 2002; Fernández-Viejo et al., 2011; Roca et al., 2011; Tugend et al., 2014; Cadenas and Fernández-Viejo, 2017; Cadenas et al., 2018).

The Bay of Biscay-Parentis rift system is interpreted to encompass the North Iberian, Armorican, and Western Approaches margins, and the Parentis Basin (Figure 1.6). The crustal structure of the Bay of Biscay-Parentis system based on previous rift domain mapping is interpreted to be highly segmented showing significant along strike crustal variabilities (Thinon et al., 2003; Tugend et al., 2014; Cadenas et al., 2018). Its diverse present day structure is interpreted to be a result of spatial variations in the timing and orientation of principle stresses during rifting, occurrence of inherited structures and pre-rift salt, and each region's exposure to compressional deformation during the Pyrenean Orogeny (Thinon et al., 2003; Ferrer et al., 2008; Jammes et al., 2009, 2010b, 2010c; Roca et al., 2011; Tugend et al., 2014; Cadenas et al., 2018, 2020; Lagabrielle et al., 2020).

1.2.1.2.1 The North Iberian margin

The North Iberian margin consists of the region between northwest Galicia and west of France that corresponds to the southern margin of the Bay of Biscay (Figure 1.6). This margin plays host to sedimentary basins such as the Asturian Basin (Cadenas and Fernández-Viejo, 2017), major lithospheric structures such as the Ventaniella Fault (Fernandez-Viejo et al., 2014; Cadenas et al., 2018) and interpreted transfer zones such as the Santander Transfer Zone (Roca et al., 2011), and continental blocks such as the Landes High and Le Danois High (Ferrer et al., 2008; Tugend et al., 2014; Cadenas et al., 2018). The crustal architecture along the North Iberian margin based on previous rift domain mapping significantly varies from west to east (Tugend et al., 2014; Cadenas et al., 2018). Along the western North Iberian margin, a narrow necking region, bounded to the east by the Ventaniella Fault, is interpreted. At the central part of the North Iberian margin, a region of hyperthinned crust is interpreted to be underlying the Asturian Basin and Santander Transfer Zone. The Le Danois crustal block (~ 20 km thick) separates the hyperthinned Asturian Basin from the underthrust hyperextended domains to the north (Cadenas et al., 2018). Ocean-ward of the Le Danois High, uncertainties still remain regarding the nature and structure of this under thrusted domain relative to the undisputed regions of oceanic crust further west (Sibuet et al., 2004; Tugend et al., 2014; Cadenas et al., 2018). These uncertainties are primarily associated with crustal thickening of a former distal margin during the Pyrenean Orogeny and the present day distinction between hyperthinned continental crust, exhumed mantle, and oceanic crust within this region interpreted as a fossil accretionary wedge (Alvarez-Marrón et al., 1997; Gallastegui et al., 2002; Fernández-Viejo et al., 2012; Cadenas et al., 2018). However, seismic refraction results obtained along the North Iberian margin (Ruiz et al., 2017) suggest an area of exhumed mantle

with minor magmatic additions oceanward of the Le Danois High. The easternmost region of the North Iberian margin consists of the Landes High and surrounding areas of slightly thinned crust (necking region) in its vicinity. The crustal thickness of the Landes High varies from ~ 20-35 km as deduced from gravity inversion results (Tugend et al., 2014) (Figure 1.7).

1.2.1.2.2 The Parentis Basin

The offshore Parentis Basin (Figure 1.6) is characterized as a smooth-slope sedimentary basin located between the Landes High and the southern edge of the Armorican margin (Brunet, 1984; Bois et al., 1997; Ferrer et al., 2008, 2012; Jammes et al., 2009; Tugend et al., 2014, 2015b; Lagabrielle et al., 2020). Corresponding to what is called in the literature as a smooth-slope sedimentary basin, the Parentis Basin exhibits gradually dipping smooth slopes towards the center of the basin, a smooth basement top, a lack of seismically imaged normal faulting, and a region of significantly thinned crust (<10 km) within the center of the basin (Pinet et al., 1987; Jammes et al., 2010a; Tugend et al., 2015b; Lagabrielle et al., 2020). Hyperextension is interpreted to have occurred from Valanginian/Barremian to Late Aptian time based on age correlations calibrated by wells and interpreted seismic sections (Ferrer et al., 2008; Jammes et al., 2010a; Tugend et al., 2015b). However, a Late Jurassic increase in subsidence calculated from exploration well data and a thickening of Late Jurassic sedimentary sequences interpreted from seismic reflection profiles could suggest a Late Jurassic initiation of significant crustal thinning within the Parentis Basin (Brunet, 1984; Bois et al., 1997). In fact, the mode of crustal thinning within the Parentis Basin has been a subject of debate in the literature (Bois et al., 1997; Ferrer et al., 2008; Jammes et al., 2010a; Lagabrielle et al., 2020). This is primarily due to a lack of significant normal faulting interpreted on seismic sections within the center of the basin (Lagabrielle et al., 2020). One

explanation for this phenomenon suggests an asymmetrical mode of opening within the southern Parentis Basin, whose structure is depicted as a lower plate sag basin with crustal thinning controlled by a detachment system at basement level (Jammes et al., 2010a). In addition, Jammes et al. (2010b) highlight the presence of a thick pre-rift salt decollement promoting extreme crustal thinning within a ductile regime, causing layers below and above the pre-rift salt layer to deform differently. Following the end of extension during the mid-Cretaceous, the Parentis Basin was partially re-activated during the Late Cretaceous and Cenozoic as a result of compressional deformation caused by the Alpine Orogeny (Ferrer et al., 2008; Tugend et al., 2014; Tavani et al., 2018). This compressional deformation within the Parentis Basin was partially buffered by the presence of the Landes High along its southern border (Ferrer et al., 2008).

1.2.1.2.3 The Armorican and Western Approaches margins

The Armorican and Western Approaches margins correspond to segments of the northern Bay of Biscay margins (Figure 1.6). The Armorican margin, immediately north of the Parentis Basin, is interpreted to have a general continent to oceanward variation in crustal architecture, with a narrow necking zone interpreted inboard of a zone of hyperthinned crust whose structure is characterized by large scale detachment faulting and extensional allochthons (Thinon et al., 2002, 2003; Tugend et al., 2014, 2015b). In addition, the Armorican margin hosts a wide deep basin (Armorican Basin) whose basement shows atypical velocity structure that is usually interpreted as exhumed mantle (Thinon et al., 2003; Tugend et al., 2014) and localized volcanic edifices (Thinon et al., 2003). The exterior boundary of this exhumed mantle domain approximately corresponds to the landward limit of oceanic crust (LaLOC) (Tugend et al., 2014; Nirrengarten et al., 2018). The Western Approaches margin, further north, is characterized by a wider necking domain in

comparison to the Armorican margin (Thinon et al., 2003; Tugend et al., 2014). In addition, S-reflections, oceanward faults and "classical" tilted fault blocks are all commonly described throughout the Western Approaches margin (De Charpal et al., 1978; Barbier et al., 1986; Le Pichon and Barbier, 1987).

The Armorican Shear Zone (Figure 1.6), a set of onshore inherited Variscan structures that extend into offshore northeast-southwest trending transfer zones, is interpreted as the boundary separating the Armorican and Western Approaches margins (Tugend et al., 2014). Along the Western Approaches and Armorican margins, a number of transfer zones delimit different margin segments which are characterized by architectural variations (Thinon et al., 2003; Tugend et al., 2014).

1.2.1.3 Pyrenees

The Pyrenean mountain range encompasses well-preserved remnants of what has been debated as either a former rifted margin (Olivet, 1996; Sibuet et al., 2004; Jammes et al., 2009; Lagabrielle et al., 2010; Mouthereau et al., 2014; Tugend et al., 2014; Teixell et al., 2018; Gómez-Romeu et al., 2019; Saspiturry et al., 2019), or a compressional setting that experienced subduction and subsequent slab break-off (Sibuet et al., 2004; Vissers and Meijer, 2012; Vissers et al., 2016; van Hinsbergen et al., 2020). The Pyrenean realm hosts several Cretaceous sedimentary basins in the so-called Northern Pyrenean zone (e.g. Basque-Cantabrian and Arzacq-Mauleon basins) (Mattauer and Henry, 1974) bordered by rigid continental blocks (e.g. Ebro Block and Landes High) (Tugend et al., 2015a) and is segmented by previously interpreted transfer zones (e.g. Pamplona and Toulouse transfer zones) (Larrasoana et al., 2003; Jammes et al., 2009; Tugend et

al., 2014; Tavani et al., 2018). The current crustal structure of the Pyrenees demonstrates significant along-strike variability (Figure 1.7) (Diaz et al., 2016; Wang et al., 2016; Chevrot et al., 2018). Furthermore, the architectural variations observed along strike of the Pyrenees are a product of Atlantic and Tethys related tectonic events that initiated during the Paleozoic. Following the collapse of the Variscan Orogeny during the late Carboniferous to Early Permian (Burg et al., 1994a; 1994b), the Pyrenean realm and Bay of Biscay were subjected to minimal amounts of rift-related deformation and widespread evaporite deposition up until the Early Jurassic (Jammes et al., 2010b; Saspiturry et al., 2019; Duretz et al., 2020; Lagabrielle et al., 2020). Following this Late Triassic to Early Jurassic rift phase, a period of tectonic quiescence was experienced within the Bay of Biscay and Pyrenean domains prior to a second phase of rifting that was initiated by the early opening of the North Atlantic Ocean during the latest Jurassic to Early Cretaceous. This second phase of rifting marked the onset of significant crustal thinning and syn-rift deposition within the Bay of Biscay (Montadert et al., 1979; Brunet, 1984; Thinon et al., 2002; Jammes et al., 2010b; Ferrer et al., 2012; Tugend et al., 2015a; Cadenas et al., 2018) and localized rift-related deformation and subsidence within the Pyrenean realm (Jammes et al., 2009; Tugend et al., 2014; Saspiturry et al., 2019). During the Aptian-Albian, the onset of sea-floor spreading within the Bay of Biscay (Montadert et al., 1979; Thinon et al., 2003; Sibuet et al., 2004) led to the eastward migration of significant rift related deformation from the Bay of Biscay into the Pyrenean realm (Tugend et al., 2015a). This resulted in hyperextension, mantle exhumation, and alkaline magmatism within the Pyrenean realm during the Aptian-Albian (Jammes et al., 2009; Lagabrielle et al., 2010; Roca et al., 2011; Tugend et al., 2014) and high temperature metamorphism during the Aptian-Santonian (Clerc et al., 2015). By the Cenomanian, rift-related

deformation and continental breakup within the Pyrenees is interpreted to have ceased (Debroas et al., 1987, 1990; Garcia-Mondejar et al., 1996, 2005, Saspiturry et al., 2019) and the onset of Alpine-related compressional deformation within the Pyrenees is interpreted to have begun during the Late Santonian (Garrido-Megias and Rios, 1972; McClay et al., 2004).

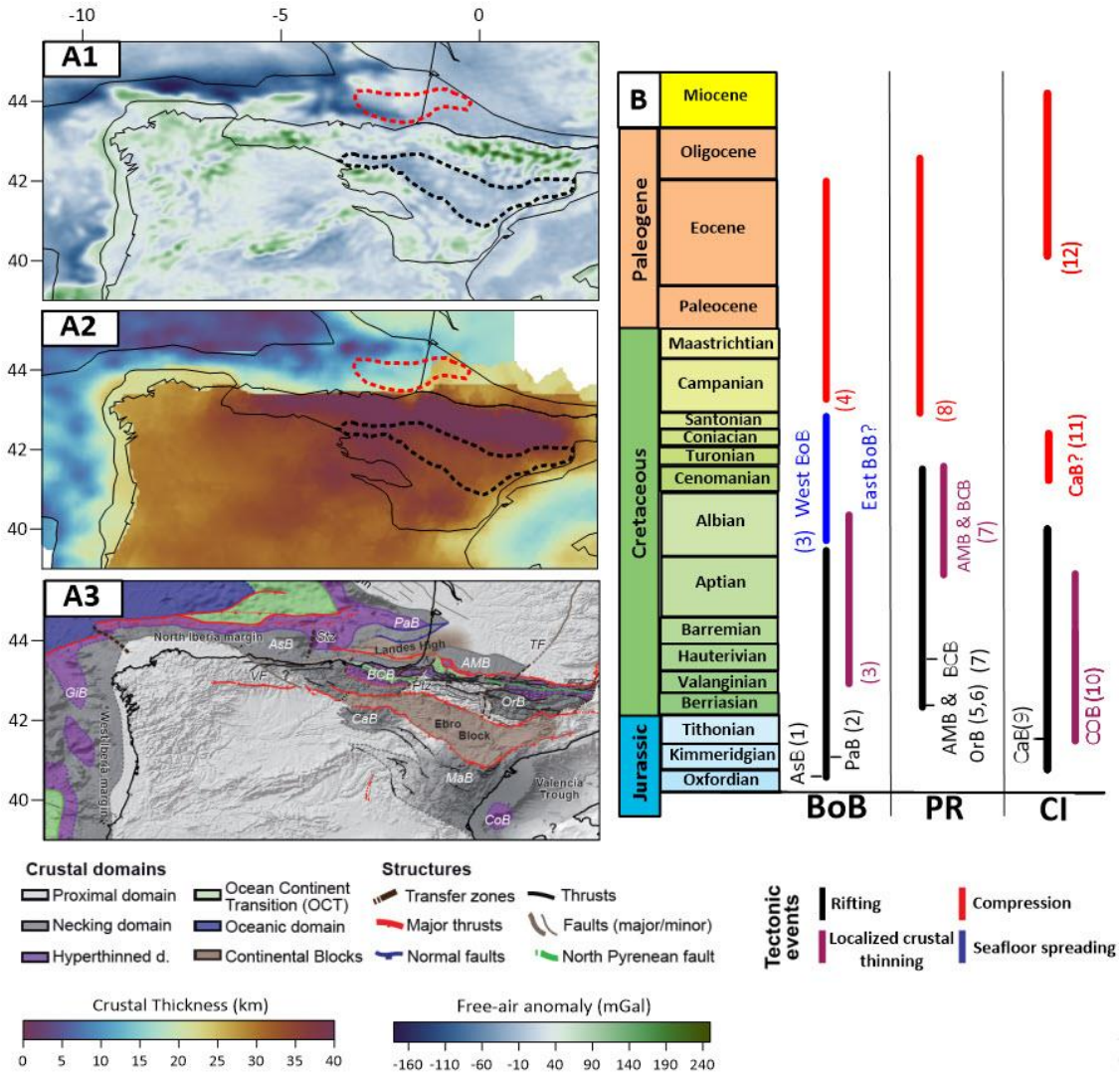

Figure 1.7 A1) WGM2012 free-air gravity anomaly throughout the Iberian interior and offshore margins extracted from the Bureau Gravimétrique International (BGI) database. Overlain is the

geometry of the Ebro Block (black dashed polygon) from Tugend et al. (2015) and Landes High (red dashed polygon) from King et al. (2021). A2) Moho depth obtained via teleseismic receiver function data within the Iberian interior from Diaz et al. (2016) and offshore gravity inversion crustal thickness estimates from King et al. (2020, 2021). A3) Map of Iberian rift domains modified after Tugend et al. (2015a). B) Timing of geological events within the Bay of Biscay (BoB), Pyrenean realm (PR) and Central Iberia (CI) modified after Tugend et al. (2015a). Numbered references used for the timing of geological events within specific regions can be found in Appendix A. AMB = Arzaq-Mauleon Basin AsB = Asturian Basin, BCB = Basque-Cantabrian Basin, CaB = Cameros Basin, COB = Columbret Basin, GIB = Galicia Interior Basin, MaB = Maestrat Basin, OrB = Organya Basin, PaB = Parentis Basin, Ptz = Pamplona transfer zone, Stz = Santander transfer zone, TF = Toulouse Fault, VF = Ventaniella Fault.

1.2.1.4 Central Iberian Ranges

The Central Iberian Ranges are a NW-SE trending mountain belt located south of the Ebro Block (Figure 1.6). Their present day structure comprises a series of sedimentary basins such as the South Iberian, Maestrat, and Cameros basins that evolved during North Atlantic and Alpine Tethys rifting events prior to being inverted during the Alpine Cycle (Salas et al., 2001; Martín-Martín et al., 2015; Rat et al., 2019; Vergés et al., 2020). Two main extensional episodes have been documented within Central Iberia; 1) Triassic to Early Jurassic and 2) Late Jurassic to Early Cretaceous (Salas et al., 2001). Unlike the Bay of Biscay, the Pyrenees and offshore extensions of the Central Iberian rift system such as the Columbret Basin (Etheve et al., 2018), evidence of hyperextension has not been documented within the Central Iberian rift, despite clear evidence of syn-rift and rift-related subsidence during the Late Jurassic to Early Cretaceous (Salas et al., 2001).

The onset of contraction experienced within Central Iberia remains relatively poorly constrained compared to observations within the Pyrenees and Bay of Biscay (Rat et al., 2019). Despite the main phase of compression being proposed to have occurred from the Eocene to Miocene in the majority of previous studies (Salas et al., 2001; Vacherat et al., 2016, 2017), evidence of Late Cretaceous compressional deformation has also been identified within Central Iberia, possibly caused by far-field stresses experienced during Pyrenean rifting (Casas-Sainz and Gil-Imaz, 1998).

1.2.2 Tectonic history of the Newfoundland and Irish margins

1.2.2.1 Newfoundland Margin

The present day architecture of the Newfoundland margin exhibits a large degree of structural variability between its northern and southern extents. The northern extent of the Newfoundland margin is interpreted to comprise the Orphan Basin and Bonavista Platform (Figure 1.8). The Orphan Basin encompasses NE-SW trending basins and crustal blocks, formed over the Avalonian terrane (King et al., 1985) (Figure 1.5), and is approximately delimited to the east and west by the eastern edge of the Bonavista Platform and western edge of the Flemish Cap, respectively. The interior of the Orphan Basin is commonly subdivided into three regions that include the East and West Orphan basins, and the Central Orphan High dividing the East and West Orphan basins by NE-SW trending blocks of relatively thicker crust (~ 15-20 km thick) (Figure 1.4B). The East and West Orphan basins are classified as failed rifts comprised of hyperextended crust, crustal detachments, and highly rotated fault blocks (Chian et al., 2001; Welford et al., 2012, 2020; Cawood et al., 2021a, 2021b; Neuharth et al., 2021). The opening and resultant structural complexity of the Orphan Basin has been interpreted to have been largely influenced by the clockwise rotation of the Flemish Cap, a previously identified continental block (Sibuet et al.,

2007; Péron-Pinvidic and Manatschal, 2010; Nirrengarten et al., 2018; Yang et al., 2021) whose rotation primarily took place during Late Jurassic to Early Cretaceous rifting.

South of the Orphan Basin and Flemish Pass (Figure 1.8), the Newfoundland continental shelf is made up of the Grand Banks. The Grand Banks correspond to relatively thicker crust (~ 25-30 km thick) (Figure 1.4B) that encompasses numerous sedimentary basins, such as the Jeanne D'Arc Basin (Sinclair, 1995), which are of significant interest for hydrocarbon exploration and production. The southern extent of the Grand Banks is interpreted as the Southern Grand Banks Tail (Figure 1.8), which is surrounded by several sedimentary basins (e.g. Whale, Horseshoe, and Carson-Salar basins) that developed synchronously with basins along the southwest Iberian margin (Alves and Cunha, 2018). The morphologies of basement terranes in the vicinity of the Southern Grand Banks Tail have been debated in previous studies due to a lack of basement well penetrations (Ady and Whittaker, 2018; Waldron et al., 2019). These debates often arise from uncertainties associated with the offshore extension of ancient terrane boundaries mapped onshore, leading to uncertainty regarding the Avalonia, Meguma, or Variscan basement affinity of the southern Grand Banks (King et al., 1985; Ady and Whittaker, 2018; Waldron et al., 2019).

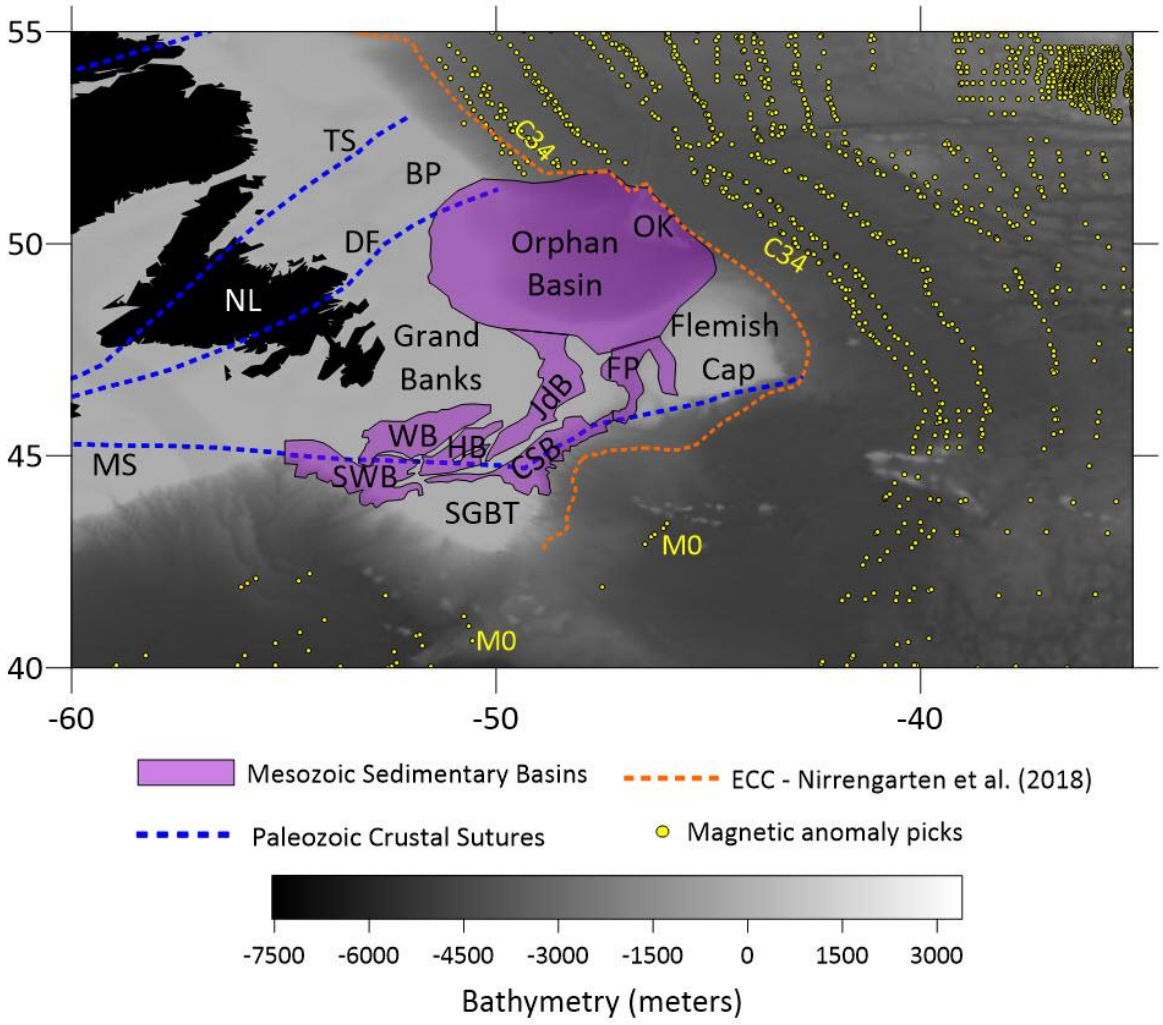

Figure 1.8 Bathymetric map (WGS 1984 coordinate system) of the Newfoundland and Labrador margin overlain with previously defined crustal structures and sedimentary basins. Magnetic anomaly locations and sedimentary basin outlines extracted from Nirrengarten et al. (2018), and crustal sutures extracted from Welford et al. (2012). BP = Bonavista Platform, CSB = Carson-Salar Basin, DF = Dover Fault, FP = Flemish Pass, HB = Horseshoe Basin, JdB = Jeanne d'Arc Basin, NL = Newfoundland and Labrador, SGBT = Southern Grand Banks Tail, SWB = South Whale Basin, TS = Taconian Suture, WB = Whale Basin.

1.2.2.2 Irish Margin

In this thesis, the Irish margin is interpreted to encompass the Goban Spur, Porcupine Basin and Porcupine Bank, and the Rockall Basin and Rockall-Hatton Bank (Figure 1.9). Throughout the Irish margin, notable changes in orogenic basement terranes observed onshore via geological field mapping have been projected and inferred to extend offshore (Figure 1.5). For example, basement terranes underlying the Goban Spur are interpreted to encompass Variscan domain rocks (Dingle and Scrutton, 1979) (Figure 1.5). Northwest of the Variscan Front (Figure 1.9), several NE-SW trending orogenic terrane boundaries have been interpreted offshore across the Porcupine and Rockall basins, suggesting segmentation of the Irish margin into several different basement terranes ranging from Archean to mid-Paleozoic in age (Readman et al., 2005; Tyrrell et al., 2007, 2010; Chenin et al., 2015; Schiffer et al., 2019; Yang et al., 2021). Additionally, several independent continental blocks have been previously interpreted along the Irish margin such as the Porcupine Bank and Rockall Bank (Péron-Pinvidic and Manatschal, 2010; Yang et al., 2021) and these are situated adjacent to the Porcupine and Rockall basins, respectively (Shannon, 1991; Hauser et al., 1995; O'Reilly et al., 1996; Readman et al., 2005; Prada et al., 2017).

The rotation and independent kinematics of the Porcupine and Rockall-Hatton banks during North Atlantic rifting are considered to be key contributors to the current crustal structure of the Porcupine and Rockall basins, respectively (Nirrengarten et al., 2018; Peace et al., 2019b; Yang et al., 2021). Within the Porcupine Basin, hyperextended crust is observed throughout the centre of the basin (O'Reilly et al., 2006; Welford et al., 2010, 2012; Chen et al., 2018; Watremez et al., 2018), which is bordered by thicker regions of crust near the Porcupine Bank and Goban Spur to the west and south, respectively.

The Rockall Basin is a NE-SW trending basin situated between the Porcupine Bank to the south and the Rockall-Hatton Bank to the north. Similar to the Porcupine Basin, the Rockall Basin is interpreted as a failed rift comprised of hyperextended crust throughout the center of the basin (O'Reilly et al., 2006; Welford et al., 2010, 2012; MacMahon et al., 2020). However, in contrast to the Porcupine Basin, the Rockall Basin is interpreted to have experienced volcanism during rifting, leading to numerous igneous features (e.g. sills) within its present day structure as inferred by previous seismic studies (Scrutton and Bentley, 1988; Funck et al., 2017; MacMahon et al., 2020).

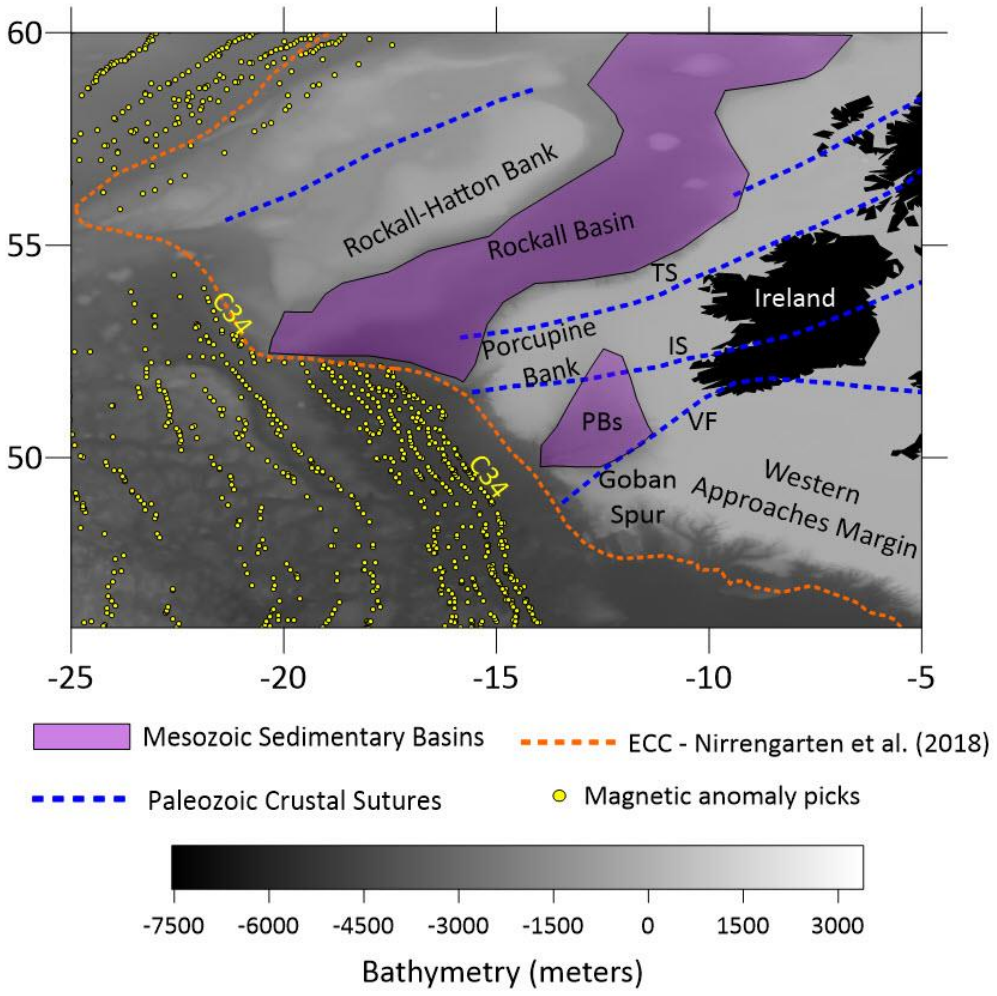

Figure 1.9 Bathymetric map (WGS 1984 coordinate system) of the Irish margin overlain with previously defined crustal structures and sedimentary basins. Magnetic anomaly locations and sedimentary basin outlines extracted from Nirrengarten et al. (2018), and crustal sutures extracted from Welford et al. (2012). IP = Iapetus Suture, PBs = Porcupine Basin, TS = Taconian Suture, VF = Variscan Front.

1.3 Scientific problems and research objectives

1.3.1 Scientific problems

Although the Newfoundland, Irish, and Iberian margins have been relatively well studied compared to other rifted margins worldwide, there are numerous scientific questions and issues that remain unresolved:

1. Despite an abundance of previously published plate tectonic reconstructions of Iberia, discrepancies still exist regarding their consequences for the timing of deformation within the Atlantic Ocean, and their implications for the plate kinematic evolution of the Bay of Biscay and Pyrenees. However, the majority of these previously published plate reconstructions of Iberia exclude deformation and the kinematics of continental blocks surrounding the Iberian micro-plate. Thus, the plate kinematics of Iberia have yet to be studied using deformable plate tectonic reconstructions that allow for detailed assessments of continental block kinematics.
2. Rigid plate tectonic reconstructions often produce overlap of continental domains and can pose challenges when trying to compare their outputs with geophysical and geological data observations acquired within regions that have been significantly deformed. To address

these issues, deformable plate reconstructions are used to calculate crustal stretching and crustal thickness estimates within plate kinematic models that can be quantitatively compared with present-day estimates. However, further methodological improvements are required in order to address the assumptions used in previously published deformable plate models such as uniform pre-rift crustal thickness assumptions and the rigid nature of continental blocks.

3. Rifting and subsequent opening of the modern North Atlantic Ocean initiated within the supercontinent Pangaea, which formed via the accretion and orogenesis of ancient Appalachian and Caledonian terranes. As a result, Paleozoic terrane boundaries and variations in crustal morphologies can be geologically mapped onshore present-day. However, the offshore extension of these terrane boundaries and their potential role during subsequent North Atlantic rifting are poorly understood.
4. The pre-rift nature of the crust prior to North Atlantic rifting is generally unknown and often assumed to be uniform in previously published 2-D structural restoration and deformable plate modelling studies. Thus, new approaches are needed in order to study the pre-rift template of the southern North Atlantic Ocean and its potential variabilities that are often ignored.
5. Quantifying uncertainties of deformable plate tectonic reconstructions is difficult due to the additional uncertainties that accompany geophysical data and modelling techniques (e.g., geophysical inversion) that are used for their inputs. Thus, new and improved approaches for making quantitative correlations between deformable plate models and

interpretations made from independent observations such as seismic interpretations, 2-D structural restorations, and well data are needed.

1.3.2 Research Objectives

The objectives of this doctoral research are to use potential field data, crustal thickness estimates calculated from 3-D gravity inversion, previously published 2-D seismic interpretations and structural restorations, and previously published and newly presented plate kinematic models of the southern North Atlantic Ocean to:

1. Evaluate the plate kinematic and crustal thickness evolution of previously published and newly presented plate kinematic models of Iberia using a deformable plate modelling approach.
2. Assess the impact of continental blocks and their interplay with the kinematics of larger tectonic plates and micro-plates (e.g., Iberia) during the opening of the modern North Atlantic Ocean.
3. Determine if previously published discrepancies regarding the plate kinematics of Iberia can be reduced using a deformable plate modelling approach and models that include continental block kinematics.
4. Examine the potential impact of orogenic inheritance on the pre-rift templates of the Newfoundland, Irish, and Iberian margins and its role on the nature and spatial extent of subsequent rift-related deformation.

5. Investigate how previously published deformable plate reconstruction approaches can be improved using new workflows that involve less assumptions and limitations compared to those used in previously published deformable plate modelling studies.
6. Provide new approaches that can improve our ability to quantitatively assess the uncertainties associated with deformable plate models and make quantitative comparisons between their results and similar estimates calculated by other techniques such as 2-D structural restorations of seismic interpretations.

1.4 Thesis outline

Chapter 2 describes the methodologies used in this thesis. In particular, this chapter provides a detailed overview of rigid and deformable plate tectonic reconstructions and their previous applications to study the plate kinematic history of the southern North Atlantic Ocean.

Chapter 3 examines the role of the Galicia Bank on the regional plate kinematics and deformation experienced along the West Iberian margin. Following an assessment of numerous plate kinematic scenarios and their comparisons with present day crustal thickness estimates and previously published seismic and well data interpretations, the kinematic role of the Galicia Bank and its potential interplay with inherited Variscan structures is revealed. This chapter is published in *"King, M. T., Welford, J. K., & Peace, A. L. (2020). Investigating the role of the Galicia Bank on the formation of the North West Iberian margin using deformable plate tectonic models. Tectonophysics, 789, 228537. https://doi.org/10.1016/j.tecto.2020.228537"*.

Chapter 4 investigates the plate kinematics and deformation experienced within the Bay of Biscay. This work was carried out by expanding the preferred deformable plate model presented

in Chapter 3 into the Bay of Biscay to assess newly presented and previously published rigid reconstructions of Iberia using a deformable plate modelling approach. Following a comparison between present-day crustal thickness estimates calculated by each deformable plate model and gravity inversion, models that included continental blocks (e.g., Landes High and Ebro Block) and their independent kinematics provided the best correlations with present-day crustal thickness estimates and the timing of deformation suggested from previous studies. This chapter has been published as *"King, M. T., Welford, J. K., Cadenas, P., & Tugend, J. (2021). Investigating the plate kinematics of the Bay of Biscay using deformable plate tectonic models. Tectonics, 40, e2020TC006467. https:// doi.org/10.1029/2020TC006467"*.

Chapter 5 expands upon the preferred deformable plate models presented in Chapters 3 and 4 and aims to investigate newly presented and previously published plate reconstructions of the Pyrenees, and Iberia as a whole. An evaluation of five different deformable plate models of Iberia suggest that the pre-rift positions of the Ebro Block and Landes High were likely located within the Bay of Biscay prior to their progressive eastward motion into the Pyrenean realm. These continental block motions and resultant oblique phases of rifting are deemed necessary in order to reproduce the deformation experienced within these regions in accordance with geological field observations within the Pyrenees and Central Iberia, and offshore interpretations made within the Bay of Biscay. This chapter has been published as *"King, M. T., Welford, J. K., & Tugend, J. (2023). The role of the Ebro Block on the deformation experienced within the Pyrenean realm: insights from deformable plate tectonic models. Journal of Geodynamics, 101962. https://doi.org/10.1016/j.jog.2023.101962"*.

Chapter 6 presents a new deformable plate modelling workflow that reduces the modelling assumptions considered in Chapters 3-5. This newly presented workflow allows for deformation to be experienced within continental blocks, the reconstruction of crustal thickness estimates and alternative datasets back through time, and the inclusion of proximal rift domains which permits the definition of rift domain boundaries *a priori.* Using the southern North Atlantic Ocean as an example, these newly presented capabilities allow for the pre-rift template, crustal evolution of continual blocks and sedimentary basins, and the potential impact of orogenic inheritance to be studied along rifted margins, and other tectonic regimes. This chapter is published in *"King, M. T., & Welford, J. K. (2022). Advances in deformable plate tectonic models: 1. Reconstructing deformable continental blocks and crustal thicknesses back through time. Geochemistry, Geophysics, Geosystems, 23, e2022GC010372. https://doi. org/10.1029/2022GC010372"*.

Chapter 7, a companion contribution to chapter 6, presents a detailed application of the deformable plate modelling workflow presented in chapter 6 to study the crustal evolution of the southern North Atlantic Ocean. Using two deformable plate models, this application revealed the pre-Jurassic template of the Newfoundland, West Iberia, and Irish margins and strong correlations between across strike variations in pre-Jurassic crustal thickness and the offshore extension of Appalachian and Caledonian orogenic terrane boundaries. Furthermore, the crustal thickness evolution of each model provided insight into the formation and origin of continental blocks, and the partitioning of deformation during the opening of the southern North Atlantic Ocean caused by the interplay between continental block kinematics and inherited structures. This chapter is published in *"King, M. T., & Welford, J. K. (2022). Advances in deformable plate tectonic models:*

2. Reconstructing the southern North Atlantic back through time. Geochemistry, Geophysics, Geosystems, 23, e2022GC010373. https://doi. org/10.1029/2022GC010373".

Chapter 8 was submitted to the journal of Marine and Petroleum Geology in January 2023 and is titled *"Beyond 2-D: validating 2-D structural restorations using deformable plate tectonic models"*. This chapter presents a new workflow for deforming 2-D seismic line interpretations back through time within deformable plate models that account for 3-D plate kinematics and deformation. This workflow allows for the reconstructed length, linearity, and orientation of 2-D seismic line interpretations to be visualized within deformable plate models through time and provides a quantitative method of comparison with results calculated by 2-D structural restorations of seismic interpretations that assume rift perpendicular kinematics and uniform pre-rift templates. Following an application of this workflow using previously published 2-D seismic lines that have been structurally restored and deformable plate models within the Orphan Basin, the ability to account for continental block motions and variable pre-rift templates within deformable plate models reveals geologically significant discrepancies regarding the total amount of Mesozoic extension calculated by 2-D structural restorations of seismic interpretations within the Orphan Basin.

Chapter 9 summarizes the kinematic and crustal evolution of the Newfoundland, Irish, and Iberian margins based on the deformable plate modelling results presented in each manuscript chapter. In addition, this final chapter discusses the main conclusions of this thesis and provides suggestions that should be considered in future studies of the southern North Atlantic Ocean, and rifted margins in general.

Chapter 2

2 Methodology

2.1 Plate tectonic reconstructions

2.1.1 Rigid plate tectonic reconstructions

Rigid plate tectonic reconstructions are used to visualize and investigate the plate kinematic evolution of rigid tectonic plates and other geological features back through time. Traditionally, rigid plate reconstructions provide an excellent tool for investigating global and regional-scale plate kinematic evolution (Bullard et al., 1965; García-Mondéjar, 1996; Srivastava et al., 2000; Stampfli and Borel, 2002; Vissers and Meijer, 2012; Seton et al., 2012; Sibuet et al., 2012; Heine et al., 2013; Matthews et al., 2016; Barnett-Moore et al., 2018; Nirrengarten et al., 2018; van Hinsbergen et al., 2020). Since the introduction of plate tectonic theory, the applications and methodology associated with plate tectonic reconstructions have evolved significantly. Considering the evolution of rigid plate tectonic reconstructions focused within the Atlantic Ocean, initial attempts recognized similar margin symmetries along both sides of the Atlantic Ocean, which led to the simple approach of fitting together conjugate transects interpreted along the coastlines of South America and Africa (Bullard et al., 1965). Following these initial attempts, new approaches were proposed that consisted of fitting together conjugate sets of oceanic magnetic anomalies, fracture patterns, and bathymetric features, and their integration with paleomagnetic

data collected from rock samples (Srivastava et al., 2000; Sibuet et al., 2004, 2007; Gong, 2008; Neres et al., 2012; Vissers et al., 2016).

Over the last decade, plate tectonic reconstructions, and the datasets used in their design, have become more freely available and reproducible using newly developed open-source software packages such as GPlates (Müller et al., 2018). These software packages are commonly used to integrate previous plate reconstruction attempts using magnetic anomaly, fracture patterns, and paleomagnetic data with the timing of plate motion inferred from independent geological and geophysical studies (Seton et al., 2012; Barnett-Moore et al., 2018; Gurnis et al., 2018; Müller et al., 2018, 2019; Nirrengarten et al., 2018; Peace et al., 2019b). In GPlates, the motions of large tectonic plates, micro-plates, continental blocks, and other features, such as individual points or lines, are governed by finite rotations in accordance with Euler's Displacement Theorem (Cox and Hart, 1986). These finite rotations can be defined in GPlates, or elsewhere, and are characterized by a latitude, longitude, and angle of rotation, which govern the motion and displacement of tectonic features about an Euler pole. In GPlates, each individual feature considered must be assigned a unique plate identification number (Plate ID). The integration of this plate ID with finite rotations is used to create Total Reconstruction Poles. The motion of any feature in GPlates is governed by Total Reconstruction Poles. A Total Reconstruction Pole includes a plate ID for the feature of interest (i.e. moving plate), a relative plate ID that defines what the feature moves relative to, a particular point in time, and a finite rotation. Collectively, these define the position and displacement of the feature throughout geological time.

However, a common assumption used in the majority of previously published plate tectonic reconstruction studies is that tectonic plates are rigid. As summarized in recent studies (Peace,

2021), this assumption is often geologically unsatisfying because it can lead to significant overlap between conjugate tectonic plates and plate boundaries back through time due to their inability to experience deformation. As a result, despite an abundance of previous published plate reconstruction studies of the southern North Atlantic Ocean, questions still remain in this region regarding concepts such as the nature of pre-rift templates, the heavily disputed plate kinematics of Iberia (Barnett-Moore et al., 2016), and temporal evolution of regional stress directions and deformation caused by the interplay of large tectonic plates (e.g., North America), micro-plates (e.g., Iberia), and continental blocks (e.g., Flemish Cap).

2.1.2 Deformable plate tectonic reconstructions

In light of recent advances to the GPlates software, users now have the capability to build deformable plate tectonic reconstructions (Gurnis et al., 2018). Deformable plate tectonic reconstructions provide an approach for quantifying deformation within plate tectonic reconstructions. In particular, deformable plate models can be used to quantify temporal variations in crustal stretching (dilatational strain rate), crustal thickness, and stretching (beta) factors, providing more information to address limitations commonly associated with rigid plate models.

To construct a deformable plate tectonic model in GPlates (Figure 2.1), the first step is to define the model inputs required to build a deformable model. These model inputs are typically designed and constrained using independent geophysical and geological observations acquired from seismic, potential field, or well data. In GPlates, hard boundaries surrounding the zone of deformation must be designed in order to construct a deformable plate model. These hard boundaries can be used to construct a deformable plate model in the form of a continuously closed

polygon (Figure 2.1), or a model that includes a dynamically evolving exterior plate boundary (Figure 2.2). The latter of these approaches is more commonly used to evaluate the opening of oceans and the timing of breakup between conjugate rifted margins (Peace et al., 2019b). This approach is accomplished by partitioning exterior boundaries, such as continent-ocean boundaries or the edge of continental crust, into smaller segments that are assigned a timing of appearance which corresponds to a time where these hard boundaries along conjugate margins are no longer overlapping. The necking line, a boundary where thinning of the lithosphere is interpreted to begin (Nirrengarten et al., 2018), is commonly used as the interior hard boundary for deformable plate models (Welford et al., 2018; Peace et al., 2019b). These hard boundaries define the limits of where deformation will take place, and thus, do not take into account any additional deformation that could be experienced outside of these hard boundaries. This assumption is a model requirement, but problematic for a real geological scenario. This is simply due to the fact that deformation is likely to be experienced regionally and not confined within delineated regions with hard boundaries.

In addition to these hard boundaries for the deformable zone, features such as polygons representing continental blocks or individual lines and points representative of geological structures can be added into the interior of deformable regions. Continental blocks or rigid features placed within deformable regions are incapable of experiencing deformation using the GPlates deformable modeling methodology. Although continental blocks/ribbons are generally defined as being relatively undeformed (~20-35 km thick) (Péron-Pinvidic and Manatschal, 2010), this assumption implies that continental blocks/ribbons must remain rigid throughout the entirety of deformable models. This limitation is geologically unsatisfying given the variable crustal

thicknesses of continental blocks/ribbons previously interpreted throughout the southern North Atlantic such as the Flemish Cap and Porcupine Bank (Sibuet et al., 2007; Péron-Pinvidic and Manatschal, 2010; Welford et al., 2010, 2012).

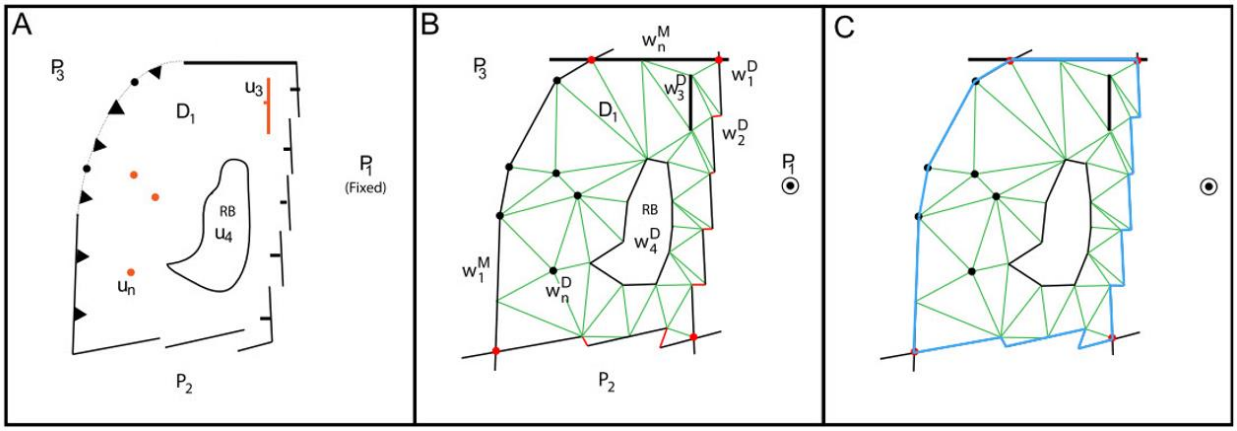

Figure 2.1 General workflow and data required for building deformable plate models with a continuously closed polygon in GPlates from Gurnis et al. (2018). A) Geological data used to create a region of deformation (D1). The deformable region encompasses a fixed tectonic plate (P1), other tectonic plates (P2 and P3) that govern the motion of exterior boundaries such as subduction zones and other fault boundaries, rigid blocks (RB) and individual points or lines that move with a local velocity (u) with respect to plate 1 (P1). B) Delaunay triangulation mesh designed based on the model inputs described in (A). The motion of each model input along the margins (M) or within the topological network (D) can be defined by a linear velocity (u) or angular velocity (w). Orange lines and points represent areas where individual boundaries are connected to form the topological network polygon. C) Same as (B) but highlighting the complete topological network polygon (blue).

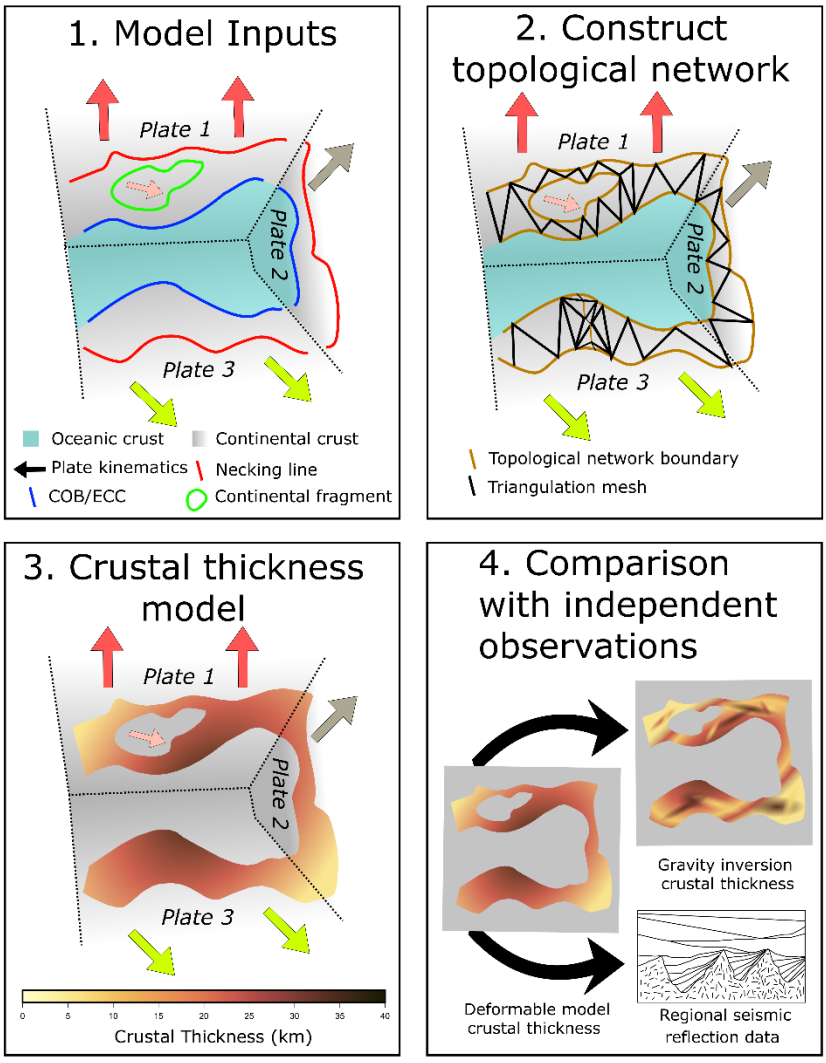

Figure 2.2 General GPlates deformable plate modelling workflow that encompasses a dynamically evolving exterior plate boundary originally from Peace et al. (2019b) and modified after King et al. (2020).

Following the definition of deformable model inputs, these features are used to construct a topological network (Figure 2.2). Within the topological network, a Delaunay triangulation mesh is created and used to measure variations in strain rate throughout geological time as described by

Gurnis et al. (2018). For each triangle within the mesh, the velocity at each vertex of a triangle can be calculated according to their stage rotations. Using the velocity calculated at the three vertices of the triangle, the velocity and strain rate at any point within the triangle can be determined. The dilatational strain rate ($\dot{\varepsilon}_D$), divergence of the horizontal velocity field on a spherical surface (Eqn. 2.1), is expressed as

$$\dot{\varepsilon}_D = div(\vec{u}) = \frac{1}{Rsin\theta}\left[\dot{u_\theta} cos\theta + sin\theta \frac{\partial \mu_\theta}{\partial \theta} + \frac{\partial \mu_\varphi}{\partial \varphi}\right] \qquad \textit{Eqn. 2.1}$$

where R, φ, θ, μ_φ , and u_θ represent the radius of the Earth, longitude, colatitude, velocity in the longitude and colatitude directions, respectively. To project one point in a spherical triangular element to Cartesian coordinates, it can be assumed that the velocity and coordinate of this point in spherical coordinates can be expressed as linear functions of its corresponding Cartesian coordinates. The coefficients of these linear values can be determined by the values at the three vertices of the triangle:

$$\begin{cases} \varphi = (\varphi_2 - \varphi_1)x + (\varphi_3 - \varphi_1)y + \varphi_1 \\ \theta = (\theta_2 - \theta_1)x + (\theta_3 - \theta_1)y + \theta_1 \\ u_\varphi = (u_{\varphi 2} - u_{\varphi 1})x + (u_{\varphi 3} - u_{\varphi 1})y + u_{\varphi 1} \\ u_\theta = (u_{\theta 2} - u_{\theta 1})x + (u_{\theta 3} - u_{\theta 1})y + u_{\theta 1} \end{cases} \qquad \textit{Eqn. 2.2}$$

where (x, y) correspond to the Cartesian coordinates of the point. Alternatively the Cartesian points can be expressed in spherical coordinates:

$$\begin{pmatrix} x \\ y \end{pmatrix} = \begin{pmatrix} \theta_3 - \theta_1 & \varphi_1 - \varphi_3 \\ \theta_1 - \theta_2 & \varphi_2 - \varphi_1 \end{pmatrix} \begin{pmatrix} \varphi - \varphi_1 \\ \theta - \theta_1 \end{pmatrix} / \, Det(A) \qquad \textit{Eqn. 2.3}$$

$$A = \begin{pmatrix} \varphi_2 - \varphi_1 & \varphi_3 - \varphi_1 \\ \theta_2 - \theta_1 & \theta_3 - \theta_1 \end{pmatrix}$$

where the derivative of the Cartesian coordinates relative to spherical coordinates (Eqn. 2.4) is constant for linear triangle elements.

$$\begin{bmatrix} \partial x/\partial \varphi \\ \partial x/\partial \theta \\ \partial y/\partial \varphi \\ \partial y/\partial \theta \end{bmatrix} = \begin{bmatrix} \theta_3 - \theta_1 \\ \varphi_1 - \varphi_3 \\ \theta_1 - \theta_2 \\ \varphi_2 - \varphi_1 \end{bmatrix} \Big/ Det(A) \qquad \textit{Eqn. 2.4}$$

Finally, the spatial derivatives of the velocity using spherical coordinates (Eqn. 2.5) can be used to calculate dilatational strain rate (Eqn. 2.1) under spherical coordinates.

$$\frac{\partial u_\varphi}{\partial \varphi} = \frac{\partial u_\varphi}{\partial x}\frac{\partial x}{\partial \varphi} + \frac{\partial u_\varphi}{\partial y}\frac{\partial y}{\partial \varphi} = \frac{(u_{\varphi 2} - u_{\varphi 1})(\theta_3 - \theta_1) + (u_{\varphi 3} - u_{\varphi 1})(\theta_1 - \theta_2)}{Det(A)}$$
$$\frac{\partial u_\theta}{\partial \theta} = \frac{\partial u_\theta}{\partial x}\frac{\partial x}{\partial \theta} + \frac{\partial u_\theta}{\partial y}\frac{\partial y}{\partial \theta} = \frac{(u_{\theta 2} - u_{\theta 1})(\varphi_1 - \varphi_3) + (u_{\theta 2} - u_{\theta 1})(\varphi_2 - \varphi_1)}{Det(A)} \qquad \textit{Eqn. 2.5}$$

Following the calculation of dilatational strain rate within a topological network, other quantities such as crustal thickness and stretching (beta) factors can be determined. Assuming that no net mass is lost or generated during deformation within a lithospheric block associated with horizontal convergence or divergence generating vertical thickening or thinning (incompressible lithospheric block), the crustal thickness (H) evolution of the lithospheric block is in agreement with the conservation of mass equation:

$$\frac{dH}{dt} = -H \cdot \dot{S} \qquad \textit{Eqn. 2.6}$$

where $\dot{S}$ is equivalent to the surface dilatation rate ($\dot{\varepsilon}_D$). This ordinary differential equation (Eqn. 2.6) is solved using the Runge-Kutta method in GPlates to calculate temporal variations in crustal thickness using the dilatation rate at each time frame considered within a deforming network.

Deformable plate models built using GPlates offer an advantageous approach to study complex plate kinematic problems. Considering recent applications, deformable plate models have proven to be a very useful tool for investigating the plate kinematic evolution of the North Atlantic Ocean (Welford et al., 2018; Peace et al., 2019b), and other tectonic regimes (Flament et al., 2014; Müller et al., 2019; Cao et al., 2020). One of the key advantages of this approach is the ability to investigate previously published rigid plate kinematic models by integrating deformable regions within continental domains to calculate temporal variations in strain rate and crustal thickness. A comparison of these calculations with similar estimates obtained from gravity inversion and seismic refraction profiles provides valuable insight regarding the kinematic implications of previously published rigid plate models. For example, lithospheric boundaries (ex. continent-ocean boundaries) and large tectonic plates, micro-plates or continental blocks are key inputs that are often used to construct deformable plate models. Thus, deformable plate models offer an approach to investigate the impact of these features on the kinematics and deformation associated within complex geological scenarios. This has been demonstrated in recent plate kinematic studies of the North Atlantic Ocean, where the inclusion of continental blocks situated between larger tectonic plates are interpreted to have highly influenced strain partitioning during rifting and the present day crustal architecture of rifted margins (Nirrengarten et al., 2018; Peace et al., 2019b).

However, deformable plate models built in GPlates also involve several limitations. A combination of numerical modelling (Pérez-Gussinyé et al., 2003; Ranero and Pérez-Gussinyé,

2010; Brune et al., 2014; Brune, 2018; Glerum et al., 2020), analogue modelling (Withjack and Jamison, 1986) and laboratory rock studies (Ashyby and Verrall, 1978) have demonstrated that deformation within the crust and upper mantle is depth-dependent and influenced by rheology, both of which are not considered within deformable plate models built in GPlates. Thus, it is imperative that results calculated by deformable plate models are assessed in detailed correlation with observations inferred from independent geological, geophysical, and modelling studies. This is a crucial step in order to validate the results produced by deformable plate models within regions that may be highly influenced by heterogeneities such as inherited structures, lithological and compositional variations, or complex surface processes related to dynamic topography and sedimentation (Figure 2.3).

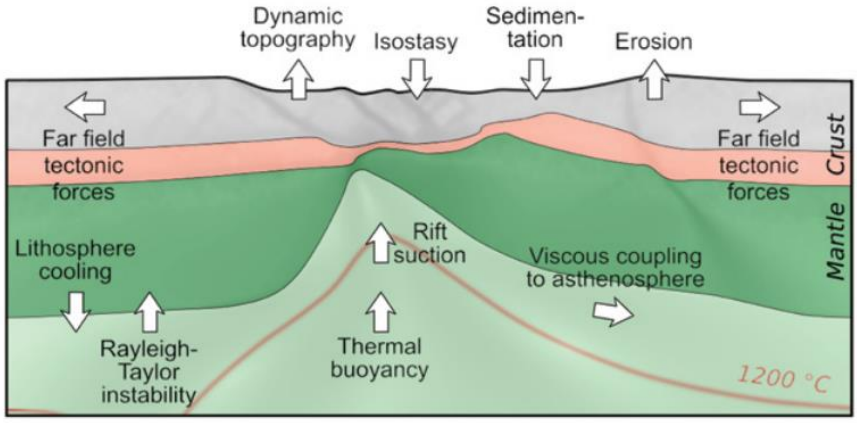

Figure 2.3 Processes and forces interpreted to occur during rifting modified from Brune (2018).

2.1.3 Previous plate tectonic reconstructions of the southern North Atlantic Ocean

The plate kinematics of the Iberian micro-plate have served as a long-standing problem and area of interest in previously published plate tectonic reconstruction studies of the southern North Atlantic Ocean (Srivastava et al., 2000; Sibuet et al., 2004; Gong et al., 2008; Jammes et al., 2009; Vissers and Meijer, 2012; Barnett-Moore et al., 2016; Nirrengarten et al., 2018; Causer et al., 2019; Angrand et al., 2020; van Hinsbergen et al., 2020). Subject to the independent geological and geophysical studies used to constrain plate tectonic models, numerous discrepancies arise when comparing previously published plate reconstruction attempts of Iberia (Barnett-Moore et al., 2016). These previously published attempts can be synthesized into three main scenarios when considering the most notable discrepancies along the Iberia-Eurasia plate boundary during the Late Jurassic to Mid-Cretaceous (Figure 2.4). One scenario (Figure 2.4a) proposes a transition from transtensional to rift-perpendicular extension from the Late Jurassic to Mid-Cretaceous (Jammes et al., 2009). Another scenario (Figure 2.4b) suggests pure strike-slip motion along the Iberia-Eurasia plate boundary (Choukroune and Mattauer, 1978; Olivet, 1996; Stampfli and Borel, 2002). The third scenario (Figure 2.4c) implies a scissor-type opening within the Bay of Biscay and subsequent subduction in the Pyrenees (Sibuet et al., 2004; Vissers and Meijer, 2012).

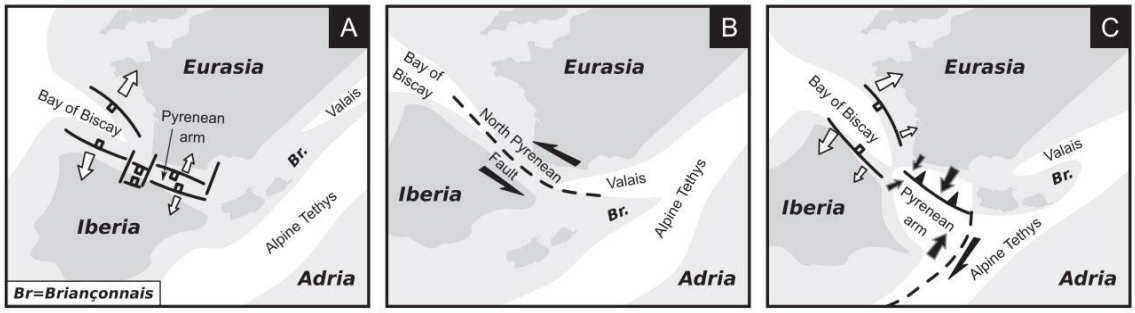

Figure 2.4 Previously published rigid plate tectonic reconstruction scenarios along the Iberia-Eurasia plate boundary during the Mid-Cretaceous taken from Tavani et al. (2018).

The three contrasting plate kinematic scenarios of Iberia primarily originate from the choice of the paleomagnetic, geophysical, and geological datasets considered in their design, and coincidently, how these datasets and observations are interpreted. For example, the nature and origin of marine magnetic anomalies such as the J-magnetic anomaly have been highly disputed. To the north of the Newfoundland-Azores Fracture Zone (Figure 1.3), the J-magnetic anomaly is often interpreted to correspond to the M0 (Figure 1.8), M3, or M4 magnetic anomalies and is highly asymmetric along the southeastern Newfoundland and West Iberian margins (Bronner et al., 2011; Nirrengarten et al., 2017; Grevemeyer et al., 2022). For previously published models that interpret the J-magnetic anomaly as synchronous oceanic crust that formed during sea-floor spreading along the southeastern Newfoundland and West Iberian margins and that honour paleomagnetic data collected throughout Iberia (Sibuet et al., 2004; Vissers and Meijer, 2012; Vissers et al., 2016; van Hinsbergen et al., 2020), the third scenario is preferred, which implies a phase of compression between Iberia and Europe during the Early Cretaceous and subsequent subduction within the Pyrenees (Figure 2.4c). This model also proposes that the pre-Alpine template of the Pyrenean realm formed via compressional stresses, advocating that crustal thinning

and mantle exhumation were caused by slab break-off and off-scraping of the upper crust (Vissers et al., 2016). In contrast, recent studies have questioned the validity of M-series magnetic anomalies within the North Atlantic Ocean as plate kinematic inputs (Bronner et al., 2011; Nirrengarten et al., 2017; Causer et al., 2019), the validity of paleomagnetic data collected throughout Iberia (Neres et al., 2012; Barnett-Moore et al., 2016, 2017), and the lack of evidence for slab break-off in the Pyrenees from seismic tomography sections (Barnett-Moore et al., 2016, 2017). Furthermore, these datasets have also demonstrated poor correlations with geological observations that suggest the Pyrenees are a former rifted margin (Jammes et al., 2010a; Lagabrielle et al., 2010; Masini et al., 2014; Tugend et al., 2014; Saspiturry et al., 2019). Meanwhile, alternative models that have proposed a rift-perpendicular scenario (Figure 2.4a) or Early Cretaceous strike-slip (Figure 2.4b) between Iberia and Europe have also been unsuccessful in mutually supporting geological and plate kinematic observations between the Pyrenean realm and North Atlantic Ocean, respectively (Barnett-Moore et al., 2016).

Recently, plate kinematic models of Iberia that were built upon previously published rift-perpendicular (Jammes et al., 2009) and strike-slip scenarios (Olivet, 1996) have emphasized the need to separate Iberia into a series of micro-blocks and continental ribbons (Tugend et al., 2015a; Barnett-Moore et al., 2018; Nirrengarten et al., 2018). In addition, the need to account for Late Permian and Triassic related deformation and Western Tethys kinematics (Angrand et al., 2020; Angrand and Mouthereau, 2021), and reconstruction techniques using pre-defined strike-slip corridors (Frasca et al., 2021) have also been highlighted in recent plate kinematic studies of Iberia. However, despite the recent availability of software to create deformable plate tectonic models, all known plate reconstructions of Iberia have been conducted using rigid plate modelling approaches.

Thus, investigating the plate kinematics of Iberia and surrounding continental blocks using a deformable plate modelling approach is deemed to be a promising avenue for assessing previously published rigid plate models, their consequences, and the deformation experienced throughout Iberia's continental domains.

2.2 Constrained 3-D Gravity Inversion using GRAV3D

Geophysical inversion is a non-unique, and iterative process implemented by geoscientists to estimate models of physical property distributions based upon data collected from a geophysical survey. Due to the non-uniqueness associated with inversion, there will always be numerous valid solutions that can minimize a model objective function and achieve the desired tolerance with respect to a given data misfit criterion.

3-D gravity inversion is commonly used to investigate the present-day crustal structure of tectonic regimes (Welford and Hall, 2007; Alvey et al., 2008; Welford et al., 2010, 2012, 2018; Kusznir et al., 2020). In this thesis, crustal thickness estimates that were previously published along the Newfoundland and Irish continental margins (Welford et al., 2007, 2010, 2012) and newly presented in this thesis along the West Iberian margin and Bay of Biscay (Chapters 3 and 4, respectively) are calculated by inverting satellite altimetry free-air gravity data (Anderson et al. 2008; Sandwell et al., 2014) using the GRAV3D minimum-structure inversion algorithm (Li and Oldenburg, 1996, 1998). Due to the fact that offshore continental margins are below sea level and often host thick sedimentary basins, it is critical to build a constrained 3-D reference density model prior to inverting gravity data acquired within these regions so that variations in water depth, sediment thickness, and depth-dependent density trends can be accounted for. Using GRAV3D, 3-

D reference density models are discretized into rectangular prisms that can be assigned different sizes, reference densities and allowable density ranges, and depth-weighting parameters that aim to counteract the natural decay of density anomalies from the surface due to gravity data having no inherent depth resolution. Identical to that implemented in Welford et al., 2010, the reference density anomaly models in this thesis (relative to a background density of 2850 kg/m^3) are designed using a mesh depth of 35 km and rectangular prisms that span 5 x 5 km laterally and 500 m deep. Previously published compilations of publicly available bathymetric data (ETOPO1 1 arc-minute global relief model) and depth to basement estimates from the NOAA (Divins, 2003) are used to constrain the depth of the water and sedimentary columns, respectively. Furthermore, identical to the setup presented in Welford et al., 2010, the reference density models used in this thesis implement allowable density ranges (delimited by bounds) relative to a background reference density (2850 kg/m^3) for seawater (-1820 kg/m^3), the sediments (-1180 kg/m^3 to -130 kg/m^3), and the crust and mantle (-410 kg/m^3 to 520 kg/m^3). Once a specified target misfit is calculated between the observed and predicted gravity data, the gravity inversion algorithm converges and provides a 3-D relative density model that can be used to extract a density iso-surface interpreted to represent the Moho (corresponding to a relative density contrast of 170 kg/m^3). Subsequently, the depth to basement estimates are then subtracted from the inverted Moho depth estimates to obtain estimates of crustal thickness.

It should be emphasized that crustal thickness estimates calculated via 3-D gravity inversion are highly sensitive to the quality of the inversion inputs such as the sampling of data points, and resolution of gravity data and depth to basement estimates. The lack of higher resolution and more densely sampled offshore open-access datasets available throughout the North

Atlantic Ocean (e.g., shipboard gravity data and densely spaced seismic profiles) was the primary reason why satellite free-air gravity data and global compilations of depth to basement and bathymetry estimates were used as inputs to calculate the crustal thickness estimates presented in this thesis. However, as higher resolution gravity inversion input datasets become more increasingly available, future work should focus on re-assessing the crustal thickness estimates that are heavily used in this thesis.

Chapter 3

3 Investigating the role of the Galicia Bank on the formation of the North West Iberian margin using deformable plate tectonic models

The majority of this chapter also appears in its published version *"King, M.T., Welford, J.K., Peace, A.L., 2020. Investigating the role of the Galicia Bank on the formation of the North West Iberian margin using deformable plate tectonic models. Tectonophysics 789, 228537. https://doi.org/10.1016/j.tecto.2020.228537"*.

3.1 Introduction

The West Iberian margin is one of the best studied non-volcanic (magma-poor) passive margins in the world and continues to draw attention due to its role in the rifting and subsequent opening of the southern North Atlantic (e.g., Alves et al., 2009; Pereira and Alves, 2011, 2012; Barnett-Moore et al., 2016; Alves and Cunha, 2018; Nirrengarten et al., 2018). Hosting several sedimentary basins (Figure 1.4), the West Iberian margin continues to be a subject of interest due to its frequent comparisons with the conjugate southeastern Newfoundland margin where

hydrocarbon exploration and production have been ongoing for several decades (Enachescu et al., 2010; Alves et al., 2014; Alves and Cunha, 2018).

Although the specific timing and style of rifting of the West Iberian margin have been debated (Wilson et al., 1989; Srivastava et al., 2000; Pereira and Alves, 2012), the deformation history is primarily controlled by two main rift phases: 1) Late Triassic to Early Jurassic and 2) Late Jurassic to Early Cretaceous (Alves and Cunha, 2018). In addition to these main rifting events, other geological phenomena such as the motion of continental ribbons, magmatic events, and rejuvenation of inherited structures all add to the complexity of rift systems and thus the interpretations drawn from regional seismic, potential field, and well data (Péron-Pinvidic and Manatschal, 2010; Nirrengarten et al., 2018; Peace et al., 2019b).

In this study, deformable plate tectonic models are created using the open source GPlates software (Williams et al., 2012; Matthews et al., 2016; Gurnis et al., 2018; Müller et al., 2018), version 2.2, and previously published constraints (Barnett-Moore et al., 2018; Nirrengarten et al., 2018; Welford et al., 2018; Peace et al., 2019b) to investigate the deformation history of the West Iberian margin and the importance of continental ribbons and inherited structures for this margin. The kinematic evolution and crustal thicknesses calculated from each plate model are compared to independent observations made from gravity inversion, and previous interpretations of regional seismic and well data across the margin. The aim of this approach is to investigate the role of the Galicia Bank during the formation of the North West Iberian margin, the extent and timing of deformation, and the importance of inherited Variscan structures during rifting.

3.2 Methodology

Following the methodology described in Chapter 2 (Figure 2.2), the deformable plate tectonic models presented in this chapter, built using GPlates 2.2 (Williams et al., 2012; Gurnis et al., 2018; Müller et al., 2018), were used to analyze the present day crustal architecture of the West Iberian margin and its evolution throughout geological time. Using this deformable plate modelling approach, several models were tested to analyze strain rates throughout geological time and recover present day crustal thickness estimates within regions of deformation surrounded by rigid plates. The primary objectives of this approach were to investigate the impact of the Galicia Bank and its independent movement on the North West Iberian Margin using various continental ribbon polygons and poles of rotation, to make comparisons with present day results based on seismic and potential field studies, and to evaluate the timing and connectivity of basins throughout the Mesozoic, prior to the breakup of Pangaea.

3.2.1 General model setup

In this study, a series of models were constructed that incorporate different polygon geometries representing candidate crustal configurations as well as various poles of rotation for the Galicia Bank to analyze its interplay with other continental ribbons and deformable boundaries defined in Peace et al. (2019b). The time frame considered for all deformable models is from 200 Ma to present day (0 Ma) with a starting uniform crustal thickness of 30 km at 200 Ma, despite a uniform crustal thickness being extremely unlikely. This assumption was made in view of the southern North Atlantic as a whole prior to the onset of Triassic rifting, with an initial crustal thickness value within the range of original values provided by previous studies for the West

Iberian margin, Grand Banks, and Flemish Cap (Van Avendonk et al., 2009; Welford et al., 2012; Mohn et al., 2015). The mesh points used to calculate crustal thicknesses and beta factors were generated using a 1.15625˚ spacing (GPlates density level 8) with no random offset.

To assess the validity of present day crustal thicknesses produced from deformable plate models, gravity inversion is a common method of comparison as it can be used to calculate present day crustal thicknesses similar to those computed in GPlates (Peace et al., 2019b). Crustal thickness calculated from gravity inversion was the primary method of comparison in this study. This is due to the inputs of gravity inversion used to calculate present day crustal thickness being much closer to reality in comparison to the inputs and assumptions made when producing deformable models in GPlates. Thus, to assess the results produced from deformable models created in this study, crustal thickness calculated by gravity inversion is deemed to be the most accurate representation of the West Iberian margin crustal structure in conjunction with interpretations made from previous seismic studies and well data (Boillot and Winterer, 1988; Murillas et al., 1990; Pérez-Gussinyé et al., 2003; Reston, 2005; Clark et al., 2007; Druet et al., 2018; Lymer et al., 2019).

3.2.2 Micro-continental blocks and ribbons: Defining the Galicia Bank

The kinematic role of relatively undeformed continental ribbons in the southern North Atlantic has been highlighted in several recent studies (Péron-Pinvidic and Manatschal, 2010; Nirrengarten et al., 2018; Peace et al., 2019b). Peace et al. (2019b) showed that the motions of the Flemish Cap, Orphan Knoll, Porcupine Bank, and Rockall-Hatton Bank were important in controlling resultant (present day) crustal structures via deformable plate modelling that are

comparable with the present day crustal architecture of rifted margins characterized through geophysical and geological observations. Along the West Iberian margin, the Galicia Bank is a continental ribbon (Péron-Pinvidic and Manatschal, 2010) considered to have played an important role during rifting and formation of the northern margin, yet it has not been included in any previous deformable reconstruction studies as an independent entity (Sibuet et al., 2007; Peace et al., 2019b).

To define a polygon for the boundary to a relatively undeformed unit comprising the Galicia Bank, gravity inversion was performed using the same approach as described in Welford et al. (2012) to calculate crustal thickness values over the West Iberian margin. Free-air gravity data from satellite altimetry were obtained from the Scripps Institution of Oceanography (Sandwell et al., 2014) and inverted to obtain a smoothed depth-weighted 3-D density model using the GRAV3D inversion algorithm (Li and Oldenburg, 1996, 1998). Bathymetric and depth to basement constraints, obtained from the ETOPO1 1 arc-minute global relief model and the NOAA total sediment thickness of the world's oceans and marginal seas data (Divins, 2003), were used to construct a reference density anomaly model (relative to 2850 kg/m^3) and to prescribe the allowable density ranges (delimited by bounds) for seawater, the sediments, the crust and the mantle. For a more detailed description of the inversion method, including the parameters chosen, see Welford et al. (2012).

For the majority of plate models in this study, two different polygons were interpreted and tested to define the crustal architecture of the Galicia Bank (Figure 3.1b, c). The smaller polygon (Figure 3.1b) was designed to represent the area of highest crustal thicknesses observed from the gravity inversion results. The larger polygon (Figure 3.1c) was created to capture the interpreted

overall architecture of the Galicia Bank including its deformed edges. The average crustal thickness for the Galicia Bank from the gravity inversion results is approximately 20 km. It is surrounded by areas of segmented thinned crust (<10 km) to the east within the Galicia Interior Basin and a continuous band of hyperextended crust along its western edge. The two additional geometries tested for the Galicia Bank, not shown in Figure 3.1, were designed primarily based on plate modelling constraints and model motivation. However, the geometry of the Galicia Bank used in these two models was also designed to have a similar crustal thickness and architecture to those described in Figure 3.1, but slightly altered to comply with the motivation of each model.

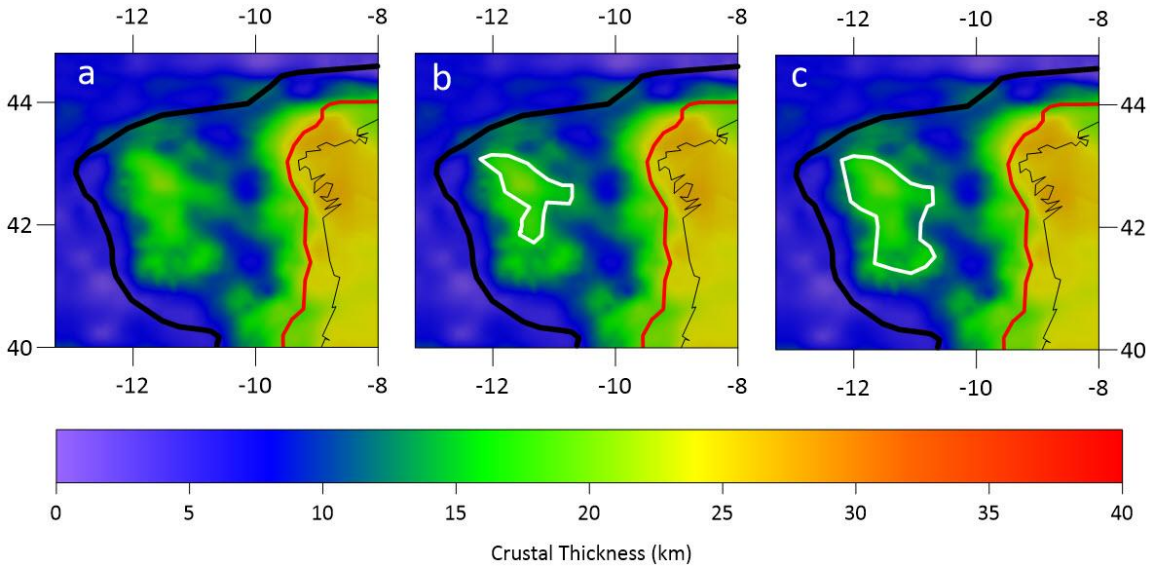

Figure 3.1 Gravity inversion crustal thickness results for the North West Iberian margin and interpreted Galicia Bank polygons. a) Crustal thickness with the necking line (red boundary) and ECC (black boundary) from Nirrengarten et al. (2018). b) Same as in (a) but with the model 2 Galicia Bank polygon outlined in white. c) Same as in (a) but with the model 3 Galicia Bank polygon outlined in white.

3.2.3 Incorporating inherited structures

The role of inherited structures during the formation of rifted margins has and continues to be a topic of scientific discussion and research (Peace et al., 2018; Phillips et al., 2019; Schiffer et al., 2019). For the West Iberian margin, inherited structures interpreted to have influenced Mesozoic rifting primarily consist of NE-SW trending Variscan transfer faults (Murillas et al., 1990). In previous deformable plate modelling studies using GPlates (Welford et al., 2018; Peace et al., 2019b), the difficulty of accounting for rift obliquity induced by inherited structures has been demonstrated through comparison of crustal thicknesses calculated by gravity inversion and deformable plate models. Due to the widespread presence of inherited structures along the West Iberian margin, particularly within the Galicia Interior Basin (Murillas et al., 1990), an attempt was made to try and incorporate inherited structures into deformable models.

In GPlates, various features with established plate IDs, such as polygons to define the geometry of continental ribbons, or simpler features such as individual lines or points, can be added into regions of deformation. To account for the styles of deformation experienced within regions of inherited structures during deformation, specific models in this study include traces of Variscan transfer faults within the Galicia Interior Basin (Figure 3.2b). Only two of the NE-SW transfer faults (Figure 3.2b) were tested in this study to avoid excessive model complexity and the potential for unpredictable results in GPlates crustal thickness calculations. These two faults (Figure 3.2b) were chosen based on their position within the center of the Galicia Interior Basin and their interpreted larger impact on the present day crustal architecture in this region. By adding these additional topological network boundaries within the interior of a deformable mesh, the

discretization of the triangular mesh was altered within regions of inherited structures. This localized change in the discretization is caused by the additional nodes being incorporated within the triangular mesh (Figure 3.2c). This proposed methodology was then used to test how deformation varied within regions of inherited structures versus models where these internal topological network boundaries were not included. This analysis primarily consisted of examining temporal variations in strain rate style (Kreemer et al., 2014), a calculation made within GPlates that can quantify the nature of tectonic stresses (e.g., rift, strike-slip, or compressional-related) and their variations with time within a topological network, and comparison of crustal thicknesses calculated from deformable plate models and gravity inversion.

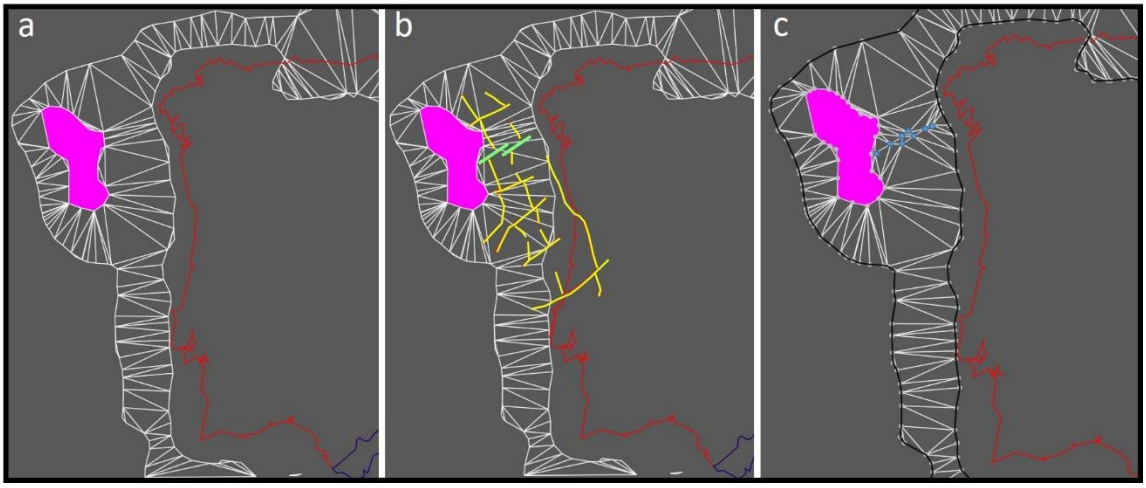

Figure 3.2 West Iberian margin topological network for the region of deformation at 0 Ma with coastlines (red).Region of deformation around the rigid Galicia Bank (pink polygon) shown within a triangular mesh. b) Same as (a) but with the major fault traces of the Galicia Interior Basin from Murillas et al. (1990) shown in yellow within the mesh. Faults highlighted in green represent transfer faults to be added into the interior of the mesh as topological network boundaries. c) New

discretized mesh in the region of the transfer faults highlighted in (b) as a result of the new nodes (blue dots) introduced into the region of deformation.

3.2.4 Poles of rotation

Poles of rotation defined in GPlates are used to govern the movement and position of tectonic plates and other features throughout geological time (Williams et al., 2012). In the deformable plate modelling workflow, poles of rotation control the amount of deformation experienced within a topological network (Gurnis et al., 2018). This is because the displacement and velocity of each tectonic plate and geological feature included along the boundaries or within the interior of a deformable mesh are controlled by poles of rotation (Gurnis et al., 2018). The poles of rotation used for this study are the poles from model 6c created by Peace et al. (2019b). The study by Peace et al. (2019b) introduced new poles of rotation based upon the poles of rotation from Nirrengarten et al. (2018) and updated the kinematics and geometries of the Flemish Cap, Orphan Knoll, Porcupine Bank, and Rockall-Hatton Bank, to provide a reasonable correlation between deformable modelling results and present day geophysical and geological observations.

However, in the study by Peace et al. (2019b), the Galicia Bank is not included as an independent plate so there are no poles of rotation provided for this feature. Thus new poles of rotation were created in this study to investigate its independent kinematic evolution. Previously published poles of rotation for the Galicia Bank are based on the J-magnetic anomaly being interpreted as an isochron at breakup (Sibuet et al., 2012). This interpretation is not consistent with the poles of rotation generated by Nirrengarten et al. (2018) as it was concluded by Nirrengarten

et al. (2017) that the J-anomaly should not be used for plate kinematic studies as it is interpreted to result from multiple and polygenic magmatic events. Thus, to address this disagreement, several poles of rotation for the Galicia Bank were tested in this study. For each model presented, although the possibility of the Flemish Cap and Galicia Bank representing one continental ribbon at 200 Ma is acknowledged, the Galicia Bank poles of rotation were designed such that the Galicia Bank does not overlap with the Flemish Cap for the entirety of each model's kinematic evolution. This is primarily due to the uncertainties associated with overlapping continental ribbons in GPlates causing mesh points to escape topological networks when calculating temporal variations in measurements such as crustal thicknesses.

3.2.5 Model specifics

For models 1-9 (Figure 3.3), each model uses the same deformable boundaries implemented in Peace et al. (2019b), with the edge of the continental crust (ECC) and necking line from Nirrengarten et al. (2018) representing the exterior and interior deformable boundaries, respectively. The primary differences between each of the tested models are the geometry and kinematics of the Galicia Bank (Table 3.1 - poles of rotation in supplementary material).

Model	Galicia Bank (GB) Included	GB Geometry	GB Starting Positon	Inherited Structures Included	GB Poles of Rotation	GB Jurassic Displacement
1	No	N/A	N/A	No	N/A	N/A
2	Yes	Small	Standard	No	Model 2	0 km
3	Yes	Large	Standard	No	Model 2	0 km

4	Yes	Small	North	No	Model 4	45 km SE
5	Yes	Alternative Small	West of Goban Spur	No	Model 5	160 km S
6	Yes	Large	South	No	Model 6	70 km NW
7	Yes	Large	NW corner connected with Flemish Cap	No	Model 7	40 km SE
8a	Yes	Large	NW corner connected with Flemish Cap	No	Model 8	130 km S
8b	Yes	Large	NW corner connected with Flemish Cap	Yes	Model 8	130 km S
9	Yes	Alternative Large	SE Flemish Cap	No	Model 9	25 km E

Table 3.1 Description of components tested in models 1-9. Galicia Bank Jurassic (200-140 Ma) displacement relative to Iberia measured using a motion path anchored on the NW corner of the Galicia Bank for all models.

Model 1, identical to model 6c from Peace et al. (2019b), is used to demonstrate the result of not including the Galicia Bank into a deformable model of the southern North Atlantic. Models 2 and 3 are the initial attempts at placing the Galicia Bank into the region of deformation with identical poles of rotation but with a smaller and a larger polygon for the Galicia Bank, respectively (Figure 3.1). Model 4 is similar to model 2 with the main difference being a further northward starting position for the Galicia Bank. Model 5 is one of two models with a different polygon geometry for the Galicia Bank, not shown in Figure 3.1. The motivation for this particular model

was to simulate a starting point for the Galicia Bank close to the position of the Goban Spur at 200 Ma with progressive southward movement of the Galicia Bank with respect to the Goban Spur. Due to the progressive rifting and rotation of the Flemish Cap away from the Central Orphan Basin (Sibuet et al., 2007), the model 5 Galicia Bank had to be made smaller compared to models 2 and 3 in order for the Galicia Bank to fit within the region of deformation between the Flemish Cap and Iberian margin necking lines, thus avoiding overlap with the Flemish Cap. Models 6, 7, 8a, and 8b all use the model 3 Galicia Bank polygon (Figure 3.1c) but test different starting points, rotations, and directions of movement for the Galicia Bank, primarily during Jurassic and Early Cretaceous time. The only difference between models 8a and 8b (poles of rotation shown in Table 3.2) was that model 8b included a discretized deformable mesh within the region of inherited structures in the Galicia Interior Basin (Figure 3.2). The motivation for model 8b was to examine whether the role of inherited structures during rifting within the Galicia Interior Basin could be observed using the GPlates deformable modelling methodology, primarily in contrast to results produced by model 8a. Model 9 (poles of rotation shown in Table 3.2) is the second model which uses a smaller Galicia Bank polygon, not previously shown in Figure 3.1. The motivation behind this model was to test the possibility of the southeastern Flemish Cap and Galicia Bank being connected until the two individual continental ribbons separated during the most significant phase of extensional deformation experienced between the Newfoundland and West Iberian margins initiating approximately 140 Ma, as suggested by previous studies (Sibuet et al., 2007).

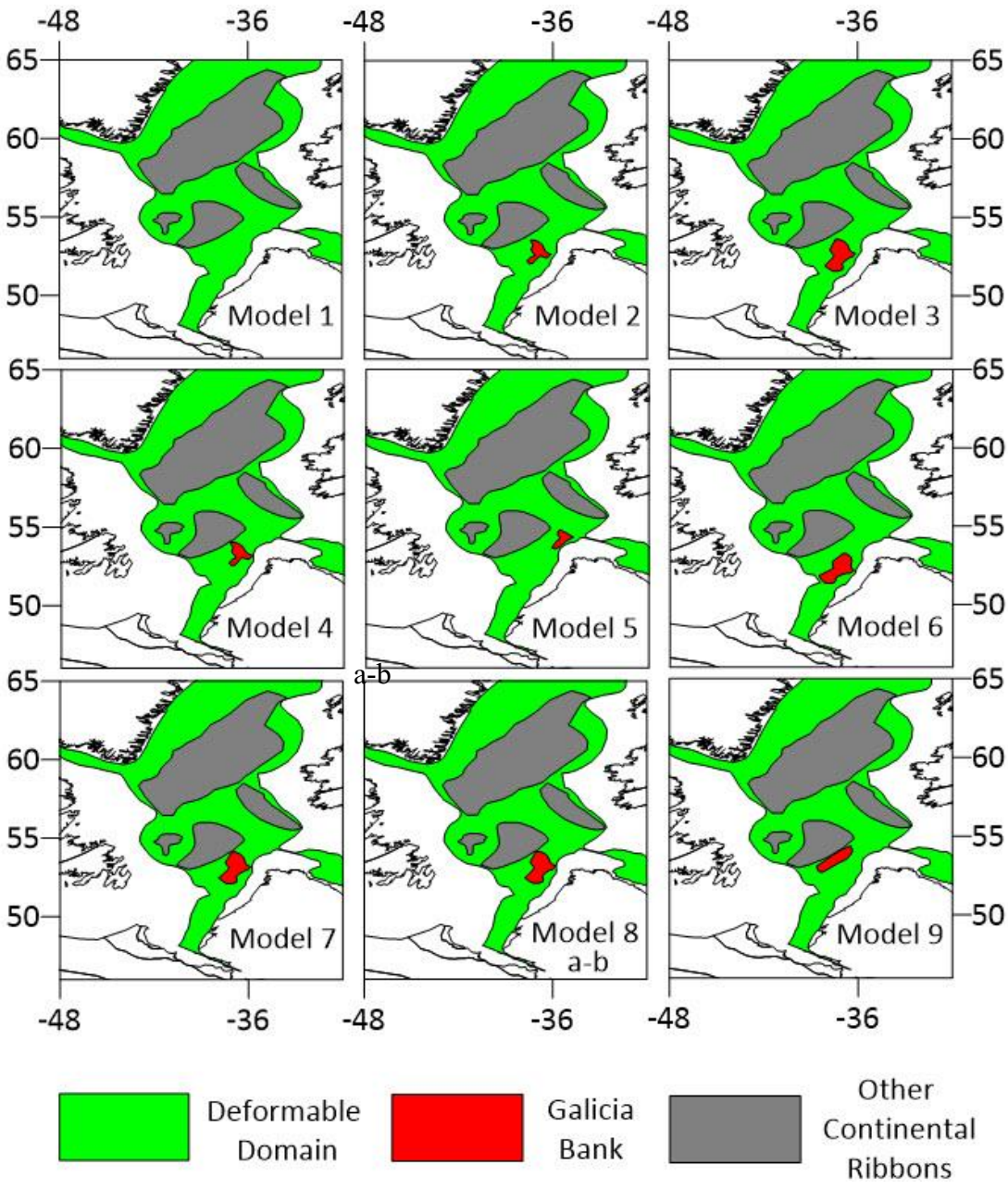

Figure 3.3 Initial setup for deformable plate models 1-9 at 200 Ma. Deformable domains represented in green, Galicia Bank in red, and other rigid continental ribbons in grey.

Model	Age	Latitude	Longitude	Angle	Fixed Plate
8a and 8b	0	0	0	0	Iberia
	112	0	0	0	Iberia
	141	23.2378	-35.7177	-3.2274	Iberia
	150	27.2124	-25.3069	-3.9459	Iberia
	162	20.9253	-21.3293	-3.041	Iberia
	173	25.347	-16.3297	-3.5748	Iberia
	179	26.995	-14.9114	-3.8864	Iberia
	189	29.6659	-11.6141	-4.4054	Iberia
	200	31.5966	-10.1489	-4.9977	Iberia
9	0	0	0	0	Iberia
	112	0	0	0	Iberia
	140	41.2659	-10.5789	-34.6767	Iberia
	142	41.2962	-10.5166	-35.2835	Iberia
	152	41.2853	-10.5897	-34.0636	Iberia
	162	41.2901	-10.4604	-34.7319	Iberia
	171	41.3473	-10.3302	-33.9604	Iberia
	181	41.2804	-10.2235	-30.5201	Iberia
	191	41.4223	-10.1264	-30.0468	Iberia
	200	41.5918	-10.2833	-30.8599	Iberia

Table 3.2 Poles of rotation used to create models 8a, 8b, and 9. All other poles are identical to Peace et al. (2019b). In all models, the Galicia Bank is moving with respect to Iberia (poles of

rotation from Nirrengarten et al. (2018)). Poles of rotation for the Galicia Bank used in models 1-7 are included in Appendix A.

3.3 Results

3.3.1 Kinematic evolution and resulting crustal thicknesses

Analysis of present day crustal thicknesses derived using deformable models 1-9 (Figure 3.4) demonstrate that variations in the initial geometry and poles of rotation for the Galicia Bank have a significant impact on the resultant present day crustal architecture of the West Iberian margin. For the southern portion of the West Iberian margin, differences in the calculated crustal thicknesses between model iterations are negligible and do not differ from Peace et al. (2019b). The most notable variations occur to the north within the Galicia Interior Basin, within northern parts of the Peniche Basin, and oceanward of the Galicia Bank.

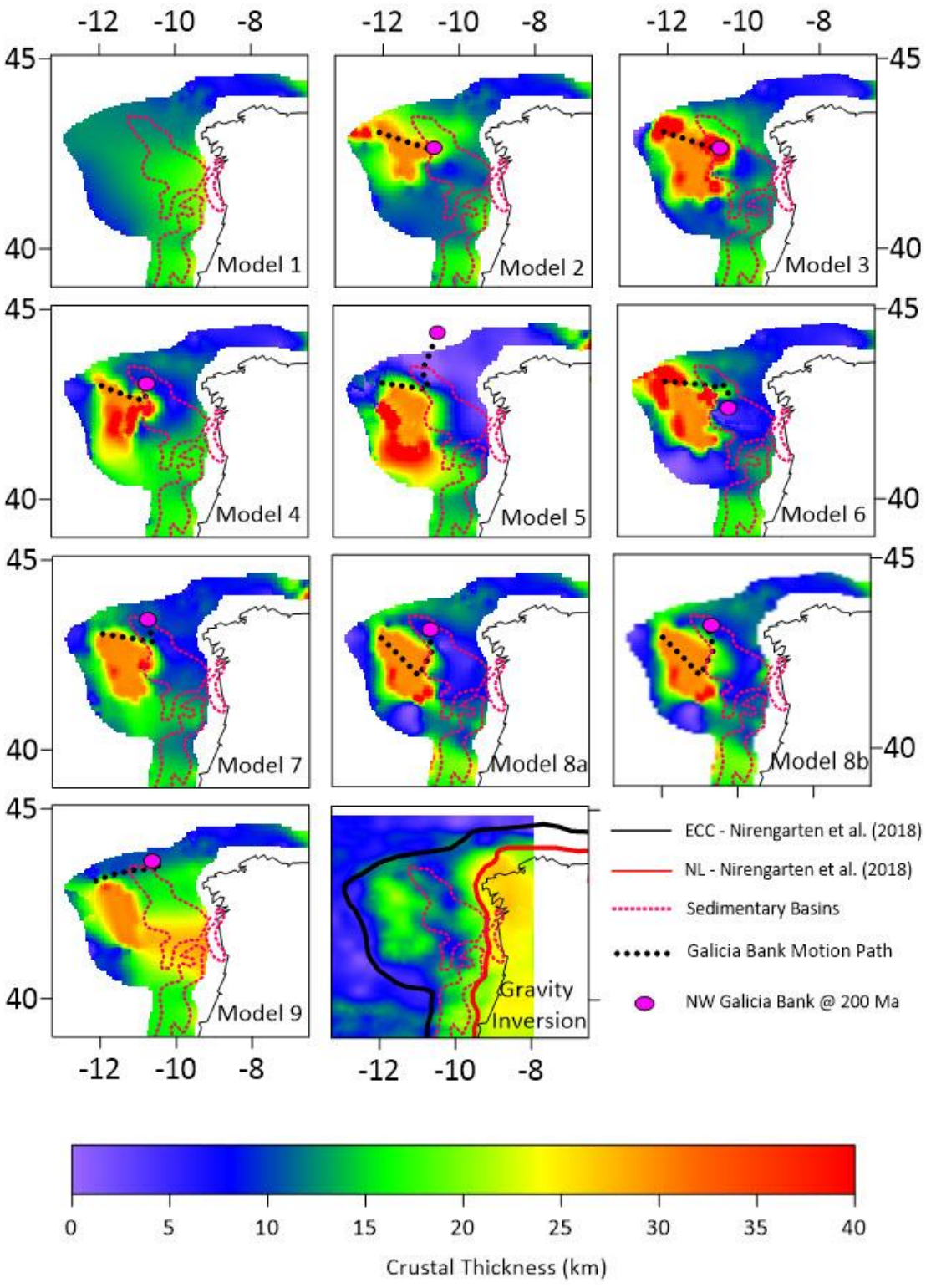
-12
-10
-8
45
40
Model 1
Model 2
Model 3
Model 4
Model 5
Model 6
Model 7
Model 8a
Model 8b
Model 9
Gravity Inversion
ECC - Nirengarten et al. (2018)
NL - Nirengarten et al. (2018)
Sedimentary Basins
Galicia Bank Motion Path
NW Galicia Bank @ 200 Ma
0
5
10
15
20
25
30
35
40
Crustal Thickness (km)

Figure 3.4 Present day (0 Ma) crustal thickness results for deformable plate models of the West Iberian margin for models 1-9. Starting points of the Galicia Bank at 200 Ma (pink circles) and Galicia Bank motion paths (black circles) for each model are relative to Iberia. Black and red boundaries displayed on gravity inversion crustal thickness map are the edge of continental crust (ECC), and the necking line (NL) from Nirrengarten et al. (2018), respectively. Iberia sedimentary basins (pink dashed lines) are the Galicia Interior Basin, Peniche Basin, and Porto Basin (referenced in Figure 1.2).

The results from model 1, which used inputs from model 6c from Peace et al. (2019b), is the only model that does not include the Galicia Bank. In model 1, crustal thicknesses within the Galicia Interior Basin and surrounding areas vary from approximately 15-20 km with thinner regions of crust to the north bordering the Bay of Biscay and the western region bordering the edge of continental crust (ECC).

Models 2 and 3 demonstrate the effect of using different sized polygons for the Galicia Bank and the resulting deformation within its vicinity. In comparison to crustal thicknesses calculated by gravity inversion, models 2 and 3 also highlight the importance of the Galicia Bank through the improved crustal thicknesses within the Galicia Interior Basin in comparison to model 1. Present day crustal thicknesses in models 2 and 3 are similar for the Galicia Interior Basin region, ranging from 7-10 km. The most notable differences between these two models are the regions of thicker crust observed in model 3 as a result of a larger Galicia Bank polygon.

Model 4 uses the same Galicia Bank polygon as model 2 but with a different starting point and thus altered poles of rotation. The motion of the Galicia Bank in model 4 has a general

southward movement and slight clockwise rotation with respect to the Flemish Cap during Late Jurassic time in contrast to models 2 and 3 where the starting and end positions of the Galicia Bank are much closer together. As a result, this change in kinematics produced different crustal thicknesses within the Galicia Interior Basin in comparison with models 2 and 3. The most notable difference is a region of thinner crust ranging from 5-10 km thick within the northern region of the Galicia Interior Basin and thicker areas of crust ranging from 15-20 km within the southern parts of the basin.

The close starting position of the Galicia Bank to the Goban Spur tested in model 5 results in significant crustal thinning within the northern Galicia Interior Basin in comparison with results from models 2-4. In model 5, the Galicia Bank underwent a significant amount of southward motion from Jurassic to Early Cretaceous time. This large amount of southward motion prior to breakup results in regions of continental crust approximately 20-40 km thick in the southern portions of the Galicia Interior Basin that are unrealistic with respect to present day observations.

The southernmost starting point of the Galicia Bank is tested in model 6. This model simulates a gradual northward propagation and counter-clockwise rotation of the Galicia Bank until early Aptian time which results in more widespread crustal thinning compared to the models previously discussed. The region of thinnest crust occurs in the southern part of the Galicia Bank, with crust less than 5 km thick. In the Galicia Interior Basin, thinning is most significant within the central part of the basin with crustal thicknesses ranging from 5-10 km thick, and thicker areas to the north ranging from 10-15 km. In the northwestern corner of the Galicia Bank, crustal thicknesses are quite high, about 40 km thick, near the ECC deformable boundary. This is interpreted to result from non-deformable boundary edge effects and interaction with the Flemish

Cap prior to separation of the Newfoundland and Iberian margins, or compression that may have potentially been distributed across the Galicia Bank if the initial model setup had allowed deformation within continental ribbons.

Models 7, 8a, and 8b share the same starting position of the Galicia Bank at 200 Ma but the longer southward distance travelled by the Galicia Bank in models 8a and 8b is the main reason for their varying amounts of deformation, primarily observed within the southern parts of the Galicia Interior Basin. This is due to the Galicia Bank travelling ~ 130 km south from the Flemish Cap (Figure 3.6) until 140 Ma when it begins to move northwest towards its present day position during the early Cretaceous rifting episode. In comparison with models 8a and 8b, model 7 only travels approximately 40 km southeast from the Flemish Cap until 140 Ma when it begins moving westward towards its present day position. In model 8a, the southward movement of the Galicia Bank into the northern parts of the Peniche Basin results in a more widespread thinned region covering the entirety of the Galicia Interior Basin with crustal thicknesses from 3-10 km. Model 8b produces similar results to those of 8a with the exception being a narrower and partially segmented thinned region within the Galicia Interior Basin. Both models 8a and 8b produce crustal thicknesses along the western edge of the Galicia Bank ranging from approximately 3-10 km and the most extensive thinning in the southern region of the Galicia Bank with crustal thicknesses of 2-5 km. These regions of thinner crust are not present in model 7 as the southern portions of the Galicia Interior Basin and Galicia Bank have calculated crustal thicknesses in the range of 15-20 km thick.

Model 9 is the only model which tested the possibility of the Galicia Bank being connected with the Flemish Cap until breakup. The present day crustal thicknesses, particularly within the

Galicia Interior Basin are much higher in comparison with the previous models discussed, ranging from approximately 15-30 km thick. These higher crustal thicknesses within the Galicia Interior Basin are a result of less deformation caused by the Galicia Bank movement in comparison to other models. In particular, the lack of crustal thinning caused by the Galicia Bank during the Late Jurassic and Early Cretaceous is due to the synchronous motion of the Galicia Bank with the southeastern Flemish Cap until breakup between the Newfoundland and Iberian margins during the Early to Mid-Cretaceous.

3.4 Discussion

3.4.1 Comparison of deformable plate modelling and gravity inversion

In this section the deformable plate modelling results described in section 3.31 are compared to estimates of crustal thickness from gravity inversion (Figure 3.4). The crustal thickness map from gravity inversion (Figure 3.4) presents several key features to be matched by the deformable plate modelling crustal thickness results (Figure 3.4). These features include the segmented regions of thinned crust (10 km or less) within the Galicia Interior Basin, significantly thinned crust to the west of the Galicia Bank (<10 km), and thinned crust (10 km or less) in the northern regions of the Galicia margin.

Starting with model 1, in contrast to all other models, this was the only model which did not include the Galicia Bank within the region of deformation. This resulted in crustal thicknesses ranging from 15-20 km within the Galicia Interior Basin, much higher than those suggested by gravity inversion. Models 2-5 and 9, show the largest discrepancies of models which include the Galicia Bank when making comparisons to crustal thicknesses calculated by gravity inversion.

Models 2-4 resulted in areas of higher crustal thickness within the Galicia Interior Basin, with a 5-15 km discrepancy compared to gravity inversion results. The rapid southward movement of the Galicia Bank in model 5 produced extensive thinning within the Galicia Interior Basin and significant thickening in the southern region of the Galicia Bank. Model 9 caused regions of thicker crust within the Galicia Interior Basin due to the Galicia Bank experiencing less independent motion during the Jurassic. Model 6 provided a closer match to crustal thicknesses suggested by gravity inversion due to the counter-clockwise rotation of the Galicia Bank, however, this also resulted in larger crustal thicknesses along the northern border of the Galicia Bank and areas of extensive thinning along its southern border. Similar to model 5, the degree of crustal thickening along the borders of the Galicia Bank in model 6 represent a large discrepancy in comparison to gravity inversion. However, due to the fact that continental ribbons and fragments are incapable of experiencing deformation in GPlates, these areas of crustal thickening could also be interpreted to represent crustal thickening that could have been distributed across the Galicia Bank if allowed in the initial model setup. Thus, if this phenomenon is considered, model 6 provides a good fit in comparison to crustal thicknesses calculated by gravity inversion throughout the North West Iberian margin. Model 7 also provided a closer match within northern regions of the Galicia Interior Basin but failed to produce the amount of thinning expected in the southern regions of the basin and Galicia Bank. Of all the models tested (Figure 3.4), the results from models 8a and 8b (Figure 2.6) provided the best crustal thickness match and will be discussed in greater detail.

For significantly thinned regions (crustal thicknesses less than 10 km) within the central part of the basin (Figure 3.6), crustal thicknesses from gravity inversion range from approximately 5-10 km and both models 8a and 8b show a similar degree of thinning within these areas, with the

exception of some localized regions with crustal thickness down to 2 km. In general, models that include a Late Jurassic and Early Cretaceous motion of the Galicia Bank toward the Galicia Interior Basin (such as models 6, 7, 8a, and 8b) produce results more akin to those observed present day in the gravity inversion estimates. In contrast, models that test minimal motion of the Galicia Bank with respect to the Flemish Cap during the Jurassic and Early Cretaceous (such as models 2, 3, and 9) do not produce crustal thickness estimates as low as those estimated from gravity inversion within the Galicia Interior Basin.

One of the main discrepancies between the gravity inversion results and those obtained from model 8a is the higher degree of thinning in the Galicia Interior Basin. In particular, the higher crustal thicknesses between the segmented thinned domains within the Galicia Interior Basin calculated by gravity inversion are replaced by areas of thinner crust in model 8a. In comparison, model 8b provides a closer match within this region as it produces a more segmented region of thinned crust within the Galicia Interior Basin as opposed to the wider thinned region shown in model 8a. Along the ocean ward edge of the Galicia Bank, models 8a and 8b provide a close match to the results obtained from gravity inversion with crustal thicknesses varying from approximately 3-8 km.

An initial crustal thickness of 30 km was assumed for all deformable plate models at 200 Ma. Crustal thicknesses within Variscan terranes along the West Iberian margin are considered to be larger than those predicted for the Newfoundland margin prior to Triassic rifting (Capdevila and Mougenot, 1988; Mohn et al., 2015). As a result, a thicker initial crustal thickness estimate, such as 34 km defined by Mohn et al. (2015), could explain the crustal thickness discrepancies

within the Galicia Interior Basin calculated by model 8a in comparison to crustal thicknesses calculated by gravity inversion.

The largest discrepancy between models 8a, 8b, and the gravity inversion results are the crustal thicknesses calculated for the Galicia Bank. The GPlates methodology does not allow deformation to take place within rigid continental fragments and ribbons, and thus the crustal thickness of continental fragments and ribbons is the same as the original crustal thickness defined throughout the entire region of deformation at 200 Ma. Due to this limitation, no deformation is experienced within the Galicia Bank in models 8a and 8b, resulting in a 10-15 km crustal thickness discrepancy for the Galicia Bank in comparison with the gravity inversion results. In addition, although the GPlates deformable modelling methodology does not allow overlapping continental fragments, the possibility of the Galicia Bank being connected to the Flemish Cap and undergoing internal deformation until breakup during the Late Jurassic to Early Cretaceous cannot be excluded. This is inferred by present day crustal thicknesses for the Galicia Bank calculated by gravity inversion being approximately 20 km, as compared to typical thicknesses of continental crust varying from 30-35 km. Thus, if the Galicia Bank is assumed to have an initial crustal thickness ranging from 30-35 km, it must have underwent some degree of crustal stretching and thinning during rifting and opening of the southern North Atlantic.

3.4.2 Comparison with regional seismic and well data

Here the plate kinematic evolution of model 8a (Figure 3.5) and model 9 (Figure 3.6) are described in comparison with the deformation history of the Northwest Iberian margin inferred from previous interpretations of regional seismic and well data (Boillot and Winterer, 1988;

Murillas et al., 1990; Pérez-Gussinyé et al., 2003; Reston, 2005; Lymer et al., 2019). For the deformable models shown in this work, the main feature driving the changes in deformation within the northern region of the West Iberian margin is the Galicia Bank and its Mesozoic kinematic history. Due to the poles of rotation for the Galicia Bank being identical for models 8a and 8b, models 8a and 9 will be described herein to focus on the motion of the Galicia Bank, its kinematic evolution, and the validity of these models in relation to interpretations made from regional seismic and well data.

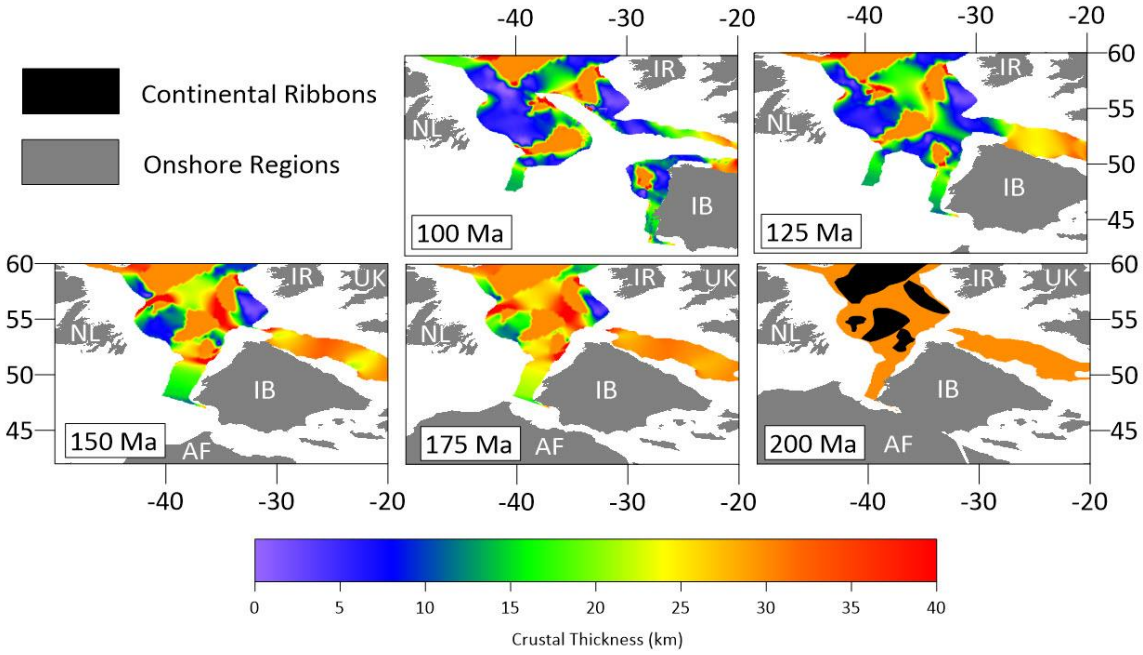

Figure 3.5 Crustal thickness evolution of model 8a at 25 Ma increments from 200 Ma to 100 Ma. AF = Africa, IB = Iberia, IR = Ireland, NL = Newfoundland, UK = United Kingdom.

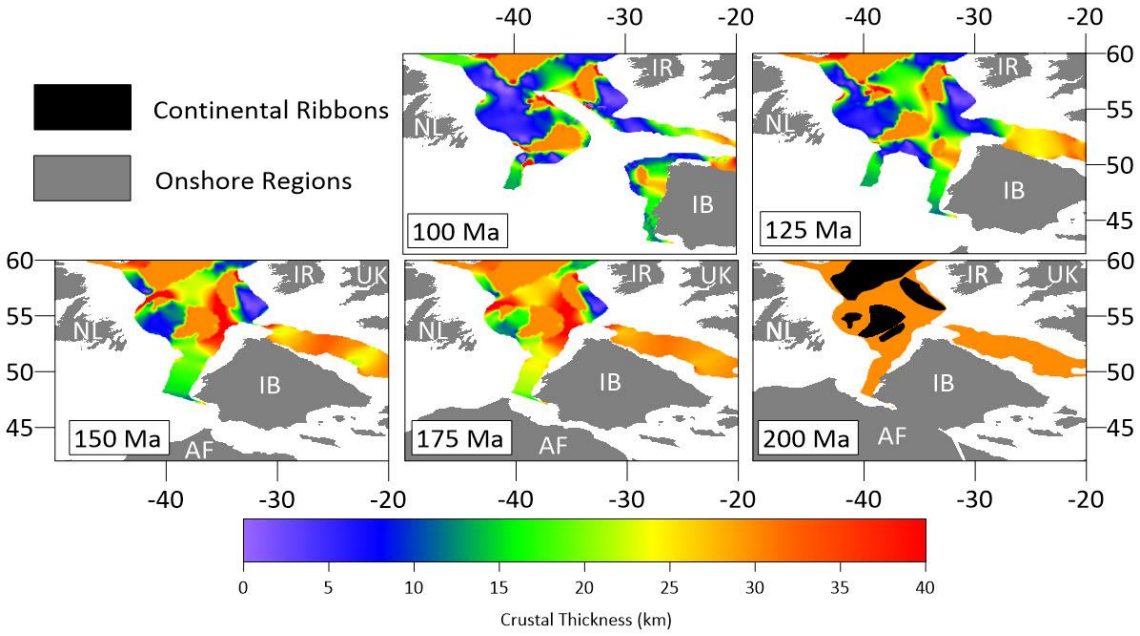

Figure 3.6 Crustal thickness evolution of model 9 at 25 Ma increments from 200 Ma to 100 Ma. AF = Africa, IB = Iberia, IR = Ireland, NL = Newfoundland, UK = United Kingdom.

Starting with model 9, this is a model that uses an alternative Galicia Bank geometry compared to those shown in Figure 3.4. The motivation for this model was to test the potential connection between the Galicia Bank and southeastern Flemish Cap prior to rift onset. This was done by simulating the Galicia Bank being attached to the southeastern Flemish Cap at 200 Ma, followed by synchronous motion of the Galicia Bank with the Flemish Cap until the initiation of breakup between the Newfoundland and Iberian margins, approximately 140 Ma. In contrast to model 8a, model 9 produced larger crustal thickness discrepancies (~10-15 km) within the Galicia Interior Basin in comparison with gravity inversion. However, aside from the discrepancies with gravity inversion, the kinematic evolution of model 9 is arguably more consistent with observations from regional seismic and well data within Northwest Iberia. Considering

interpretations of regional seismic data, hyperextension has not been documented within the Galicia Interior Basin in comparison to regions south and west of the Galicia Bank where hyperextended crust, indicative of Early Cretaceous rifting, and S reflections have been clearly imaged (Reston, 1996; Pérez-Gussinyé et al., 2003; Lymer et al., 2019). Correlating these observations with interpretations made from ODP/DSDP and exploration wells drilled throughout Northwest Iberia, minimal subsidence is frequently inferred based on Late Jurassic to Early Cretaceous shallow marine and continental sediments, in contrast to the southwest Iberian margin (Boillot and Winterer, 1988; Murillas et al., 1990; Alves and Cunha, 2018). These observations correlate with the Late Jurassic and Early Cretaceous Galicia Bank plate kinematics and resultant lack of Late Jurassic crustal thinning suggested by model 9 in contrast to model 8a within the Galicia Interior Basin.

The validity of model 8a is primarily based on its present day crustal thicknesses providing the closest match with gravity inversion (Figure 3.4). In model 8a at 200 Ma, the long axis of the Galicia Bank lies in a northeast-southwest orientation with its northwestern corner situated along side of the Flemish Cap. From 200 Ma until Oxfordian time (~160 Ma) in this model, the Galicia Bank moves south simultaneous with the clockwise rotation of the Flemish Cap. This relationship between the Flemish Cap and Galicia Bank, similar to that suggested in model 9, is in general agreement with previous regional seismic interpretations (Murillas et al., 1990), due to the interpretation of an overall tectonically quiet environment within the Galicia Interior Basin suggested by Lower-Middle Jurassic marine limestones interpreted on seismic sections and drilled within the Porto Basin (Murillas et al., 1990). From Oxfordian time until the breakup of the southeastern Newfoundland and Iberian margins (~140 Ma), thinning of the continental crust

occurs within the northern regions of the Galicia Interior Basin as the Galicia Bank moves towards Iberia in a southeastward direction. Based on the timing of deformation interpreted from seismic data at this time, an Oxfordian-Kimmeridgian extensional episode has been postulated within the Galicia Interior Basin (Murillas et al., 1990). This interpreted pre-Tithonian extensional event is evidenced by discontinuous and high-amplitude reflections within wedge-shaped sedimentary units (Murillas et al., 1990). Continental red beds interpreted from borehole data within the Porto Basin are also indicative of a local emersion event during the Late Jurassic and similar interpretations for the Galicia Interior Basin are supported based on submersible samples collected along the deep Galicia margin (Murillas et al., 1990). However, Late Jurassic thinning within the Galicia Interior Basin implied by model 8a contradicts some previously published interpretations that suggest a shallow marine depositional environment inferred by various wells drilled on structural highs along the Galician margin such as ODP wells 639, 901, and 1065 (Boillot et al., 1987; Clark et al., 2007). In addition, the amount of crustal thinning within the Galicia Interior Basin suggested by model 8a can not be reconciled by thinning estimated from observed faulting on seismic sections (Reston, 2005, 2009, 2010). However, this discrepancy could be attributed to poly-phase faulting causing any evidence of Late Jurassic rifting to be overprinted by later phases of rifting and thus being inadequately imaged on seismic sections (Reston, 2005). The amount of crustal thinning inferred by model 8a and gravity inversion are also consistent with numerical modelling beta factors ranging from approximately 3.5-5.5 in the center of the Galicia Interior Basin (Pérez-Gussinyé et al., 2003). At the initiation of breakup in model 8a, the Galicia Bank moves westward, coinciding with the initiation of the most extensive deformation experienced within the Galicia Interior Basin until Aptian-Albian time (~110 Ma). The timing of this extensive

rifting episode is well documented by both regional seismic and well data interpretations and corresponds to clastic syn-deposition and faulting recorded during a Berriasian-Valanginian extensional event within the Galicia Interior Basin (Murillas et al., 1990).

In summary, models 8a and 9 can both be considered valid based on their comparisons with regional independent observations. Model 8a provided a better match with gravity inversion crustal thickness, however, the plate kinematics and timing of deformation implied by model 9 are in better agreement with interpretations frequently made from regional seismic and well data throughout the Galicia margin.

3.4.3 Assessing discrepancies within the Galicia Interior Basin

The main discrepancy between model 8a and gravity inversion crustal thickness is the larger area of thinned crust in model 8a compared to the more segmented regions of significantly thinned crust in the gravity inversion results. When comparing these present day results with the major fault patterns along the North West Iberian margin (Figure 3.7), a correlation can be seen between the occurrence of inherited Variscan transfer faults interpreted within the Galicia Interior Basin and the segmented regions of significantly thinned crust. Within the Galicia Interior Basin, areas with SW-NE oriented transfer faults interpreted by Murillas et al. (1990) correspond closely to the crustal thickness discrepancies observed when comparing the gravity inversion and model 8a results (Figure 3.7). The attempt to accommodate the effect of inherited structures within the deformable mesh for the Galicia Interior Basin in model 8b provides a closer match to gravity inversion crustal thicknesses (Figure 3.7).

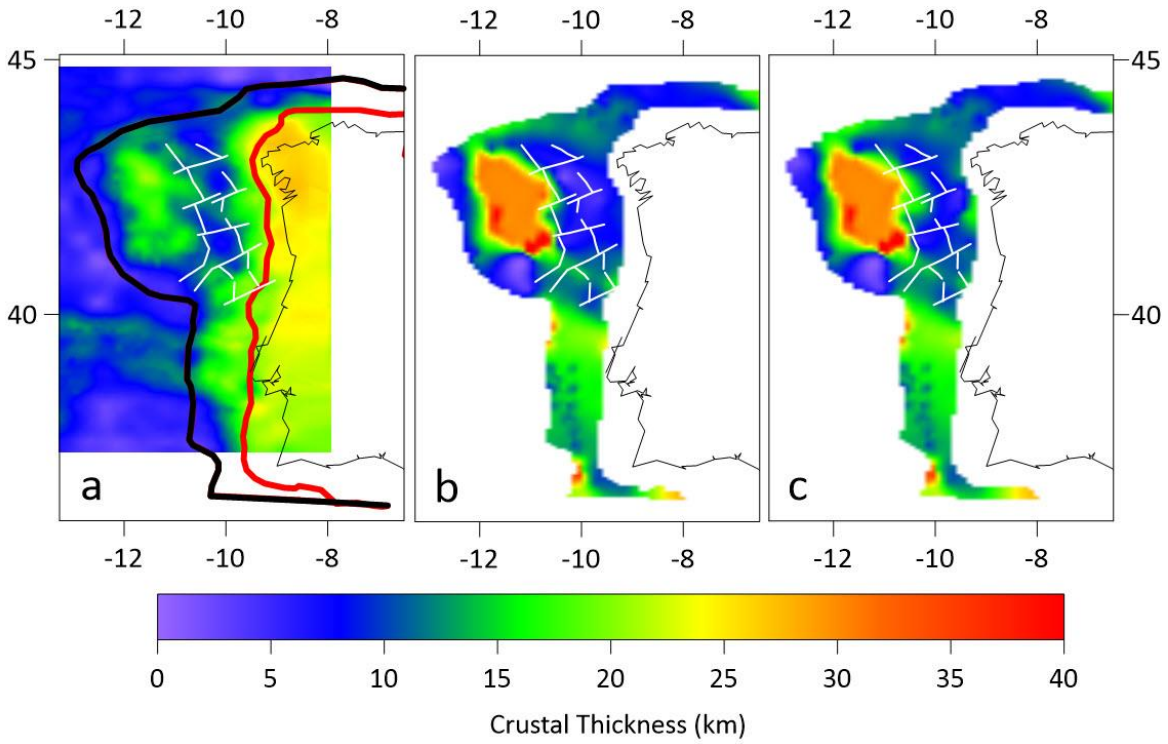

Figure 3.7 Crustal thicknesses calculated from a) gravity inversion, b) model 8a, and c) model 8b with major basin bounding faults (white) overlaid from Murillas et al. (1990). Black and red boundaries displayed on the gravity inversion crustal thickness map are the edge of continental crust (ECC), and the necking line (NL) from Nirrengarten et al. (2018), respectively.

Comparing the styles of rifting for model 8a and model 8b, the main difference driving the more realistic crustal thicknesses calculated by model 8b (Figure 3.7), involves localized transpressional events within the region of inherited structures during the Early Cretaceous rifting episode within the Galicia Interior Basin. Although interpretations made from regional seismic sections have only documented Late Cretaceous and Tertiary structures indicative of compressional events within the Galicia Interior Basin and surrounding areas (Murillas et al., 1990; Druet et al., 2018), seismic interpretation studies elsewhere (Peace et al., 2018) have demonstrated

the potential for transpressional events at rift-transform intersections, with several such comparable intersections identified within the basin. In addition, the obliquity of these inherited structures to the Early Cretaceous extension direction within the Galicia Interior Basin is deemed to be an important contributor to the segmented rift pattern as demonstrated in previous studies (Heron et al., 2019; Phillips et al., 2019). Aside from the improved results interpreted within the Galicia Interior Basin, the crustal thickness results for the rest of model 8b are the same as model 8a.

Analyzing crustal thickness profiles extracted from gravity inversion and model 8b (Figure 3.8), aside from profile b (extracted across the rigid Galicia Bank), deviations between the gravity inversion and model 8b results are minor compared to crustal scale uncertainties of approximately 2-5 km. The larger discrepancies across the Galicia Bank are to be expected due to the inability to account for deformation within rigid continental ribbons in the deformable models.

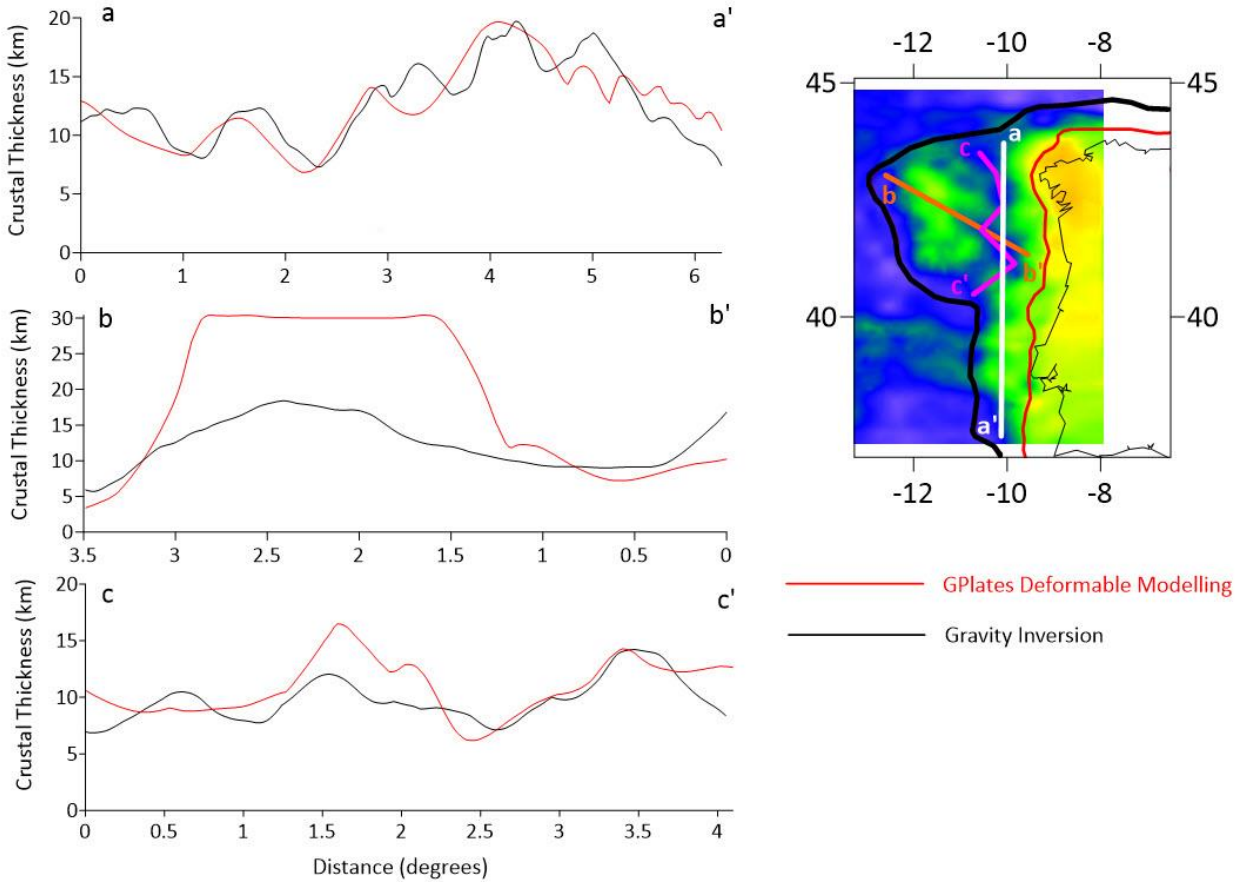

Figure 3.8 Crustal thickness profiles a) N-S, b) NW-SE across the Galicia Bank, and c) N-S through thinned areas within the Galicia Interior Basin extracted from the gravity inversion, and model 8b at 0 Ma (Figure 3.7). The black and red lines in all profiles represent the crustal thickness profiles extracted from the gravity inversion and deformable modelling, respectively. Black and red boundaries displayed on gravity inversion crustal thickness map are the edge of continental crust (ECC), and the necking line (NL) from Nirrengarten et al. (2018), respectively.

In addition to comparing crustal thicknesses calculated by gravity inversion and deformable plate models (Figure 3.8), results generated from these methods were also compared

with crustal thicknesses obtained from seismic refraction velocity modelling within the Galicia Interior Basin (Figure 3.9) (Pérez-Gussinyé et al., 2003; Druet et al., 2018).

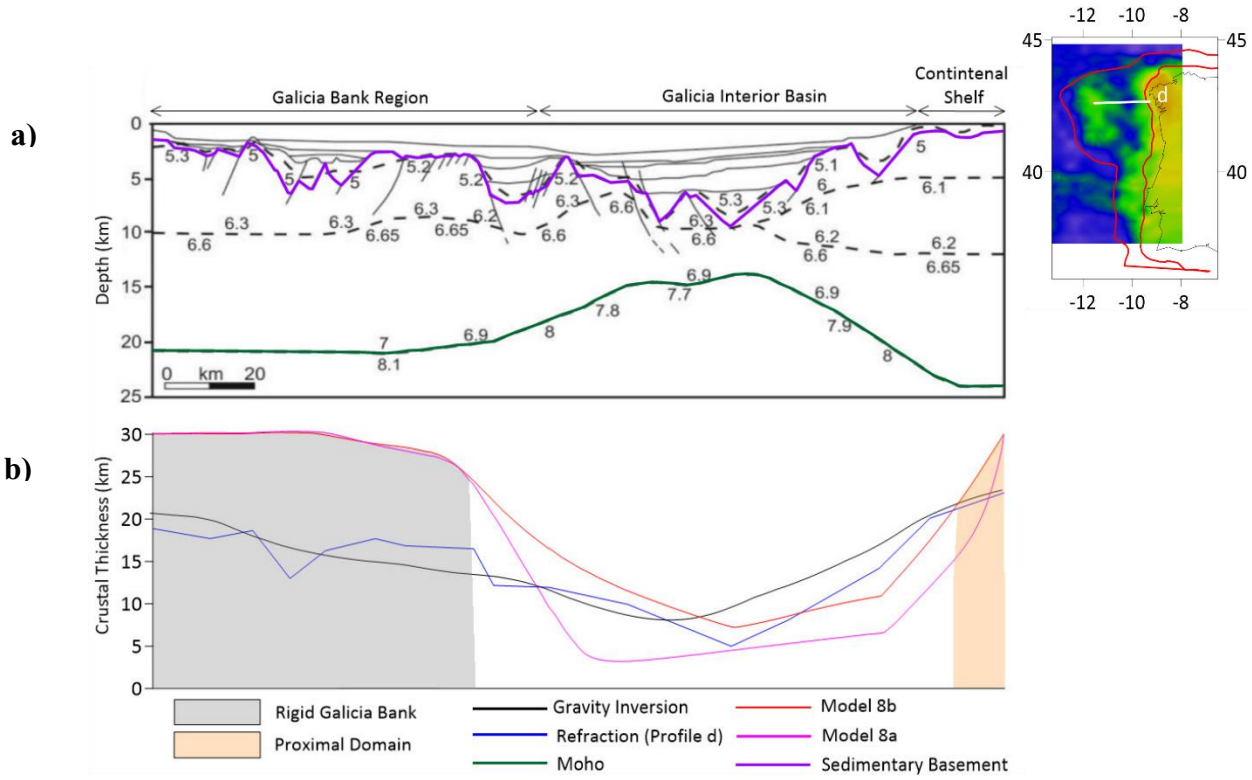

Figure 3.9 Comparison of refraction modelling, and crustal thicknesses calculated by gravity inversion and deformable modelling. a) Refraction model with labelled seismic velocities (km/s) along profile d modified after Druet et al. (2018) and originally from Pérez-Gussinyé et al. (2003). b) Comparison of crustal thickness profiles extracted along profile d for refraction modelling, gravity inversion, and models 8a and 8b calculated in GPlates.

First, when comparing crustal thickness results calculated by gravity inversion and refraction modelling along profile d, a good crustal scale match is observed with deviations of approximately 1-5 km. Comparing these results with crustal thicknesses calculated by models 8a

and 8b, model 8b provides a closer match to crustal thicknesses calculated by refraction modelling and gravity inversion. In comparison with model 8b, model 8a has a steeper decrease in crustal thickness moving east away from the rigid Galicia Bank and suggests crustal thicknesses ranging from 4-10 km within the Galicia Interior Basin in comparison with 7-10 km inferred by model 8b. Due to refraction profile d extending into the proximal domain, a domain not included in the deformable plate models, both crustal thickness profiles for models 8a and 8b in Figure 3.9 were extended by 30 km to match the length of the refraction and gravity inversion profiles, and to represent the crustal thicknesses predicted within this relatively undeformed domain. Consistent with independent comparisons of crustal thicknesses calculated by gravity inversion and deformable plate models (Figure 3.8), the largest discrepancy is observed within the Galicia Bank region, primarily caused by the inability of continental ribbons to undergo deformation in GPlates.

3.5 Conclusions

Deformable plate tectonic modelling of the West Iberian margin using GPlates has been performed using previously published constraints and the integration of the Galicia Bank as an independent continental ribbon, which was newly defined in this study. Comparison of these deformable models with gravity inversion results and previous interpretations from regional seismic and well data provide detailed insight into the plate kinematics and present day architecture of the West Iberian margin. The main findings of this work include:

1. The Galicia Bank played an important role during the formation of the North West Iberian margin, particularly within the Galicia Interior Basin.

2. Despite limited support from regional seismic and well data, models that included Late Jurassic extension invoked by the Galicia Bank's independent motion provided a better correlation with gravity inversion crustal thickness results within the Galicia Interior Basin.

3. The Galicia Bank and Flemish Cap may have been previously connected as a singular continental ribbon that experienced internal deformation during the Jurassic prior to breakup between the Newfoundland and Iberian Margins ~140 Ma. This scenario shows strong correlations with interpretations made from regional seismic and well data.

4. Inheritance of pre-existing Variscan structures along the North West Iberian margin played an important role with respect to the style of deformation and resulting present day crustal architecture of the margin. In particular, these pre-existing Variscan structures are interpreted to have controlled where deformation was transferred and partitioned during the early stages of extension experienced within the Galicia Interior Basin.

Chapter 4

4 Investigating the Plate Kinematics of the Bay of Biscay Using Deformable Plate Tectonic Models

The bulk of this chapter can also be found in its published version *"King, M. T., Welford, J. K., Cadenas, P., & Tugend, J. (2021). Investigating the plate kinematics of the Bay of Biscay using deformable plate tectonic models. Tectonics, 40, e2020TC006467. https:// doi.org/10.1029/2020TC006467".*

4.1 Introduction

The plate kinematic evolution of the Bay of Biscay during rifting and subsequent opening of the southern North Atlantic (Figure 1.3) has been a subject of debate for several decades (Srivastava et al., 1990; García-Mondéjar, 1996; Sibuet et al., 2004; Gong et al., 2008; Jammes et al., 2010c; Tugend et al., 2014, 2015a; Barnett-Moore et al., 2016; Cadenas et al., 2018; Nirrengarten et al., 2018). Bounded by several continental margins that host numerous sedimentary basins (Figure 1.6), the Bay of Biscay has drawn significant interest for independent geological and geophysical studies that provide valuable insight into its regional plate kinematic evolution and natural resource potential (Boillot et al., 1979; Brunet, 1984; Bois et al., 1997; Thinon et al.,

2002, 2003; Jammes et al., 2009, 2010c; Tugend et al., 2015b; Cadenas and Fernández-Viejo, 2017).

Subject to western European tectonic events dating back to the Paleozoic, the present day crustal structure of the Bay of Biscay is the product of poly-phase and multi-stage rifting that initiated within a complex pre-rift template encompassing inherited Variscan to Late Carboniferous- Early Permian structures and crustal heterogeneities (Matte, 1991, 2001; Burg et al., 1994; Jabaloy et al., 2002; Tavani et al., 2018; Schiffer et al., 2019; Cadenas et al., 2020). From the Triassic to Early Cretaceous, the Bay of Biscay experienced transtensional and extensional tectonics that caused significant crustal thinning prior to the onset of compressional deformation during the Alpine Orogeny (Olivet 1996; Sibuet et al., 2004; Roca et al., 2011; Tugend et al., 2015a; Cadenas et al., 2018; Nirrengarten et al., 2018). As a result of its complex evolution, interpretations derived from regional seismic, potential field, and well data within the Bay of Biscay will often accompany uncertainties regarding temporal variations in plate kinematics and stress orientations.

In this study, deformable plate tectonic models of the Bay of Biscay are built using the GPlates software (Williams et al., 2012; Müller et al., 2018), version 2.2, and recently published constraints along the North Iberian, Armorican, and Western Approaches margins (Tugend et al., 2014, 2015b; Cadenas et al., 2018; Nirrengarten et al., 2018; Peace et al., 2019b; Angrand et al., 2020). The deformable plate models presented will be used to analyze temporal variations in deformation within the Bay of Biscay and assess the kinematic role of continental blocks and their impact on its present day crustal structure. To validate the kinematic evolution and resultant crustal thicknesses calculated by deformable plate models, each model is analyzed in comparison with

previously published and newly presented gravity inversion crustal thickness estimates, and interpretations made from previously published seismic and well data. The objective of this approach is to investigate the plate kinematics of the Landes High, Le Danois High, and Ebro Block, and the timing, style, and extent of deformation experienced within the Bay of Biscay (Figure 1.7).

4.2 Methodology

To study the plate kinematic evolution of the Bay of Biscay, the deformable plate tectonic modelling methodology discussed in Chapter 2 (Figure 2.2), and applied in Chapter 3 and previously published studies (Flament et al., 2014; Gurnis et al., 2018; Welford et al., 2018; Müller et al., 2019; Peace et al., 2019b), was implemented using the GPlates software, version 2.2 (Müller et al., 2019). Using this approach, deformable plate tectonic models were constructed to analyze the plate kinematics of continental blocks within the Bay of Biscay, and resultant present day crustal thickness estimates within deformable regions. The primary objective of this work was to investigate the independent motion of previously recognized micro-blocks such as the Landes High, Le Danois High, and Ebro Block during rifting and opening of the Bay of Biscay using various continental block geometries and poles of rotation. Subsequently, a comparison between present day crustal thickness estimates and observations from potential field, seismic studies, and well data, provided a good metric for deducing the most probable plate kinematic scenario and the timing and extent of deformation experienced within the Bay of Biscay.

4.2.1 General model setup

In this study, five deformable plate tectonic models of the Bay of Biscay were built using the GPlates software (Williams et al., 2012; Müller et al., 2018), version 2.2. Identical to previous deformable plate model setups (Peace et al., 2019b; King et al., 2020), the time frame considered for four out of five deformable models (models 1 and 3-5) is from 200 Ma to present day (0 Ma) with a uniform 30 km crustal thickness estimate assumed at 200 Ma. One deformable plate model (model 2) based on the Late Permian to Mid-Cretaceous rigid plate tectonic reconstruction of Iberia from Angrand et al. (2020), was designed using a time frame of 270 Ma to present day. A uniform crustal thickness of 30 km at 270 Ma was also chosen for this deformable plate model. The initial 30 km crustal thickness estimate considered for all deformable plate models was chosen to capture potential minor crustal thinning caused by Triassic rifting over the continental shelves adjacent to the Bay of Biscay (De Charpal et al., 1978; Montadert et al., 1979; Ruffell, 1995; Cadenas et al., 2020), a phenomenon not considered for four out of the five deformable models tested. A 0.15625˚ mesh point spacing (GPlates density level 8) with no random offset was used for all crustal thickness calculations. A mesh point spacing (distance between points used to calculate crustal thicknesses within topological networks) of 0.15625˚ was considered an appropriate value to obtain regional-scale crustal thickness trends within the Bay of Biscay and was a more computationally feasible value in contrast to smaller point spacing options when making calculations in GPlates. Estimates of crustal thickness obtained from alternative methods/techniques such as gravity inversion serve as the primary method of comparison for investigating the validity of deformable plate models, in conjunction with observations from seismic and well data.

4.2.2 Gravity inversion: A compilation of different approaches

In this study, three different gravity inversion crustal thickness calculations are considered to examine the present day architecture of the Bay of Biscay and to compare with crustal thicknesses calculated in the Bay of Biscay by deformable plate models. One gravity inversion crustal thickness calculation obtained using the scheme of Welford et al. (2010, 2012) will be visualized throughout this study (Figure 4.1), while the other two gravity inversion calculations obtained using an alternative inversion scheme (Greenhalgh and Kusznir, 2007; Alvey et al., 2008; Chappell and Kusznir, 2008; Cowie and Kusznir, 2013; Tugend et al., 2014) can be found in Appendix A.

Gravity inversion crustal thickness estimates (Figure 4.1) were produced using the same minimum-structure gravity inversion methodology applied in previous studies over areas such as the Irish margin (Welford et al., 2010), Newfoundland margin (Welford et al., 2012), and West Iberian margin (King et al., 2020). Using the GRAV3D inversion algorithm (Li and Oldenburg, 1996, 1998), a smoothed depth-weighted 3-D density anomaly model was obtained by inverting the DTU10GRA free-air gravity dataset from the DTU National Space Institute (Anderson, 2010). To construct a reference density anomaly model (relative to 2850 kg/m^3) and account for appropriate density ranges (delimited by bounds) for the seawater, sediments, crust, and mantle, this inversion scheme used depth to basement and bathymetric constraints from the NOAA total sediment thickness of the world's oceans and marginal seas data (Divins, 2003) and the ETOPO1 1 arc-minute global relief model, respectively. A more detailed explanation regarding the inversion scheme and parameters chosen can be found in Welford et al. (2012).

4.2.3 Present day crustal structure: Insights from gravity inversion and seismic refraction

In this section, Moho depths derived from each gravity inversion method are compared with those derived from previously published seismic refraction lines throughout the Bay of Biscay (Figure 4.1) (Ayarza et al., 1998; Fernández-Viejo et al., 1998; Thinon et al., 2003; Ruiz et al., 2017), to investigate the present day crustal structure of the Bay of Biscay and address discrepancies.

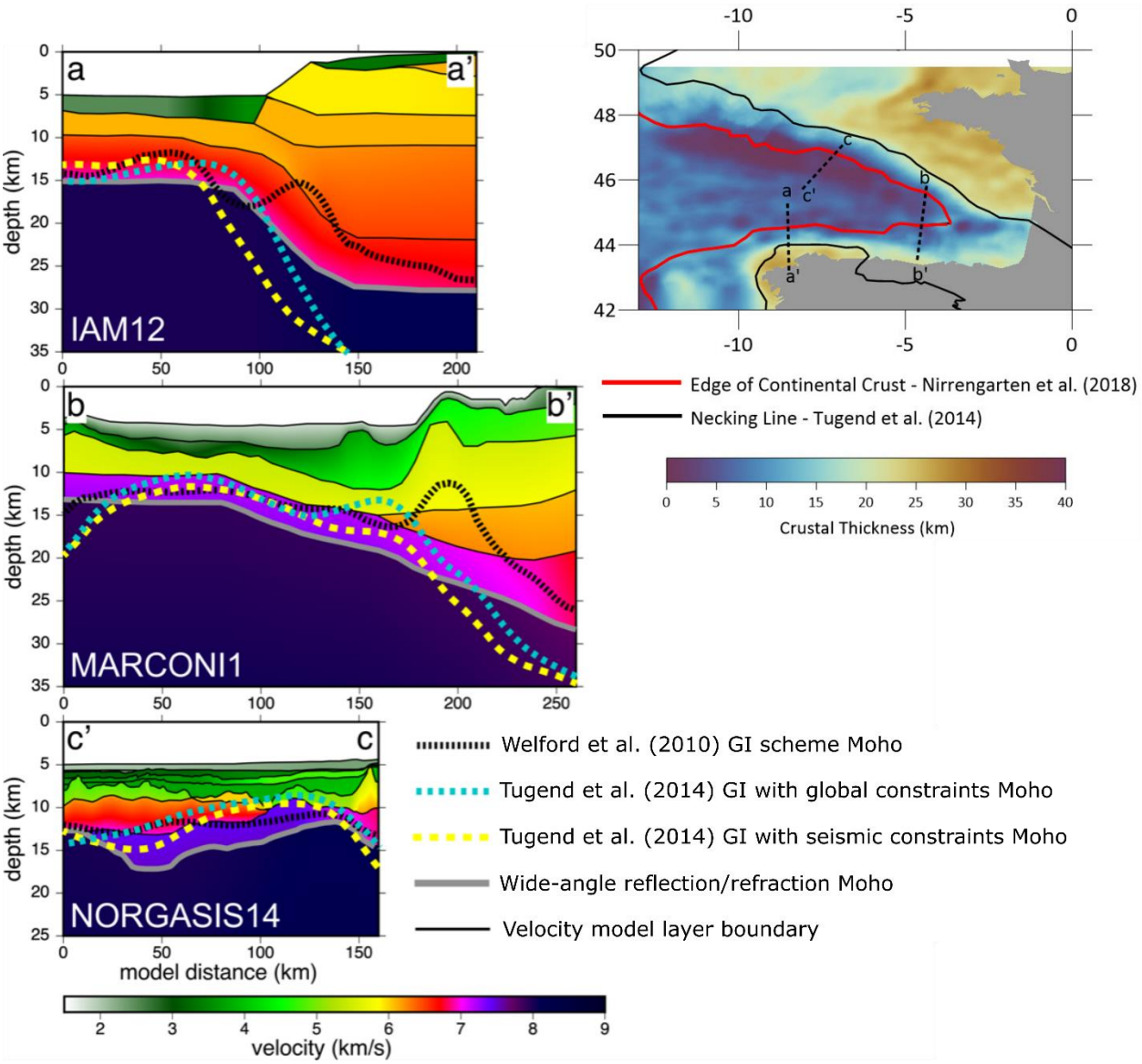

Figure 4.1 Comparison of Moho depths derived from gravity inversion (GI) and previously published seismic refraction velocity models. Profile locations are shown on the gravity inversion crustal thickness map calculated using the inversion scheme from Welford et al. (2010, 2012). a) Moho depth comparisons along IAM-12 (line a-a' on crustal thickness map) (Fernández-Viejo et al., 1998). b) Moho depth comparisons along Marconi 1 (Ruiz et al., 2017) (line b-b' on crustal

thickness map). c) Moho depth comparisons along Norgasis 14 (Thinon et al., 2003) (line c-c' on crustal thickness map).

As demonstrated in Figure 4.1, all three gravity inversion results are in general agreement with Moho depths interpreted from various seismic refraction velocity models throughout the Bay of Biscay (Fernández-Viejo et al., 1998; Thinon et al., 2003; Ruiz et al., 2017). Considering lines IAM-12 and Marconi 1 along the North Iberian margin (Figure 4.1a, b), the calculated Moho depths from each gravity inversion demonstrate an approximate ± 5 km discrepancy compared to Moho depths obtained from seismic refraction. The magnitude of these crustal thickness discrepancies is deemed appropriate given the depth resolution non-uniqueness challenges of gravity inversion. Examining the Norgasis 14 refraction line along the Armorican margin (Figure 4.1c), Moho depths calculated by gravity inversion also demonstrate an approximate ± 5 km discrepancy with the Moho horizon interpreted from the seismic refraction velocity model (Thinon et al., 2003). With reference to the high velocity body interpreted inboard of the oceanic domain along Norgasis-14 by Thinon et al. (2003), interestingly, the Moho depth calculated using the scheme of Welford et al. (2010, 2012) is nearly identical to the horizon representing the top of the high velocity body. This observation is primarily a result of the assumption that the Moho can be characterized by a constant density isosurface. Here, that assumption results in anomalously high crustal densities corresponding to mantle.

4.2.4 Model inputs: Deformable boundaries and continental blocks

The timing and magnitude of deformation produced via deformable plate tectonic models are dependent on the timing and geometry of deformable model boundaries associated with the motion of larger tectonic plates and the independent motion of features within deformable regions such as continental blocks. Throughout the southern North Atlantic, the timing and extent of these phenomena have and continue to be a topic of scientific interest, and research (Péron-Pinvidic and Manatschal, 2010; Welford et al., 2010; Tugend et al., 2014; Nirrengarten et al., 2018; Peace et al., 2019b; Neuharth et al., 2021).

In this study, the exterior deformable boundary used for all models is the edge of the continental crust (ECC) used in Chapter 3 (Figure 4.1), but slightly modified in the region west of the present day Landes High to avoid overlap between the ECC and Landes High during the Mid-Late Cretaceous opening of the Bay of Biscay. The interior deformable boundary implemented in this work is a combination of two previously published geometries of the necking line, a rift domain boundary where onset of the main thinning of the continental crust and lithosphere is interpreted (Tugend et al., 2014; Nirrengarten et al., 2018) (Figure 4.1). The necking line from Tugend et al. (2014) encompasses the Bay of Biscay, Pyrenees, and central regions of Iberia (Figure 1.4) and was expanded by Nirrengarten et al. (2018) to encompass additional regions throughout the southern North Atlantic (Figure 1.3).

The independent motion of relatively undeformed continental blocks and their significant role in shaping the present day crustal architecture of rifted margins throughout the southern North Atlantic have been highlighted in Chapter 3 and previous deformable plate modelling studies

(Peace et al., 2019). In the Bay of Biscay, the Landes High, Le Danois High, and Ebro Block are continental blocks of different size defined in previous potential field, rigid plate reconstruction, and seismic studies, and are considered to have played an important role in partitioning/distributing transtensional and extensional deformation during rifting and the short-lived opening of this region (Tugend et al., 2015a; Cadenas et al., 2018; Nirrengarten et al., 2018). To investigate the independent role of each of these continental blocks on the Bay of Biscay present day crustal architecture, various geometries and poles of rotations for these continental blocks are tested in the deformable models presented herein.

To define polygons whose geometry is representative of these relatively undeformed continental blocks, a combination of previous and newly defined polygons are used within the interior of deformable plate models. All models that include the Ebro Block use the geometry defined in Tugend et al. (2014), except for one model which uses the geometry defined in Angrand et al. (2020). Considering the Le Danois High, the geometry defined in Cadenas et al. (2018) is used in all models that include the Le Danois High. For the Landes High, two different polygon geometries are tested. One Landes High geometry consists of that defined in Tugend et al. (2014). The other consists of a newly defined geometry based on gravity inversion crustal thickness (Appendix A). The motivation for this new Landes High geometry was primarily based on gravity inversion crustal thickness estimates provided in Tugend et al. (2014) (Appendix A), and the new geometry was designed to include the additional regions of relatively undeformed continental crust surrounding the Landes High geometry defined in Tugend et al. (2014).

4.2.5 Poles of rotation

Poles of rotation defined within GPlates, or elsewhere, are used to govern the temporal kinematic variations of major tectonic plates, micro-plates, continental blocks, and individual points or lines (Williams et al., 2012; Müller et al., 2018). Consequently, the deformation experienced within topological networks designed in GPlates is governed by the poles of rotation associated with the boundaries of deformable regions and interior rigid features used to construct deformable plate models (Gurnis et al., 2018).

As discussed in Chapter 2, the poles of rotation and associated plate kinematics of Iberia have and continue to be a subject of scientific debate (Olivet, 1984; 1996; García-Mondéjar, 1996; Srivastava et al., 2000; Sibuet et al., 2004; Gong et al., 2008; Jammes et al., 2009; Barnett-Moore et al., 2016; Vissers et al., 2016; Nirrengarten et al., 2018; Causer et al., 2019). Building upon the work presented in Chapter 3, the Iberia poles of rotation used in this study are the poles defined in Nirrengarten et al. (2018), except for one model that uses the poles of rotation defined in Angrand et al. (2020). Additionally, the poles of rotation for all models that include the Ebro Block and select models that include the Landes High are from Nirrengarten et al. (2018) aside from the one model using poles of rotation from Angrand et al. (2020). For some models that include the Landes High, new poles of rotation were defined based on the motivation for each model (Table 4.1). The poles of rotation used for the Le Danois High were all newly defined in this study (Table 4.1). The Le Danois High poles were designed based on model motivation so as to avoid overlap with the Landes High and Ebro Block throughout the entirety of all models to avoid escaping mesh points within deformable plate models caused by overlapping continental blocks.

Continental Block	Poles of Rotation	Age	Latitude	Longitude	Angle	Reference Plate
Landes High	This Study	200	46.1322	9.1813	-3.1577	Ebro Block
	Nirrengarten et al. (2018)	122	30.56	-1.68	-7.34	Ebro Block
	Nirrengarten et al. (2018)	122	44.29	-0.79	-23.27	Europe
	Nirrengarten et al. (2018)	100	43.99	-1.75	-6.53	Europe
	Nirrengarten et al. (2018)	86	0	0	0	Europe
	Nirrengarten et al. (2018)	0	0	0	0	Europe
Le Danois High	This study	200	42.8989	-6.5973	-24.59	Iberia
	This study	160	42.2887	-5.5266	-34.5511	Iberia
	This study	140	48.2862	-2.7192	5.2955	Iberia
	This study	125	40.1242	4.8354	-3.7703	Iberia
	This study	120	43.99	-1.75	-6.53	Iberia
	This study	115	44.546	-4.0572	-15.9683	Iberia
	This study	86	0	0	0	Iberia
	This study	0	0	0	0	Iberia
Ebro Block	Nirrengarten et al. (2018)					

Table 4.1 Poles of rotation of the Landes High, Le Danois High, and Ebro Block used in model 4.

4.2.6 Model specifics

Five deformable plate tectonic models of the Bay of Biscay (Figure 4.2) were constructed and evaluated in this study to investigate the Mesozoic plate kinematics of the Landes High, Le Danois High, and Ebro Block. An additional five models were also considered in this analysis and can be found in Appendix A. The additional models excluded from the main text were designed to

test alternative plate kinematic scenarios for various continental blocks and deformable model boundaries. The primary differences between each model (Table 4.2) are the poles of rotation for Iberia, the time frame of interest, and the inclusion, geometries, and poles of rotation of various continental blocks.

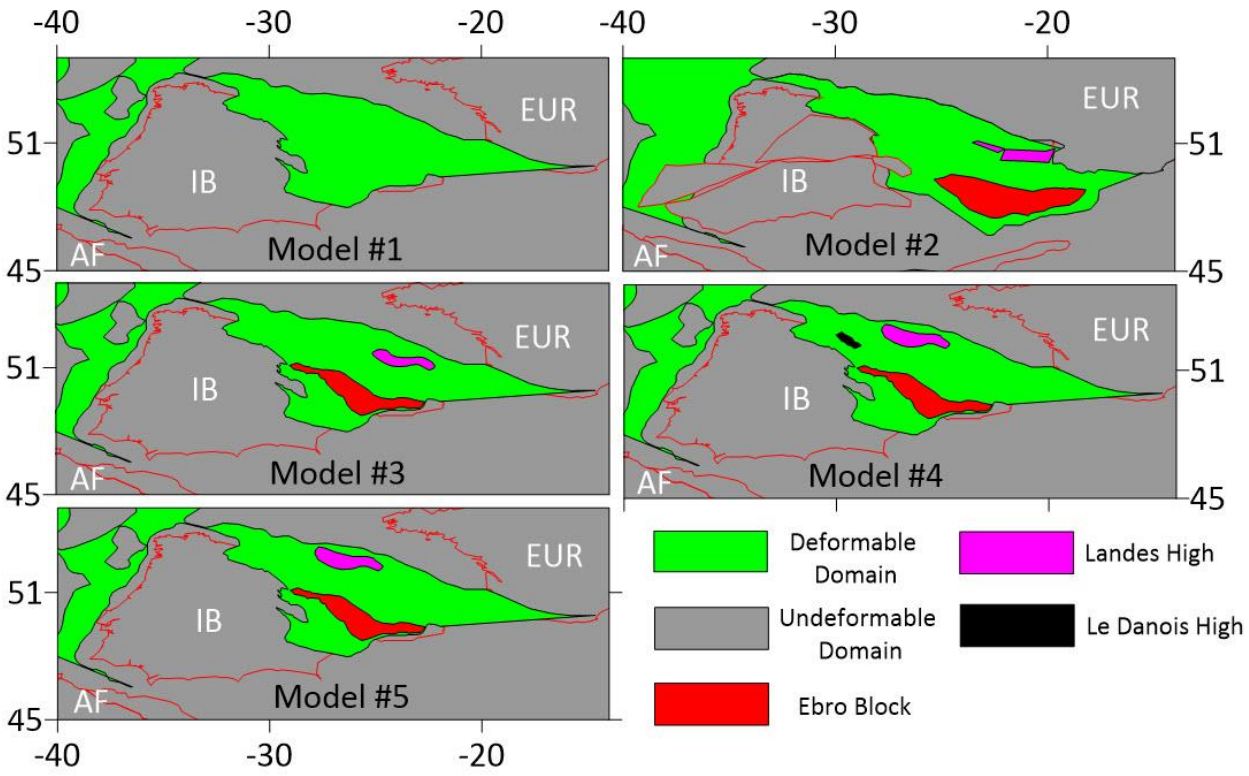

Figure 4.2 Initial setup for deformable plate models of the Bay of Biscay. All models are reconstructed back to 200 Ma, except for model 2, which is reconstructed back to 270 Ma. The deformable domain for all models is shown in green, undeformable domains in grey, Ebro Block filled in red, Landes High filled in magenta, Le Danois High filled in black, and coastlines outlined in red. AF= Africa, EUR = Europe, IB = Iberia.

Model #	Iberia Poles of Rotation	Model Start Time	Le Danois High Included	Landes High Included	Landes High Starting Point	Landes High Geometry	Ebro Block Included	Ebro block geometry
1	Nirrengarten et al. (2018)	200 Ma	No	No	NA	Tugend et al. (2014)	No	NA
2	Angrand et al. (2020)	270 Ma	No	Yes	Angrand et al. (2020)	Angrand et al. (2020)	Yes	Angrand et al. (2020)
3	Nirrengarten et al. (2018)	200 Ma	No	Yes	Nirrengarten et al. (2018)	Tugend et al. (2014)	Yes	Tugend et al. (2014)
4	Nirrengarten et al. (2018)	200 Ma	Yes	Yes	This study	This study	Yes	Tugend et al. (2014)
5	Nirrengarten et al. (2018)	200 Ma	No	Yes	This study	This study	Yes	Tugend et al. (2014)

Table 4.2 Description of boundary conditions for all deformable plate models tested in this study.

Model 1 is the simplest model as no continental blocks are included within the region of deformation. The motivation for this model was to investigate the impact of not having continental blocks included within deformable plate tectonic reconstructions along the Iberia-Eurasia plate boundary, similar to that proposed in previous rigid plate tectonic reconstruction studies (Sibuet et al., 2004; Vissers et al., 2016). Model 2, identical to the rigid plate reconstruction of Angrand et al. (2020), includes the Ebro Block and Landes High using the geometries and poles of rotation proposed by Angrand et al. (2020). This is the only model that uses a time frame of 270 Ma to present day (0 Ma) and is also the only model that does not use poles of rotation for Iberia defined in Nirrengarten et al. (2018). Model 3 includes the Landes High and Ebro Block using the poles of rotation defined in Nirrengarten et al. (2018). The geometries of the Ebro Block and Landes High are identical to those defined in Tugend et al. (2014). The reconstruction of the southern North Atlantic from Nirrengarten et al. (2018) was the first to provide independent poles of rotation for the Landes High and Ebro Block, and the motivation for model 3 was simply to investigate the kinematic role of these continental blocks using a deformable plate modelling approach. Model 4 is the first model where the Le Danois High, defined in Cadenas et al. (2018), is introduced. The motivation for including the Le Danois High is based upon recent seismic and potential field studies which interpret the Le Danois High as a rift-inherited basement block with a distinct evolution during extensional and compressional stages of deformation experienced along the North Iberian margin (Cadenas et al., 2018, 2020). The geometry of the Le Danois High is the same as that defined in Cadenas et al. (2018) and new poles of rotation for the Le Danois High are defined in this study. Model 4 also includes the Landes High and Ebro Block with a newly defined geometry and poles of rotation for the Landes High. This new geometry of the Landes High is

designed based on gravity inversion crustal thickness estimates (Appendix A) and its new poles of rotation are designed to simulate the Landes High starting further west within the Bay of Biscay at 200 Ma, causing the Landes High to move more independently from the Jurassic to Mid-Cretaceous as proposed in previous studies focussing on the Bay of Biscay plate kinematics (Tugend et al., 2014, 2015a). Model 5 is identical to model 4 but it does not include the Le Danois High. The motivation for this model was to investigate the effect of the Le Danois High on deformation.

4.3 Results

4.3.1 Kinematic evolution and resulting crustal thickness

Herein, the present day crustal thickness results calculated by deformable plate models described in the previous section are analyzed (Figure 4.3). For models 1-5, the inclusion of various continental blocks, and their varying poles of rotation and geometries, produced highly variable present day crustal thickness results throughout the Bay of Biscay.

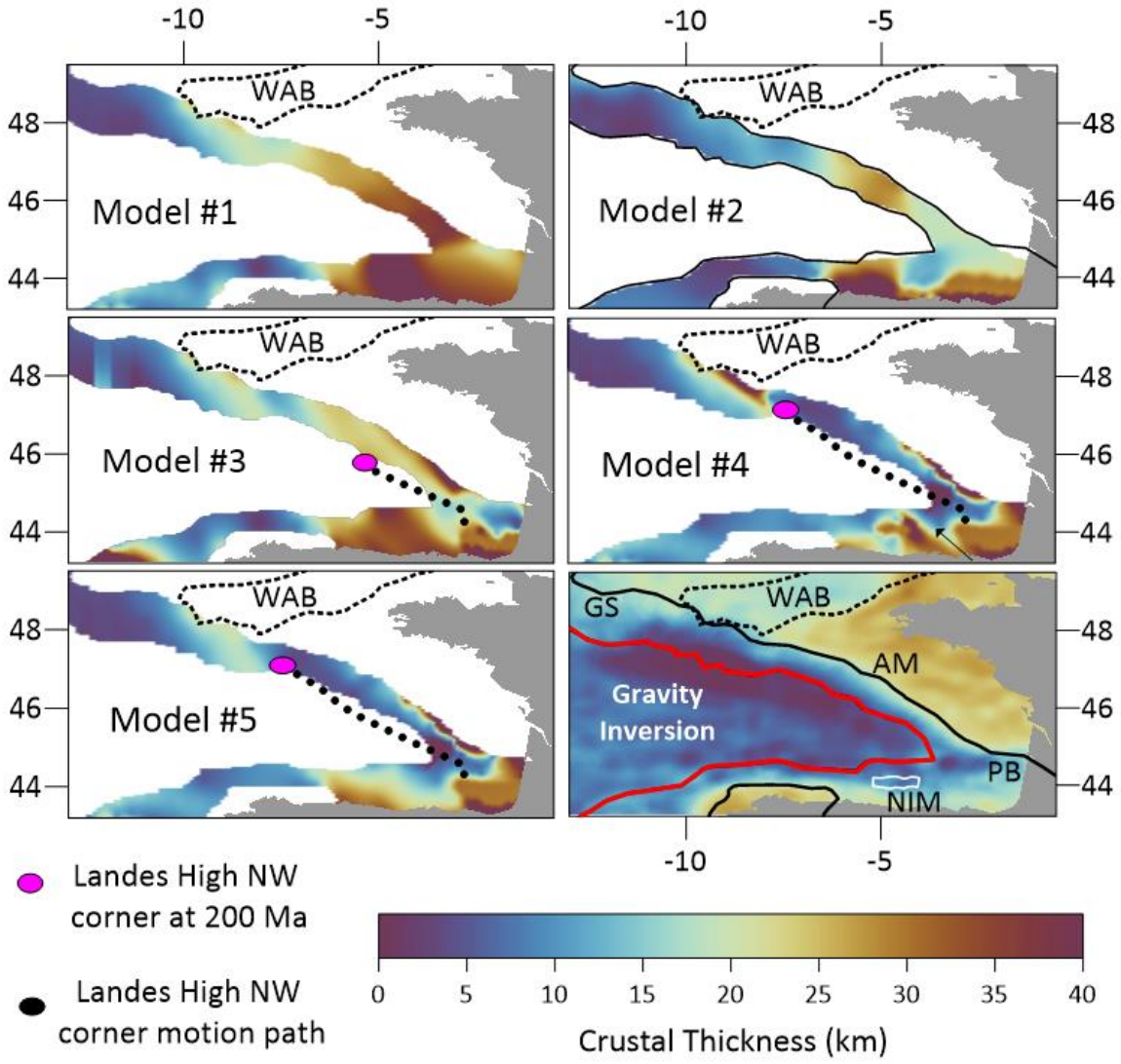

Figure 4.3 Present day (0 Ma) crustal thickness results for deformable plate models 1-5 and gravity inversion crustal thickness estimates. The starting point for the northwest corner of the Landes High (magenta circle) and the Landes High motion path at 10 Ma increments (black circles) with respect to Iberia, are shown for each model. Outline of the Western Approaches Basins (dashed black line) used to distinguish the boundary between the Armorican and Western Approaches margins. Interior (necking line, outlined in black) and exterior (ECC, outlined in red) deformable

model boundaries and Le Danois High geometry (white polygon) displayed on the gravity inversion crustal thickness map. AM = Armorican margin, GS = Goban Spur, NIM = North Iberian margin, PB = Parentis Basin, WAB = Western Approaches Basins.

Model 1 is the only model that does not include any continental blocks within the interior deformable region. In model 1, crustal thicknesses along the North Iberian margin range from ~ 30-40 km. Within the Parentis Basin and along the Armorican margin, crustal thicknesses also vary from ~ 30-40 km. Moving northward towards the Western Approaches margin and Goban Spur, a gradual decrease in crustal thickness is observed with regions of thinner crust ranging from 15-20 km along the Western Approaches margin and regions of significantly thinned crust (~ 2-10 km) in the vicinity of the Goban Spur.

Model 2 is identical to the plate reconstruction of Iberia proposed by Angrand et al. (2020). Along the North Iberian margin within the vicinity of the Le Danois High, crustal thicknesses vary from ~ 40 km land-ward to ~25 km ocean-ward. An area of localized thinned crust ~10-15 km thick is observed within the so-called Santander Transfer Zone (Roca et al., 2011), west of the Landes High, as well as within another localized region of the Parentis Basin varying from ~ 15-20 km thick. To the north of the Parentis Basin along the Armorican margin, crustal thicknesses vary from ~ 15-30 km, with a localized area of increased crustal thickness ~ 25-30 km thick within the central region of the Armorican margin. Moving further north, crustal thicknesses vary from ~ 10-15 km along the Western Approaches margin to areas of ~ 5-10 km thick along the Goban Spur margin.

In model 3, the independent kinematics of the Landes High resulted in regions of thinner crust within the northern Bay of Biscay and Parentis Basin in comparison to models 1 and 2. Along the Western Approaches and northern regions of the Armorican margin, crustal thicknesses generally range from 15-25 km with a localized area of thinned crust (~10 km) in the southern region of the Western Approaches margin. Within the Parentis Basin, crustal thicknesses range from ~5-10 km within the center of the basin and 10-15 km along the basin edges. Along the North Iberian margin, present day crustal thicknesses are identical to those calculated in model 1, with the exception of the 30 km crustal thickness of the rigid Landes High.

Model 4 is the only model that includes the Le Danois High as a continental block, in addition to the Landes High and Ebro Block. In proximity to the Le Danois High, a localized crustal thinning is observed within the Asturian Basin (10-15 km). Regions of significantly thinned crust (10 km or less) are observed west and ocean-ward of the rigid Le Danois High. In model 4, a NW-SE oriented indented region of thinned crust (indicated by the black arrow in Figure 4.3) is observed west of the Landes High ranging from ~10-15 km until a localised area of thicker crust (~35-40 km) is observed east of the Le Danois High near the so-called Santander Transfer Zone. Within the Parentis Basin, symmetric crustal thinning is observed in the center of the basin (~5-10 km), and crustal thicknesses along its northern and southern borders increase to as high as 30 km. A region of significantly thinned crust (< 5 km) occurs ocean ward of the Parentis Basin. From the southern Armorican margin to the Goban Spur margin, crust thicknesses calculated by model 4 vary considerably. Across strike of the southern Armorican margin, there is a gradual northeast to southwest decrease in crustal thickness ranging from 40 km near the continent-ward edge to approximately 8-15 km near the ocean ward edge. Across the north Armorican margin, a localised

wide region of thinned crust (~5-10 km) is observed until a widely distributed increase in crustal thickness (~15-20 km) is observed along the Western Approaches margin. This broad region of thicker crust along the Western Approaches margin continues northwestward until significant crustal thinning occurs within the Goban Spur vicinity.

Aside from crustal thickness variations along the North Iberian margin and south of the Western Approaches Basin, model 5 produces near identical crustal thickness results to those calculated by model 4 along the Western Approaches and Armorican margins, and within the Parentis Basin. Along the North Iberian margin, however, there is a continuous decrease in crustal thickness varying from ~30 km near the coastline to ~5-15 km near the exterior deformable boundary. Immediately west of the Landes High, similar to model 4, an indented region of thinner crust ranging from 5-15 km is observed. In proximity to the Le Danois High, the observed crustal thickness ranges from 20 to 30 km.

4.4 Discussion

4.4.1 Comparison of deformable plate modelling and gravity inversion

The main observations to investigate from comparing gravity inversion crustal thickness maps to deformable plate models include the symmetric crustal thinning within the Parentis Basin, localized crustal thinning within the Santander Transfer Zone and Asturian Basin, and approximate gradual continent to ocean-ward crustal thinning along the North Iberian margin, Armorican and Western Approaches margins (Figure 4.3).

4.4.1.1 Comparison of deformable plate modelling and gravity inversion: Models 1-3

Model 1 reveals significant present-day crustal thickness discrepancies in comparison to gravity inversion crustal thickness estimates. The most significant variations are the larger crustal thicknesses (~ 15-20 km thicker) calculated along the North Iberian margin, Parentis Basin, and Armorican margin.

Model 2 also demonstrates several discrepancies. Within the vicinity of the Asturian Basin and the Le Danois High, a gradual ocean-ward thinning is achieved, however, the magnitude of crustal thicknesses calculated by model 2 are ~ 10-15 km thicker compared to gravity inversion estimates. Crustal thicknesses calculated by model 2 within the so-called Santander Transfer Zone (Roca et al., 2011), west of the Landes High, show good correlations with those calculated by gravity inversion, however, crustal thicknesses within the Parentis Basin calculated by model 2 are ~ 10-15 km thicker. Along the Armorican margin, crustal thicknesses calculated by model 2 are generally larger than those calculated by gravity inversion by ~ 10-15 km. Transitioning northwards from the Armorican to the Western Approaches margin, model 2 demonstrates similar crustal thicknesses to those calculated by gravity inversion with slightly thicker areas of crust (~ 5 km) within ocean-ward areas of the Western Approaches Basins.

Model 3 produced similar unrealistic crustal thickness results along the North Iberian and Armorican margins, however, a notable difference is the region of localized crustal thinning (~5-10 km) within the Parentis Basin. This localized crustal thinning within the Parentis Basin, similar to that observed from gravity inversion, demonstrates the importance of the Landes High and its independent motion causing crustal thinning within this region. The removal of unrealistic significant crustal thickening within the Parentis Basin in models 2 and 3 also demonstrates the

role of the Landes High as a regional buffer of compressional deformation during the Alpine Orogeny (Ferrer et al., 2008), preventing significant crustal thickening within the Parentis Basin during the Late Cretaceous and Cenozoic.

4.4.1.2 Comparison of deformable plate modelling and gravity inversion: Models 4 and 5

Considering all models tested, crustal thicknesses calculated by models 4 (Figure 4.3) and 5 (Figure 4.4) provided the best crustal-scale match with gravity inversion crustal thickness estimates and these will be discussed in greater detail.

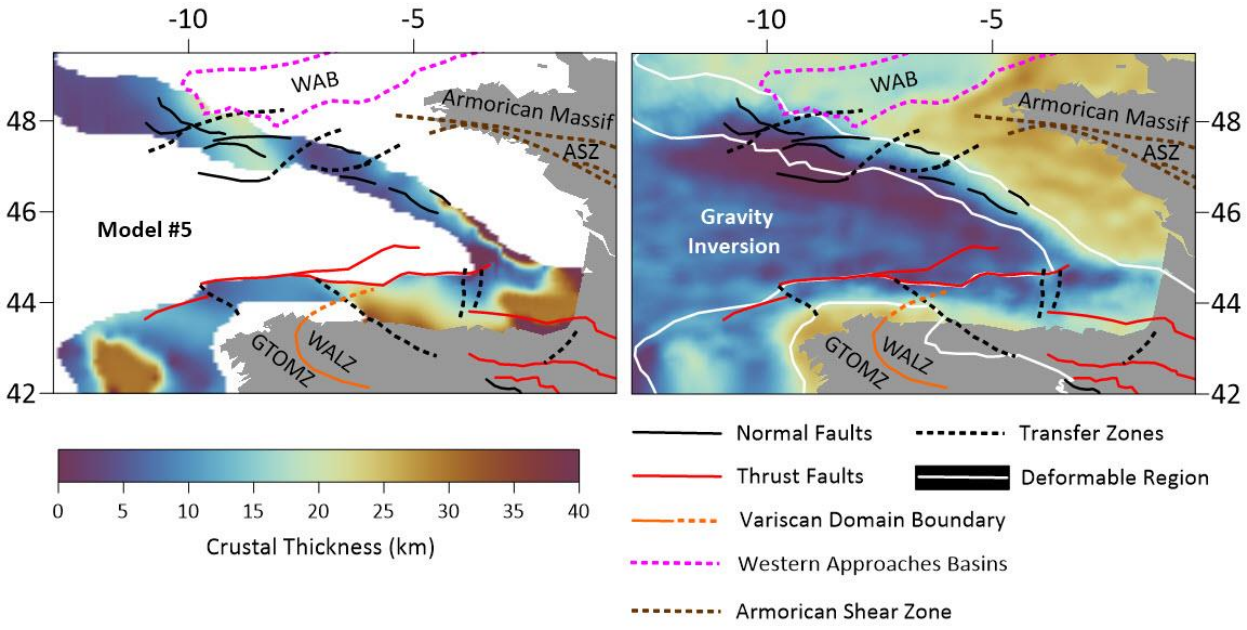

Figure 4.4 Comparison of crustal thickness maps produced from deformable plate model 5 and gravity inversion estimates. Overlain on each crustal thickness map are Bay of Biscay structures compiled by Tugend et al. (2014) and references therein, and deformable model boundaries used to construct all deformable plate models (white). Variscan domain boundaries (orange) compiled

from Farias et al. (1987) and Martinez-Catalan (2014). ASZ = Armorican Shear Zone, GTOMZ = Galicia-Tras Os Montes Zone WAB = Western Approaches Basins.

Model 4 introduces the Le Danois High, as well as a new geometry and poles of rotation for the Landes High. The kinematics of the Le Danois High in model 4 and their interplay with the Landes High correlate with localized crustal thinning within the Asturian Basin (~10-15 km), similar to present-day crustal thicknesses measured by Cadenas et al. (2018). West and north of the rigid Le Danois High in model 4, significantly thinned regions of crust (~5-10 km) are observed, demonstrating good correlations with gravity inversion estimates. Within the Santander Transfer Zone, an area of localized crustal thinning (~ 5-15 km) is observed, analogous to crustal thicknesses calculated by gravity inversion. The crustal thickness of the Le Danois High itself (30 km) demonstrates the main discrepancy between crustal thickness calculations made in this region by gravity inversion. In addition, larger crustal thicknesses along the eastern edge of the Le Danois High (~ 35-40 km) are observed, in contrast to those calculated by gravity inversion. It is important to note that the present-day crustal thickness of the Le Danois basement block results from Mesozoic crustal thinning and subsequent Alpine crustal thickening, which led to underthrusting of highly thinned crust underneath the Le Danois rift-inherited crustal block (Cadenas et al., 2020). Thus, these discrepancies with the results calculated by model 4 are interpreted to be a result of the assumption that all continental blocks are rigid and unable to experience deformation within deformable models built in GPlates. Although the crustal geometry of the Le Danois High and crustal thinning within the Asturian Basin have been clearly identified in previous seismic studies (Cadenas et al., 2018), these features are not as clearly identified in the gravity inversion crustal thickness maps considered. Given that gravity inversion results are largely dependent on input

sedimentary thicknesses, this phenomenon is likely a result of regional and local structural features such as the Asturian Basin not being included within the regional compilation of sedimentary thicknesses used in each gravity inversion calculation. Within the Parentis Basin, crustal thicknesses calculated by model 4 show good correlations with gravity inversion estimates, with crustal thicknesses ranging from 5-10 km within the basin center, and increasing to as high as 30 km along its northern and southern edges. Along the southern Armorican margin, crustal thickness values range from 30-40 km continent-ward to ~5 km ocean-ward, showing a good general correlation with gravity inversion results. The largest crustal thickness discrepancy between model 4 and gravity inversion estimates near the Parentis Basin is the region of significantly thinned crust (<5 km) calculated by model 4 near the southeast corner of the Bay of Biscay. Along the north Armorican margin, similar to the south, gravity inversion crustal thickness estimates generally suggest a gradual decrease in crustal thickness ocean-ward. Comparing this with crustal thicknesses calculated by model 4 in this region, a wide area of thinned crust (~ 5-10 km) is indicated as opposed to the sharp ocean-ward transition of decreasing crustal thickness suggested by gravity inversion estimates. Based on observations from previous seismic studies (Thinon et al., 2003), crustal thinning along the Armorican margin is restricted within a narrow domain, suggesting localized crustal stretching within this region. Considering the starting position of the Landes High in model 4, the Landes High at 200 Ma is situated within this region and in close proximity to the hard interior deformable boundary. Thus, the overestimation of crustal stretching and thinning calculated by model 4 in this region could be a result of the significant deformation accommodated by the motion of the Landes High away from its starting position. Further north along the Western Approaches margin, a wide area of larger crustal thicknesses (~15-20 km) is

calculated by each deformable model in contrast to a wide necking region and ocean ward crustal thinning (~5-15 km) suggested by gravity inversion estimates.

Model 5 is identical to model 4 aside from the exclusion of the Le Danois High in model 5. Considering all models, present day crustal thickness estimates calculated by model 5 provide the best correlations with those calculated by gravity inversion estimates. Along the North Iberian margin, model 5 captures similar variations in crustal thickness to those observed in each gravity inversion crustal thickness map considered, as demonstrated by crustal thickness profiles (Figure 4.5). In particular, the localized crustal thinning observed within the Santander Transfer Zone and the gradual ocean ward thinning of the crust in proximity of the Le Danois High. In contrast to model 4, crustal thickness variations within the vicinity of the Le Danois High suggested by previous seismic studies (Cadenas et al., 2018, 2020) are not captured in model 5 due to the omission of the Le Danois High. However, this is preferred as the inclusion of the Le Danois High in model 4 causes too much regional deformation relative to its small size as compared to other continental blocks considered. The large amounts of regional deformation caused by the Le Danois High in model 4 can also be associated with the difficulty of accounting for multi-stage and poly-phased deformation within deformable plate models built using GPlates, which are interpreted to have specifically affected the central North Iberian margin (Cadenas et al., 2020). Arguably, the largest discrepancy in crustal thicknesses calculated in all models along the North Iberian margin is the crustal thickness of the Landes High, which remains a constant value of 30 km for all models as rigid blocks are not permitted to deform in GPlates. Based on gravity inversion, crustal thicknesses for the relatively undeformed Landes High range from ~ 20-35 km.

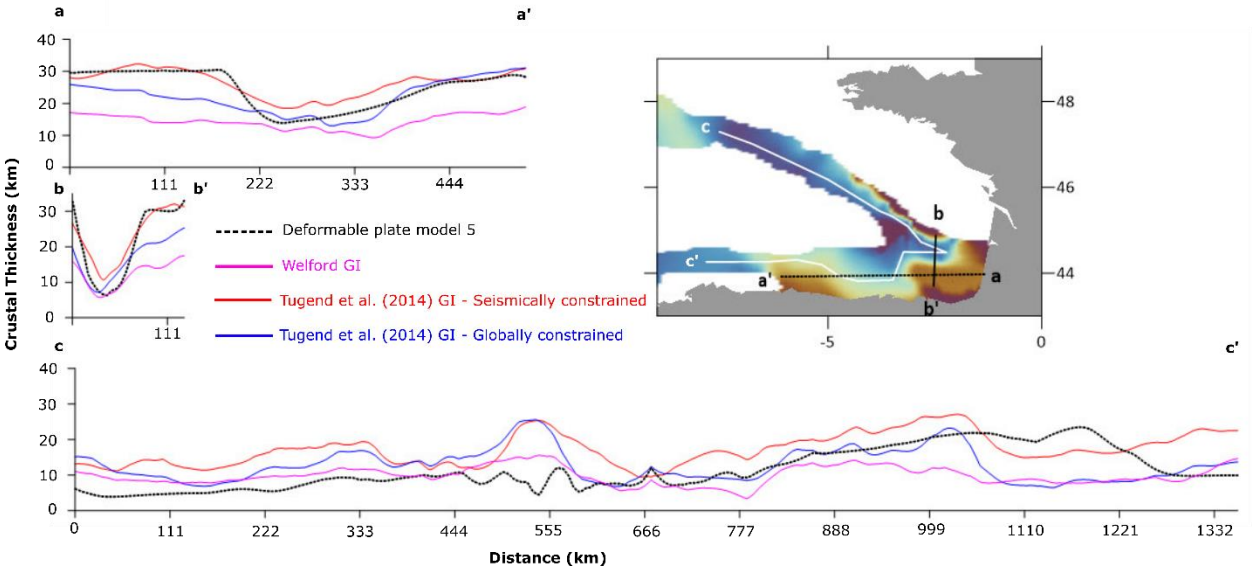

Figure 4.5 Crustal thickness profiles extracted from deformable plate model 5 and all three gravity inversion crustal thickness estimates considered. Profile a-a' (black dashed line), b-b' (solid black line), and c-c' (solid white line) locations and interior continental regions (solid grey) shown on crustal thickness map (top right panel).

4.4.2 Comparison of deformable plate modelling with regional seismic and well data

In this section, the plate kinematic evolution of model 5 (Figures 4.6 and 4.7) is analyzed in comparison to interpretations made from previously published seismic and well data throughout the Bay of Biscay (De Charpal et al., 1978; Montadert et al., 1979; Avedik et al., 1982; Brunet, 1984; Pinet et al., 1987; Alvarez-Marrón et al., 1996; Bois et al., 1997; Gallastegui et al., 2002; Thinon et al., 2003; Ferrer et al., 2008; Roca et al., 2011; Fernández-Viejo et al., 2011; Tugend et al., 2014, 2015b; Cadenas and Fernández-Viejo, 2017; Cadenas et al., 2018, 2020). In model 5, the kinematics of the Landes High play a major role in the variations in Mesozoic deformation

experienced within the Bay of Biscay. The Ebro Block, although included within the interior of deformable model 5, exerts minimal influence on the deformation experienced within the Bay of Biscay in contrast to its significant role during deformation within the Pyrenean realm (Tugend et al., 2015a; Angrand et al., 2020).

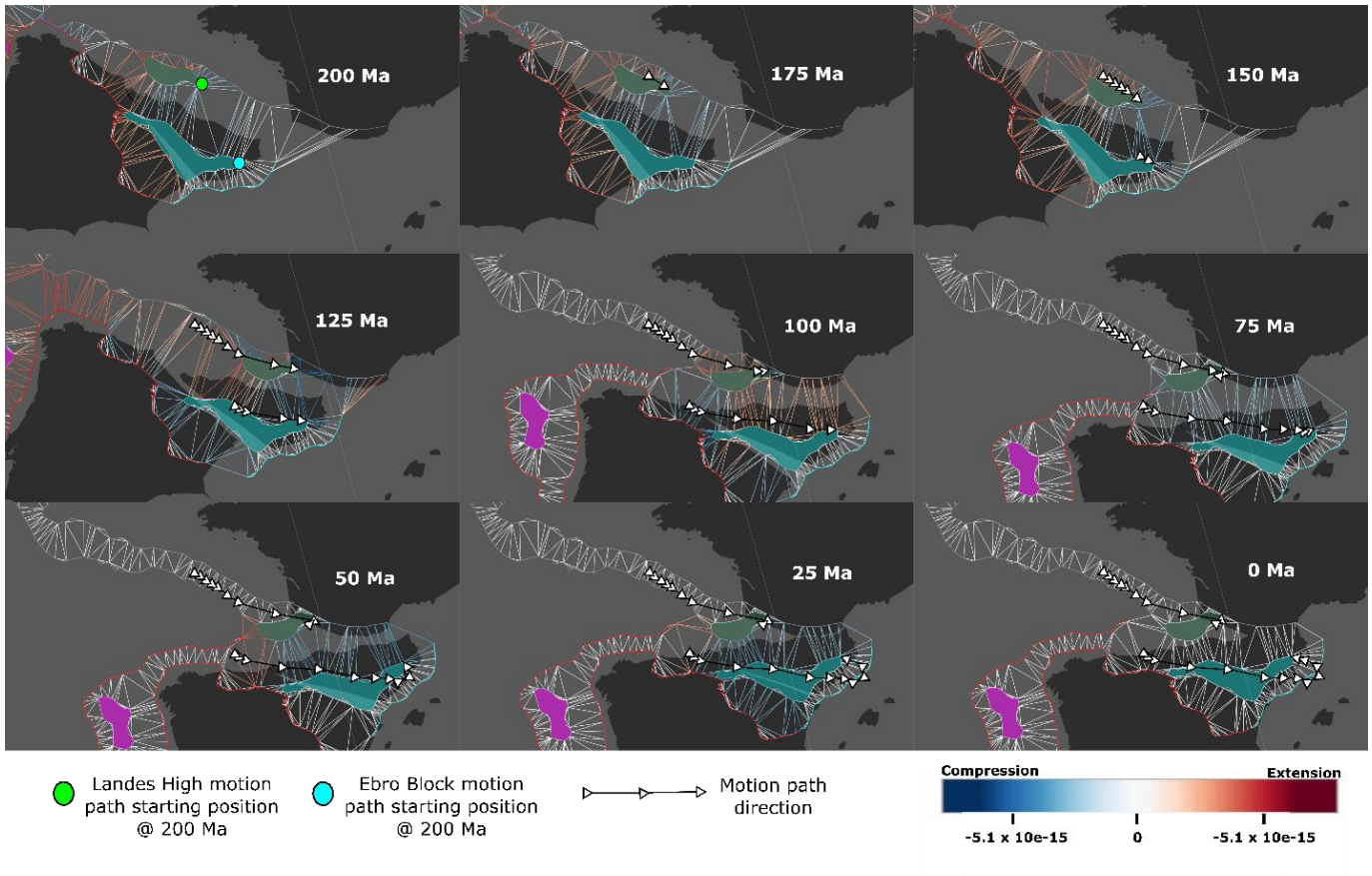

Figure 4.6 Temporal variations in strain rate within the interior of deformable plate model 5 and the kinematics of the Ebro Block (turquoise), Landes High (green), Galicia Bank from Chapter 3 (magenta), deformable boundaries, and larger tectonic plates in model 5 relative to Europe.

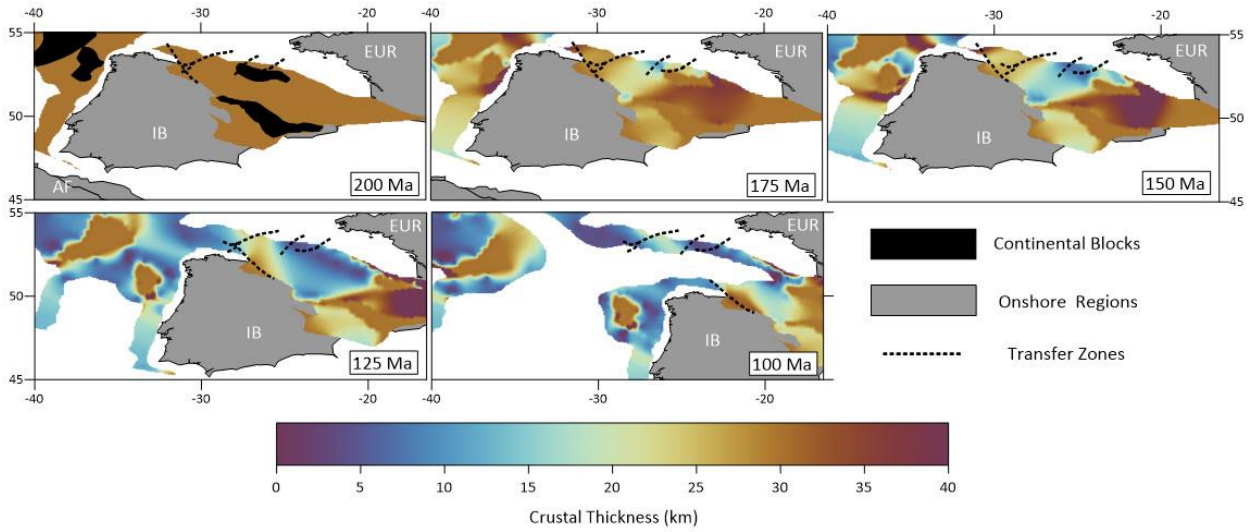

Figure 4.7 Model 5 crustal thickness evolution and the reconstructed orientations of present day transfer zones from 200-100 Ma at 25 Ma increments. IB = Iberia, EUR = Europe, and AF = Africa.

4.4.2.1 Mesozoic rift evolution within the Bay of Biscay

Model 5 tests a starting point for the Landes High near the Western Approaches Basin, with its long axis aligned approximately east-west at 200 Ma. From 200 Ma to ~150 Ma, the slow eastward motion of the Landes High in model 5 causes limited transtensional deformation to occur within the Bay of Biscay, and minimal crustal thinning. These results are generally consistent with little post-Triassic subsidence and crustal thinning inferred by Early-Mid Jurassic shallow marine lithologies dredged and penetrated by exploration and deep ocean drilling program wells and similar pre-rift units interpreted on seismic sections (Pastouret and Auffret, 1976; Montadert et al., 1977, 1979; Bois et al., 1997; Thinon et al., 2002, 2003; Tugend et al., 2014, 2015b; Cadenas et al., 2018). In the latest Jurassic (~ 150-145 Ma), the increasing velocity of the Landes High moving southeast corresponds to an increase in crustal thinning (~10-20 km) experienced along the

Western Approaches, Armorican, and North Iberian margins in model 5. The increasing velocity of the Landes High relative to Iberia during this time and the initiation of significant crustal thinning within the Bay of Biscay suggested by model 5 correlate with increasing subsidence rates during this time documented by exploration well data within the Parentis Basin (Figure 4.8) (Brunet, 1984; Bois et al., 1997). During the Early Cretaceous (~145-100 Ma), the most significant rifting episode is experienced within the Bay of Biscay, consistent with subsidence curves derived from Deep Sea Drilling Program (DSDP) results (Montadert et al., 1977). Throughout the Early Cretaceous (~145-100 Ma), the Landes High continues to travel eastward with the progressive opening of the Bay of Biscay until it reaches its present day position at ~ 100 Ma. This period of time also corresponds to the largest velocity pulse of the Landes High relative to Iberia, directly corresponding to the largest pulse in subsidence velocity recorded within the Parentis Basin (Figure 4.8) (Bois et al., 1997). Model 5 produces areas of hyperextended crust along the North Iberian, Armorican, and Western Approaches margins by 125 Ma, corresponding well to the onset (Berriasian-Barremian) and end (Aptian) of hyperextension documented from previous seismic, well data and subsidence analyses within the Northern Biscay margin (Montadert et al., 1977; Thinon et al., 2002, 2003; Tugend et al., 2014, 2015b). However, in the central North Iberian margin, borehole constrained seismic interpretations define a period of transtensional deformation accommodated by local crustal thinning within narrow and laterally confined basins, interpreted as pull-apart basins from the Upper Jurassic to Barremian (Cadenas et al., 2020). In contrast to that suggested by model 5, the onset of hyperextension leading to high degrees of crustal thinning and mantle exhumation is interpreted to initiate during the Aptian due to the emplacement and activity of extensional detachment faults (Cadenas et al., 2020). Comparing the onset of hyperextension

suggested by model 5 and borehole constrained seismic interpretations (Cadenas et al., 2020), model 5 predicts significant crustal thinning along the central North Iberian margin to have ceased during the early Aptian (~ 125 Ma). This discrepancy between model 5 and that suggested by borehole constrained seismic interpretations (Cadenas et al., 2020) is interpreted to be caused by the inability to model deformation caused by rheological and depth-dependent processes in deformable plate kinematic models. This results in a lack of significant crustal thinning calculated by model 5 along the central North Iberian margin during the Aptian-Albian.

By 100 Ma, significant crustal thinning is calculated by model 5 within the Parentis Basin. The present-day crustal architecture of the Parentis Basin has caused many to question and postulate explanations regarding the mode of deformation responsible for the significant crustal thinning observed within this region (Pinet et al., 1987; Bois et al., 1997; Ferrer et al., 2008; Jammes et al., 2010a; Lagabrielle et al., 2020). Some authors emphasize the presence of a thick pre-rift salt layer and a ductile mode of deformation (Lagabrielle et al., 2020), while others propose an asymmetric opening of a lower plate sag basin with crustal thinning induced by a top-basement detachment system (Jammes et al., 2010a). However, in all cases, a common consensus is reached that supports the observation of gently dipping smooth slopes along its basin edges, a lack of steeply dipping normal faults capable of explaining the crustal thinning documented towards the basin axis, and the presence of a thick pre-rift salt layer responsible for decollement of the pre-rift sedimentary cover along the sedimentary basement (Jammes et al., 2010a, 2010b; Ferrer et al., 2012; Lagabrielle et al., 2020). Aside from localized areas and rift systems (De Charpal et al., 1978; Montadert et al., 1979; Ferrer et al., 2012; Zamora et al., 2017; Cadenas et al., 2020), this pre-rift salt decollement layer is not as prevalent along the North Iberian, Armorican, and Western

Approaches margins. The mode of deformation within these regions is interpreted to be similar to that interpreted along the Iberia-Newfoundland margins (Thinon et al., 2003; Tugend et al., 2014; Cadenas et al., 2018, 2020; Lagabrielle et al., 2020), and primarily consists of upper crustal thinning caused by brittle deformation, an abundance of normal faulting, and the occurrence of extensional allochthons (Peron-Pinvidic et al., 2013; Lagabrielle et al., 2020).

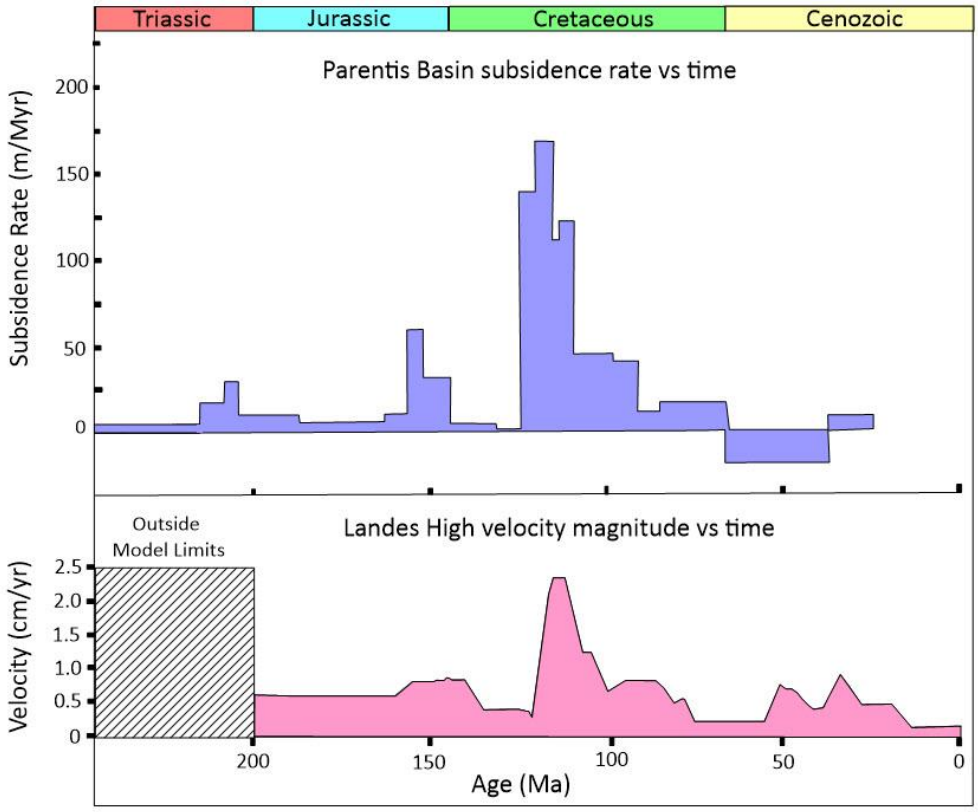

Figure 4.8 Comparison of Landes High velocity magnitude (cm/year) versus time (Ma) in model 5 (bottom panel) and subsidence rate (m/Ma) versus time (Ma) from Bois et al. (1997) (top panel). Aside from model 2, Triassic subsidence velocities originally calculated by Brunet et al. (1984) are outside the time frame considered for deformable plate models (200 Ma to present day).

4.4.2.2 Compressional re-activation within the Bay of Biscay

Beginning in the Late Cretaceous, the orientation of stress fields along the Iberia-Eurasia plate boundary were significantly modified as a result of the collision between Iberia and Eurasia during the Alpine Orogeny. Considering the impact of compressional deformation within the Northern Bay of Biscay, an area encompassing the Western Approaches and Armorican margins, these regions are interpreted to have experienced only minor reactivations in the Late Cretaceous and Eocene (Thinon et al., 2001). However, the pre-orogenic template of the southern Bay of Biscay is interpreted to have been significantly modified by compressional deformation during the Alpine Orogeny, resulting in variable amounts of tectonic inversion and crustal thickening along strike of the North Iberian margin (Alvarez-Marrón et al., 1997; Gallastegui et al., 2002; Ferrer et al., 2008; Cadenas et al., 2018, 2020). Analogous to previous plate kinematic studies (Roest and Srivastava, 1991; Rosenbaum et al., 2002), the crustal thickness evolution of model 5 (Figure 4.9) suggests that extension across the Iberia-Eurasia plate boundary ceased during the Campanian (~ 83 Ma). However, the onset of compressional deformation throughout the entire Pyrenean-Cantabrian Orogeny and particularly, the North Iberian margin, still remains a matter of debate. The onset of Alpine contraction within the Parentis Basin has been ascribed to the Late Cretaceous, with major deformation occurring from Eocene to Middle Miocene (e.g., Ferrer et al., 2008; Roca et al., 2011). Well calibrated seismic interpretations constrained ages of syn-orogenic sequences within the continental platform of the central and western North Iberian margin, ranging from Upper Eocene to Lower Miocene (e.g., Gallastegui et al., 2002; Cadenas and Fernández-Viejo, 2017). Within the abyssal plain in the western North Iberian margin, Álvarez-Marrón et al. (1997) dated syn-orogenic sequences within the accretionary wedge from Middle Eocene to Middle

Miocene through projection and extrapolation of ODP-118 onto the IAM-12 profile, located at the western corner of the Bay of Biscay. However, the lack of timing constraints within the abyssal plain also contributes to uncertainties regarding the age of syn-orogenic sequences constraining the onset and end of contractional deformation. From the evolution of model 5 (Figure 4.9), minor crustal thickening is observed within the so-called Santander Transfer Zone during the Late Cretaceous. However, considering the hard exterior boundaries used to construct deformable plate models, the proximity of these hard boundaries to other rigid features such as continental blocks can often produce edge effects, a phenomenon that could have an impact on the magnitude of this localized compressional deformation experienced in areas such as the Santander Transfer Zone during the Late Cretaceous. Although compressional re-activation may have initiated during the Late Cretaceous, major crustal thickening along the southern Bay of Biscay in model 5 does not occur until Eocene onwards, in agreement with time constraints deduced from syn-orogenic sequences within the continental platform in the North Iberian margin and with the major period of compression within the Parentis Basin. This would support and suggest that the onset of compressional deformation was unlikely to be synchronous along the Iberia-Eurasia plate boundary.

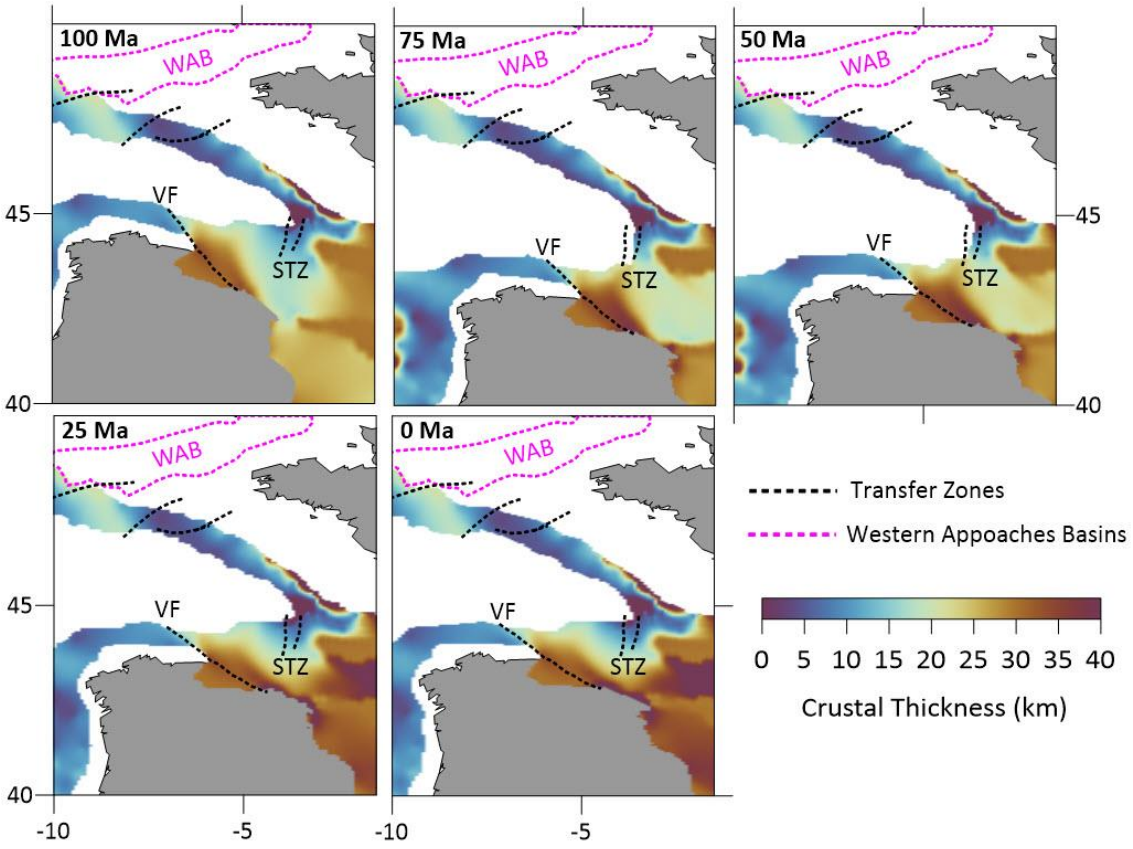

Figure 4.9 Model 5 crustal thickness evolution from 100 Ma to present and the reconstructed orientations of present day transfer zones and the English Channel from Tugend et al. (2014) and references therein. STZ = Santander Transfer Zone, VF = Ventaniella Fault, WAB = Western Approaches Basins.

During the Alpine Orogeny, the majority of compressional deformation experienced along the North Iberian margin was focused within and outboard of the hyperthinned domain, resulting in the formation of an accretionary wedge at the toe of the continental slope (Alvarez-Marrón et al., 1997; Gallastegui et al., 2002; Fernández-Viejo et al., 2012), and under thrusting of highly thinned crust and exhumed mantle to the south underneath the continental platform (Roca et al., 2011; Fernández-Viejo et al., 2012; Cadenas et al., 2020). Considering recent studies that focus on

the tectonic evolution of the southern Bay of Biscay (Cadenas et al., 2020), the Le Danois High is considered to be a rift related crustal block with an independent evolution during the subsequent Alpine Orogeny. Within this region, compressional deformation is interpreted to be accommodated beneath the Le Danois crustal block caused by under thrusting of hyperthinned and exhumed domains, resulting in uplift and tilting of the block (Cadenas et al., 2020). Based on seismic interpretations within the Asturian Basin, minor-reactivation of rift-related structures contrasts with that experienced in areas outboard (Cadenas and Fernández-Viejo, 2017; Cadenas et al., 2018). Comparing these observations with the crustal thickness evolution of model 5 within the southern Bay of Biscay during the Alpine Orogeny (Figure 4.9), these changes in structure and rift-related crustal thickness are not observed. This is mainly due to the resolution of crustal thickness variations that can be calculated by deformable plate models built in GPlates, and more importantly, the fact that localized deformation associated with the re-activation of basement morphologies within outer rift domains, as interpreted along the North Iberian margin, cannot be accounted for using GPlates.

4.4.3 Assessing discrepancies between deformable plate models and independent observations

4.4.3.1 Analyzing the interplay of inheritance and rifting within the Bay of Biscay

In comparison to previously published geological and geophysical observations, deformable plate model 5 provides good crustal-scale correlations both in terms of present-day structure and temporal evolution of deformation. However, although regional scale crustal thickness variations within the Bay of Biscay are captured, model 5 still demonstrates localized

crustal thickness discrepancies within areas where major lithospheric boundaries and heterogeneities have been previously interpreted.

Considering crustal thicknesses calculated by model 5 within the Western Approaches margin and similar estimates calculated by gravity inversion, crustal thicknesses calculated by model 5 are ~ 5-10 km thicker. For the westernmost North Iberian margin, an area conjugate to the Western Approaches margin, crustal thicknesses calculated by model 5 within hyperthinned domains (Cadenas et al., 2018, 2020) are also ~ 5-10 km thicker compared to gravity inversion estimates. To explain these discrepancies, two different scenarios, or their combination, are proposed.

One scenario emphasizes the role of Variscan trends within these two regions during rifting within the Bay of Biscay. Along strike of the Northern Bay of Biscay rifted margin, significant changes in crustal architecture have been documented to occur in the vicinity of the interpreted offshore prolongation of the Armorican Shear Zone (Thinon, 1999; Tugend et al., 2014). Within the western North Iberian margin, we suggest that the offshore prolongation of the onshore limit between the Galicia-Tras Os Montes Zone (GTOMZ) and the Western Asturian Leonese Zone (WALZ) (e.g., Farias et al., 1987; Martínez-Catalán et al., 2014) occurs in the area showing anomalous thicker crust. Based on the reconstructed orientations of these offshore prolonged major lithospheric boundaries at 200 Ma (Figure 4.10), these two regions of thicker crust calculated by model 5 appear to be highly compartmentalized by these previously interpreted transfer zones, possibly following former Variscan domain boundaries (between GTOMZ and WALZ) or post-Variscan lithospheric structures (ASZ). Another interesting observation in proximity to the Western Approaches margin at 200 Ma is the presence and orientation of the Armorican Shear

Zone and the offshore Ventaniella-Cantabrian Fault (Fernandez-Viejo et al., 2014). Based on previous interpretations made from seismic and potential field data (Tugend et al., 2014; Cadenas et al., 2018), the Armorican Shear Zone and Ventaniella Fault along the Armorican and North Iberian margins, respectively, are interpreted to have played a significant role in shaping the crustal architecture of present day necking domains. In particular, the Ventaniella Fault is interpreted to represent the boundary between the necking and proximal domains along the western North Iberian Margin (Cadenas et al., 2018). The transfer zone in the inferred prolongation of the Armorican Shear Zone was interpreted at the boundary between the wider necking zone along the Western Approaches margin in contrast to the narrow necking zone along the Armorican margin (Tugend et al., 2014). Considering these observations and crustal thicknesses calculated within these regions by model 5, we suggest that inherited structures played a key role in distributing deformation and the resultant crustal thinning within this region, a phenomenon that cannot currently be reproduced by deformable plate models built using GPlates.

In addition, another scenario not captured by model 5 is the potential role of Permian to Early Liassic rift basins within the English Channel that may have previously thinned the crust as a result of intra-continental rifting (Ruffell, 1995). Model 2 was the only deformable plate model that included Late Permian-Triassic related deformation. Comparing crustal thicknesses calculated by model 2 and gravity inversion within this region, a good crustal-scale correlation is observed despite slightly higher crustal thicknesses (~ 5 km) calculated by model 2 within ocean-ward regions of the Western Approaches margin. However, a uniform crustal thickness of 30 km during the Late Permian – Triassic considered in model 2 is deemed highly unlikely given the expectation of larger crustal thickness variations within this region as a result of compressional deformation

experienced during the Variscan Orogeny (Matte, 2001). Although crustal thinning caused by orogenic collapse could potentially result in crustal thicknesses closer to the 30 km estimate prior to the Jurassic (Ziegler, 1988; Matte, 1991), crustal thicknesses within the Bay of Biscay are still considered to be highly variable prior to Late Triassic and Early Jurassic rifting, suggesting that localized strain partitioning and deformation were more likely to be influenced by inherited structures. In addition, significant widespread crustal thinning calculated by all deformable plate models along the Goban Spur margin (5 km or less) in contrast to estimates calculated by gravity inversion (10-20 km) also suggest that the orientation of major lithospheric boundaries and their interplay with regional stress directions played a key role in localizing deformation during Mesozoic rifting.

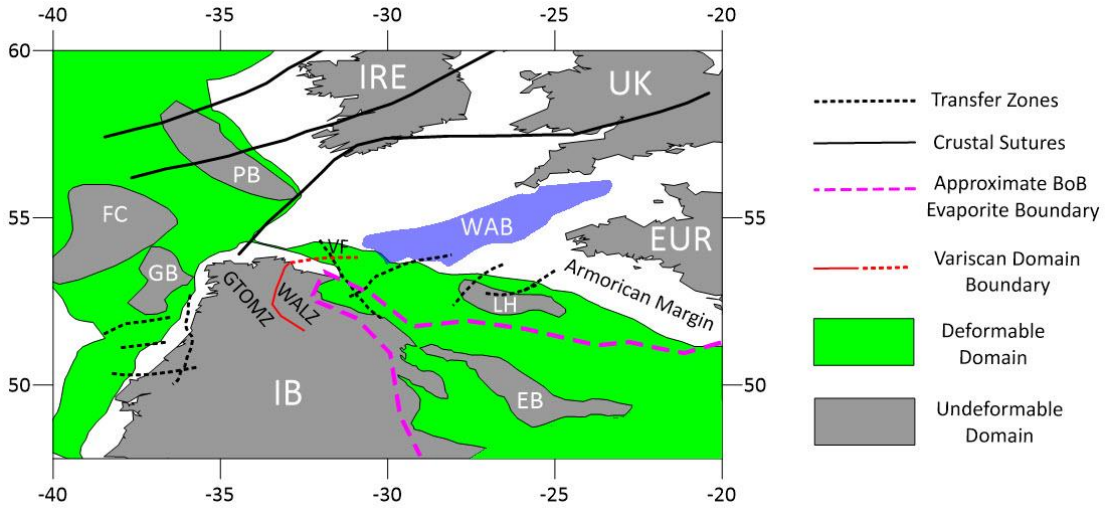

Figure 4.10 Reconstruction of model 5 at 200 Ma with crustal sutures (solid black lines) from Welford et al. (2012), reconstructed position of present day transfer zones (dashed black lines) from Tugend et al. (2014), and an approximate boundary of regions within the Bay of Biscay (BoB) and beyond affected by pre-rift evaporites (magenta dashed line) modified after Lagabrielle

et al. (2020). EB = Ebro Block, EUR = Europe, FC = Flemish Cap, GB = Galicia Bank, GTOMZ = Galicia-Tras Os Montes Zone, IB = Iberia, IRE = Ireland, LH = Landes High, PB = Porcupine Bank, UK = United Kingdom, VF = Ventaniella Fault, WAB = Western Approaches Basin, WALZ = West Asturian-Leonese Zone.

4.4.3.2 Investigating the interplay of continental blocks and transfer zones

The position of the Landes High at 200 Ma tested in model 5 and its interplay with the reconstructed orientation of interpreted transfer zones (Figure 4.10) provide interesting observations along the Western Approaches margin. One observation is the intersection of the Landes High with an interpreted northeast-southwest trending offshore prolongation of one branch of the Armorican Shear Zone. Based on this relationship, it is postulated that the transfer zone at this location potentially localized deformation and delimited the Landes High throughout the Jurassic as a result of the crustal stretching induced from its interplay with this branch of the Armorican Shear Zone and progressive eastward motion. This could partially explain the relatively undeformed nature of the Landes High suggested by gravity inversion crustal thickness estimates. In addition, this observation can also provide clues about the origin of the Le Danois High. In particular, whether the Le Danois High has always been an independent continental block or whether it was originally connected to the Landes High and later detached as a result of deformation experienced within the Landes High. Considering the first scenario, having the Le Danois High act as an independent continental block as tested in model 4 seemed to cause too much regional deformation given its small size in comparison to other continental blocks. In contrast, considering previous paleo geographic maps of the Bay of Biscay (Tugend et al., 2015a), it can be postulated that the Landes High was once a larger continental block having undergone

deformation during the Mid-Late Cretaceous. This scenario would also support recent seismic interpretation within the Bay of Biscay (Cadenas et al., 2020) suggesting that the Le Danois High corresponded to a rift-related continental block which developed particularly from the Aptian to Albian due to the emplacement of extensional detachment faults. However, future studies in this region are needed in order to address these theories regarding the deformation history and potential link between these two continental blocks.

4.4.4 Implications for Iberian plate kinematics and deformation

Considering traditional plate reconstruction studies of the Iberian plate that propose subduction in the Pyrenees (Vissers and Meijer, 2012), strike-slip motion along the Northern Pyrenean Fault (Olivet, 1996; Stampfli and Borel, 2002), or transtensional and rift-perpendicular motion along the Iberia-Eurasia plate boundary (Jammes et al., 2009), all of these reconstructions propose Iberia to act as single, rigid, tectonic plate. In light of more recent studies that consider the Iberian plate kinematics (Nirrengarten et al., 2018; Angrand et al., 2020), the partitioning of Iberia into continental blocks and micro-plates such as the Ebro Block and Landes High (introduced in Tugend et al., 2014; 2015a) provides a more robust and dynamic approach to investigate temporal variations in strain partitioning along the Iberia-Eurasia plate boundary. Rigid plate tectonic reconstructions can often lead to inappropriate overlap of continental domains and a limited ability to make comparisons with results obtained from independent geological and geophysical observations. This study presents the first deformable plate tectonic reconstruction of the area allowing for the investigation of deformation experienced within continental domains based on previously published, and newly presented plate kinematic models. The preferred

kinematic model suggests oblique rifting within the Bay of Biscay from the Jurassic to Early Aptian (~ 125 Ma) in agreement with previous reconstructions made by Nirrengarten et al. (2018). However, an independent assessment of the Landes High plate kinematics conducted herein, and its interplay with the Ebro Block provide an improved model of the Bay of Biscay plate kinematics based on regional scale crustal thickness correlations with gravity inversion estimates and observations from seismic and well data. Considering the models tested herein, models that exclude the Landes High as an independent continental block often underestimate the amount of deformation experienced within the Bay of Biscay. This observation also suggests that kinematic models proposing subduction within the Pyrenean realm or pure strike slip along the Northern Pyrenean Fault are highly unlikely due to their inability to account for the deformation experienced within the Bay of Biscay, in addition to their limited ability to reconcile geological and geophysical observations (Barnett-Moore et al., 2016; Tavani et al., 2018). Moreover, the results of this study suggest that continuing to modify the poles of rotation for Iberia using updated oceanic magnetic anomaly and paleomagnetic constraints is not the only approach when continuing to address problems related to the Mesozoic plate kinematics of Iberia. In contrast, giving more detailed consideration to the kinematics of continental blocks and their interplay with major lithospheric boundaries throughout Iberia using methodologies such as deformable plate tectonic reconstructions and numerical models may be a more advantageous approach moving forward to address problems related to Iberian plate kinematics. Integrating results calculated by deformable plate models with observations from independent datasets and numerical models is important to understand the development of present-day crustal structure associated with lithospheric heterogeneities and depth-dependent deformation. Considering the current state of deformable

plate modeling capabilities, these phenomena are not easily understood using deformable plate models alone.

4.5 Conclusions

The deformable plate tectonic models presented in this work have provided insight into the plate kinematic evolution of the Bay of Biscay-Parentis rift system. A comparison of deformable plate models with previously published and newly presented gravity inversion results, and interpretations from regional seismic and well data, provided a good metric for investigating the evolution of the Bay of Biscay. The main findings of this work include:

1. Oblique extension and strain partitioning prior to the opening of the Bay of Biscay were largely influenced by the independent plate kinematics of the Landes High and its interplay with the Ebro Block. As suggested by previous studies using alternative methodologies and datasets, the preferred plate kinematic model suggests that models proposing subduction in the Pyrenees or pure strike slip motion along the North Pyrenean Fault are very unlikely.
2. Deformable plate models that include the Landes High produce a region of thinned crust centered within the Parentis Basin, analogous to that observed present day. Thus, the formation of the Parentis Basin is considered to be largely dependent on the Landes High kinematics.
3. Based on the deformable modelling results presented, the Ebro Block is interpreted to have minimal impact on the deformation experienced within the Bay of Biscay in contrast to its significant influence eastward within the Pyrenean realm.

4. Deformable plate models that consider the Le Danois High as a rigid independent continental block appear to over-estimate the amount of regional deformation experienced along the North Iberian margin as a result of its independent kinematics. Moreover, continental blocks similar in size to that of the Le Danois High (~ 3000km^2) appear to be at the limit of continental block sizes that should be included within deformable models built in GPlates.
5. Major lithospheric boundaries such as the Ventaniella Fault and Armorican Shear Zone appear to have played a significant role in rift segmentation and shaping the present day crustal architecture of the Bay of Biscay. It is likely that these lithospheric boundaries follow inherited/pre-existing Variscan and Late Carboniferous-Early Permian structural trends.
6. More generally, as opposed to assessing the kinematics of large rigid tectonic plates during time frames where oceanic magnetic anomaly constraints are lacking, considering the independent kinematics of continental blocks and their impact on the deformation experienced along the Iberia-Eurasia plate boundary represents an alterative approach moving forward to develop a more detailed understanding of strain partitioning along the Iberia-Eurasia plate boundary.

Chapter 5

5 The role of the Ebro Block on the deformation experienced within the Pyrenean realm: insights from deformable plate tectonic models

Most of the material presented in this chapter can be found in its published version *"King, M. T., Welford, J. K., & Tugend, J. (2023). The role of the Ebro Block on the deformation experienced within the Pyrenean realm: insights from deformable plate tectonic models. Journal of Geodynamics, 101962. https://doi.org/10.1016/j.jog.2023.101962".*

5.1 Introduction

Reconciling the kinematics of large tectonic plates and their evolution during the opening and closing of ocean basins has served as a frequent and effective method for reconstructing the positions and geometries of previous supercontinents (Bullard et al., 1965; Roest and Srivastava, 1991; Seton et al., 2012; Matthews et al., 2016). Considering recent plate reconstructions of the North Atlantic Ocean (Barnett-Moore et al., 2018; Nirrengarten et al., 2018; Peace et al., 2019b), an increasing emphasis has been given to understanding the kinematics of micro-plates (e.g. Iberia) and smaller continental blocks (e.g. Galicia Bank and Flemish Cap), also referred to as continental

ribbons (Péron-Pinvidic and Manatschal, 2010), in order to more accurately rectify the temporal variations in strain partitioning experienced along its offshore margins. Amongst all reconstructions that accompany Atlantic and/or Western Mediterranean plate motions, the kinematics of Iberia and surrounding continental blocks continue to serve as a heavily disputed topic of debate (Barnett-Moore et al., 2016, 2017; van Hinsbergen et al., 2017). As a consequence, the plate kinematics of the Pyrenean realm, a present day mountain belt situated between Spain and France (Figure 1.6), continues to be investigated in accordance with geological field observations, crustal restorations, and interpretations made from crustal and lithospheric-scale geophysical surveys.

The Pyrenean, Bay of Biscay and Central Iberian rift systems have been demonstrated to have a complex geological history due to their segmentation into several rift arms and diachronous formation (Tugend et al., 2015a). The present-day crustal structure of the Pyrenees has been interpreted to encompass the fossil remnants of a hyperextended rift system (Jammes et al., 2009; Lagabrielle et al., 2010; Roca et al., 2011; Masini et al., 2014; Tugend et al., 2014; Saspiturry et al., 2020), formed via Atlantic and Tethyan related tectonic events, that underwent subsequent inversion and uplift as a result of compressional deformation experienced during the Pyrenean Orogeny. Based on geological field observations within the Pyrenees, significant crustal thinning and mantle exhumation are considered to have initiated during the Aptian-Albian (Lagabrielle and Bodinier, 2008; Jammes et al., 2009; Lagabrielle et al., 2010; Masini et al., 2014; Tugend et al., 2014; Saspiturry et al., 2019; Ducoux et al., 2021), leading to the establishment of the Pyrenean pre-orogenic template and progressive cessation of rift-related deformation during the Cenomanian. Although the existence of hyperextended crust and exhumed mantle domains within

the Pyrenean pre-orogenic template is generally well agreed upon, the nature of Late Permian to Cretaceous tectonic events leading to its formation are still debated. In particular, attempts at establishing the link between interpretations made from regional plate kinematic models and field observations have proven to be problematic. Discrepancies include the crustal evolution of continental blocks such as the Ebro Block and the general kinematics along the Iberia-Eurasia plate boundary due to uncertainties related to the interpretation of offshore M-series magnetic anomalies (Nirrengarten et al., 2017; Causer et al., 2019; Szameitat et al., 2020) and paleomagnetic data collected throughout Iberia (Neres et al., 2012; Barnett-Moore et al., 2016, 2017).

The majority of global plate reconstruction studies (Seton et al., 2012; Matthews et al., 2016) and original reconstructions focussed on Iberia (Olivet, 1996; Sibuet et al., 2004; Vissers and Meijer, 2012; Barnett-Moore et al., 2016; van Hinsbergen et al., 2020) have been conducted with Iberia acting as a single, rigid plate. In light of modern rift domain mapping studies throughout Iberia (Roca et al., 2011; Tugend et al., 2014) and the call for attention to the kinematics of continental blocks such as the Ebro Block and Landes High (Tugend et al., 2015a), recent reconstructions have treated Iberia as a collection of rigid continental blocks (Nirrengarten et al., 2018; Angrand et al., 2020; Angrand and Mouthereau, 2021; Frasca et al., 2021). Furthermore, recent developments in plate reconstruction software have provided the opportunity to build deformable plate tectonic reconstructions (Ady and Whittaker, 2018; Gurnis et al., 2018). Using the GPlates software (Müller et al., 2018), deformable plate models have proven to be advantageous for investigating the timing and extent of deformation experienced within continental domains and the kinematics of continental blocks throughout the North Atlantic (Peace et al., 2019b). Additional insight on these phenomena were provided via locally updated models

after Peace et al. (2019) along the West Iberian margin in Chapter 3 and within the Bay of Biscay in Chapter 4. The capability of accounting for temporal variations in dilatational strain rate, crustal thickness and stretching (beta) factors also allows for more direct comparisons between plate reconstructions and independent observations. Some commonly used examples include comparisons with crustal thickness estimates derived using gravity inversion, and the timing of deformation inferred by crustal restorations and borehole-constrained seismic sections.

In this study, deformable plate tectonic reconstructions are used to investigate the most recent plate kinematic models of the Pyrenees (Nirrengarten et al., 2018; Angrand et al., 2020; Angrand and Mouthereau, 2021; Frasca et al., 2021) and newly presented models shown herein. A primary objective of this work is to investigate the role of the Ebro Block, a previously recognized continental block situated between the Iberian Ranges and the Pyrenees (Tugend et al., 2014, 2015a), on the pre-Alpine deformation experienced within the Pyrenean realm. In addition, the interplay of the Ebro Block with the kinematics of Iberia and the Landes High are assessed in order to gain a better understanding of the deformation experienced throughout the Pyrenees, Central Iberia, and Bay of Biscay using a deformable plate modelling approach. Our goal is not to discard previously published plate kinematic models of Iberia, but to quantitatively assess their consequences when a deformable plate modelling approach is implemented.

5.2 Methodology

In this study, deformable plate tectonic reconstructions, built using GPlates 2.2 (Müller et al., 2018), are used to investigate previously published and newly presented plate kinematic models of the Pyrenees using the workflows discussed in Chapter 2. In particular, the kinematics

of the Ebro Block, a continental block previously recognized within the Pyrenees (Tugend et al., 2014, 2015a; Nirrengarten et al., 2018; Angrand et al., 2020; Angrand and Mouthereau, 2021), are investigated to gain a better understanding of the block's impact on the orientation of regional stress directions and partitioning of deformation within the Pyrenean realm prior to the Pyrenean Orogeny. The kinematic and crustal thickness results of each model are then compared to one another and correlated with geological and geophysical observations in order to gain a better understanding of their implications on the regional Mesozoic deformation experienced within the Pyrenees, Central Iberia, and Bay of Biscay.

Although our goal is to investigate the kinematic role of the Ebro Block, a decision also had to be made regarding the plate kinematics of Iberia itself (see Chapter 2 for a detailed summary). Considering previously published plate models that suggest a 35 degree rotation of Iberia during the Aptian and resultant subduction within the Pyrenees (Sibuet et al., 2004; Gong et al., 2008; Vissers and Meijer, 2012; van Hinsbergen et al., 2020), none of these models have considered the Ebro Block as an independent continental block. Furthermore, models that suggest Mesozoic subduction within the Pyrenees also demonstrate a conflict with observations from geological field mapping such as the occurrence of inverted extensional structures and thick Albo-Cenomanian syn-rift sequences indicative of an Early Cretaceous extensional setting, rather than a compressional one (Lagabrielle and Bodinier, 2008; Tugend et al., 2014; Saspiturry et al., 2021). As a result, the kinematic models of Iberia tested herein all suggest an approximate 20 degree rotation of Iberia during the Early Cretaceous and treat the Ebro Block as an independently moving continental block between Iberia and Europe (Nirrengarten et al., 2018; Angrand et al., 2020; Frasca et al., 2021). Similar to the scenario suggested in recent plate reconstruction studies that

include Iberia (Barnett-Moore et al., 2018; Le Breton et al., 2021), our modelled scenario permits Early Cretaceous extension or transtension to be experienced along the Iberia-Eurasia plate boundary and also mitigates any Early Cretaceous ill-supported compression and subsequent subduction between Iberia and Europe.

5.2.1 Model selection and setup

In this study, six deformable plate models, four previously published and two newly presented, that encompass the Pyrenees, Central Iberia, and Bay of Biscay, are considered (Figure 5.1). Model 1 is identical to deformable plate model 1 presented in Chapter 4. Model 2 is the same plate kinematic model as Nirrengarten et al. (2018). Model 3 represents the Late Permian (270 Ma) to Mid-Cretaceous reconstruction of Iberia from Angrand et al. (2020). Model 4 is identical to the 200 Ma to present day reconstruction of Iberia from Frasca et al. (2021). Models 5 and 6 are newly presented models that are built off of the preferred plate model for the Bay of Biscay (Chapter 4). The motivation for models 5 and 6 is to test two different kinematic scenarios for the Ebro Block from the Triassic (250 Ma) to present day and its interplay with the Landes High. Additionally, model 6 is also used to test the spatial-temporal extent of rift-related deformation within Central Iberia. Similar to previous deformable plate modelling studies focussed throughout the offshore margins of the North Atlantic (Peace et al., 2019b; King et al., 2020, 2021), a 30 km initial crustal thickness estimate is implemented at the start time of each model. Although crustal thicknesses were likely to be variable prior to and during the collapse of the Variscan Orogeny, a crustal thickness of 30 km is chosen for consistency with previous work. Considering the variability in model start times (i.e. the exclusion of Triassic related deformation in models 1, 2

and 4), an initial 30 km crustal thickness estimate is also chosen for consistency between models and represents the minimum crustal thickness expected prior to Triassic rifting based on the potential for minor crustal thinning caused by orogenic collapse and rifting during the Late Permian - Triassic transition (Montadert et al., 1979; Saspiturry et al., 2019; Angrand et al., 2020). A GPlates density level 8 (0.15625°) mesh point spacing is used to calculate crustal thicknesses for each deformable plate model. This value is deemed appropriate based on the sampling between mesh points used to calculate crustal thicknesses and computational feasibility, however, finer mesh point spacings were also tested and yielded similar results.

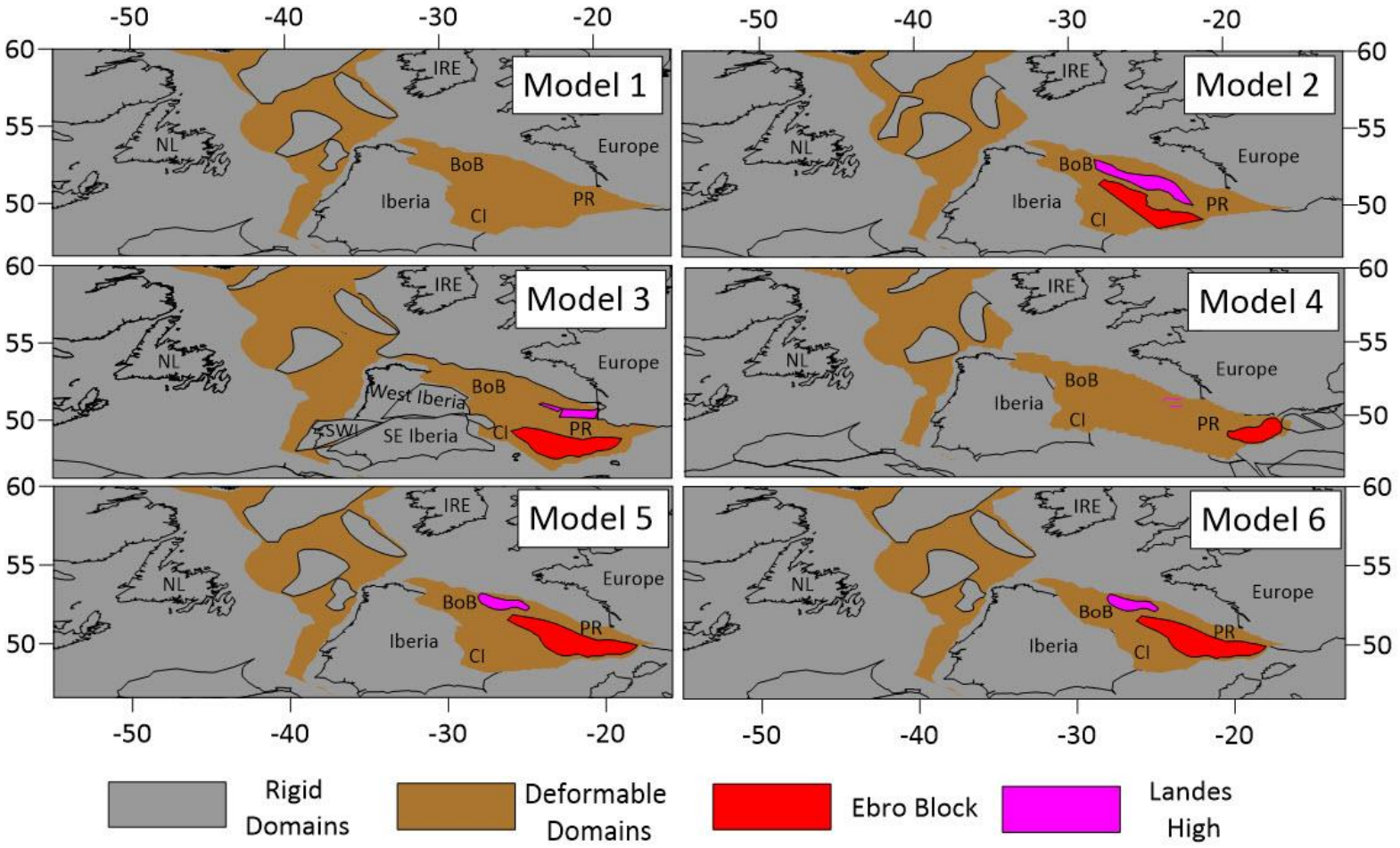

Figure 5.1 Reconstruction of models 1 to 6 relative to Europe at the start time for each model. BoB = Bay of Biscay, CI = Central Iberia, IRE = Ireland, NL = Newfoundland, PR = Pyrenean Realm, SWI = Southwest Iberia.

5.2.2 Model design and implementation of previously published rigid plate models

Deformable plate models, built via the design of topological networks in GPlates (Gurnis et al., 2018), are constructed using topological plate boundaries representing the extent of deformable domains and optional features placed within the interior of deformable regions such as rigid continental blocks. In this study, the exterior deformable plate boundary used for each model is the edge of continental crust (ECC) originally implemented by Peace et al. (2019) and modified within the Bay of Biscay in Chapter 4. The interior deformable boundary for all models is the necking line originally defined by Tugend et al. (2014) within the Bay of Biscay and Pyrenees that was later extended throughout the rest of the southern North Atlantic by Nirrengarten et al. (2018).

In order to evaluate the kinematics and deformation induced by the Ebro Block using a deformable plate modelling approach, previously published rigid plate reconstructions considered herein require the addition of topological networks needed to evaluate deformation within specified continental domains. For model 3, the model boundaries required to build a topological network are assigned plate IDs according to the partitioning of Iberia as specified in the previously published reconstruction (Figure 5.2). Since model 3 encompasses a more partitioned Iberian plate (i.e. Ebro Block, southeast/southwest Iberia and west Iberia) in comparison to all other models, segments of the necking line throughout Iberia in model 3 are partitioned and assigned plate IDs according to the plate ID of their specific Iberian micro-plate.

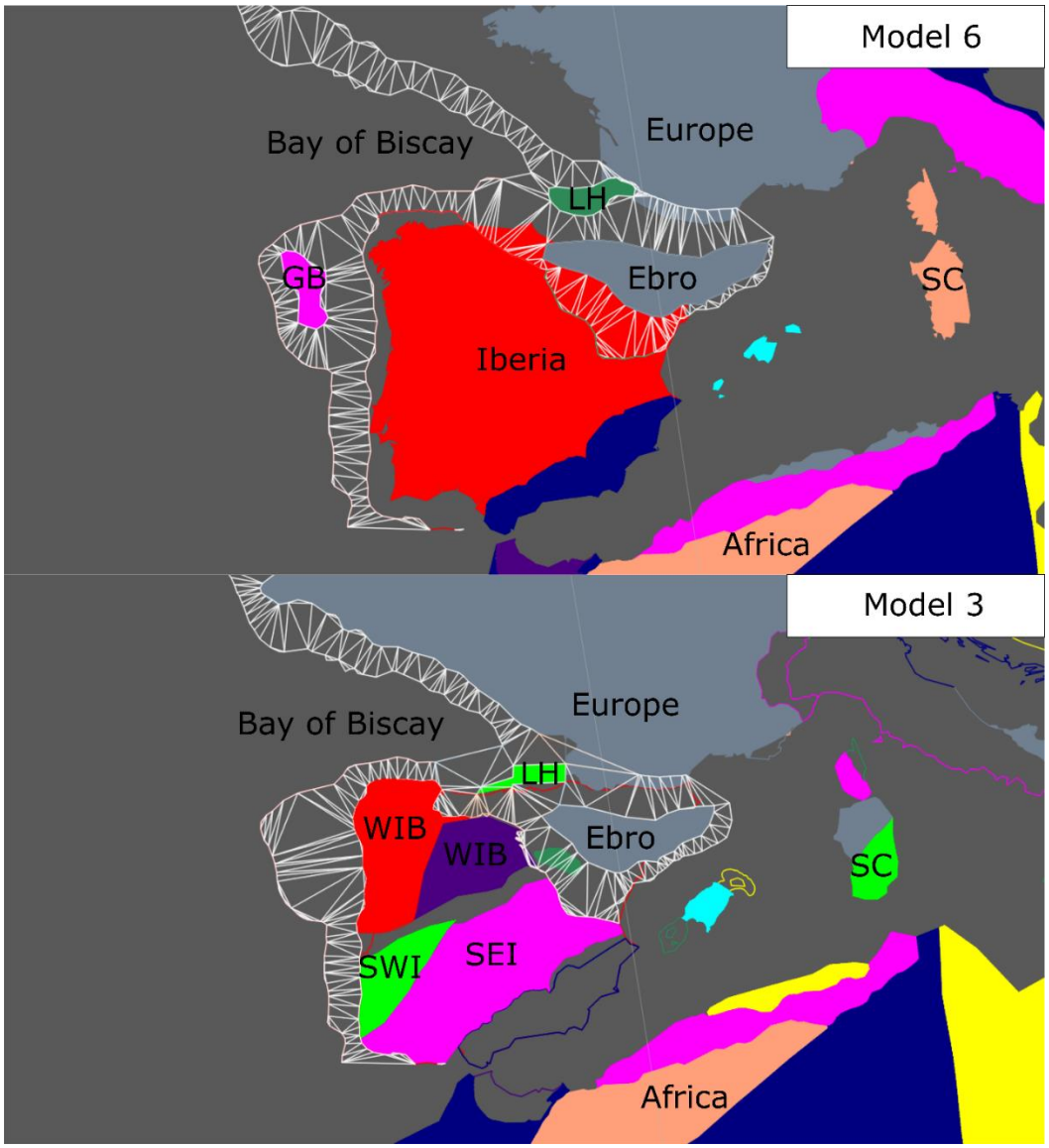

Figure 5.2 Present day definition of topological networks and overall plate tectonic framework for models 6 (this study) and 3 (Angrand et al., (2020) using orthographic projection. Rigid plate polygons placed within the interior and along the exterior of deformable regions (shown by the triangulation mesh) are filled in with solid colours. GB = Galicia Bank, LH = Landes High, SC = Sardinia-Corsica, SEI = Southeast Iberia, SWI = Southwest Iberia, WIB = West Iberia.

5.2.3 Model Details

For the six constructed deformable plate models of the Pyrenees, the key variabilities between each model are the poles of rotation and structure of the Iberian plate, and the poles of rotation and geometries for the Ebro Block and Landes High.

Model 1 is identical to model 1 in Chapter 4. The motivation for this model is to simulate a scenario where no continental blocks are considered within the Bay of Biscay or Pyrenees. Model 2 is identical to that presented in Nirrengarten et al. (2018). The motive for this model is to examine the impact of the Landes High and Ebro Block geometries and kinematics from Nirrengarten et al. (2018) on the Pyrenean realm. The Iberia poles of rotation for models 1 and 2 are from Nirrengarten et al. (2018) and the model time frames are from 200 Ma to present day. Model 3 represents the reconstruction of Iberia from Angrand et al. (2020). In model 3, the Ebro Block is considered as a single continental block whose kinematics are primarily responsible for the deformation experienced throughout the Ebro-Eurasia and Ebro-Central Iberia strike slip systems (Angrand et al., 2020). Model 4 is identical to the reconstruction of Iberia from Frasca et al. (2021). The motivation for including this model is to test the impact of using strike-slip corridors as plate kinematic inputs on the Pyrenean realm using a deformable plate modelling approach and to compare its results with other recently published plate models of Iberia from Nirrengarten et al. (2018) and Angrand et al. (2020) (models 2 and 3, respectively). In model 4, the Ebro Block is included as an independent rigid continental block using the geometry and poles of rotation from Frasca et al. (2021), however, the Landes High is not. Moreover, the Landes High in Frasca et al. (2021) is included as a pair of rigid necking lines that move relative to Europe from the Aptian

(126 Ma) to Cenomanian (97 Ma). Thus, the two Landes High necking lines (represented as topological lines in GPlates) are included within the model 4 deformable mesh.

Models 5 and 6 are newly presented models that are built off of the preferred Bay of Biscay model from Chapter 4 to encompass Triassic deformation (250 Ma to 200 Ma) and new geometry and kinematics for the Ebro Block. The motivation for models 5 and 6 is to study the impact of regional extension directions within the Pyrenees and their implications on the deformation experienced within the Pyrenean realm and Central Iberia. To do this, models 5 and 6 test two different scenarios for the Cretaceous kinematics of the Ebro Block, which largely control the orientation of regional extension directions within the Pyrenean realm and Central Iberia, a topic that has been highly debated within previous plate kinematic (Barnett-Moore et al., 2016) and crustal restoration studies (Lescoutre et al., 2021). Model 5 is designed to simulate Earliest Cretaceous (145 Ma) to Cenomanian (97 Ma) north-south extension within the Pyrenees induced by the southward motion of the Ebro Block within the Pyrenean realm. In contrast, model 6 is designed to simulate a transtensional model of the Pyrenees and Central Iberia throughout the Cretaceous. The geometry of the Ebro Block used in models 5 and 6 is modified after Angrand et al. (2020) in order to extend the Ebro Block further westward near the western extent of the Basque-Cantabrian Basin, as suggested by previous rift domain mapping studies (Tugend et al., 2014; Cadenas et al., 2018). The necking line (interior deformable plate boundary) used in model 6 is from Cadenas et al. (2018), and is a modified version of the necking line from Tugend et al. (2014) that proposes the Ventaniella Fault as the necking line boundary along the North Iberian margin and Cantabrian interior (Figure 1.5). In addition, model 6 is the only model where separate poles of rotation are assigned to the Central Iberian necking line, allowing the Central Iberian

interior to expand and contract with time relative to the kinematics of the Ebro Block. The motive for this approach is to test the impact of a spatial-temporal evolving Central Iberian interior on the amount of contraction observed within Central Iberia. This contraction is caused by Iberia's rotation towards the southward moving Ebro Block during the Aptian-Albian, a phenomenon documented in previous reconstructions (Angrand and Mouthereau, 2021), but ill-supported by independent observations (Salas et al., 2001; Rat et al., 2019).

Model #	Start Time	Iberia Poles	Ebro Block Included	Ebro Block Geometry	Ebro Block Poles	Landes High Included	Landes High Geometry	Landes High Poles	Necking Line Geometry
1	200 Ma	Nirrengarten et al. (2018)	No	NA	NA	No	NA	NA	Tugend et al. (2014)
2	200 Ma	Nirrengarten et al. (2018)	Yes	Nirrengarten et al. (2018)	Nirrengarten et al. (2018)	Yes	Nirrengarten et al. (2018)	Nirrengarten et al. (2018)	Tugend et al. (2014)
3	270 Ma	Angrand et al. (2020)	Yes	Angrand et al. (2020)	Angrand et al. (2020)	Yes	Angrand et al. (2020)	Angrand et al. (2020)	Tugend et al. (2014)
4	200 Ma	Frasca et al. (2021)	Yes	Frasca et al. (2021)	Frasca et al. (2021)	Yes	Frasca et al. (2021)	Frasca et al. (2021)	Frasca et al. (2021)
5	250 Ma	Nirrengarten et al. (2018)	Yes	This study	This study	Yes	King et al. (2021)	This study	Tugend et al. (2014)
6	250 Ma	Nirrengarten et al. (2018)	Yes	This study	This study	Yes	King et al. (2021)	This study	Cadenas et al. (2018)

Table 5.1 Description of the poles of rotation and geometries of Iberia and various continental blocks used to construct each deformable plate model considered.

5.3 Results

Differences in the kinematics and geometries of Iberia, the Ebro Block, and the Landes High and the spatial-temporal extent of deformable plate models produce highly variable temporal

variations in crustal thickness within the Bay of Biscay, Central Iberia, and Pyrenean realm. Temporal variations in crustal thickness are analyzed from the start time of each model until Cenomanian time (~ 97 Ma), when rift-related deformation is interpreted to have ended and the pre-orogenic template of the Pyrenees is considered to have been achieved.

5.3.1 Kinematic evolution and resulting crustal thicknesses

5.3.1.1 Late Permian and Triassic (270 - 200 Ma)

The role of Late Permian and Triassic related deformation on the stratigraphic architecture of basins has been highlighted by several recent studies within the Pyrenees (Saspiturry et al., 2019; Angrand et al., 2020; Lagabrielle et al., 2020). Both models 1 and 2 exclude Late Permian and Triassic related deformation. Thus, a constant crustal thickness along the Iberia-Eurasia plate boundary at 200 Ma is observed in models 1 and 2 (Figure 5.3). In model 3, the reconstruction of Iberia from Angrand et al. (2020), minor crustal thinning (5 km or less) is observed between the Ebro Block and Eurasia and within most of the Bay of Biscay. The largest amounts of Late Permian and Triassic crustal thinning in model 3 are calculated between the Ebro Block and southwest Iberia (~ 10 km of thinning) and in the vicinity of the Goban Spur and northwest Iberia (~ 10-15 km of thinning). Model 4, the reconstruction of Iberia from Frasca et al. (2021), also excludes Late Permian and Triassic related deformation. Therefore, a constant crustal thickness of 30 km is observed along the Iberia-Eurasia plate boundary and within Central Iberia. Models 5 and 6 demonstrate similar results following Triassic related deformation, with minimal amounts of crustal thinning (5 km or less) experienced between the Ebro Block and Eurasia aside from a

localized region of thinned crust (10 km or less) observed between the Landes High and Ebro Block.

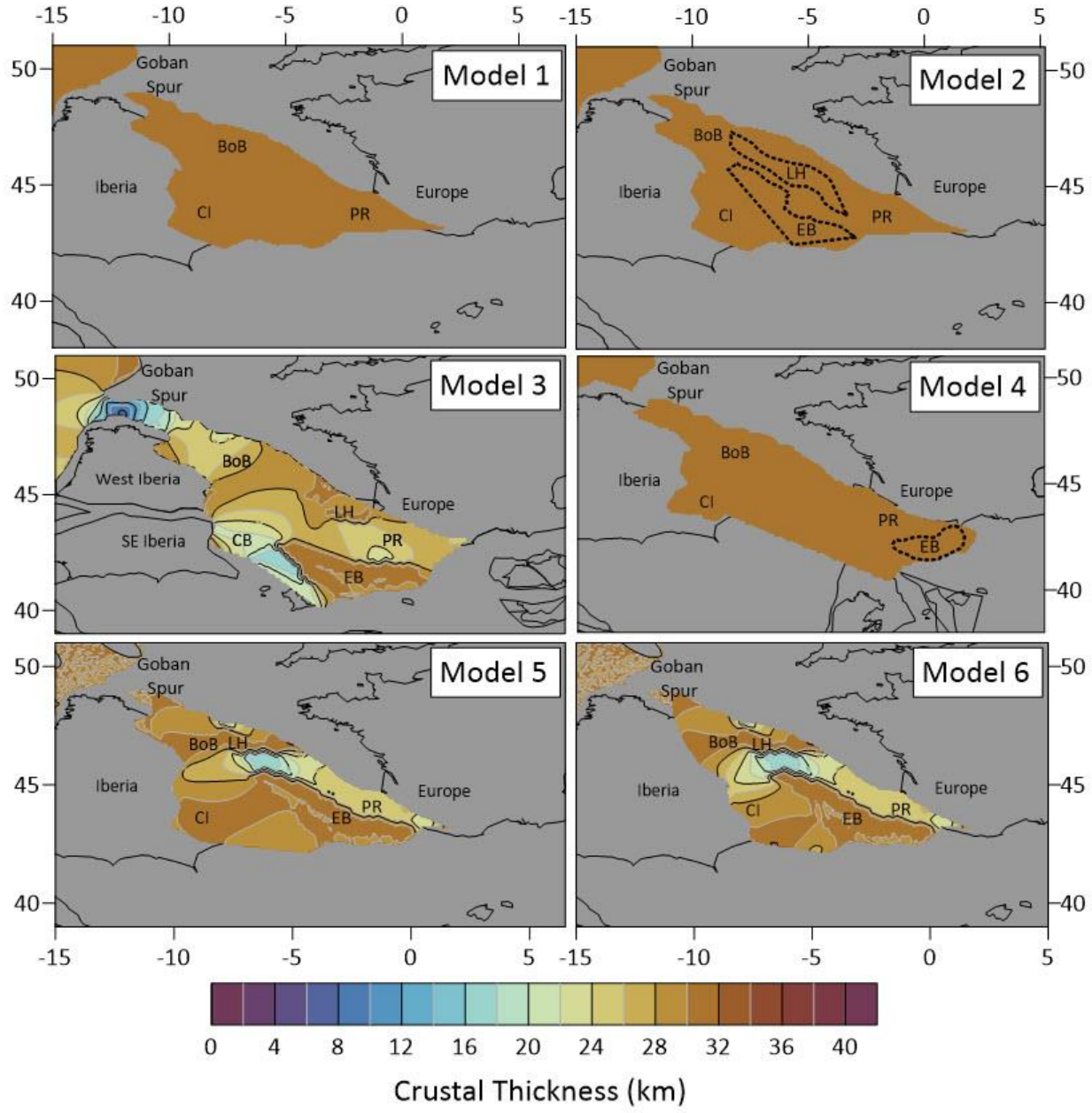

Figure 5.3 Crustal thickness results for models 1 to 6 at 200 Ma. All models are reconstructed relative to Europe. The black dashed polygons in models 2 and 4 represent the geometries of the

Ebro Block and Landes High (not included in model 4) implemented in each model. BoB = Bay of Biscay, CI = Central Iberia, EB = Ebro Block, LH = Landes High, PR = Pyrenean Realm.

5.3.1.2 Pre-Cretaceous (prior to 145 Ma)

Near the end of the Jurassic (150 Ma), each model experiences variable amounts of crustal thinning along the Iberia-Eurasia plate boundary (Figure 5.4). In model 1, very little crustal thinning is experienced along the Iberia-Eurasia plate boundary by 150 Ma, as regional crustal thicknesses range from about 25 to 30 km. For model 2, similar crustal thicknesses to those calculated by model 1 are observed aside from regions within the western Bay of Biscay that experienced slightly more crustal thinning (crust ~ 20 to 25 km thick). In model 3, crustal thicknesses between the Ebro Block and Eurasia and within the Bay of Biscay range from approximately 15 to 25 km. In areas south of the Ebro Block, crustal thicknesses range from 10 to 15 km, with the thinnest regions of crust (~ 10 km) observed within the southeastern portion of Central Iberia. In model 4, very little crustal thinning is observed as crustal thicknesses range from about 25 to 30 km throughout the Bay of Biscay, Pyrenees and Central Iberian domains. Model 5 and model 6 indicate near identical crustal thickness results near the end of the Jurassic. Similar to model 2, significant crustal thinning is observed within the Bay of Biscay for both models and crustal thicknesses within the Pyrenean realm range from approximately 15 to 25 km. Within Central Iberia, crustal thicknesses calculated by model 5 range from approximately 25 to 30 km, slightly different than model 6 which exhibits a region of thinner crust (~ 15 to 20 km thick) within the southeastern extent of Central Iberia.

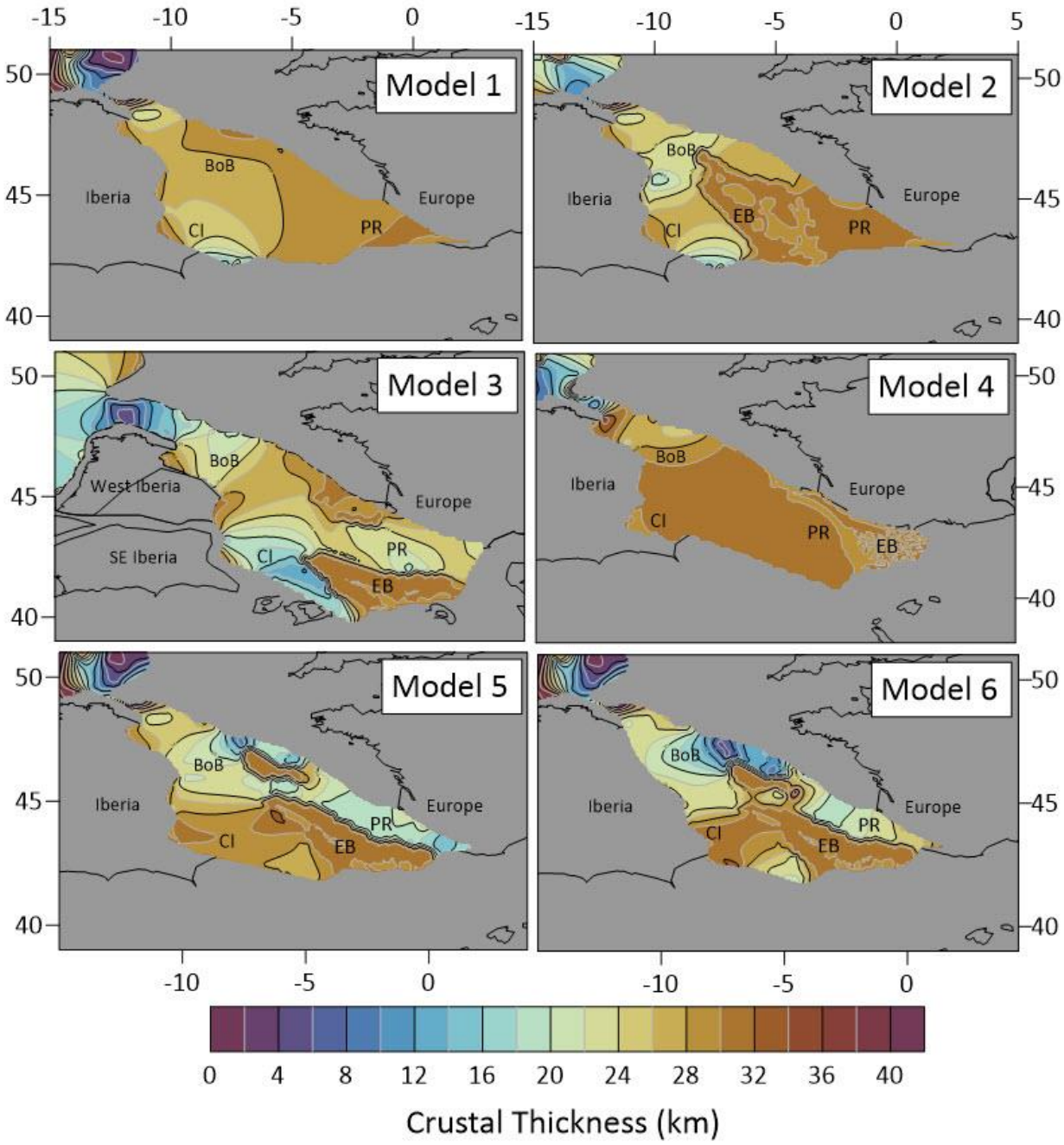

Figure 5.4 Crustal thickness results for models 1 to 6 at 150 Ma. All models are reconstructed relative to Europe. BoB = Bay of Biscay, CI = Central Iberia, Ebro Block, PR = Pyrenean Realm.

5.3.1.3 Early Cretaceous (145 – 130 Ma)

The early to mid-Cretaceous represents a time period when the kinematics of Iberia and surrounding continental blocks have been highly debated (Gong et al., 2008; Jammes et al., 2009; Tugend et al., 2015a; Barnett-Moore et al., 2016; Nirrengarten et al., 2018; Tavani et al., 2018; Frasca et al., 2021; Lescoutre et al., 2021). As expected, this time period also corresponds to the largest variabilities in crustal thickness results calculated by deformable plate models. Considering the results of each model during the Barremian (~ 130 Ma) (Figure 5.5), crustal thicknesses calculated by model 1 throughout the Bay of Biscay, Pyrenees, and Central Iberia remain similar to those observed during the Late Jurassic (150 Ma) at approximately 20 to 30 km. Model 2 demonstrates the continued development of significant crustal thinning along the North Iberian and Armorican margins within the Bay of Biscay (~ 8 to 15 km thick), however, crustal thicknesses within the Pyrenean realm range from approximately 30 to 40 km. Within the southeastern and northwestern regions of Central Iberia, crustal thicknesses calculated by model 2 range from approximately 10 to 15 km and between these two regions, an area of thicker crust (~ 15 to 20 km thick) is observed. In model 3, crustal thicknesses within the Pyrenees and Central Iberia are nearly identical to those observed during the Late Jurassic (150 Ma). Within the Bay of Biscay, crustal thicknesses in the vicinity of the North Iberian and Armorican margins range from approximately 25 to 35 km and about 15 to 25 km along the Northwest Iberian and Western Approaches margins. Crustal thicknesses calculated by model 4 at 130 Ma are nearly identical to those at 150 Ma. The main differences are the additional crustal thinning within the Bay of Biscay (crust ~ 20 to 25 km thick) and minimal thickening (crust ~ 30 to 35 km thick) within the Pyrenean realm and Central Iberia. Model 5 exhibits similar crustal thickness estimates in the Bay of Biscay as observed in

model 2. However, within the Pyrenean realm, significant crustal thinning (~ 5 to 10 km thick) is observed within the eastern Pyrenees and crustal thicknesses ranging from 10 to 20 km are seen within the western and central Pyrenees. Within Central Iberia, a wide region for which the crust gets gradually thinner towards the Bay of Biscay is observed with crustal thicknesses ranging from 20 to 25 km. Similar to model 5, crustal thicknesses calculated by model 6 within the Bay of Biscay are near identical to those calculated by model 2. In addition, crustal thicknesses calculated within Central Iberia by model 6 are also very similar to those calculated by model 2. Within the Pyrenean realm, between the Landes High and Ebro Block, crustal thicknesses range from approximately 20 to 35 km. Near the northeastern extents of the Ebro Block, crustal thicknesses are slightly thinner, ranging from about 15 to 20 km.

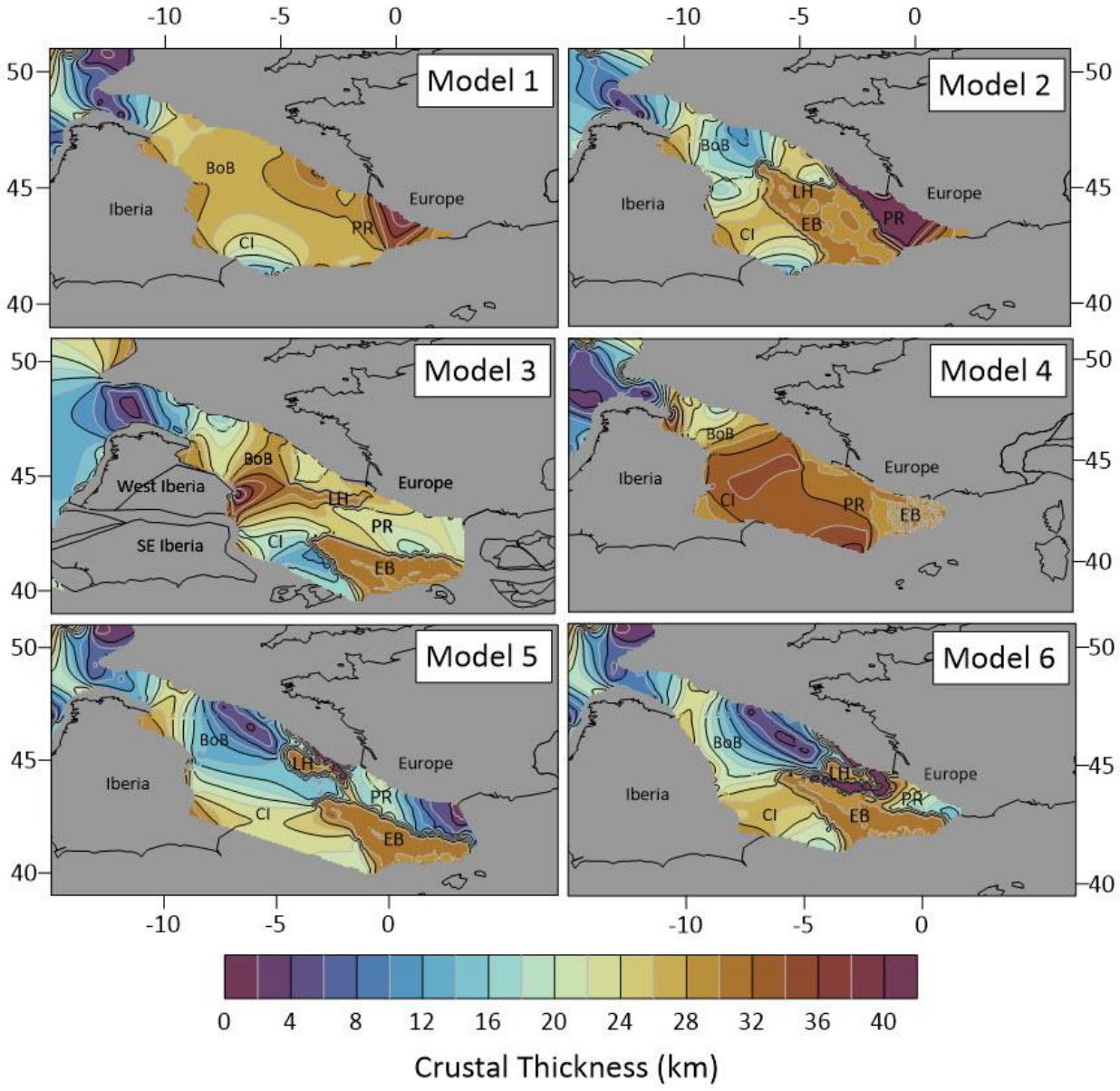

Figure 5.5 Crustal thickness results for models 1 to 6 at 130 Ma. All models are reconstructed relative to Europe. BoB = Bay of Biscay, CI = Central Iberia, EB = Ebro Block, LH = Landes High, PR = Pyrenean Realm.

5.3.1.4 Early to Mid-Cretaceous (130 – 110 Ma)

During the latest Aptian (~ 110 Ma), the Bay of Biscay began to open via sea-floor spreading, which led to the migration of significant rift-related deformation into the Pyrenean realm (Montadert et al., 1979; Thinon et al., 2003; Sibuet et al., 2004; Tugend et al., 2015a; Nirrengarten et al., 2018). Considering crustal thicknesses calculated by model 1 during this time period (Figure 5.6), crustal thicknesses along the North Iberian margin and Armorican margin vary regionally from approximately 30 to 40 km, with gradually thinner areas of crust (~ 10 to 15 km thick) along the Northwest Iberian and Western Approaches margins. Within the Pyrenees, crustal thicknesses calculated by model 1 range from about 25 to 35 km and get progressively thinner (~ 20 km thick) near the eastern extent of the Pyrenees and central Iberia. In model 2, significantly thinned crust (~ 5 to 15 km) is observed along the Armorican margin and in the vicinity of the Parentis Basin (green star in model 5 panel of Figure 5.6). Along the North Iberian margin, crustal thicknesses range from approximately 15 to 30 km. Within the Pyrenees, localized regions of thinned crust (~ 10 km thick) are segmented by regions of thicker crust (~ 30 to 40 km thick) from west to east. Crustal thicknesses calculated by model 2 within Central Iberia at 110 Ma vary from about 20 to 25 km. Crustal thicknesses calculated by model 3 at 110 Ma within the Bay of Biscay are almost identical to those calculated by model 3 at 130 Ma aside from additional crustal thinning within the Parentis Basin (~ 15 to 20 km thick) and thickening along the eastern portion of the North Iberian margin and westernmost Basque-Cantabrian Basin (~ 35 to 40 km thick). Crustal thicknesses within the Pyrenees are regionally consistent ranging from 15 to 25 km. Within the southeastern region of Central Iberia, a localized area of thinned crust (~ 15 km) is observed that gradually thickens to about 20 to 25 km within areas to the east and west. In model 4, crustal

thinning continues within the western Bay of Biscay and Parentis Basin (crust ~ 15 to 25 km). In addition, the onset of significant crustal thinning (~ 5 to 15 km thick) is observed within the eastern Pyrenees while little crustal thinning (crust ~ 20 to 30 km thick) is observed within the central and western Pyrenees. Within Central Iberia, crustal thicknesses range from about 30 to 40 km. Model 5 and model 6 provide similar crustal thickness results to those of model 2 within the Bay of Biscay. Between the Ebro Block and Eurasia, several segmented regions of significantly thinned crust are observed in model 5 at 110 Ma. Within the eastern Pyrenees, crustal thicknesses are less then 10 km. An additional region of significantly thinned crust (~ 8 to 10 km thick) is observed within the Basque-Cantabrian Basin (magenta star in Figure 5.6) in model 5 and is segmented by two regions of relatively thicker crust (~ 15 to 25 km thick) aligned with the eastern and western extents of the Landes High to the north. Within Central Iberia, crustal thicknesses are quite high, ranging from approximately 40 to 50 km. Model 6 also demonstrates segmented regions of significantly thinned crust between the Ebro Block and Eurasia at 110 Ma. The most significantly thinned crust calculated by model 6 (< 10 km thick) is observed within the eastern Pyrenees along with smaller patches of thinned crust (~ 10 km thick) within the central and western Pyrenees. Within the central Pyrenees, crustal thicknesses calculated by model 6 range from about 20 to 25 km, with regions of slightly thicker crust (30 to 35 km thick) along the westernmost portion of Central Iberia.

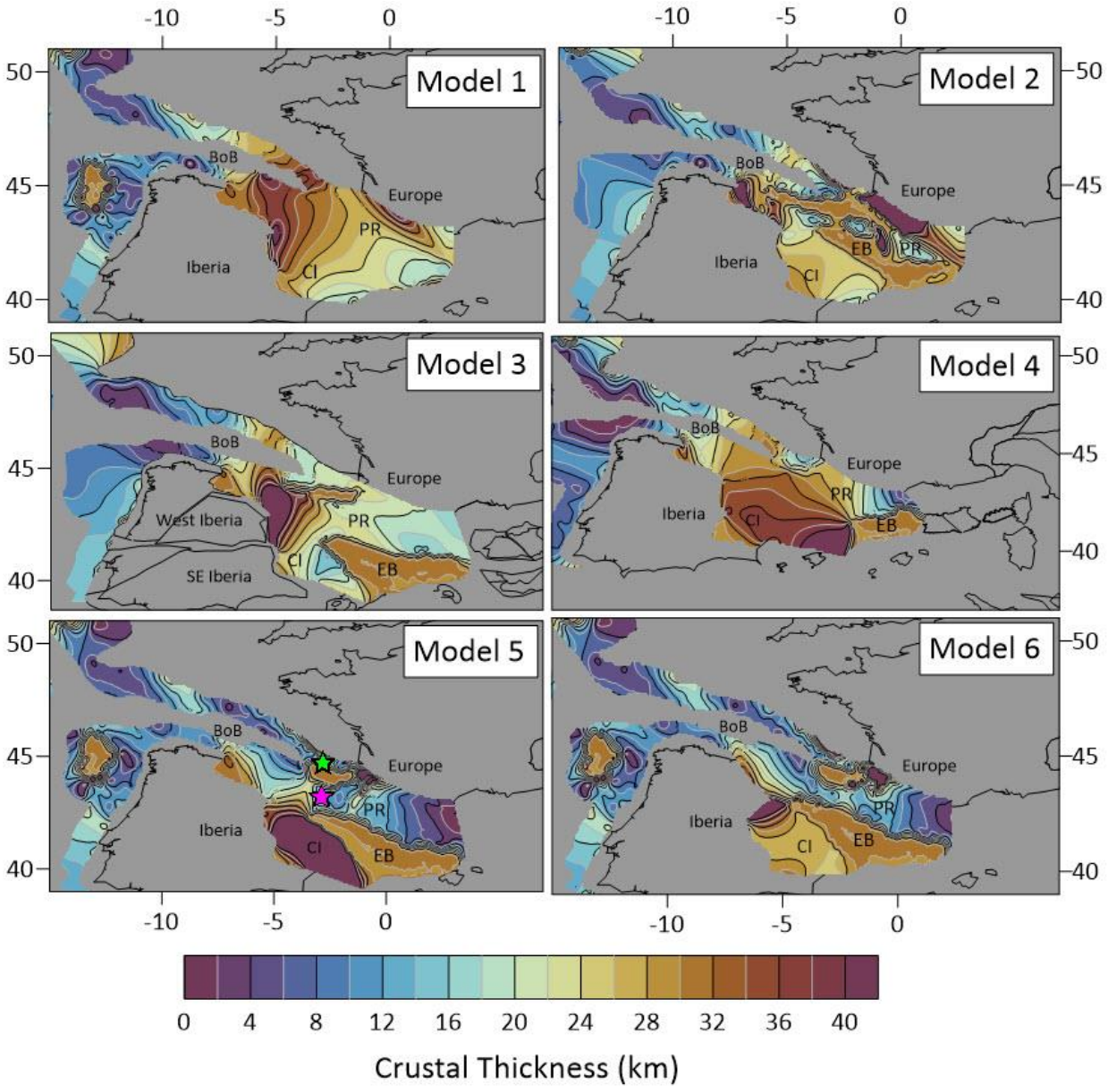

Figure 5.6 Crustal thickness results for models 1 to 6 at 110 Ma. The green star highlights the Parentis Basin and the magenta star shows the location of the Basque-Cantabrian Basin. All models are reconstructed relative to Europe. BoB = Bay of Biscay, CI = Central Iberia, EB = Ebro Block, PR = Pyrenean Realm.

5.3.1.5 Post-Aptian (110 Ma) evolution

Following the end of rift-related deformation, the pre-orogenic template of the Pyrenees is interpreted to have been achieved by Cenomanian time (Jammes et al., 2009; Lagabrielle et al., 2010; Clerc and Lagabrielle, 2014; Masini et al., 2014; Tugend et al., 2014). This is suggested by a lack of field evidence for post-Cenomanian extension, despite previous studies that suggest its continuation into the Santonian (Clerc et al., 2016). Significant variability is observed when examining the crustal thickness results of all deformable plate models during the Cenomanian (Figure 5.7). Considering models 1 and 2, crustal thickness results are largely the same as those calculated at 110 Ma aside from localized crustal thinning in model 2 within the Parentis Basin (~ 5 to 10 km thick) and within the segmented Pyrenean depocenters (~ 10 to 15 km thick), and with minor thinning (~ 15 to 20 km thick) within the southeastern portion of Central Iberia observed in model 1. Examining the Cenomanian crustal thickness results of models 3 and 4 within the Pyrenees and Bay of Biscay, in general, they are also very similar to those observed at 110 Ma. The most significant variations between models 3 and 4 at 110 Ma and 97 Ma are the regions of thickened crust (~ 30 to 50 km thick) within Central Iberia. In model 5, a wide region of significantly thinned crust (< 10 km thick) is observed within the east and central Pyrenees. Within the Basque-Cantabrian Basin (magenta star in Figure 5.7), adjacent to a region of thicker crust (15 to 20 km thick) along its eastern extent, an additional area of significantly thinned crust (5 to 10 km thick) is observed next to another region of thicker crust (20 to 30 km thick) along its western extent. Within Central Iberia, crustal thicknesses calculated by model 5 by the Cenomanian are the largest of all models tested (> 50 km thick). Similar to model 5, model 6 also exhibits a wide region of significantly thinned crust (< 10 km thick) within the eastern Pyrenees during the Cenomanian.

Adjacent to a north-northwest-south-southeast trending region of relatively thicker crust (~ 15 km thick) within the central Pyrenees (red arrow in Figure 5.7), additional regions of significantly thinned crust (~ 5 to 10 km thick) are observed within the Basque-Cantabrian Basin and areas southwest of the Landes High. Cenomanian crustal thicknesses calculated by model 6 within Central Iberia are similar to those calculated at 110 Ma, varying between 25 to 30 km aside from a localized region of thicker crust (~ 30 to 40 km thick) in the vicinity of the Cameros Basin (yellow star in the model 6 panel of Figure 5.7).

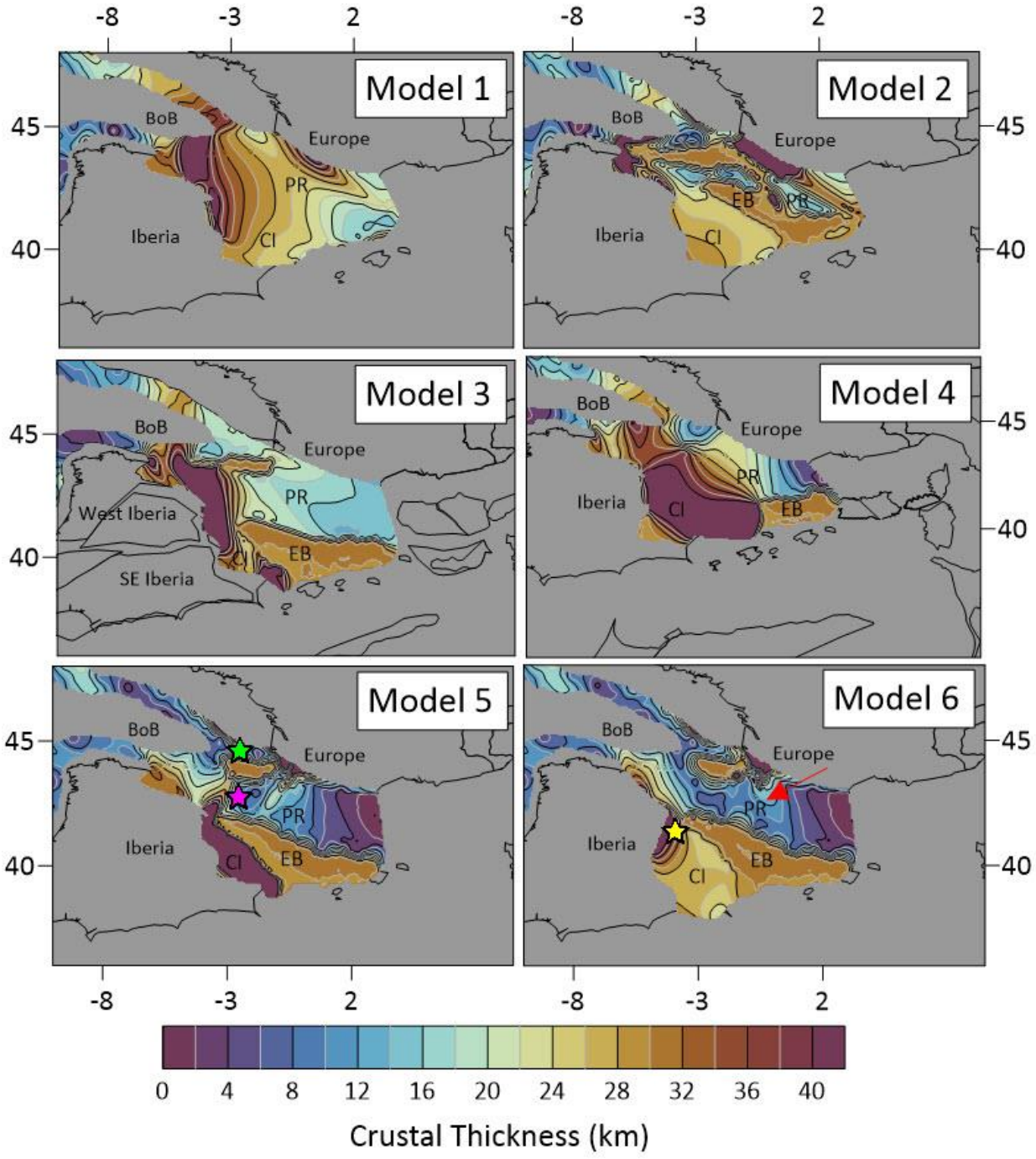

Figure 5.7 Crustal thickness results for models 1 to 6 during the Cenomanian (97 Ma). The green star highlights the Parentis Basin and the magenta star shows the location of the Basque-Cantabrian Basin. The yellow star highlights the localized region of thicker crust within the Cameros Basin.

All models are reconstructed relative to Europe. BoB = Bay of Biscay, CI = Central Iberia, EB = Ebro Block, PR = Pyrenean Realm.

5.4 Discussion

5.4.1 Comparison of deformable plate models with independent observations

The well preserved pre-Alpine fossil remnants within the Pyrenees have permitted numerous geological (Lagabrielle et al., 2010; Clerc and Lagabrielle, 2014; Vacherat et al., 2017; Tavani et al., 2018) and geophysical (Choukroune et al., 1990; Tugend et al., 2014, 2015a, 2015b; Wang et al., 2016; Chevrot et al., 2018) observations to be made that have provided insight regarding the timing and extent of deformation experienced within the Pyrenean realm. Given the wealth of geological and geophysical data collected throughout the Pyrenees, a frequent topic of discussion persists of establishing the link between interpretations made from these datasets with observations from global and regional plate reconstructions that incorporate Iberian plate kinematics. Herein, the results of models 1 to 6 are compared and contrasted with natural observations made within the Pyrenean realm, Bay of Biscay, and Central Iberia. The primary topics of interest for making comparisons are the timing and extent of deformation experienced within these regions from the Triassic to Early Cretaceous, the segmentation, size, and crustal thickness template of sedimentary basins through time, and the crustal structure of the Pyrenean pre-orogenic template.

5.4.1.1 Pyrenean Realm and Bay of Biscay

Following the collapse of the Variscan Orogeny during the Permian, a Late Triassic to Early Jurassic phase of rifting occurred within the Bay of Biscay and the Pyrenean realm (Jammes

et al., 2010b; Saspiturry et al., 2019; Duretz et al., 2020; Lagabrielle et al., 2020). As suggested in previous work (Vargas et al., 2009; Saspiturry et al., 2019; Cadenas et al., 2020), this phase of rifting is interpreted to have caused minimal pre-Jurassic crustal thinning and subsidence. Comparing these observations with the results of deformable plate models that accommodate Triassic deformation (models 3, 5, and 6) (Figure 5.3), pre-Jurassic crustal thicknesses calculated by each model range from about 25 to 30 km thick, in general agreement with observations that suggest minimal pre-Jurassic deformation. However, some notable discrepancies include the localized regions of thinner crust near the Goban Spur and in the southeast Central Iberian Interior calculated by model 3, and a confined region of thinner crust between the western edge of the Ebro Block and eastern edge of the Landes High in models 5 and 6. For models 5 and 6, this localized region of thinner crust is interpreted to be caused by the rigid nature of the Ebro Block and Landes High that prevents extensional deformation from being distributed throughout their interiors. Furthermore, the occurrence of pre-Jurassic deformation within the Ebro Block has also been suggested by pre-Jurassic subsidence analysis within the Ebro Basin (Desegaulx and Moretti, 1988).

Throughout the Jurassic, the Pyrenees and Bay of Biscay were relatively tectonically quiet prior to a second phase of transtensional rifting that took place during the Late Jurassic to Early Cretaceous. This rift phase induced the onset of significant crustal thinning and syn-rift deposition within the Bay of Biscay (Montadert et al., 1979; Bois et al., 1997; Thinon et al., 2002, 2003; Tugend et al., 2014; Cadenas et al., 2018). Comparing these observations with the results of deformable plate models, crustal thicknesses calculated by models 2, 5, and 6 generally replicate these observations due to the interplay of the Landes High and Iberian plate kinematics.

Furthermore, models that exclude the kinematics of the Landes High (models 1 and 4) or propose that it was attached to Europe (model 3), appear to underestimate the amount of Late Jurassic to Early Cretaceous deformation experienced within the Bay of Biscay. Thus, as suggested in Chapter 4 and previous studies (Tugend et al., 2015a), the independent kinematics of the Landes High and its interplay with surrounding blocks exhibit an influential role on the deformation experienced within the Bay of Biscay. Within the Pyrenean realm, Late Jurassic to Early Cretaceous transtensional deformation led to rift-related subsidence, sedimentation, and necking of the crust (Tugend et al., 2015a; Saspiturry et al., 2019, 2021). These observations are analogous to Early Cretaceous crustal thicknesses calculated by models 3 and 6 within the Pyrenean realm (crust ~ 10 to 25 km thick) (Figure 5.5). Considering other models during this time frame, the Early Cretaceous eastward acceleration of the Ebro Block in model 5 leads to a region of hyperextended crust (crust 10 km thick or less) within the eastern Pyrenees. The timing of hyperextension calculated by model 5 (~ 130 Ma) is much earlier compared to the Aptian-Albian timing of hyperextension and mantle exhumation inferred from independent field observations within the Pyrenees (Lagabrielle and Bodinier, 2008; Jammes et al., 2009; Lagabrielle et al., 2010; Clerc and Lagabrielle, 2014; Tugend et al., 2014). Moreover, crustal thicknesses calculated by models 1, 2, and 4 by 130 Ma are indicative of proximal rift domains (crust 25 km thick or more). Thus, these models demonstrate a lack of Early Cretaceous deformation within the Pyrenean realm which is interpreted to be caused by either a lack of Ebro Block motion during the Early Cretaceous (e.g. models 2 and 4) or its exclusion as an independent block within deformable plate models (e.g. model 1).

During the Aptian-Albian, continental breakup was initiated in what is now the Pyrenean realm which led to the onset of hyperextension, mantle exhumation, and segmentation of sedimentary basins along strike of the Pyrenees (Jammes et al., 2009; Masini et al., 2014; Tugend et al., 2015a; Teixell et al., 2018; Espurt et al., 2019). These observations are approximately analogous to onset of significant crustal thinning within the Pyrenees calculated by model 6 (~ 115 Ma). In particular, the timing of hyperextension calculated by model 6 during the Aptian is primarily induced by the southeastward motion of the Ebro Block away from the Landes High and Europe. Moreover, an irregular Aptian-Albian crustal thickness template is also observed along strike of the Pyrenees in model 6. More specifically, this comprises a relatively wider and more significantly thinned region of crust within the eastern Pyrenees (crust 7 km thick or less) versus more localized and less significantly thinned regions (crust 8 to 10 km thick) within the western Pyrenees. Considering other deformable plate models tested herein, only model 5 also achieves regions of hyperextended crust within the Pyrenees during the Aptian-Albian, despite its early onset during the Early Cretaceous. However, in spite of a lack of crustal thicknesses indicative of hyperextended crust, model 2 demonstrates Aptian-Albian segmentation of Pyrenean sub-basins between the Ebro Block and Landes High. This phenomenon has been proposed in previous studies of the Pyrenees (Biteau et al., 2006; Tugend et al., 2014, 2015a) and is suggested to have formed via Late Jurassic to Early Cretaceous transtensional rifting along the Iberia-Eurasia plate boundary that progressively led to the development of localized and distinct rift systems. In model 2, the segmentation of rift basins appears to be induced by localized rift-related deformation experienced between the southeastward moving Ebro Block and the Landes High. Furthermore, the extent of this segmentation is approximately correlated with the length of these two blocks along strike,

suggesting that the geometries of these two blocks and their independent kinematics impact the extent and distribution of Cretaceous rift basins within the Pyrenees.

By Cenomanian time, the cessation of continental breakup within the Pyrenees led to the establishment of the Pyrenean pre-orogenic template. The pre-orogenic crustal structure of the Pyrenees is proposed to consist of sedimentary basins that were segmented along strike by major lithospheric boundaries and floored by domains of hyperextended crust and exhumed mantle (Larrasoana et al., 2003; Lagabrielle and Bodinier, 2008; Jammes et al., 2009; Lagabrielle et al., 2010; Roca et al., 2011; Tugend et al., 2015a; Lescoutre et al., 2021). Models 2 and 6 provide results that are most analogous to both the timing of pre-Cenomanian deformation and the pre-orogenic template of the Pyrenees according to field observations. In particular, Cenomanian crustal thicknesses calculated by model 6 are indicative of hyperextended rift domains that vary in size and thickness along strike of the Pyrenees in a similar manner to that calculated during the Aptian-Albian (Figure 5.8). In addition, model 2 is successful in achieving segmented corridors of thinned crust along strike of the Pyrenees, despite their classification as necking domains (Figure 5.8). However, although crustal thicknesses calculated by models 2 and 6 provide the best correlations with natural observations within the Pyrenees, shortcomings such as the size of hyperextended domains, the amount of Pyrenean extension, and the implications of these models within the Iberian Ranges are also identified and discussed in detail within the subsequent sections.

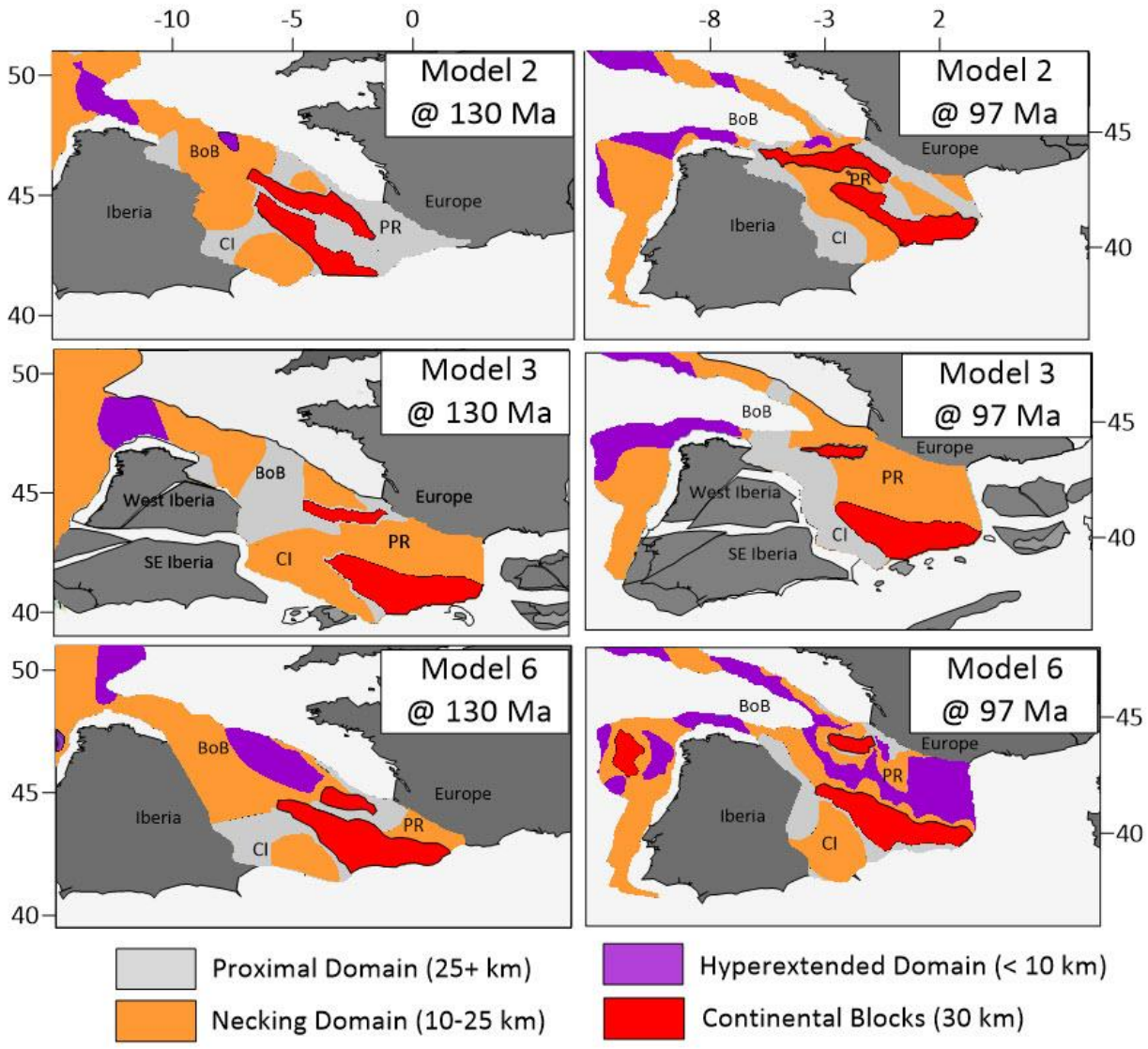

Figure 5.8 Rift domain maps designed based on the crustal thicknesses calculated by models 2, 3, and 6 at 130 Ma (left column) and 97 Ma (right column).

5.4.1.2 Central Iberia

The puzzling plate kinematics of Central Iberia represent a problem that is typically less studied than those of the Pyrenees and Bay of Biscay. Due to a limited amount of constraints, the kinematics of Central Iberia often represent an inconsequential output of reconstructions that are

more focused on the Pyrenean realm and Bay of Biscay, and thus, are less independently studied using plate reconstructions. Considering previous geological observations throughout Central Iberia (Salas et al., 2001; Rat et al., 2019; Vergés et al., 2020), the onset of rift-related deformation is interpreted to have begun during the Late Jurassic (~ 150 Ma) and ended during the Albian (~ 106 Ma), despite recent studies that suggest the continuation of rift-related deformation until Santonian time (Clerc et al., 2016; Frasca et al., 2021). Given that models 2 to 6 provide the most geologically reasonable results within the Pyrenean realm compared to independent observations, the evolution of model 1 within Central Iberia will not be discussed.

Model 2, the reconstruction from Nirrengarten et al. (2018), provides good correlations with independent observations within the Central Iberian Range (Salas et al., 2001; Rat et al., 2019). The initiation of crustal necking in the vicinity of Central Iberian basins (Figure 5.8), such as the Cameros Basin, by 150 Ma generally agrees with the Late Jurassic onset of rift-related deformation and subsidence proposed within Central Iberia (Salas et al., 2001). In addition, continued crustal thinning within Central Iberia in model 2 until the Aptian and lack of crustal thicknesses indicative of hyperextended crust also correlate well with the timing and extent of rifting documented by previous studies within the Central Iberian Range (Salas et al., 2001; Rat et al., 2019). Furthermore, despite discrepancies observed within the Pyrenean pre-orogenic template, a lack of crustal thickening calculated within Central Iberia from the Aptian to Cenomanian by model 2 supports interpretations that propose an Eocene-Miocene onset of compressional deformation within Central Iberia. However, minor Late Cretaceous compressional deformation within Central Iberia has also been proposed based on outputs from previous plate kinematic models (Angrand and Mouthereau, 2021), despite a lack of constraints.

In model 3, necking of the crust induced by the eastward motion of the Ebro Block from southeast Iberia is observed within Central Iberia following the end of the Triassic. Near the end of the Jurassic (150 Ma), rift-related deformation and subsequent crustal thinning continue within Central Iberia, resulting in a wider necking domain. Comparing these observations with the timing of rift-related deformation suggested by independent observations (Salas et al., 2001), the degree of crustal thinning calculated by model 3 throughout the Triassic and Jurassic appears to be more than that previously recognized. In addition, a lack of crustal thinning calculated by model 3 during the Early Cretaceous also suggests a lack of correspondence with the continuation of rift-related deformation within Central Iberia during this time frame. During Aptian-Albian time, shortening is observed, resulting in crustal thicknesses approximately 30 to 50 km. This phenomenon is observed within the majority of deformable plate models tested and is primarily caused by the approximate eastward motion of Iberia towards the southward moving Ebro Block from the Early to Mid-Cretaceous.

Overall, model 4 demonstrates poor correlations between crustal thickness estimates calculated from the Jurassic to Mid-Cretaceous with those inferred from independent observations within Central Iberia. One discrepancy is the lack of Late Jurassic to Early Cretaceous crustal thinning calculated by model 4 in comparison to what is suggested by independent observations (Rat et al., 2019). Additionally, from the Early (130 Ma) to Mid-Cretaceous (110 Ma), crustal shortening is observed within northern and central regions of Iberia that have been previously interpreted as strike-slip systems, similar to those observed in model 3 (Angrand et al., 2020; Angrand and Mouthereau, 2021; Frasca et al., 2021).

For model 5, a significant degree of crustal thickening (> 50 km) is calculated due to the large amount of southward displacement of the Ebro Block throughout the Cretaceous. Thus, the validity of model 5 is deemed insufficient due to its consequences within the Central Iberian rift.

Model 6 was the only model that varied the spatial-temporal extent of deformation within the Central Iberian domain. Throughout the entirety of model 6, the spatial extent of deformation within Central Iberia was controlled by the kinematics of the Ebro Block in an attempt to mitigate the amounts of compressional deformation experienced within Central Iberia as observed in models 3, 4 and 5. Aside from the region of deformation within Central Iberia being slightly narrower in model 6, models 5 and 6 demonstrate similar crustal thicknesses calculated from the Triassic to Early Cretaceous. By the Early Cretaceous (130 Ma) (Figure 5.8), crustal thicknesses calculated by model 6 indicate necking of the crust within Central Iberia, in general agreement with the lack of hyperextended crust documented within the Central Iberian basins following the end of the Late Jurassic to Early Cretaceous rift phase (Rat et al., 2019). From the Barremian (130 Ma) to Cenomanian (97 Ma), transtensional deformation and southeastward expansion of the Central Iberian domain, coeval with the southeastward motion of the Ebro Block, are observed. Apart from localized areas of compression in the vicinity of the Cameros Basin (yellow star in Figure 5.7) (35 to 40 km thick), crustal thicknesses throughout Central Iberia range from approximately 20 to 30 km by the Cenomanian. Compared to previous plate kinematic models of Iberia, the Cenomanian (~ 97 Ma) end of rift related deformation within Central Iberia suggested by model 6 is similar to that suggested by Angrand et al. (2020) (100 Ma), but earlier compared to the reconstruction from Frasca et al. (2021) (83 Ma). Thus, based on currently available constraints, model 6 seems to provide the best correlations with independent observations, while

also mitigating Mid-Cretaceous compressional deformation as observed within all other models tested.

In summary, models 2 and 6 provide the best results within Central Iberia as compared to independent observations, while model 6 also provides the most relevant estimates of crustal thinning within the Pyrenean realm. Comparing all models tested, the regional extension directions within the Pyrenean realm and Central Iberia appear to play a role in the amount of Middle to Late Cretaceous shortening experienced within Central Iberia (Figures 5.9 and 5.10). For models 2 and 6, approximately NNW-SSE directed extension within the Pyrenean and Central Iberia rifts appears to mitigate the amount of shortening experienced within Central Iberia. Furthermore, in models 3 and 4, approximately N-S extension and WNW-ESE trending strike slip motion within the Pyrenees and Central Iberia, respectively, result in larger amounts of shortening within Central Iberia. Thus, far-field stresses from the Pyrenean rift and its interplay with stress directions within Central Iberia appear to play a key role in the deformation experienced within Central Iberia during the Mid-Cretaceous.

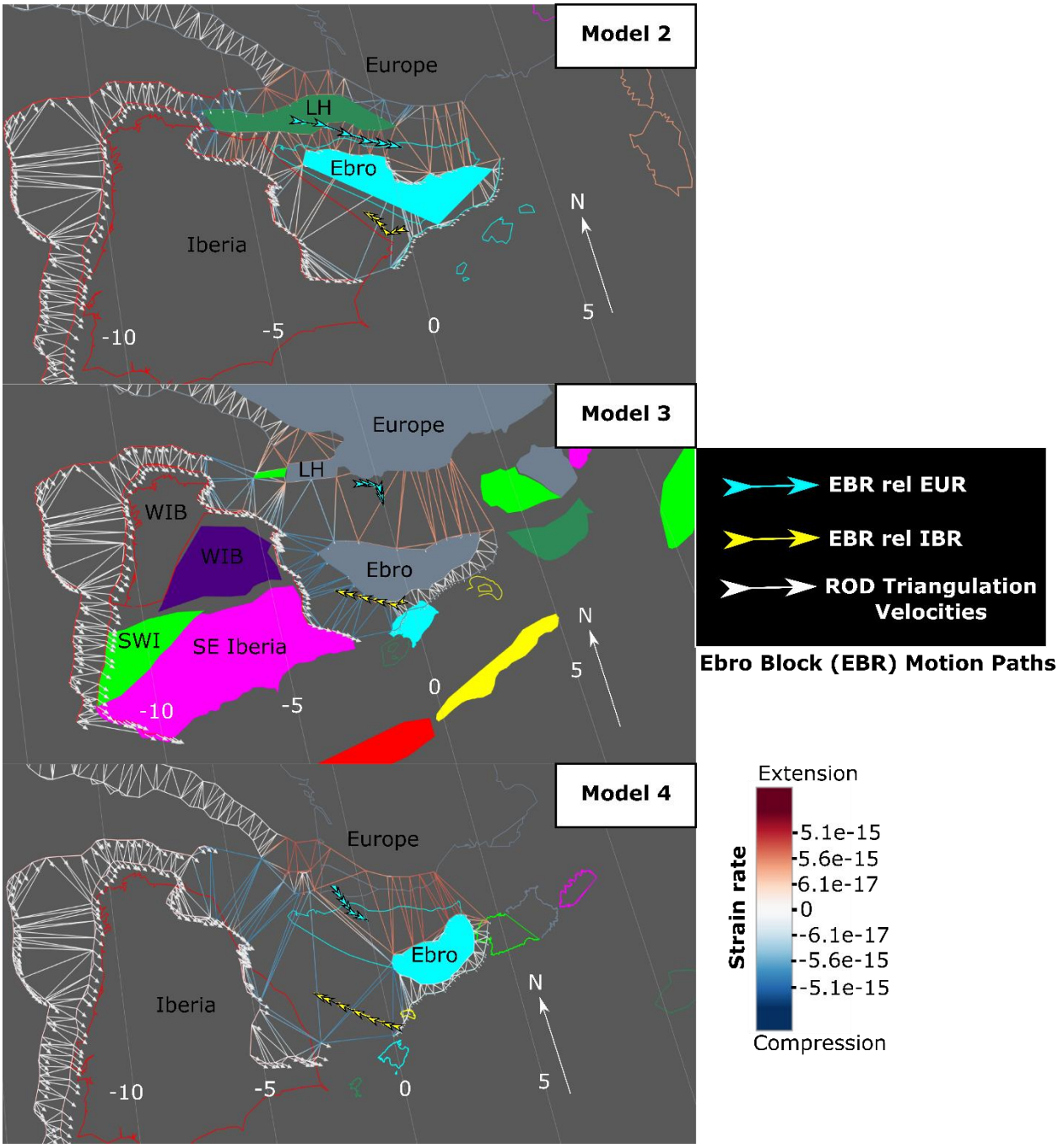

Figure 5.9 Motion paths of the Ebro Block (EBR) relative to Europe (cyan) and Iberia (gold) from the Aptian (126 Ma) to Cenomanian (97 Ma) in models 2 to 4. The time step used to calculate motion paths (distance between triangles) is 5 Ma. CB = Central Iberia, EUR= Europe, IBR=

Iberia, LH = Landes High, ROD = Region of deformation, SWI = South West Iberia, WIB = West Iberia.

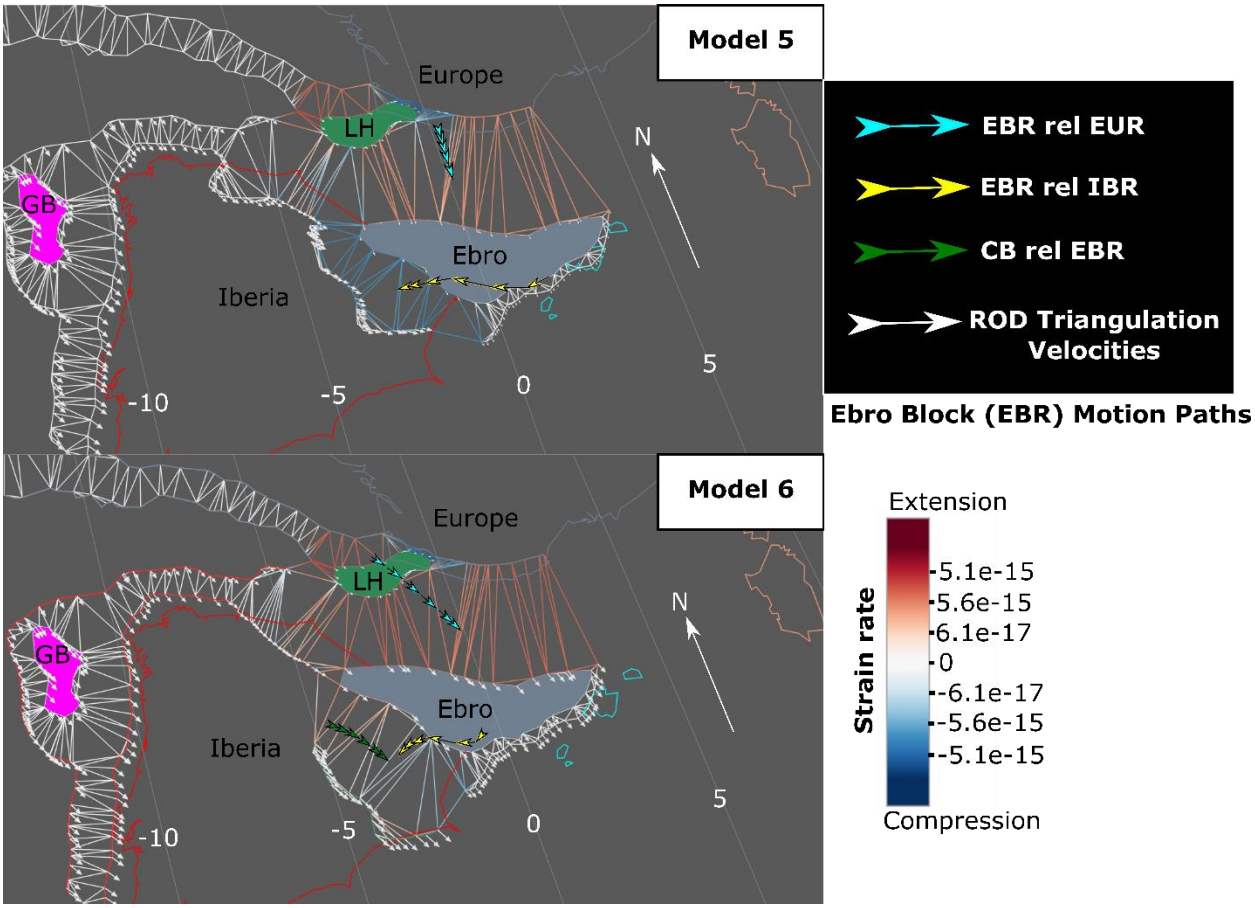

Figure 5.10 Motion paths of the Ebro Block (EBR) relative to Europe (cyan) and Iberia (gold) from the Aptian (126 Ma) to Cenomanian (97 Ma) in models 5 and 6. The time step used to calculate motion paths (distance between triangles) is 5 Ma. CB = Central Iberia, EUR= Europe, IBR= Iberia, LH = Landes High, ROD = Region of deformation, SWI = South West Iberia, WIB = West Iberia.

5.4.2 Evaluating the kinematics of the Ebro Block

The variability in the kinematics and geometry of the Ebro Block for each deformable plate model considered (Table 5.2) significantly impact the deformation and subsequent evolution of rift domains within the Pyrenean realm and surrounding regions (Figure 5.8). In this section, the kinematics of the Ebro Block in each model are evaluated by assessing its displacement relative to Europe and its resultant influence on orientation of regional extension directions and crustal thicknesses calculated within the Pyrenean realm (Figures 5.9 and 5.10).

In model 1, the exclusion of the Ebro Block as a rigid block within the interior of deformable regions fails to produce the amount of deformation expected within the Pyrenees, emphasizing the importance of the Ebro Block's inclusion within deformable plate models of Iberia.

For model 2, the use of the Ebro Block geometry and poles of rotation from Nirrengarten et al. (2018) results in segmented necking domains throughout the Pyrenean realm (Figure 5.10). However, crustal thicknesses indicative of hyperextension (< 10 km thick) by the Cenomanian are not achieved by model 2. This is interpreted to be related to the starting position and lack of Ebro Block motion away from Iberia up until the Early Cretaceous, resulting in the largest amount of Ebro Block Cretaceous displacement (~ 523 km) calculated amongst all models considered.

In model 3, the kinematics of the Ebro Block produce more widespread deformation throughout the Pyrenean realm in comparison to model 2. The Jurassic displacement of the Ebro Block in model 3 (176 km) is the largest of all models tested. As a consequence, this causes the onset of crustal necking by 150 Ma within Central Iberia (Figure 5.4), which is earlier than

expected based on previous interpretations that suggest the onset of rift-related deformation was during the Late Jurassic and continued until the Albian (Salas et al., 2001). However, considering the minimal amounts of Jurassic deformation previously documented within the Pyrenees (Jammes et al., 2009; Gómez-Romeu et al., 2019; Saspiturry et al., 2019, 2021), reasonable Late Jurassic crustal thicknesses are calculated by model 3 ranging from approximately 20-25 km thick. In addition, model 3 is the only model where the Ebro Block displacement is greater during the Jurassic than during the Cretaceous. Most of the Ebro Block displacement during the Cretaceous in model 3 takes place from the Aptian to Cenomanian, resulting in approximately N-S extension within the Pyrenees and about 80 km of displacement between the Ebro Block and Europe. Furthermore, despite similarities between the Ebro Block displacement calculated by model 3 and the amount of extension documented by recent crustal restoration studies within the western Pyrenees (Teixell et al., 2018; Gómez-Romeu et al., 2019; Lescoutre et al., 2021), a lack of crustal thicknesses indicative of hyperextension and mantle exhumation by the Cenomanian is observed, conflicting with interpretations made from geological field mapping and crustal restorations (Lagabrielle and Bodinier, 2008; Lagabrielle et al., 2010; Teixell et al., 2018).

Model 4 is the only model that considers a smaller geometry of the Ebro Block compared to its present day extent (Figure 1.5), interpreted from previous rift domain mapping studies (Tugend et al., 2015a), and a starting position attached to southeastern France at 200 Ma (Figure 5.1). Additionally, in contrast to all models tested, most of the Ebro Block displacement relative to Europe takes place from the Aptian to Cenomanian (80 km), with no displacement occurring throughout the Jurassic. This appears to have a significant impact on the deformation experienced within the Pyrenean realm. Most notably, the motion of the Ebro Block away from Europe during

the Aptian induces the onset of significant crustal thinning (crust < 10 km thick) within the eastern Pyrenees. However, following approximately 80 km of displacement and N-S directed extension between the Ebro Block and Europe from the Aptian to Cenomanian, hyperextended crust is not generated within the central and western Pyrenees and regions throughout the Bay of Biscay (Figure 5.7). This observation demonstrates poor correlations with previous interpretations of the western and central Pyrenean pre-orogenic template (Jammes et al., 2010a; Lagabrielle et al., 2010; Masini et al., 2014; Tugend et al., 2014; Saspiturry et al., 2019, 2021).

The kinematics of the Ebro Block in models 5 and 6 are constructed using identical Triassic and Jurassic poles of rotation, however, differences between their Cretaceous poles of rotation have a notable impact on the extent of Cretaceous deformation experienced within the Pyrenees. In models 5 and 6, minimal Jurassic displacement of the Ebro Block (39 km) is observed, similar to the lack of Ebro displacement during the Jurassic measured by model 4 (0 km). During the Earliest Cretaceous (145 – 130 Ma), the acceleration of the Ebro Block in model 5 produces the largest rate of motion for the Ebro Block (~ 35km/Myr) measured by all models considered (Figure 5.11). In addition, the 336 km of Cretaceous displacement for the Ebro Block is the third largest of all models tested. From the Barremian to Cenomanian, approximately 160 km of displacement and N-S directed extension is observed between the Ebro Block and Europe in model 5, a larger value compared to calculations made from crustal restorations (~ 80-100 km). Furthermore, despite achieving significant crustal thinning within the Pyrenean realm, the Cretaceous southward motion of the Ebro Block in model 5 produces unrealistic crustal thickening within Central Iberia.

In model 6, a key difference compared to model 5 is the NNW-SSE Early to Mid-Cretaceous regional extension direction within the Pyrenees induced by the motion of the Ebro

Block relative to Europe (Figure 5.10). By simulating a transtensional (sinistral sense) Early to Mid-Cretaceous rift within the Pyrenees, Cenomanian crustal thicknesses indicative of a hyperextended crust are achieved within the Pyrenean realm (Figure 5.12) and the amount of crustal shortening observed within Central Iberia in previous models is minimized. However, similar to model 5, approximately 140 km of displacement between the Ebro Block and Europe is documented from the Early to Mid-Cretaceous, a value that is also larger than previous values proposed by Pyrenean crustal restorations (~ 80-100 km) (Teixell et al., 2018 and references therein; Gómez-Romeu et al., 2019; Lescoutre et al., 2021).

In summary, an interesting correlation is observed between models that achieve hyperextended crustal thicknesses within the Pyrenees and the amounts of extension derived from previous restoration studies of the Pyrenees (Tugend et al., 2014; Teixell et al., 2018; Gómez-Romeu et al., 2019; Lescoutre et al., 2021). For model 6, crustal thicknesses indicative of hyperextended crust are achieved throughout the Pyrenees by the Cenomanian, however, the amount of Aptian to Cenomanian Ebro Block displacement (~ 140 km) appears to be larger than extension amounts previously documented within the Pyrenees (~ 80-100 km). However, considering models where the Ebro Block displacement is nearly equivalent to previous estimates of Pyrenean extension, regions of significant crustal thinning are not achieved, aside from model 4 within the eastern Pyrenees.

Model #	Ebro Included	Ebro Block Poles of Rotation	Jurassic Displacement relative to Europe	Cretaceous Displacement relative to Europe	Aptian-Cenomanian displacement relative to Europe	Mid-Cretaceous extension direction	Pyrenean hyperextended crust by Cenomanian time?
1	No	N/A	N/A	N/A	N/A	NW-SE	No
2	Yes	Nirrengarten et al. (2018)	37 km (ESE)	523 km (ESE)	340 km (ESE)	WNW-ESE	No
3	Yes	Angrand et al. (2020)	176 km (ESE)	118 km (ESE)	82 km (S)	N-S	No
4	Yes	Frasca et al. (2021)	0 km	80 km (S)	80 km (S)	N-S	Yes
5	Yes	This study	39 km (SSE)	336 km (SSE)	160 km (S)	N-S	Yes
6	Yes	This study	39 km (SSE)	370 km (SSE)	140 km (SSE)	NNW-SSE	Yes

Table 5.2 Detailed output parameters of each model pertaining to the Ebro Block kinematics and its displacement during various time periods. Displacement calculations are made using a motion path (relative to Europe) situated on the northeastern corner of the Ebro Block in each model.

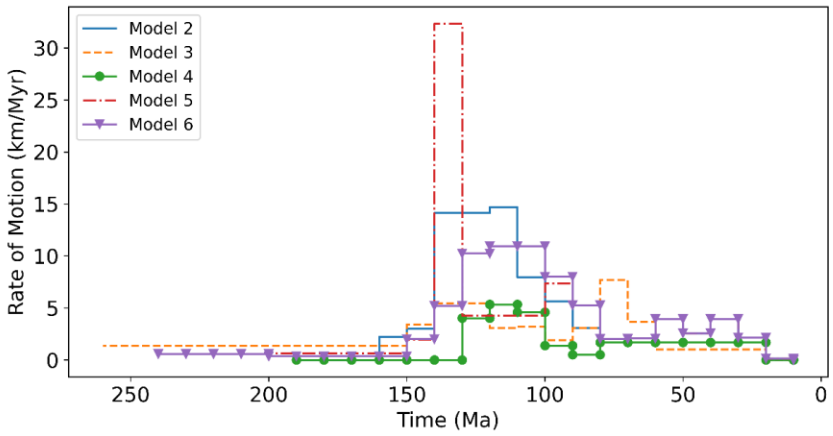

Figure 5.11 Ebro Block rate of motion (km/Myr) calculated using a motion path (relative to Europe) along the northeastern edge of the Ebro Block for models 2 to 6.

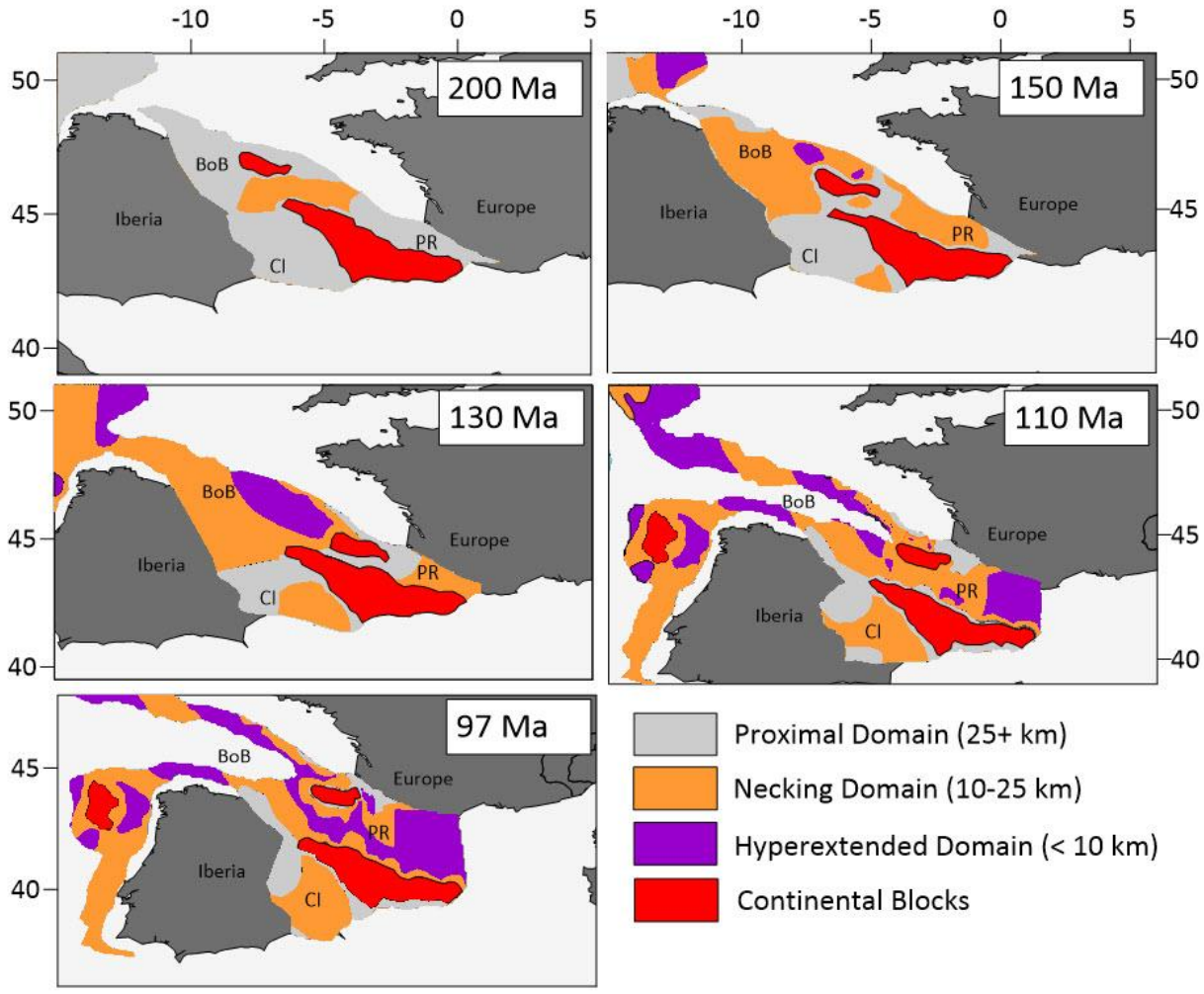

Figure 5.12 Temporal evolution of rift domains for model 6 defined based on crustal thicknesses calculated by model 6.

5.4.3 Assessing model discrepancies and limitations

5.4.3.1 Pyrenean pre-orogenic setting

Based on our investigation of the Ebro Block kinematics and their impact on the extent and timing of Pyrenean deformation, interesting relationships and discrepancies arise when making comparisons between results calculated by deformable plate models and independent observations.

One notable discrepancy is the variability in pre-orogenic crustal thicknesses calculated by each model within the Pyrenean realm. Cenomanian crustal thickness estimates calculated by model 6 seem to provide the best correlations with observations supporting hyperextension within the Pyrenees caused by significant crustal thinning experienced during the Aptian-Albian (Lagabrielle and Bodinier, 2008; Lagabrielle et al., 2010; Tugend et al., 2014). In addition, the results of model 6 also appear to be in general agreement with the timing of rift-related deformation experienced within the Bay of Biscay and Central Iberia. However, when comparing estimates of Early to Mid-Cretaceous extension calculated by previous crustal restorations within the Pyrenees to those derived from model 6, the amount of Pyrenean extension experienced in model 6 is about 40-60 km greater than the highest values previously documented (~ 80-100 km). While the uncertainties and difficulties associated with reconstructing hyperextended and exhumed domains within present day mountain belts can potentially explain the mismatch, the limitations of deformable plate modelling must also be recognized. A combination of geological field mapping (Lagabrielle et al., 2010; Clerc and Lagabrielle, 2014; Tavani et al., 2018) and numerical modelling studies (Jammes et al., 2010a, 2014; Duretz et al., 2020; Saspiturry et al., 2021) have demonstrated that deformation within the Pyrenean realm was influenced by various factors such as depth-dependent rheology and surface processes. Considering the current capabilities of deformable plate models built using GPlates, deformable plate models assume pure-shear deformation and exclude any depth-dependent phenomena. Thus, future work should focus on combining results derived from deformable plate models with geodynamic plate-mantle models in order to more diligently assess the impact of depth-dependent deformation on the results shown in this study. Based on the deformable plate modeling results presented, it is postulated that the amount of Ebro Block

displacement could be larger than that previously proposed within studies of the Pyrenean realm. However, the inability to capture rheological and depth-dependent processes in the considered deformable plate models could also be a cause for the larger amounts of Ebro Block displacement needed to produce significant crustal thinning within the Pyrenees. Assessing the impact of these processes on the results of deformable plate models would be beneficial for investigating the outputs of the models presented herein, in particular, when making comparisons between models that provide an appropriate amount of extension and strain partitioning expected within the Pyrenean realm (model 2) versus models that achieve significantly thinned pre-orogenic crustal thicknesses within the Pyrenees, despite having wider domains of deformation than potentially expected (model 6).

Another discrepancy is the variable pre-orogenic template of the Pyrenees from west to east. For all models that achieve significantly thinned regions of crust in the Pyrenees by the Cenomanian, the most significant crustal thinning is experienced within the eastern Pyrenees. This observation appears to contradict previous interpretations that attempt to explain the variability between the Pyrenean crustal structure from west to east and its subsequent impact on the variable present day crustal structure along strike of the Pyrenees. In recent studies, the eastern Pyrenees have been demonstrated to be relatively starved of Mesozoic sediments (Grool et al., 2018) and are considered to have developed within a transtensional setting with narrower rift domains (Ford and Vergés, 2020) in comparison to those westward (Clerc and Lagabrielle, 2014; Jammes et al., 2014; Chevrot et al., 2018; Teixell et al., 2018). In addition, the pre-orogenic crustal structure of the eastern Pyrenees is postulated to be dominated by crustal massifs and localized basins that formed during rifting within a weaker Variscan crust throughout the central and eastern Pyrenees.

Due to significant uncertainties, variations in the kinematics and geometries of crustal massifs within the Pyrenean realm are considered to be beyond the scope of this work. However, their inclusion within deformable plate models could potentially provide results more akin to previous interpretations of the eastern Pyrenean crustal structure, with perhaps extensional deformation more distributed into localized rift sub-basins in the eastern Pyrenees compared to the west.

5.4.3.2 Orientation of Aptian-Albian extension within the Pyrenees

An additional discrepancy amongst all models tested is the orientation of Mid-Cretaceous extension within the Pyrenean realm. Previous geological field mapping (Jammes et al., 2009; Masini et al., 2014; Tavani et al., 2018; Lescoutre et al., 2021) and plate kinematic studies within the Pyrenees (Angrand et al., 2020; Frasca et al., 2021) (models 3 and 4) have proposed approximately N-S or NNE-SSW directed extension during the Aptian-Albian. Comparing all models tested, NNW-SSE directed extension induced by the Aptian-Albian kinematics of the Ebro Block in models 2 and 6 provide the best results with respect to minimizing discrepancies between large and local scale deformation previously documented within rift basins throughout the Bay of Biscay, Pyrenees, and Central Iberia. Although a NNW-SSE Aptian-Albian regional extension direction is slightly different to that previously proposed by geological field mapping within the Pyrenees (Masini et al., 2014; Tavani et al., 2018; Saspiturry et al., 2019; Lescoutre et al., 2021), it should be noted that local extension directions can be guided by phenomena such as pre-existing structures and smaller block rotations. For example, most of the transfer zones that segment the Pyrenean rift system (e.g., Pamplona and Toulouse fault zones) are interpreted to follow pre-existing structural trends (Tugend et al., 2014; Saspiturry et al., 2019). As a result, their trend can not be solely relied upon as a precise plate kinematic indicator. Thus, extension directions

documented within rift basins throughout the Pyrenees are expected to be highly variable, and not necessarily reflective of regional extension directions at the scale of plate boundaries inferred from plate kinematic models.

5.4.3.3 Crustal shortening within Central Iberia

Each deformable plate model presented in this work demonstrates some degree of crustal shortening within Central Iberia, most notably in the vicinity of the Cameros Basin (Figure 1.4) during the Early to Mid-Cretaceous. For each model, this shortening appears to be caused by the eastward motion of Iberia towards the southward moving rigid Ebro Block (Figures 5.9 and 5.10). In addition, models 3 and 4 also experience crustal shortening during the Early to Mid-Cretaceous within the Basque Cantabrian Basin and North Iberian margin due to the southward motion of the Landes High towards Iberia. Throughout the Iberian interior, Middle to Late Cretaceous compressional deformation has been rarely documented (Rat et al., 2019; Angrand and Mouthereau, 2021). Given the impact of this pre-Eocene shortening on the evolution of crustal thicknesses within Central Iberia, the assumption of rigid model boundaries and blocks within the interior of deformable regions and the lack of consideration for processes such as erosion could potentially amplify the amount of crustal thickening calculated by deformable plate models. Thus, future studies are needed in order to assess the amounts of pre-Eocene compressional deformation experienced throughout Central Iberia and their relationship to the crustal thickness evolution experienced within regions that have been debated as either strike-slip (Angrand et al., 2020; Cadenas et al., 2020; Frasca et al., 2021) or orthogonal and transtensional rift systems (Salas and Casas, 1993; Salas et al., 2001; Tugend et al., 2015a; Verges et al., 2020). Given the results of the deformable plate models presented, models that propose a transtensional rift within Central Iberia

and the Pyrenees (models 2 and 6) provide the best results with regard to mitigating compressional stresses within Central Iberia. In addition, these models also achieve the best correlations with independent observations regarding the amount of crustal thinning and distribution of rift-related deformation expected throughout the Pyrenean pre-orogenic template.

5.4.4 Implications for Iberian plate kinematics: a deformable plate modelling perspective

The work presented herein represents the first deformable plate modelling study focussed on the Pyrenean realm. Similar to that observed along the West Iberian margin (Chapter 3), Bay of Biscay (Chapter 4), and elsewhere throughout the Atlantic (Peace et al., 2019b), the kinematics of continental blocks appear to play a significant role in the pre-Alpine deformation experienced within the Pyrenees, and throughout Iberia as a whole. With respect to previous rigid plate reconstruction studies of Iberia (Nirrengarten et al., 2018; Angrand et al., 2020; Angrand and Mouthereau, 2021; Frasca et al., 2021), the partitioning of Iberia into continental blocks and micro-plates has also allowed previous authors to more clearly reconcile geological observations throughout Iberia that were less supported by studies treating Iberia as a lone tectonic plate (Olivet, 1996; Sibuet et al., 2004; Jammes et al., 2009; Vissers and Meijer, 2012). Moreover, the initial position and kinematics of the Landes High and Ebro Block in model 6, a model interpreted as having the strongest correlations with independent observations, provide insight regarding the nature of the Iberia-Eurasia plate boundary. As suggested in previous studies (Tugend et al., 2015a; Cadenas et al., 2020; Angrand and Mouthereau, 2021), the Iberia-Eurasia plate boundary appears to be a diffuse and discontinuous plate boundary that is highly compartmentalized by rigid blocks,

sedimentary basins and inherited structures. Following an analysis of the deformable plate models considered in this study, temporal variations in strain partitioning along the Iberia-Eurasia plate boundary and within Central Iberia appear to be highly variable and largely impacted by transtensional stresses. In addition, significant variability in the results calculated by deformable plate models appears to be mostly due to the inclusion and kinematics of continental blocks. Thus, understanding their origin and evolution appears to be equally, if not more important than the kinematics of Iberia itself, especially within the Pyrenean realm. Considering future directions for plate kinematic studies, emphasis should be given to verifying phenomena inferred from deformable and rigid plate models by using thermo-mechanical numerical modelling studies that encompass depth-dependent deformation and sedimentary processes. Examples of such phenomena include the processes related to the formation of continental blocks (Neuharth et al., 2021) and the complex interactions between regional stress directions and localized heterogeneities inherited from previous tectonic events (Jammes et al., 2014; Heron et al., 2019; Jammes and Lavier, 2019; Phillips et al., 2019). A clearer understanding of these concepts could potentially improve explanations for local plate kinematic observations within the Pyrenees that can be difficult to reconcile using global and regional plate kinematic models alone. Furthermore, future studies should focus on expanding the models shown herein to accommodate plate kinematic models of the Western Mediterranean (van Hinsbergen et al., 2020; Le Breton et al., 2021). This could allow the kinematics and deformation experienced within regions surrounding previously recognized blocks and plates (e.g. Sardinia-Corsica and Adria) to be more clearly understood.

5.5 Conclusions

Deformable plate tectonic models have been used to gain insights regarding the timing and extent of Mesozoic deformation experienced throughout Iberia. In particular, this study provides a detailed investigation of the Ebro Block kinematics and their interplay with surrounding continental blocks (e.g. Landes High) and micro-plates (e.g. Iberia) during rift-related deformation experienced within the Pyrenean realm. The main conclusions of this work are:

1. The Ebro Block played a significant role in the partitioning of strain within the Pyrenean realm prior to the Pyrenean Orogeny. Models that suggest a transtensional tectonic setting within the Pyrenees and approximately NNW-SSE regional extension directions during the Mid-Cretaceous (model 6) are successful in achieving crustal thicknesses indicative of hyperextended crust within the Pyrenees, while also mitigating the amount of pre-Eocene shortening experienced within Central Iberia.
2. Most of the models investigated herein (all except model 3) suggest very little motion of the Ebro Block during the Jurassic. Thus, the majority of Jurassic deformation experienced along the Iberia-Eurasia plate boundary was likely confined within the Bay of Biscay and Central Iberia.
3. For deformable plate models that generate pre-orogenic crustal thicknesses indicative of hyperextension within the Pyrenees (models 4, 5, and 6), hyperextension is commonly initiated within the eastern Pyrenees. In addition, the eastern Pyrenees represent the widest and most significantly thinned region calculated by all deformable plate models within the Pyrenean realm.

4. The interplay between the Landes High and the Ebro Block in models 2, 3, and 6 plays a critical role in the partitioning of deformation within the Bay of Biscay and Pyrenean realm, respectively. Within the Pyrenees, the interplay between the Landes High and Ebro Block kinematics in model 6 results in a region of thicker crust in the vicinity of the Pamplona transfer zone and localized thinning within the Basque-Cantabrian Basin. Models that exclude the Landes High as an independently moving continental block (models 1 and 4) appear to underestimate the amount of deformation experienced within the Bay of Biscay.
5. Considering the close proximity of the Ebro Block to Europe during the Triassic and its kinematics in most of the plate models considered, the Iberia-Eurasia plate boundary should not be considered a continuous boundary, rather, a disconnected and diffuse boundary whose morphology changes subject to the orientation and kinematics of surrounding continental blocks and inherited structures.
6. Using a deformable plate modelling approach allows for the kinematic role of continental blocks to be more diligently assessed within the Pyrenees and highlights their importance relative to the kinematics of Iberia itself (emphasized by the results of model 1). Thus, in our opinion, future improvements made to deformable plate models and methods used to study continental blocks will allow the model discrepancies presented herein to be addressed more clearly.
7. The aim of our approach is not to disregard current plate kinematic models of Iberia, but rather, to quantitatively assess their consequences when a deformable plate modeling approach is used.

Chapter 6

6 Advances in deformable plate tectonic models (Part A): reconstructing deformable continental blocks and crustal thicknesses back through time

The majority of the work presented in this chapter can be found in its published version *"King, M. T., & Welford, J. K. (2022). Advances in deformable plate tectonic models: 1. Reconstructing deformable continental blocks and crustal thicknesses back through time. Geochemistry, Geophysics, Geosystems, 23, e2022GC010372. https://doi. org/10.1029/2022GC010372"*.

6.1 Introduction

Plate tectonics describes the motion of tectonic plates through geological time and is largely responsible for the dynamic exterior and interior geological structure of the Earth. For early plate tectonic studies, many of the fundamental aspects of plate tectonics were discovered by simple reconstructions of conjugate coastlines and oceanic fracture zones (Bullard et al., 1965), paleomagnetism (Gong et al., 2009; Neres et al., 2012), and the identification of oceanic spreading and transforms along the seafloor (Dietz, 1961; Wilson, 1965). Despite the significant advancement of plate tectonic theory via these traditional methods and interpretations, the methods and approaches used to study plate tectonics continue to rapidly advance. In particular, the

visualization and representation of plate motions via plate tectonic reconstructions continue to be commonly used and investigated.

Traditionally, most common plate reconstruction approaches consist of reconstructing rigid plates and other geological features of interest according to their rotations about Euler poles. Furthermore, the scope and time frame of plate kinematic studies can vary quite substantially, from global scale studies over several supercontinent cycles (Matthews et al., 2016), to more regional studies focussed on a single orogeny or opening of an ocean (Sibuet et al., 2004; van Hinsbergen et al., 2020). Recently, GPlates (Müller et al., 2018), an open-source software used to build and visualize plate tectonic reconstructions, has become increasingly popular. In addition, an automated form of GPlates, pyGPlates, offers an alternative way of expanding GPlates functionality using the python programming language. Ultimately, both options provide an environment where users can construct, visualize, and investigate both rigid and deformable plate tectonic models.

Deformable plate tectonic models are becoming an increasingly used method for studying plate kinematics and temporal variations in strain rate and crustal thickness (Peace, 2021). In Chapters 3-5, deformable plate models are used to investigate the interplay of deformation and plate kinematics throughout Iberia, and the southern North Atlantic Ocean as a whole. Despite their ability to more diligently assess the kinematics of microplates, continental blocks, and temporal variations in crustal thickness, the deformable plate models presented in Chapters 3-5, and elsewhere (Peace et al., 2019b; Cao et al., 2020), depend on numerous assumptions that can be geologically unsatisfying. Some notable examples include the lack of consideration for deformation within continental blocks, a uniform crustal thickness assumption at a start time of

interest, and the nature and geometry of rigid model boundaries which define the extents of where deformation takes place. As a result, these assumptions can often lead to model edge effects surrounding rigid continental blocks and boundaries, and discrepancies when making comparisons between crustal thicknesses calculated by deformable plate models and present day estimates.

In this study, we present a new deformable plate modelling workflow (Figure 6.1) and application within the southern North Atlantic (Figure 1.4) using pyGPlates and GPlates. In particular, we demonstrate how deformation can be accounted for within continental blocks, the ability to avoid uniform crustal thickness assumptions by reconstructing present day gravity inversion crustal thickness estimates, and the capability of designing deformable plate models without the need for well-constrained landward boundaries of deformation. Following a description of these deformable plate modelling strategies, their application is assessed using a previously published deformable plate model of the southern North Atlantic (Peace et al., 2019b). The reasoning for this choice of application is based on the considerable amount of constraints available throughout the southern North Atlantic, and its geological complexity and compatibility with other tectonic regimes, regardless of time frame, as a Mesozoic rift that initiated within a Paleozoic mountain belt (Nirrengarten et al., 2018; Waldron et al., 2019). In addition, the North Atlantic also represents a region that has been relatively well studied using rigid plate tectonic reconstructions (e.g. Barnett-Moore et al., 2018) that have been subsequently used to construct global deforming plate models that incorporate constraints such as present day gravity inversion crustal thickness estimates and seismic data (Müller et al., 2019). The results of this application provide insight regarding the kinematic role of continental blocks during North Atlantic rifting, the pre-Jurassic (200 Ma) template of continental blocks and sedimentary basins throughout the

North Atlantic, and the impact of reactivated Appalachian and Caledonian orogenic terranes during the breakup of the supercontinent Pangaea.

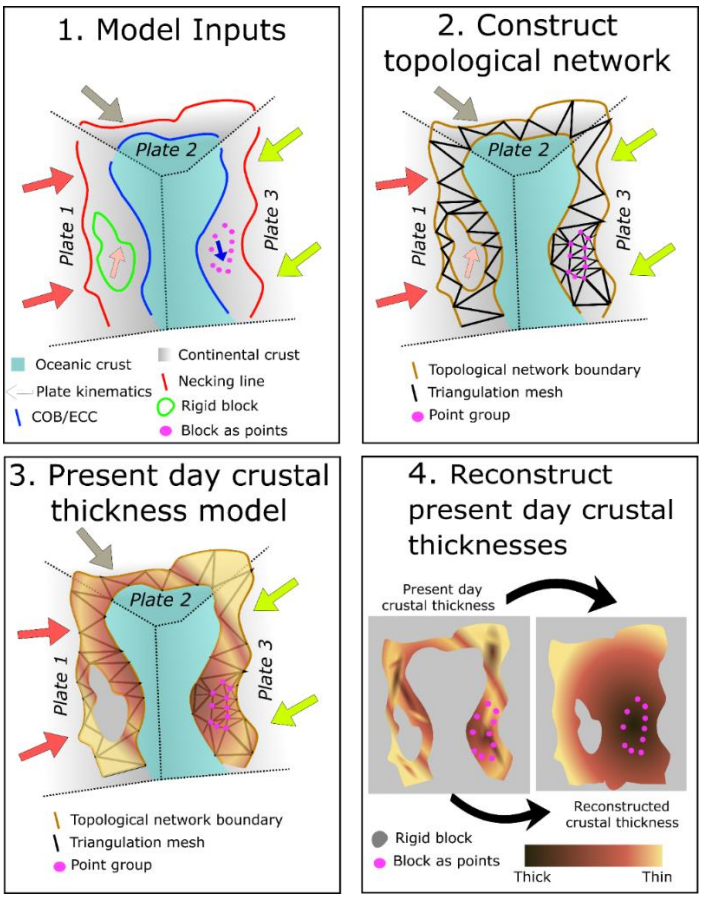

Figure 6.1 Deformable plate tectonic modelling workflow for this study modified after Peace et al., (2019) and King et al., (2020.2021).

6.2 Methodology

6.2.1 Designing deformable continental blocks

Assumptions about the rigidity of continental blocks and how those assumptions impact crustal thickness estimates calculated by deformable plate models have been discussed throughout this thesis. More specifically, given the fact that continental blocks are often assumed to be rigid (e.g., Chapters 3-5), this implies that they remain the same constant crustal thickness throughout the entirety of a model simulation, a phenomenon proven to be problematic based on present day crustal thickness estimates of continental blocks throughout the North Atlantic (Welford and Hall, 2007; Welford et al., 2010, 2012; King et al., 2020).

For the design of continental blocks implemented in previous deformable plate modelling studies, such as the Flemish Cap (Figure 6.2) (Peace et al., 2019b), continental blocks are typically designed as rigid polygons. This approach prevents the triangulation mesh used to quantify deformation within deformable plate models from penetrating the interior of a continental block. As a consequence, this often leads to the generation of modelling edge effects surrounding the exterior of rigid blocks due to the inability to model compression and extension that would typically be distributed throughout the block itself. Thus, a solution proposed herein that allows deformation to take place within continental blocks is through the use of individual points placed within the interior of deformable meshes. For their implementation, the points are designed according to the geometry of continental blocks inferred from previous plate models, gravity inversion, and seismic constraints (Figure 6.2). By using a group of points designed in the shape of a polygon, this allows the triangulation mesh within a topological network to interpolate within

continental blocks. For the kinematics of the points, the group of points corresponding to a continental block are assigned a plate ID for the continental block of interest (e.g. Flemish Cap in Figure 6.2). Thus, the points move identically to a rigid polygon, however, they enable internal deformation to be experienced within the block itself.

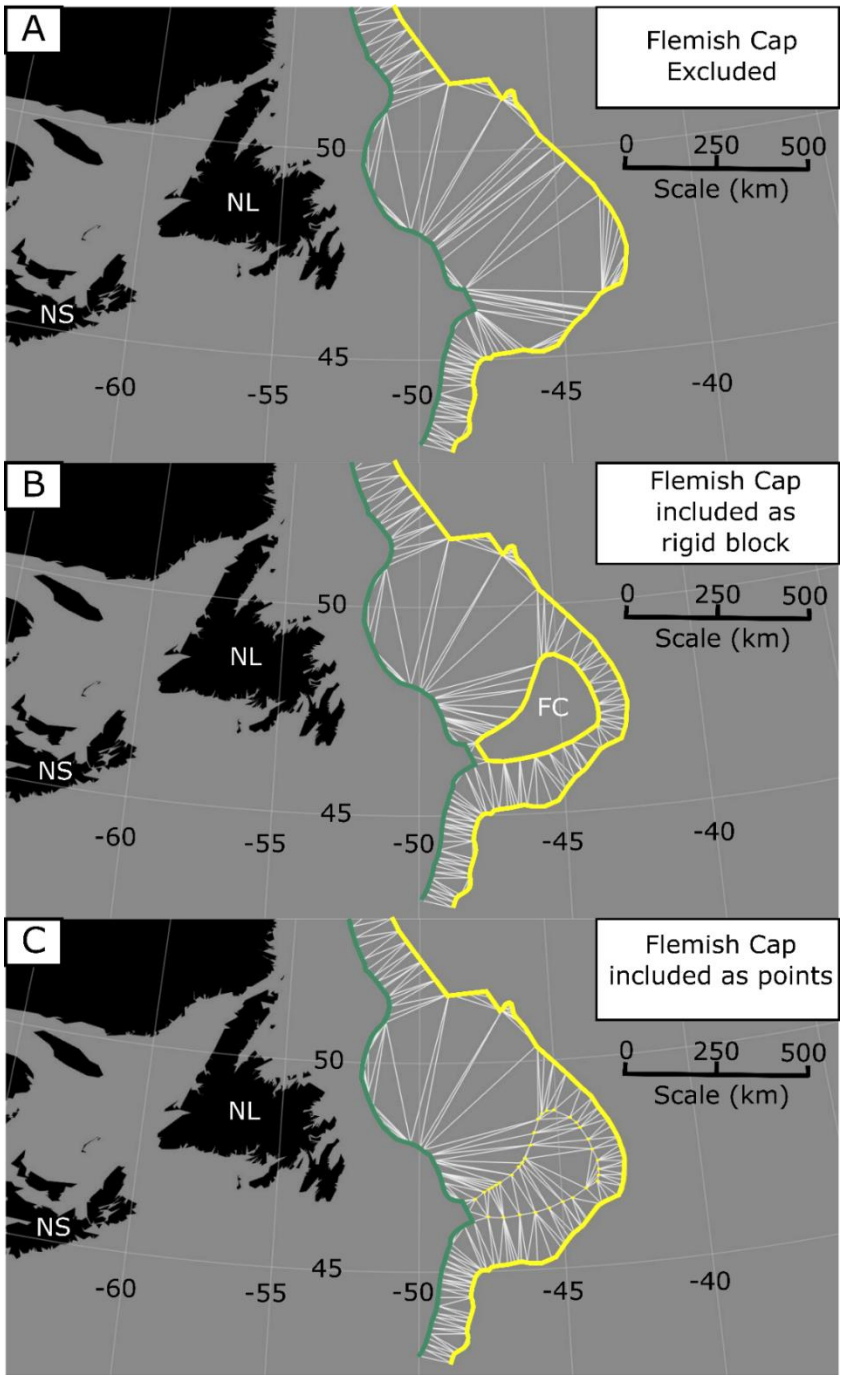

Figure 6.2 Variabilities in the mesh discretization of a deformable plate model caused by different model inputs. A) Deformable plate model along the Newfoundland margin that excludes continental blocks. The exterior and interior boundaries of deformation used in each model are the

edge of continental crust (ECC) (yellow) and necking line (green) from Peace et al. (2019), respectively. B) Deformable plate model that includes the Flemish Cap (FC) as a rigid polygon within the triangulation mesh using the geometry from Peace et al. (2019). C) Deformable plate model that includes the Flemish Cap as a group of points within the triangulation mesh. The placement of the points is designed after the geometry of the Flemish Cap from Peace et al. (2019). NL = Newfoundland and Labrador, NS= Nova Scotia.

6.2.2 Reconstructing present day crustal thicknesses

To our knowledge, all deformable plate models published to date using the GPlates software have been carried out using a constant crustal thickness assumption at an initial time frame of interest. For example, chapters 3-5 and previously published deformable plate models of the North Atlantic (Peace et al., 2019b) assume a 30 km crustal thickness estimate prior to the beginning of significant rifting, approximately 200 Ma. However, despite this assumption being adequate in previous studies investigating regional plate kinematics and deformation, crustal thicknesses are likely to be highly variable at model start times due to previous tectonic events not considered within the time frame of a model.

In this study, we present an alternative approach to building deformable plate models that involves reconstructing present day crustal thicknesses back through time using pyGPlates, a python library designed to access GPlates functionality using the python programming language. Present day crustal thickness estimates can be obtained via global crustal thickness models such as Crust 1.0 (https://igppweb.ucsd.edu/~gabi/crust1.html), or from previously published gravity inversion estimates such as those calculated along the offshore rifted margins of the North Atlantic

(Welford and Hall, 2007; Chappell and Kusznir, 2008; Welford et al., 2012) (Figure 1.2). Using pyGPlates, independently obtained crustal thickness estimates are converted into a scalar coverage (e.g. crustal thickness) GPlates file (.gpml file). Subsequently, these crustal thickness estimates are uploaded into pyGPlates or GPlates, providing the ability to reconstruct the crustal thickness estimates back through time within topological networks (Figure 6.3). There are many advantages to this approach such as the ability to calculate pre-Jurassic crustal thicknesses within topological networks (Figure 6.3).

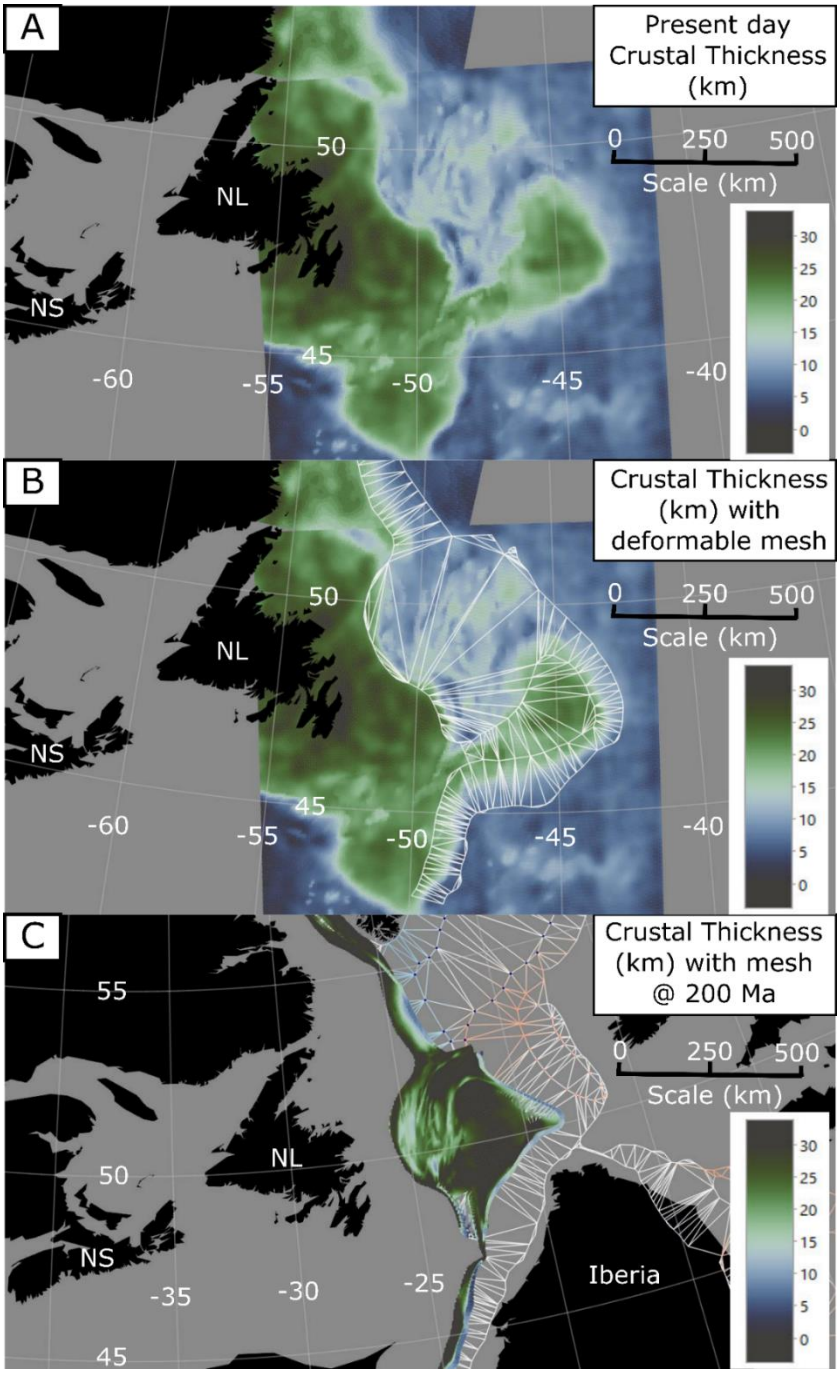

Figure 6.3 Reconstruction of crustal thickness estimates back through time within a deformable plate model. A) Gravity inversion crustal thickness estimates calculated along the Newfoundland and Labrador (NL) offshore rifted margins using the gravity inversion scheme described in

Welford et al., (2007, 2012). B) Same as (A) except with a topological network modified after Peace et al., (2019) overlying gravity inversion crustal thickness estimates. C) Reconstructed gravity inversion crustal thickness estimates at 200 Ma using the poles of rotation defined in Peace et al., (2019). Continental blocks included within the topological network are designed using points with geometries identical to the rigid polygons implemented in Peace et al., (2019). NS = Nova Scotia.

6.2.3 Expansion of deformable plate models within proximal rift domains

Rifted margins are commonly divided into different rift domains based on the mapping of their crustal structure and morphology using observations from seismic, potential field, and well data (Péron-Pinvidic and Manatschal, 2010; Peron-Pinvidic et al., 2013; Tugend et al., 2014; Nirrengarten et al., 2018). Considering previous rift domain mapping studies throughout the southern North Atlantic (Tugend et al., 2014; Nirrengarten et al., 2018), the definition of rift domains has proven to be useful for defining the boundaries in which deformation takes place within deformable plate models (Peace et al., 2019b). The necking line, a boundary where significant rift-related deformation and crustal thinning is interpreted to initiate, has been commonly used in previous studies as an interior deformable model boundary (Peace et al., 2019b; King et al., 2020, 2021).

When deformable plate models are investigated via the reconstruction of present day crustal thicknesses back through time and the extent of crustal thickness estimates extends into proximal domains (Figure 6.3), this provides the opportunity to expand deformable plate models landward beyond the extent of necking domains (Figure 6.4). This approach is advantageous for

several reasons. Arguably, the most impactful reasons are the ability to study deformation experienced within proximal domains and the potential for investigating the geometries of rift domain boundaries a priori, such as the necking line and the reconstructed edges of continental crust (RECC) (Nirrengarten et al., 2018) via the reconstruction of present day crustal thicknesses. More specifically, this offers a quick and comprehensive approach for identifying rift domain boundaries as opposed to previous approaches where rifted margins are sampled along numerous present day transects in order to determine the reconstructed geometries of rift domain boundaries (Nirrengarten et al., 2018). In addition, by expanding the size of deformable regions, this also helps mitigate modelling edge effects induced by close proximity of rigid model boundaries.

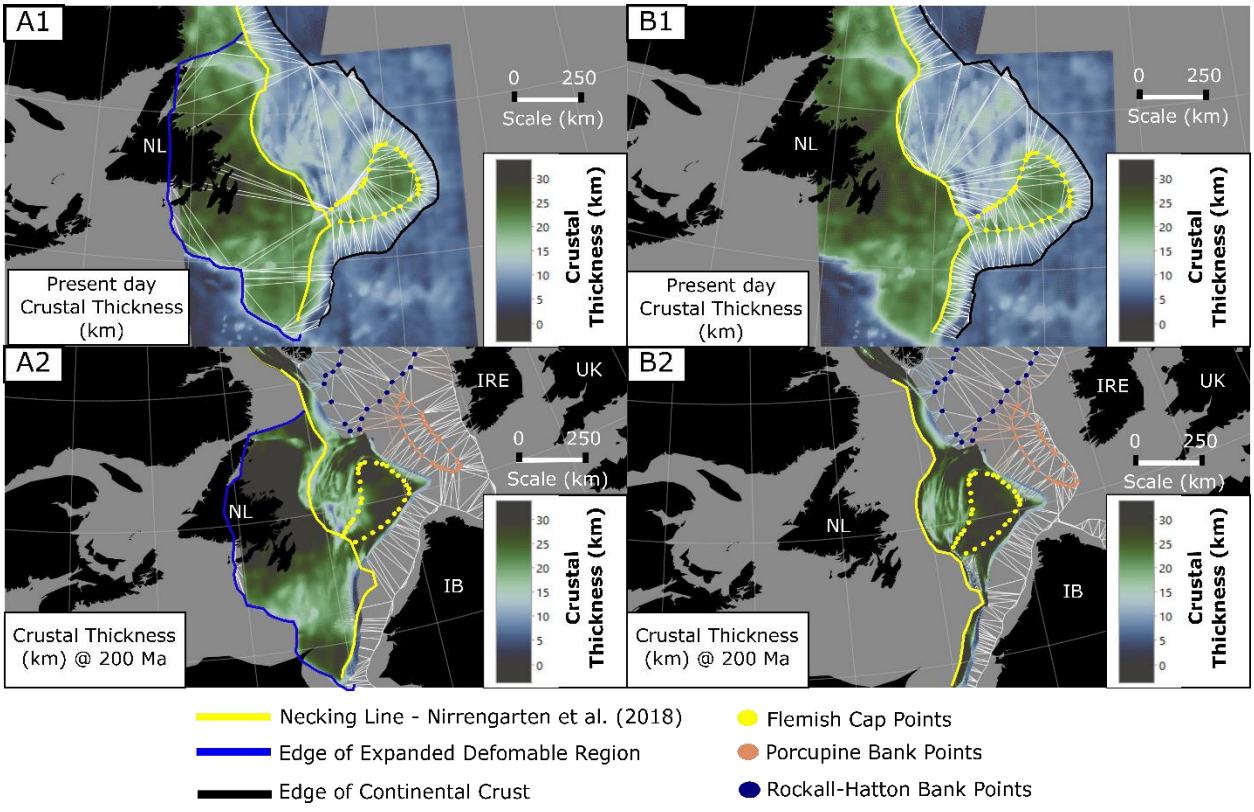

Figure 6.4 Reconstructing crustal thickness estimates back through time within deformable plate models with different interior boundaries. A1) Present day gravity inversion crustal thickness estimates with expanded topological network overlain. A2) Reconstructed crustal thickness estimates and expanded topological network at 200 Ma using the poles of rotation from Peace et al. (2019). B1) Same as (A1) except for a topological network that uses the necking line from Nirrengarten et al. (2018) as the interior topological network boundary (yellow line). B2) Same as (A2) except for a topological network that uses the necking line from Nirrengarten et al. (2018) as the interior topological network boundary. IB = Iberia, IRE = Ireland, NL = Newfoundland and Labrador, UK = United Kingdom.

6.2.4 Reconstructing alternative datasets within topological networks

Aside from crustal thickness estimates, the pyGPlates workflow discussed herein also provides the ability to convert other datasets (e.g. residual magnetic anomaly) into an appropriate GPlates file format that can be reconstructed within topological networks (Figure 6.5). Potential field datasets are often used to examine the present day crustal structure of tectonic regimes (Bronner et al., 2011; Szameitat et al., 2018a, 2020). Thus, the ability to reconstruct datasets (e.g. residual magnetic or free-air anomalies) according to the kinematics of features within topological networks can allow one to analyze the extent and orientation of potential field anomalies and structures throughout geological time (Figure 6.5). For example, within the North Atlantic, this approach could be used to study the onshore-offshore extent of structures throughout the North Atlantic that are interpreted to be inherited from previous Appalachian and Caledonian orogenic events.

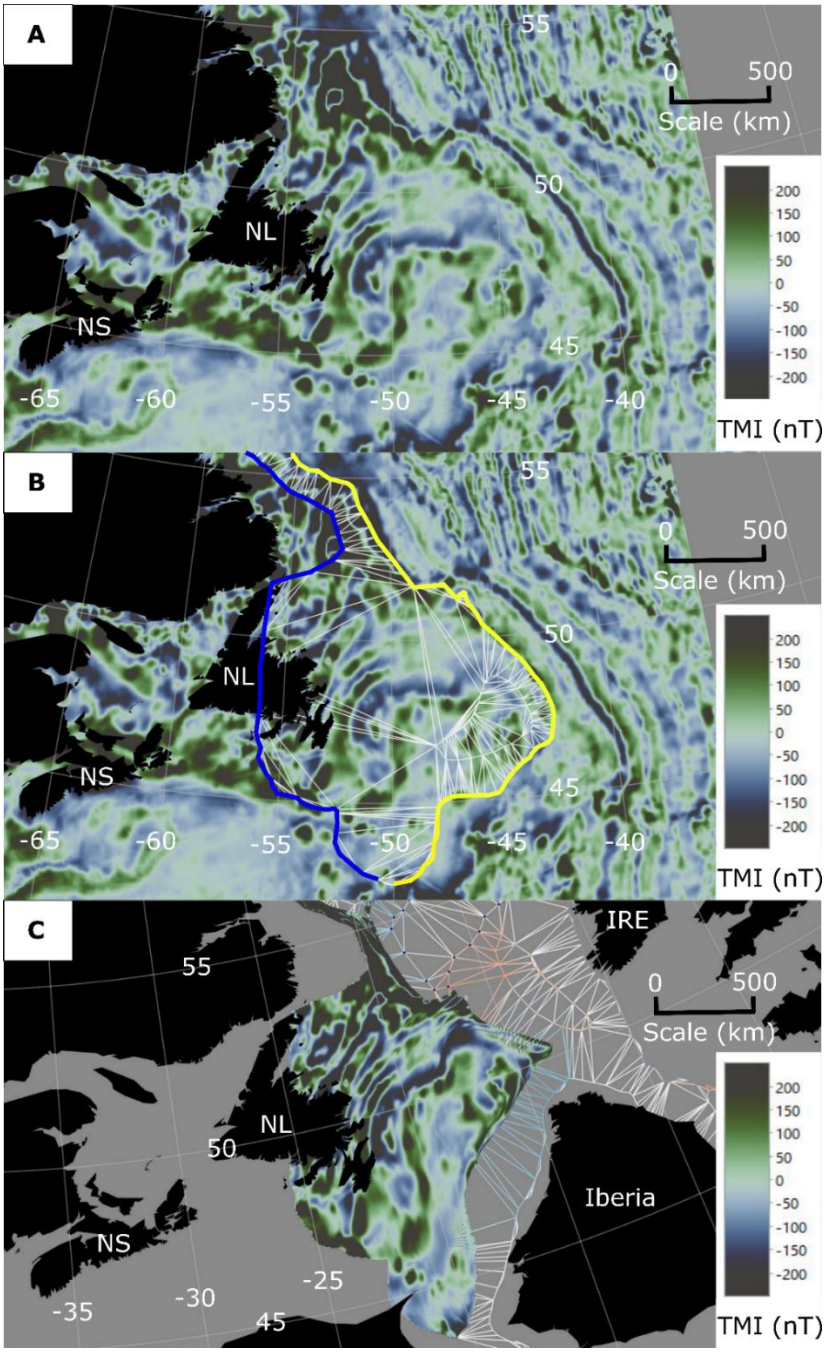

Figure 6.5 Reconstructing magnetic anomalies back through time within a deformable plate model. A) EMAG3 residual magnetic anomaly map along the Newfoundland margin. B) Same as (A) except with a topological network that is extended within the overlain proximal domain. The

yellow line represents the ECC from Nirrengarten et al., (2018) and the blue line represents the landward topological network boundary. C) Reconstructed residual magnetic anomaly along the Newfoundland margin at 200 Ma. NL = Newfoundland and Labrador, NS = Nova Scotia, TMI = Total Magnetic Intensity.

6.3 Application and Results

6.3.1 Application – Newfoundland, Irish, and West Iberian offshore rifted margins

In this section, previously published deformable plate models (Peace et al., 2019b) and gravity inversion crustal thickness estimates (Welford and Hall, 2007; Welford et al., 2012; King et al., 2020) along the Newfoundland, Irish, and West Iberian offshore rifted margins (Figure 6.6) are used to test the approaches and methodologies described in the previous section.

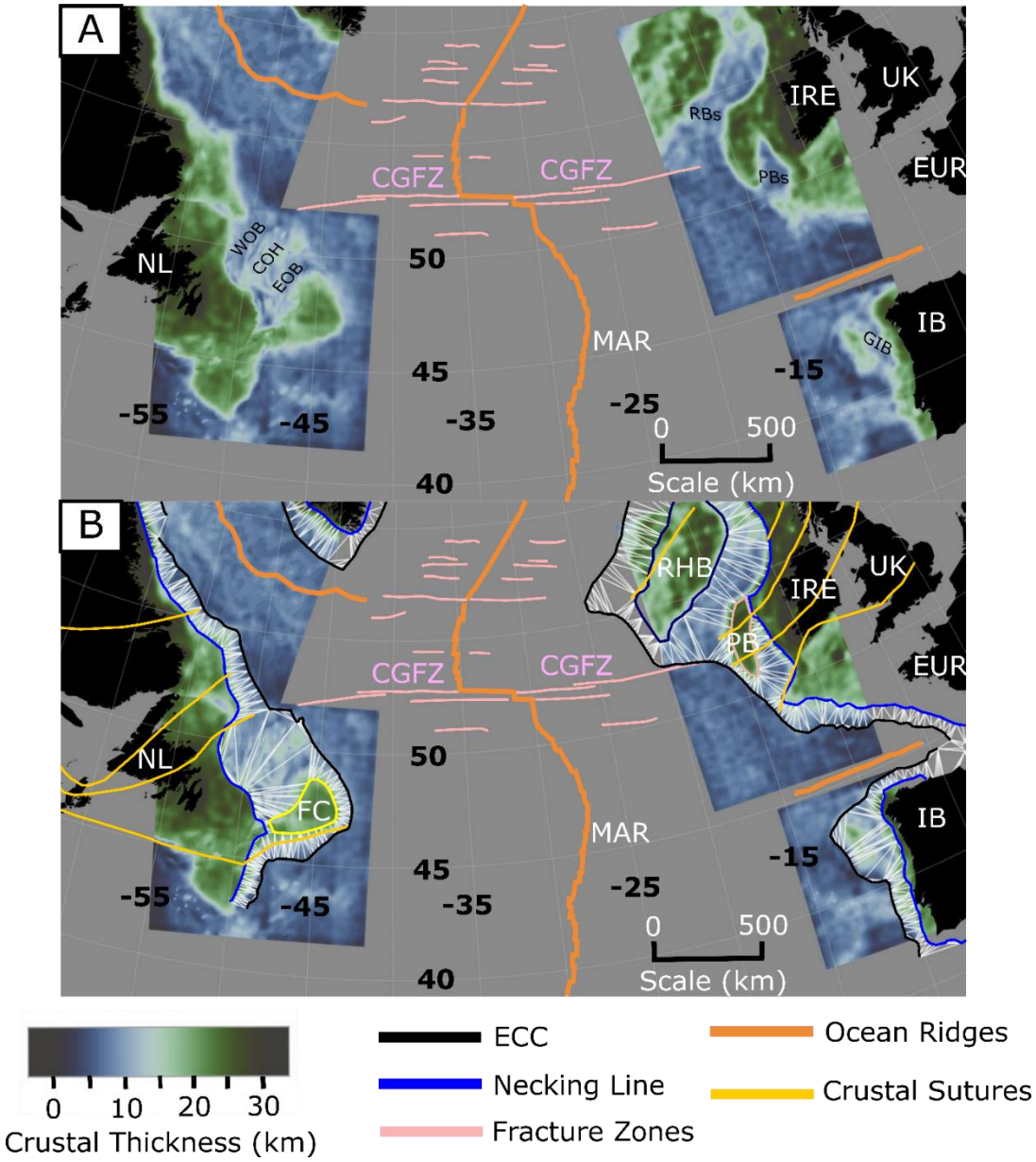

Figure 6.6 Deformable plate model inputs used in this study. A) Gravity inversion crustal thickness estimates calculated along the Newfoundland, Labrador, Ireland, and West Iberian offshore margins. B) Same as (A) except with the geometries of the necking line and edge of continental crust (ECC) from Nirrengarten et al. (2018) and the orientation of ancient crustal sutures throughout the North Atlantic from Welford et al. (2012) overlain. A topological network

(triangulation mesh) designed using rift domain boundaries (necking line and ECC) and continental blocks (rigid polygons) of the Flemish Cap, Porcupine Bank, and Rockall-Hatton Bank are also overlain. CGFZ = Charlie-Gibbs Fracture Zone, COH = Central Orphan High, EOB = East Orphan Basin, EUR = Europe, FC = Flemish Cap, GIB = Galicia Interior Basin, IB = Iberia, IRE = Ireland, MAR = Mid-Atlantic Ridge, PB = Porcupine Bank, PBs = Porcupine Basin, RBs = Rockall Basin, RHB = Rockall-Hatton Bank, UK = United Kingdom, WOB = West Orphan Basin.

In this study, four deformable plate models are tested to investigate the impact of the newly proposed workflow on the pre-Jurassic template and temporal evolution of crustal thicknesses along the Newfoundland, Ireland, and West Iberian offshore margins. The poles of rotation for each model are identical to the preferred deformable plate model used in Peace et al. (2019) (model 6c). However, the main differences between each model are the inclusion of continental blocks (Flemish Cap, Porcupine Bank, and Rockall Bank), their design (rigid blocks vs points), and the design of the landward boundary of deformation (Table 6.1). Model A1 excludes continental blocks from the interior of the deformable model. Models A2 and A3 include the Flemish Cap, Porcupine Bank, and Rockall-Hatton Bank. However, model A2 includes the continental blocks as rigid polygons, whereas continental blocks in model A3 are included as points using the same geometries as those used in model A2. Model A4 is identical to model A3 aside from the expansion of the landward boundary of deformation along the Newfoundland and Irish offshore margins into the proximal domain based on the extent of crustal thickness estimate coverage. The landward boundary of deformation is not expanded along the West Iberian margin due to a lack of crustal thickness estimate coverage landward of the West Iberian margin necking line. The pre-Jurassic crustal thickness results of each model (Figures 6.7 and 6.8) are reconstructed to 200 Ma.

Model	Poles of Rotation	Continental Blocks Included?	Continental Block Geometry	Continental Block Design	Deformation within proximal domains?
1	Peace et al. (2019)	No	N/A	N/A	No
2	Peace et al. (2019)	Yes	Peace et al. (2019)	Rigid Blocks	No
3	Peace et al. (2019)	Yes	Peace et al. (2019)	Points	No
4	Peace et al. (2019)	Yes	Peace et al. (2019)	Points	Yes

Table 6.1 Description of deformable model parameters used in this study.

6.3.2 Pre-Jurassic (200 Ma) crustal thickness results

The inclusion and design of continental blocks have a significant impact on the pre-Jurassic crustal thicknesses calculated by all models tested (Figures 6.7 and 6.8). In model A1, crustal thicknesses calculated at 200 Ma within the Orphan Basin following the reconstruction of present day gravity inversion estimates are highly variable from west to east. Within the West Orphan Basin (Figure 6.7), an approximately NNE-SSW trending region of crust ~ 5-15 km thick is bordered by thicker regions of crust ~ 15-20 km thick along its western and eastern extents. Within the Central Orphan High, thicker NNE-SSW trending regions of crust (20-30 km thick) are observed which segment localized regions of thinner crust (~ 10-15 km thick). In the East Orphan Basin, an area of relatively thinner crust (~ 5-15 km thick) is bordered by thicker regions of crust to the west (~ 20-25 km thick) and the Flemish Cap (~ 30-35 km thick) to the east. Along the Irish margin, the thickest regions of crust are observed within the Porcupine Bank and Rockall-Hatton Bank (~ 25-35 km thick). Within the Porcupine and Rockall basins, crustal thicknesses range from approximately 5-15 km thick within the center of each basin, gradually getting thicker (~ 20-25 km thick) towards their western and eastern extents. However, throughout the center of the Rockall

Basin, localized regions of thicker crust (~ 15-20 km thick) are observed and scattered throughout its southwest and northeastern limits. For the West Iberian margin, crustal thicknesses range from approximately 25-35 km thick with a localized area of thinner crust (~ 15 km thick) located southeast of the Flemish Cap.

In model A2, the Flemish Cap, Porcupine Bank, and Rockall Hatton Bank are included as rigid polygons within the deformable region. Within the Orphan Basin, crustal thicknesses range from about 25-35 km thick, aside from localized N-S trending regions of slightly thinner crust (~ 15-20 km thick) that are focused within the West Orphan Basin. Due to the inability to model deformation within rigid continental blocks, crustal thicknesses within the Flemish Cap remain the same as those observed present day. Similarly along the Irish margin, the Porcupine Bank and Rockall-Hatton Bank crustal thicknesses are identical to those observed present day. Within the Rockall and Porcupine basins, crustal thicknesses range from about 30-40 km thick, with regions of relatively thinner crust (~ 5-15 km thick) in the southwestern corner of the Rockall Basin (yellow star in Figure 6.7). Along the West Iberian margin, crustal thicknesses calculated by model A2 are nearly identical to those calculated by model A1. However, additional segmented localized regions of thinner crust (~ 15-20 km thick) are observed within the proto Galicia Interior Basin, east of the Galicia Bank.

Model A3 uses identical continental block geometries as model A2, but the continental blocks are designed as points rather than rigid polygons. Overall, model A3 demonstrates similar crustal thickness values as model A2 along the Newfoundland and Irish margins. However, a key difference is the thicker crustal thicknesses (~ 25-35 km thick) within the Flemish Cap, Porcupine Bank, and Rockall-Hatton Bank calculated by model A3 due to their ability to experience

deformation. In addition, the regions of slightly thinner crust throughout the Orphan Basin (~ 15-20 km thick) are more elongated in comparison to model A2 and oriented approximately NNE-SSW. Crustal thicknesses calculated along the West Iberian margin in model A3 are the same as those in model A2.

Model A4 expands the interior deformable model boundary to include proximal domains along the Newfoundland and Irish margins. Within the Orphan Basin, pre-Jurassic crustal thicknesses calculated by model A4 are very similar to those calculated by model A3. Some key differences include the widening and northerly expansion of the relatively thinner region of crust (15-20 km thick) within the West Orphan Basin (red star in Figure 6.8) and the widening of the thinner region of crust (~ 8-10 km thick) to the southwest of the Flemish Cap (yellow star in Figure 5.8b). Westward of the Orphan Basin, along the Bonavista Platform, crustal thicknesses range from about 25-30 km thick. Towards the south along the Newfoundland Grand Banks, crustal thicknesses are slightly thinner (~ 15-25 km thick) until the southern tail of the Grand Banks where crustal thicknesses are relatively thicker (~ 25-30 km thick). Aside from slightly thinner crustal thicknesses calculated within the proto Porcupine Basin (~ 15 km thick), crustal thicknesses calculated by model A4 along the Irish margin are similar to those calculated by model A3. Within the proximal domains along the Irish margin, crustal thicknesses range from about 20-30 km thick. Crustal thicknesses calculated by model A4 along the West Iberian margin are mostly identical to those calculated by models A2 and A3.

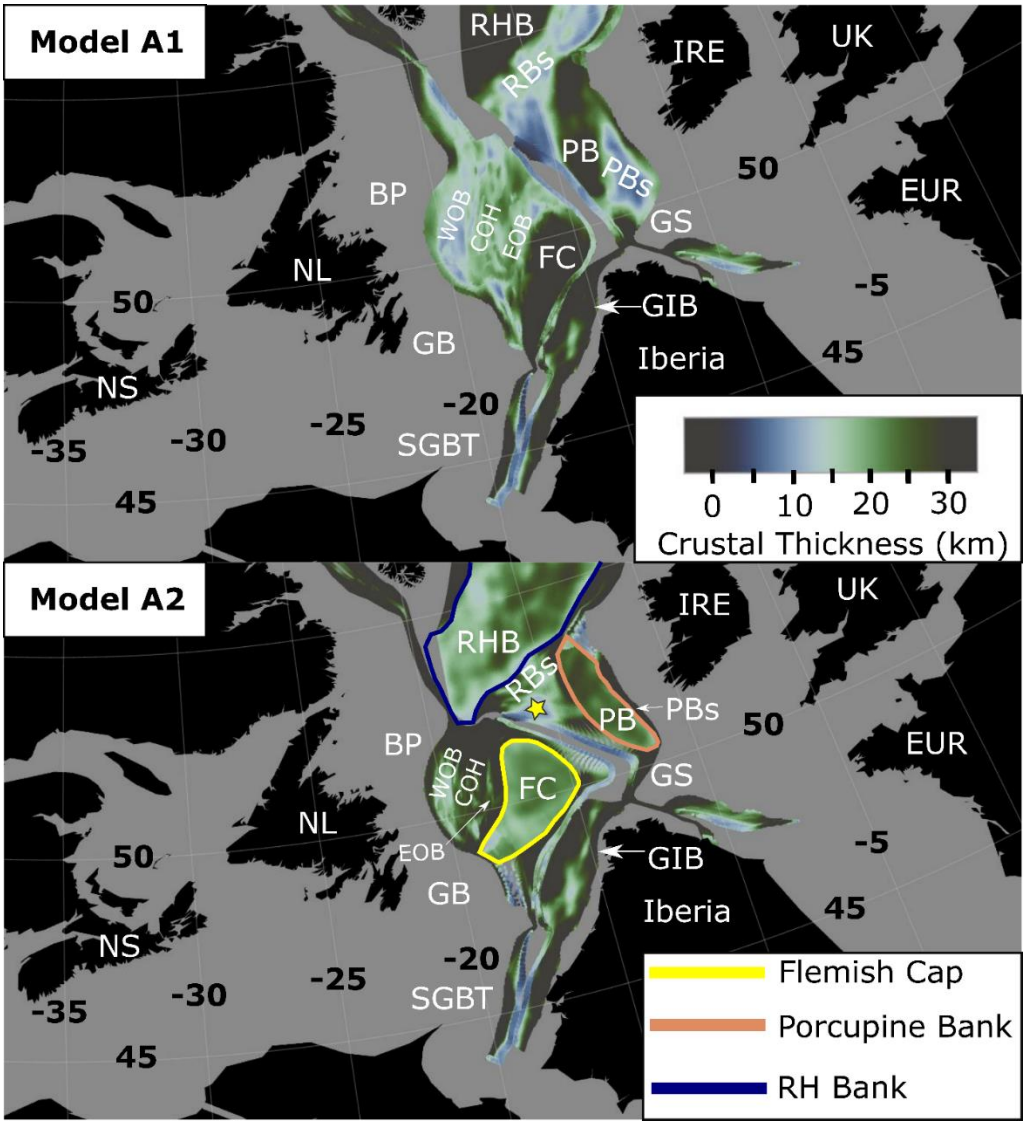

Figure 6.7 Crustal thickness results of models A1 and A2 calculated at 200 Ma. The yellow star in model A2 represents an area of localized thinner crust within the Rockall Basin. BP = Bonavista Platform, COH = Central Orphan High, EOB = East Orphan Basin, EUR =Europe, FC = Flemish Cap, GB = Grand Banks, GIB = Galicia Interior Basin, GS = Goban Spur, IRE = Ireland, NL, Newfoundland, NS= Nova Scotia, PB = Porcupine Bank, PBs = Porcupine Basin, RBs = Rockall

Basin, RHB = Rockall-Hatton Bank, SGBT = Southern Grand Banks Tail, UK = United Kingdom, WOB = West Orphan Basin.

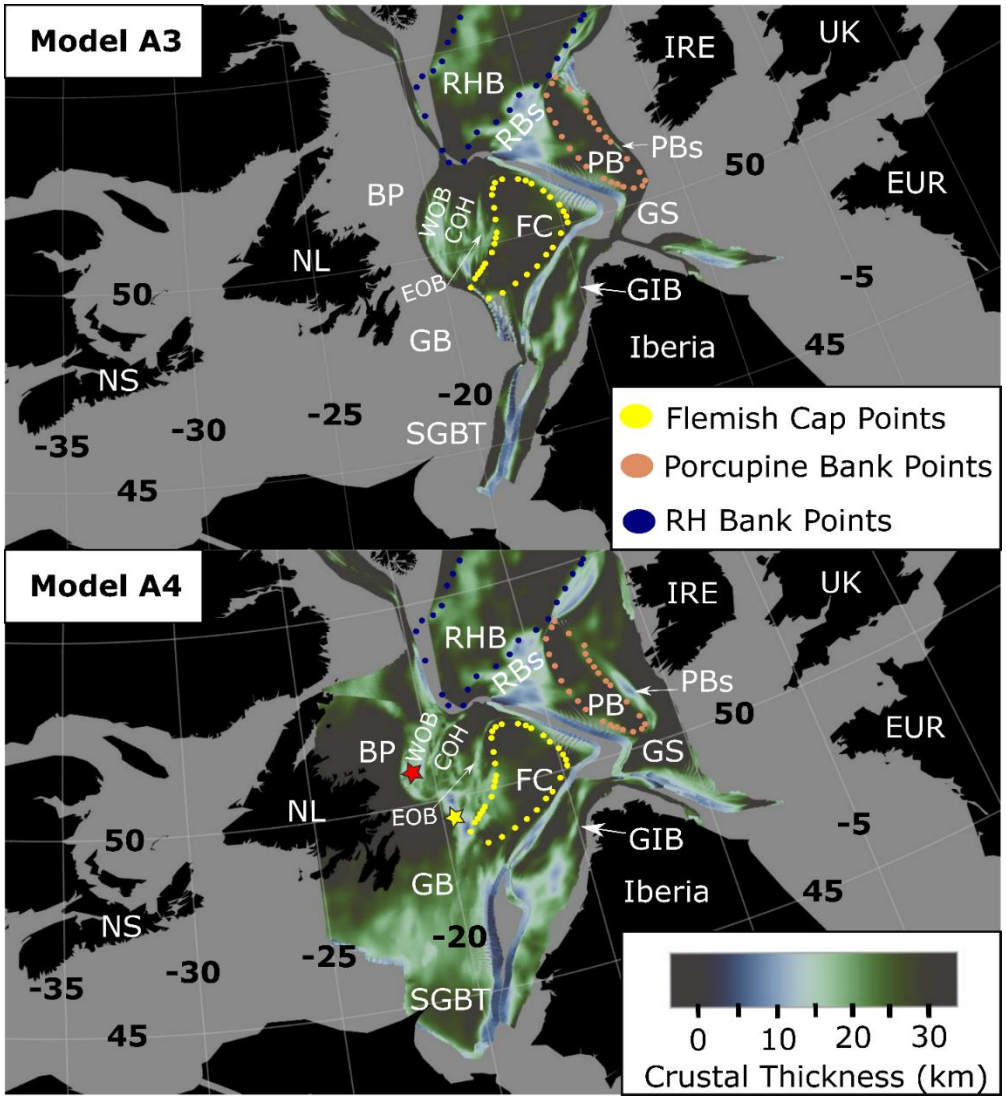

Figure 6.8 Crustal thickness results of models A3 and A4 calculated at 200 Ma. The yellow and red stars in model A4 represent regions of relatively thinner crust within the southeast and west Orphan basins, respectively. BP = Bonavista Platform, COH = Central orphan High, EOB = East Orphan Basin, EUR =Europe, FC = Flemish Cap, GB = Grand Banks, GIB = Galicia Interior

Basin, GS = Goban Spur, IRE = Ireland, NL, Newfoundland, NS= Nova Scotia, PB = Porcupine Bank, PBs = Porcupine Basin, RBs = Rockall Basin, RHB = Rockall-Hatton Bank, SGBT = Southern Grand Banks Tail, UK = United Kingdom, WOB = West Orphan Basin.

6.4 Discussion

6.4.1 Pre-Jurassic crustal thicknesses

The inclusion and variable design of continental blocks and model boundaries demonstrate a significant impact on the pre-Jurassic crustal thicknesses calculated by each deformable plate model of the southern North Atlantic. Herein, the pre-Jurassic (200 Ma) crustal thicknesses calculated by each model are assessed and compared against all models tested and previous observations regarding the pre-Jurassic template of the southern North Atlantic.

Model A1 is the only model that excludes continental blocks from the interior of topological networks. Interestingly, model A1 calculates pre-Jurassic crustal thicknesses and geometries of the Flemish Cap, Porcupine Bank, Rockall Bank, and Galicia Bank, similar to those inferred from previous studies regarding their crustal structure and pre-Jurassic nature (Funck et al., 2003; Welford and Hall, 2007; Welford et al., 2012; Nirrengarten et al., 2018; Peace et al., 2019b; King et al., 2020). However, despite calculating reasonable pre-Jurassic crustal thicknesses and geometries of these continental blocks, large crustal thickness discrepancies are observed within surrounding sedimentary basins. In particular, the Orphan and Porcupine basins are poorly restored, resulting in crustal thicknesses that are similar to those observed present day along the Newfoundland and Irish margins, respectively. Therefore, although the pre-Jurassic nature of continental blocks are restored, model A1 is deemed unsatisfactory due to its inability to

reconstruct pre-Jurassic crustal thicknesses within sedimentary basins throughout the North Atlantic that are consistent with relatively undeformed continental crust (~ 25-40 km thick).

In contrast, the inclusion of continental blocks as rigid polygons in model A2 results in pre-Jurassic crustal thicknesses throughout the southern North Atlantic that are more consistent with those inferred from previous studies of its pre-Jurassic structure (~ 30-35 km thick) (Mohn et al., 2015; Brune et al., 2017). Throughout the North Atlantic, the majority of pre-Jurassic crustal thicknesses vary from about 25-35 km thick, in agreement with previous interpretations and assumptions inferred from numerical modelling (Mohn et al., 2015; Brune et al., 2017; Neuharth et al., 2021) and deformable plate reconstruction studies (Peace et al., 2019b). However, along each margin, regions of relatively thinner crust (~ 15-25 km thick) are observed. Within the Orphan Basin, regions of NNW-SSE trending relatively thinner crust (~ 15-25 km thick) are seen throughout the basin, most notably, within the West Orphan Basin. The West Orphan Basin is acknowledged as a failed rift in previous seismic refraction (Chian et al., 2001; Welford et al., 2020) and gravity inversion studies (Welford and Hall, 2007). In addition, the onshore to offshore extension and geometry of ancient basement terranes within the Orphan Basin (Figure 5.2) are also disputed (Welford et al., 2012; Ady and Whittaker, 2018). The nature and potential cause for these reconstructed regions of relatively thinner crust are addressed in more detail within the companion contribution from this study (Chapter 7). However, it is postulated that the West Orphan Basin may have been influenced by older tectonic events (pre-200 Ma) and offshore to onshore inherited boundaries separating ancient basement terranes along the Newfoundland margin (Waldron et al., 2019). Along the West Iberian margin, within the Galicia Interior Basin, relatively thinner NE-SW trending regions of crust (~ 15-20 km thick) are observed. The location and segmentation of these

relatively thinner regions of crust demonstrate interesting correlations with previously interpreted Variscan structures within the Galicia Interior Basin (Murillas et al., 1990; King et al., 2020). Thus, similar to the interpretation for the Orphan Basin, the distribution of inherited structures and lack of consideration for pre-200 Ma tectonic events may potentially explain the variable magnitude of pre-Jurassic crustal thicknesses calculated by model A2. Furthermore, despite an improvement in the ability to reconstruct pre-Jurassic crustal thicknesses within sedimentary basins, the crustal thicknesses of the continental blocks in model A2 remain the same as their present day thicknesses due to their design as rigid polygons. Thus, the crustal thickness evolution of continental blocks is not restored by model A2.

In model A3, the use of points for designing continental blocks rather than rigid polygons allows deformation to be experienced within each block (Figure 6.8). As a result, pre-Jurassic crustal thicknesses calculated within the Flemish Cap, Porcupine Bank, and Rockall Bank range from ~ 25-35 km thick and are in better agreement with similar pre-Jurassic estimates proposed in previous studies (Whitmarsh et al., 1974; Makris et al., 1991; O'Reilly et al., 1996; Funck et al., 2003; Welford et al., 2010, 2012). Aside from the crustal thicknesses of the blocks themselves, pre-Jurassic crustal thicknesses throughout the rest of the North Atlantic are nearly identical to those calculated by model A2.

Model A4 is identical to model A3 aside from the expanded landward boundary of deformation within proximal domains in model A4 based on the landward extent of crustal thickness estimates calculated by gravity inversion (Figure 6.8). Overall, similar crustal thickness trends are observed throughout the North Atlantic as those calculated by models A2 and A3. However, the most significant differences calculated by model A4 in comparison to other models

are observed along the Newfoundland and Irish margins (Figures 6.7 and 6.8). At 200 Ma, crustal thicknesses throughout the Newfoundland margin are highly variable in magnitude and trend. Within the Orphan Basin, narrow NE-SW trending depocenters (with crust ~ 15-25 km thick) are observed, with the widest region being within the West Orphan Basin (yellow arrow in Figure 6.9). In addition, to the south of the West Orphan Basin, an approximately N-S trending region of thinner crust (~ 10-15 km thick) is observed (cyan arrow in Figure 6.10). Although the precise origin of this relatively thin pre-Jurassic crust is unknown, it is postulated that it may have been caused by older tectonic events not included within the time frame of the model. This interpretation is elaborated on in more detail within the companion contribution (Chapter 7) of this work. Within the Central Orphan Basin, the previously described depocenters are separated by regions of relatively thicker crust (~ 25-35 km thick), collectively referred to as the Central Orphan High, interpreted to correspond to the pre-Jurassic configuration of the Orphan Knoll (red star in Figure 6.9) and the Flemish Cap to the east. Along the Bonavista Platform, crustal thicknesses at 200 Ma range from about 30-35 km thick. Further south along the Newfoundland Grand Banks, crustal thicknesses vary from approximately 15-25 km thick, with the thinnest regions being situated within localized NE-SW trending regions (red arrow in Figure 6.9). Additionally, the Grand Banks demonstrate an interesting segmentation between the relatively thicker Bonavista Platform to the north (~ 30-35 km thick) and the similarly thick southern tail of the Grand Banks to the south (~ 25-30 km thick). The nature of this segmentation is discussed in more detail within the companion contribution from this study (Chapter 7). Briefly, the segmentation observed along the Grand Banks demonstrates interesting correlations with the offshore extension of the Meguma terrane boundary from Nova Scotia (Figure 1.4), suggesting that it potentially impacted the pre-Jurassic

structure and subsequent rift-related deformation experienced along the Grand Banks. Throughout the Irish margin, crustal thicknesses calculated by model A4 within proximal domains range from about 25-35 km thick. Another notable difference compared to model A3 is the relatively thinner pre-Jurassic crust (~ 10-15 km thick) calculated by model A4 within the Porcupine Basin, much thinner than that calculated by models 2 and 3 (~ 25-35 km thick).

6.4.2 Temporal crustal thickness evolution of model A4

In this section, the temporal crustal thickness evolution of model A4 along the Newfoundland, Irish, and West Iberian margins (Figure 6.9) is briefly discussed. However, it should be noted that temporal variations in crustal thicknesses calculated by models A2 and A3 are similar to those calculated by model A4. Thus, given these similarities and the fact that model A4 also includes the crustal thickness evolution of proximal domains, its evolution is chosen to be described in this section.

6.4.2.1 Newfoundland margin

Following the initiation of rift-related deformation along the Newfoundland margin, rifting and subsequent crustal thinning calculated by model A4 throughout the Jurassic (200-150 Ma) appears to be diffuse and primarily controlled by the interplay between the clockwise rotation of the Flemish Cap and the gradual separation of Iberia from southeastern Newfoundland. By 150 Ma, the southern tail of the Grand Banks is slightly thinner (~ 15-20 km thick) compared to its pre-Jurassic thickness (~ 25-30 km thick). Transitioning from the Jurassic to Early Cretaceous (150-125 Ma), significant crustal thinning (crust 10 km thick or less) is experienced within the East and West Orphan basins. These regions of significantly thinned crust are partitioned by blocks

of relatively thicker crust (~ 15-20 km thick), such as the Orphan Knoll (red star in Figure 6.9), within the Central Orphan Basin, in a region known as the Central Orphan High. Thus, similar to the smaller blocks of relatively thicker crust to the southwest, the Orphan Knoll appears to be an extensional relic of thicker crust that was once connected with the Flemish Cap and Rockall Bank along the Newfoundland and Irish margins, respectively. Furthermore, the onset of significant crustal thinning calculated by model A4 within the Orphan Basin is consistent with previous observations regarding the timing of syn-rift sedimentation within the Orphan Basin (Sibuet et al., 2007; Gouiza et al., 2017; Sandoval et al., 2019; MacMahon et al., 2020; Cawood et al., 2021a, 2021b) and the timing of significant crustal thinning inferred from previous deformable plate modelling studies (Peace et al., 2019b). By 125 Ma, sea-floor spreading begins along the southeastern Newfoundland and southwest Iberian margins (Nirrengarten et al., 2018) and continues to propagate northward from the Middle to Late Cretaceous.

6.4.2.2 Irish margin

Along the Irish margin, the majority of Jurassic (~ 200–150 Ma) crustal thinning is experienced within the Porcupine and Rockall basins as a result of the Porcupine Bank and Rockall Bank kinematics, respectively. Within the Porcupine Basin, significantly thinned crust (~ 5-15 km thick) is observed by the end of the Jurassic (~ 150 Ma) as a result of the clockwise rotation of the Porcupine Bank. At 150 Ma, the Porcupine Basin appears to be isolated and disconnected from adjacent margins and basins by relatively thicker regions of crust (~ 25-30 km thick) at the southern tail of the Porcupine Bank and the northwest limit of the Goban Spur. This observation conflicts with previous interpretations made from rigid plate models that suggest a connection between the Porcupine Basin and Galicia Interior Basin by the end of the Jurassic (Nirrengarten et al., 2018;

Sandoval et al., 2019). Within the Rockall Basin, crustal thicknesses by the end of the Jurassic range from approximately 5-15 km thick, with thicker regions of crust (20-30 km thick) along the edges of the basin surrounding the Porcupine and Rockall banks. Furthermore, by the end of the Jurassic (~ 150 Ma), crustal thicknesses calculated within the Porcupine Bank are segmented by approximately ENE-WSW trending regions of relatively thinner crust (~ 20 km thick) that are aligned with the offshore extension of ancient terrane boundaries. This observation is also in agreement with interpretations made from recent deformable plate models along the Irish margin that suggest that the Porcupine Bank experienced segmentation and shearing as a result of the interplay between its independent kinematics and offshore extension of terrane boundaries inherited from the Caledonian and Appalachian orogenic events (Yang et al., 2021). Furthermore, these regions of segmentation calculated by model A4 within the Porcupine Bank continue to widen and experience localized crustal thinning from the end of the Jurassic until the Early Cretaceous (125 Ma). By 125 Ma, the Porcupine and Rockall basins are fully opened and encompass significantly thinned crust ranging from less than 5 km thick within the center of each basin to gradually thicker crust (~ 15-30 km thick) towards their western and eastern extents.

6.4.2.3 West Iberian margin

Along the West Iberian margin, little deformation and crustal thinning is calculated by model A4 throughout the Jurassic (200-150 Ma). From the Late Jurassic to Early Cretaceous (150-125 Ma), segmented regions of significantly thinned crust (10 km or less) are observed within the Galicia Interior Basin (Figure 6.9). To the west of the Galicia Interior Basin, the Galicia Bank (Figure 6.9), a previously recognized continental block (Péron-Pinvidic and Manatschal, 2010; King et al., 2020), experiences internal deformation throughout the Early Cretaceous, leading to

crustal thicknesses within the Galicia Bank ranging from about 15-20 km thick (orange arrow in 125 Ma panel in Figure 6.9). The deformation experienced within the Galicia Bank is primarily caused by significant rift-related deformation induced by the breakup between the southeast Newfoundland and West Iberian margins. Furthermore, the Galicia Bank appears to have a similar crustal thickness evolution to that of the Orphan Knoll along the Newfoundland margin. In particular, pre-Jurassic crustal thicknesses calculated by model A4 suggest that the Galicia Bank and Flemish Cap evolved as a single continental block prior to Early Cretaceous rifting, a phenomenon suggested in Chapter 3. As a consequence, this interpretation also raises the questions as to why these two blocks separated and what contributed to their morphological variability with respect to their associated ancient basement terranes. Despite a lack of drilling on the Galicia Bank itself, the Galicia Bank is often interpreted to encompass Variscan domain crust based on the offshore extension of Variscan terranes from the Iberian and European interiors (Matte, 2001; Catalán et al., 2014). In contrast, rocks indicative of the Avalon zone have been penetrated via drilling on the Flemish Cap, suggesting that the Flemish Cap encompasses Avalonian terrane rocks (King et al., 1985). Thus, it is postulated that the Variscan Front (Figure 1.4) potentially intersected the limits of the Flemish Cap and Galicia Bank at 200 Ma. As a result, the Variscan Front may have acted as an inherited weakness which promoted the separation of the two blocks, leading to their independent crustal structure observed from gravity inversion and seismic crustal thickness estimates.

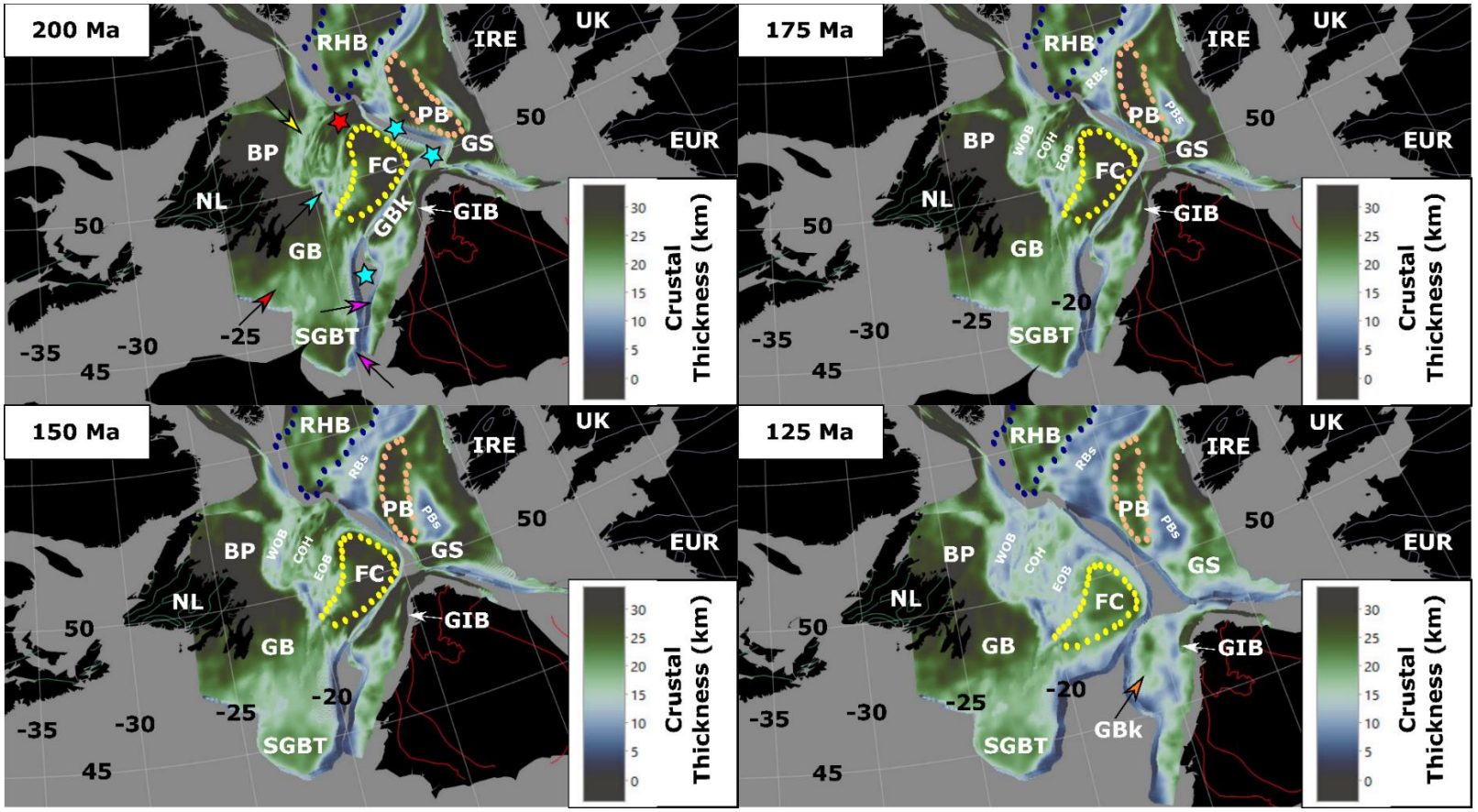

Figure 6.9 Temporal crustal thickness evolution of model A4 from 200 Ma to 125 Ma. The geometries of inherited structures (thin green and red lines) overlying the interiors of Newfoundland (NL), Ireland (IRE), United Kingdom (UK), and Europe (EUR) are from

Nirrengarten et al., (2018). Overlying the crustal thickness results are the geometries of the Flemish Cap (yellow points), Porcupine Bank (orange points), and Rockall Bank (navy blue points). The cyan stars and red star in the 200 Ma panel represent gaps between crustal thickness estimates and the pre-Jurassic position of the Orphan Knoll, respectively. The red arrow in the 200 Ma panel indicates an area of localized thinner crust within the southern Grand Banks. The magenta arrows and yellow arrow in the 200 Ma panel highlight the preserved thinner crust within ocean-continent transitions and the West Orphan Basin, respectively. The cyan arrow in the 200 Ma panel points to the region of localized thinned crust located southwest of the Flemish Pass. The orange arrow in the 125 Ma panel points to the Galicia Bank (GBk). BP = Bonavista Platform, COH = Central Orphan High, EOB = East Orphan Basin, FC = Flemish Cap, GB = Grand Banks, GBk = Galicia Bank, GIB = Galicia Interior Basin, GS = Goban Spur, NS= Nova Scotia, PB = Porcupine Bank, PBs = Porcupine Basin, RBs = Rockall Basin, RHB = Rockall-Hatton Bank, SGBT = Southern Grand Banks Tail, WOB = West Orphan Basin.

6.4.3 Model gaps and discrepancies

The pre-Jurassic configuration and crustal thicknesses calculated by each model along the Newfoundland, Irish, and West Iberian margins reveal discrepancies and gaps (cyan stars in Figure 6.9) that need to be addressed. However, although these gaps and discrepancies are briefly discussed herein, they are more thoroughly addressed and tested by subsequent models discussed in the companion contribution from this work (Chapter 7).

First, for each model at 200 Ma, gaps in crustal thickness estimates reconstructed along each margin are observed. The cause of these gaps could be due to several different aspects that are not considered in this study. One potential cause of these gaps is related to the disputed poles of rotation and restored fit of Iberia and Europe relative to Newfoundland at 200 Ma (Barnett-Moore et al., 2016). Additionally, other reasons for these restored gaps could be due to inaccurate geometries, inappropriate inclusion, and poorly constrained poles of rotation of continental blocks throughout the North Atlantic.

Another discrepancy observed from all the models shown herein is the preservation of significantly thinned crust within the continent-ocean-transitions (COTs) (magenta arrows in Figure 6.9). Similar to the occurrence of crustal thickness gaps, the preservation of significantly thinned crust within COTs could be a result of several phenomena that are not considered within this study. Analogous to the postulated causes of crustal thickness gaps, the pre-Jurassic configuration and geometries of various micro-plates and continental blocks at 200 Ma throughout the North Atlantic could lead to the preservation of ocean-ward regions of thinner crust. In addition, the lack of consideration for Triassic or older tectonic events could also partially

contribute to these observations. Furthermore, another possibility could be uncertainties related to interpreting the boundary representing the edge of continental crust that is used as the exterior topological network boundary. An exterior topological network boundary positioned further landward could potentially remove these thinner areas of pre-Jurassic crust, however, this approach would also lead to larger gaps between reconstructed crustal thicknesses along the margins.

6.4.4 Implications for future work

Deformable plate models have been successfully used to investigate the interplay between plate kinematics and deformation throughout numerous tectonic environments around the globe (Ady and Whittaker, 2018; Müller et al., 2019; Peace et al., 2019b; Cao et al., 2020; King et al., 2020, 2021; Yang et al., 2021). Considering the applications shown herein and previous studies throughout the North Atlantic, the necessity to include continental block kinematics in reconstructions of the North Atlantic continues to be emphasized in order to properly restore pre-Jurassic crustal thicknesses and crustal thinning experienced along rifted margins.

In addition, the results of this study prompt recommendations from the authors regarding the workflow and considerations for future deformable plate modelling studies. In our opinion, if similar crustal thickness constraints to those presented are available via gravity inversion or seismic data, reconstructing present day crustal thickness estimates back through time is a recommended first approach when entering the preliminary stages of building deformable plate models. This viewpoint is based on the fact that fewer assumptions are being imposed using this approach and it also provides the ability to mitigate edge effects by reducing the number of rigid

features within the model interior. As demonstrated by the results of model A1, this can also help inform the pre-Jurassic structure and position of various crustal blocks, regardless of their inclusion within a deformable plate model. In addition, depending on the extent of crustal thickness estimate coverage, landward regions outside of a particular study area can be included to help aid our understanding of their tectonic evolution, while also mitigating model edge effects caused by rigid boundaries and the need to define detailed landward boundaries of deformation. If crustal blocks are present within regions of interest, their design using a group of points is recommended in order to simulate the relatively minor amounts of deformation usually experienced within their interiors. We also note that using similar deformable plate modelling strategies to those presented in previous studies (Peace et al., 2019b; Cao et al., 2020; King et al., 2020, 2021; Yang et al., 2021) still offers a very useful methodology, especially when detailed crustal thickness constraints are lacking within regions of interest. However, the ability to avoid the modelling assumptions from those studies through the interplay of pyGPlates and GPlates presents an avenue for continuous methodological improvements of deformable plate models and their application to studying tectonic regimes.

6.5 Conclusions

In this study, new approaches are highlighted for building deformable plate models using the interplay and current capabilities of GPlates and pyGPlates. The main conclusions of this study are:

1. Using point geometries when designing continental blocks in GPlates permits the triangulation mesh of the topological network to be expanded within the interior of a block,

allowing for deformation to be experienced within its interior. Thus, it is recommended that continental blocks be designed in this fashion in order to account for deformation experienced within their interiors. Additionally, this approach can help mitigate edge effects caused by the use of rigid polygons.

2. Reconstructing present day gravity inversion crustal thickness estimates back through time allows for the pre-Jurassic template of offshore rifted margins throughout the North Atlantic to be investigated. In our opinion, if the appropriate constraints are available, this approach should be carried out prior to building models using more traditional deformable plate modelling approaches and assumptions.
3. The landward extent of crustal thickness estimates can be used as the interior model boundary when designing deformable plate models. As a result, this can allow the temporal evolution of other rift domain boundaries (e.g. the necking line) to be quantitatively defined a priori.
4. The approaches discussed in this work can be used to investigate the reconstructed geometries and thicknesses of continental blocks, even when they are not explicitly included as inputs within deformable plate models. Thus, this represents a much faster approach for restoring temporal variations in crustal thickness across rifted margins in comparison to previous approaches using 2-D seismic restorations.
5. Although the approaches discussed herein are applied to rifted margins, if suitable constraints are available, this workflow can also be applied to study the evolution of compressional tectonic regimes.

Chapter 7

7 Advances in deformable plate tectonic models (Part B): reconstructing the southern North Atlantic back through time

Most of the material presented in this chapter can be found in its published version *"King, M. T., & Welford, J. K. (2022). Advances in deformable plate tectonic models: 2. Reconstructing the southern North Atlantic back through time. Geochemistry, Geophysics, Geosystems, 23, e2022GC010373. https://doi. org/10.1029/2022GC010373"*.

7.1 Introduction

The development and present-day architecture of rifted margins have been long studied using a variety of geophysical and geological approaches. For the rifted margins of the North Atlantic, such as the southeast Newfoundland and West Iberian margin conjugate pair, an abundance of data acquired along each margin has led to considerable advancements regarding our knowledge of rift tectonics (Péron-Pinvidic et al., 2007; Tucholke et al., 2007; Manatschal et al., 2009; Péron-Pinvidic and Manatschal, 2009; Sutra et al., 2013; Peron-Pinvidic et al., 2019). Subsequently, these observations have also provided an avenue and method of comparison for investigating rifted margins with sparse data coverage and less constraints (e.g. South China Sea)

(Gozzard et al., 2019; Cao et al., 2020; Nirrengarten et al., 2020; Zhao et al., 2020). Using seismic reflection and refraction profiles (Murillas et al., 1990; Vogt et al., 1998; Funck et al., 2003; Thinon et al., 2003; Watremez et al., 2018; Sandoval et al., 2019), well data obtained from deep ocean drilling programs (King et al., 1985; Boillot and Winterer, 1988; Tucholke and Sibuet, 2006), potential field data (Srivastava et al., 2000; Bronner et al., 2011; Szameitat et al., 2018a), and geophysical modelling and inversion (Chappell and Kusznir, 2008; Welford et al., 2012), the crustal evolution of the Newfoundland, Irish, and West Iberian margins continue to be topics of active research. Furthermore, these investigative approaches also provide valuable inputs and constraints for rigid and deformable plate tectonic reconstruction studies (Heine et al., 2013; Mohn et al., 2015; Barnett-Moore et al., 2018; Nirrengarten et al., 2018; Peace et al., 2019b), allowing the tectonic evolution of the North Atlantic to be visualized and studied in more detail.

Despite advancements made using deformable plate models, previously published models have involved practical assumptions that are inadequate when considering the geological complexity of the North Atlantic Ocean (Figures 1.4 and 1.5). Examples of such complexity include the variability and segmentation of pre-Jurassic templates due to Appalachian and Caledonian orogenic boundaries (Williams, 1984; Hall et al., 1998; Ady and Whittaker, 2018; Waldron et al., 2019), poly-phase and oblique rifting events (Reston, 2005; Brune et al., 2018), continental block rotations (Sibuet et al., 2007; Tugend et al., 2015a; Nirrengarten et al., 2018; Peace et al., 2019b), and magmatic activity (Scrutton and Bentley, 1988; Peace et al., 2019a). In addition, the multiple contemporaneous rift axes and final along-strike margin segmentation of the North Atlantic (Péron-Pinvidic and Manatschal, 2010; Peron-Pinvidic et al., 2013) have also contributed to its structural complexity. As a result, limitations of previous deformable plate

models such as uniform crustal thickness assumptions at model start times and the rigid boundaries and blocks used for their design have proven to be problematic for evaluating complex plate kinematic scenarios.

In this study, the methodology introduced in the companion contribution of this work (Chapter 6) is used to evaluate the crustal evolution of the southern North Atlantic using previously published (Peace et al., 2019b) and newly presented deformable plate models. This workflow encompasses the reconstruction of deformable continental blocks and present day crustal thickness estimates calculated by gravity inversion (Figure 1.4) back through time throughout the Newfoundland, West Iberia, and Irish offshore rifted margins. The temporal variations in crustal thickness calculated by each model reveal the pre-Jurassic architecture of the southern North Atlantic. In addition, the models presented herein also provide insight into the internal deformation experienced within continental blocks and the potential impact of inherited orogenic terrane boundaries on pre-Jurassic crustal structure and subsequent margin development.

7.2 Methodology

7.2.1 Deformable plate modelling workflow

In this study, the deformable plate tectonic modelling workflow presented in the companion contribution of this study (Chapter 6) is used to investigate the plate kinematic evolution of the southern North Atlantic using two different models. As a general overview, this approach involves the reconstruction of present day gravity inversion crustal thickness estimates back through time within a topological network built using the interplay of GPlates (Müller et al., 2018) and its python programming library, pyGPlates. Despite being an advanced approach in

comparison to that implemented in Chapters 3-5, the deformable plate models presented herein still operate under the assumption that deformation occurs via uniform lithospheric stretching. Thus, this approach neglects the impact of depth-dependent stretching and the potential for larger amounts of thinning within the crust versus the lithospheric mantle, or vice versa, with the former scenario being proposed to be more influential in previous studies of the Newfoundland and Iberian margins (Crosby et al., 2011).

The crustal thickness estimates used in this study (Welford and Hall, 2007; Welford et al., 2012; King et al., 2020) are calculated using the minimum-structure 3-D gravity inversion algorithm, GRAV3D (Li and Oldenburg, 1996, 1998). This inversion algorithm allows one to calculate a smoothed depth-weighted 3-D density anomaly model that can be used to determine a proxy for the depth to Moho. The Moho proxy is defined as a density isosurface between the crust and mantle (70 kg/m^3) within the inverted 3-D density anomaly model relative to a prescribed background density (2850 kg/m^3) implemented within a reference density anomaly model. The reference density anomaly model is also constrained using bathymetry and depth to basement constraints to define allowable density ranges for the seawater, sedimentary column, crust, and mantle. Crustal thicknesses are calculated by taking the difference between the depth to basement and the Moho proxy. Due to the conservatively low density anomaly value assigned to the Moho proxy, this approach has a tendency to underestimate crustal thickness in regions with anomalously high density lower crust, such as underplated regions. For our purposes here, this underestimate becomes advantageous as it generates crustal thicknesses representative of thinned continental crust and ignores the effect of magmatic underplating, a phenomenon that does impact previously calculated crustal thickness estimates throughout the North Atlantic (Mjelde et al., 2016; Barnett-

Moore et al., 2018). For more details pertaining to the gravity inversion approach and constraints used, please refer to Welford et al. (2012).

7.2.2 Model Setup

In this study, two deformable plate models of the North Atlantic Ocean are investigated using previously published (Nirrengarten et al., 2018; Peace et al., 2019b) and newly presented plate kinematic inputs (Table 7.1). The present day crustal thickness estimates that are reconstructed back through time by each model include estimates calculated along the Newfoundland, Irish, and West Iberian margins (Welford and Hall, 2007; Welford et al., 2012; King et al., 2020).

Model B1 is identical to model A4 presented in Chapter 6. Model B1 is designed using the poles of rotation from the preferred deformable plate model (model 6c) in Peace et al., (2019b). The exterior topological boundary for model B1 consists of the edge of continental crust from Peace et al., (2019b), originally defined by Nirrengarten et al. (2018), which excludes domains of exhumed and serpentinized mantle interpreted ocean ward. In Nirrengarten et al. (2018), the edge of continental crust is mapped using previously published 2-D seismic sections and interpolated elsewhere using potential field data acquired throughout the southern North Atlantic. The interior model boundary is designed to cover proximal domain regions within the extent of crustal thickness estimates calculated using gravity inversion along the Newfoundland, Irish, and West Iberian margins. In addition, model B1 includes the same geometries of the Flemish Cap, Porcupine Bank, and Rockall-Hatton Bank as those used in Peace et al., (2019b); however, these continental blocks are designed using groups of points in order to allow deformation to be

experienced within their interiors. Model B2 is identical to model B1 aside from differences along the Newfoundland margin where a new continental block is defined for the Southern Grand Banks Tail (Figure 7.3). As highlighted in Chapter 6, pre-Jurassic crustal thicknesses calculated by model B1 along the southern tail of the Grand Banks demonstrate segmentation delimited by the offshore extension of the Meguma terrane boundary (shown as the Meguma Suture in Figure 7.1B), suggesting that the southern tail of the Grand Banks may have acted as a separate block during rifting. Thus, in an attempt to further investigate this phenomenon, the southern tail of the Grand Banks is designed as an independent crustal block (using a group of points) with newly defined poles of rotation herein. The geometry of the Southern Grand Banks Tail (SGBT) is designed according to its apparent pre-Jurassic geometry observed in model B1 (Figure 7.1).

Model	Pole of rotation	Continental blocks included	Continental block design	Model Time Frame
B1	Peace et al., (2019b)	Flemish Cap, Porcupine Bank, and Rockall-Hatton Bank	Points	200-0 Ma
B2	Peace et al., (2019b) and this study	Flemish Cap, Porcupine Bank, Rockall-Hatton Bank, and Southern Grand Banks Tail	Points	200-0 Ma

Table 7.1 Parameters and details pertaining to the design of models B1 and B2.

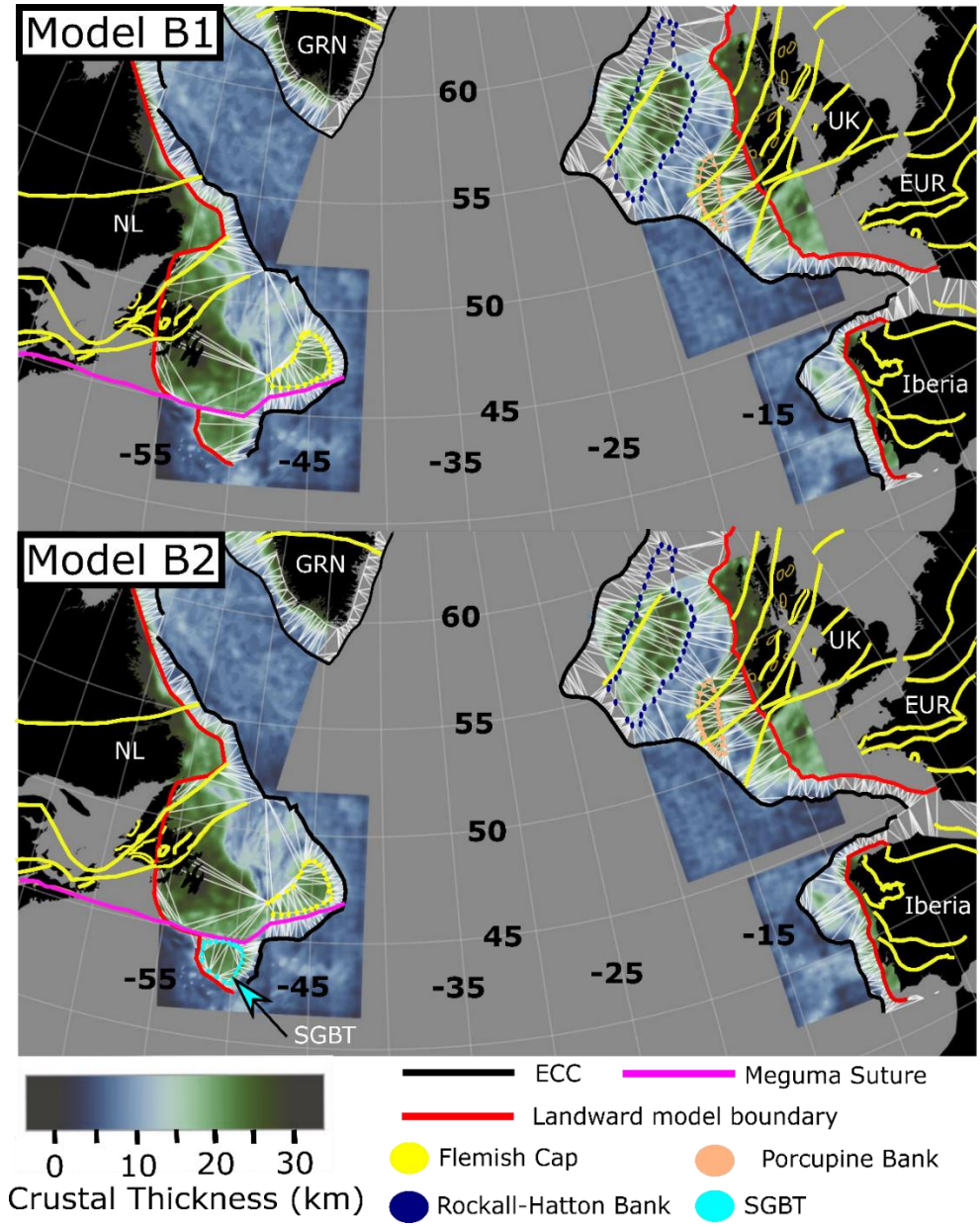

Figure 7.1 Boundaries and geometries of continental blocks used to create topological networks (triangulation meshes) for models B1 and B2. Onshore to offshore inherited structures (yellow lines) are overlain in each model, however, these are not included within the deformable mesh. ECC = edge of continental crust, EUR = Europe, GRN = Greenland, NL = Newfoundland and Labrador, SGBT = Southern Grand Banks Tail, UK = United Kingdom.

7.3 Results

7.3.1 Pre-Jurassic (200 Ma) crustal thickness

7.3.1.1 Newfoundland margin

The pre-Jurassic crustal thicknesses calculated by models B1 and B2 (Figure 7.2) demonstrate similar results aside from variations observed in model B2 along the Newfoundland margin caused by the consideration of the Southern Grand Banks Tail (SGBT). In model B1, crustal thicknesses calculated within the Orphan Basin vary from ~ 17-35 km thick. Within the Flemish Cap, crustal thicknesses vary from ~ 20-35 km thick, with the thinnest areas of crust located in the vicinity of the Flemish Pass (cyan star in Figure 7.2 for model B2) and regions southwest of the Flemish Pass (crust ~ 10-15 km thick). The east and central regions of the Orphan Basin are subdivided by localized depocenters (crust ~ 15-20 km thick) that are bordered by relatively thicker blocks of crust (~ 25-30 km thick) throughout the Central Orphan High. Within the West Orphan Basin, a wide NE-SW trending region is observed with crustal thicknesses ranging from approximately 15-20 km thick within its interior. Along the Bonavista Platform and regions further south within the Grand Banks, crustal thicknesses calculated by model B1 range from about 25-35 km thick. Further south along the Grand Banks, a relatively thinner region of crust (~ 15-25 km thick) is observed north of a relatively thicker region within the Southern Grand Banks Tail (25-35 km thick). Model B2 demonstrates near identical pre-Jurassic crustal thicknesses as model B1 along the Newfoundland margin aside from estimates calculated along the Grand Banks. Throughout the Grand Banks and within the Southern Grand Banks Tail, crustal thicknesses calculated by model B2 range from about 20-30 km thick.

7.3.1.2 Irish and West Iberian margins

Along the Irish margin, pre-Jurassic crustal thicknesses calculated by models B1 and B2 are identical (Figure 7.2). Within the Porcupine Bank, crustal thicknesses range from about 25-35 km thick aside from a localized region of relatively thinner crust (~ 20 km thick) that segments the central region of the Porcupine Bank. Within the proto Porcupine Basin, crustal thicknesses range from about 30 km thick near the basin edges to about 15 km thick within the basin center. To the northwest, within the Rockall Basin, crustal thicknesses range from about 10 km thick within the basin center to approximately 30 km thick along the basin edges. Crustal thicknesses calculated by models 1 and 2 within the Rockall-Hatton Bank range from about 20-30 km thick.

Considering the West Iberian margin, pre-Jurassic crustal thicknesses calculated by models B1 and B2 are also identical. Within the northwest Iberian margin, a thicker region of crust (~ 25-30 km thick) is calculated adjacent to the Flemish Cap, interpreted to represent the geometry and pre-Jurassic thickness of the Galicia Bank. East of the Galicia Bank, within the Galicia Interior Basin, crustal thicknesses range from about 20-30 km thick, with the thinnest regions of crust (~ 20 km thick) segmented by NW-SE trending regions of thicker crust (~ 25 km thick) (red arrows in Figure 7.2 for model B2). To the southeast of the Galicia Bank, a region of relatively thin crust (~ 15 km thick) (magenta arrow in Figure 7.4 for model B2) is observed in the vicinity of the Vigo and Porto seamounts (Murillas et al., 1990). Along the southwest Iberian margin, conjugate to the Southern Grand Banks Tail, crustal thicknesses range from about 25 km landward to about 15 km thick oceanward.

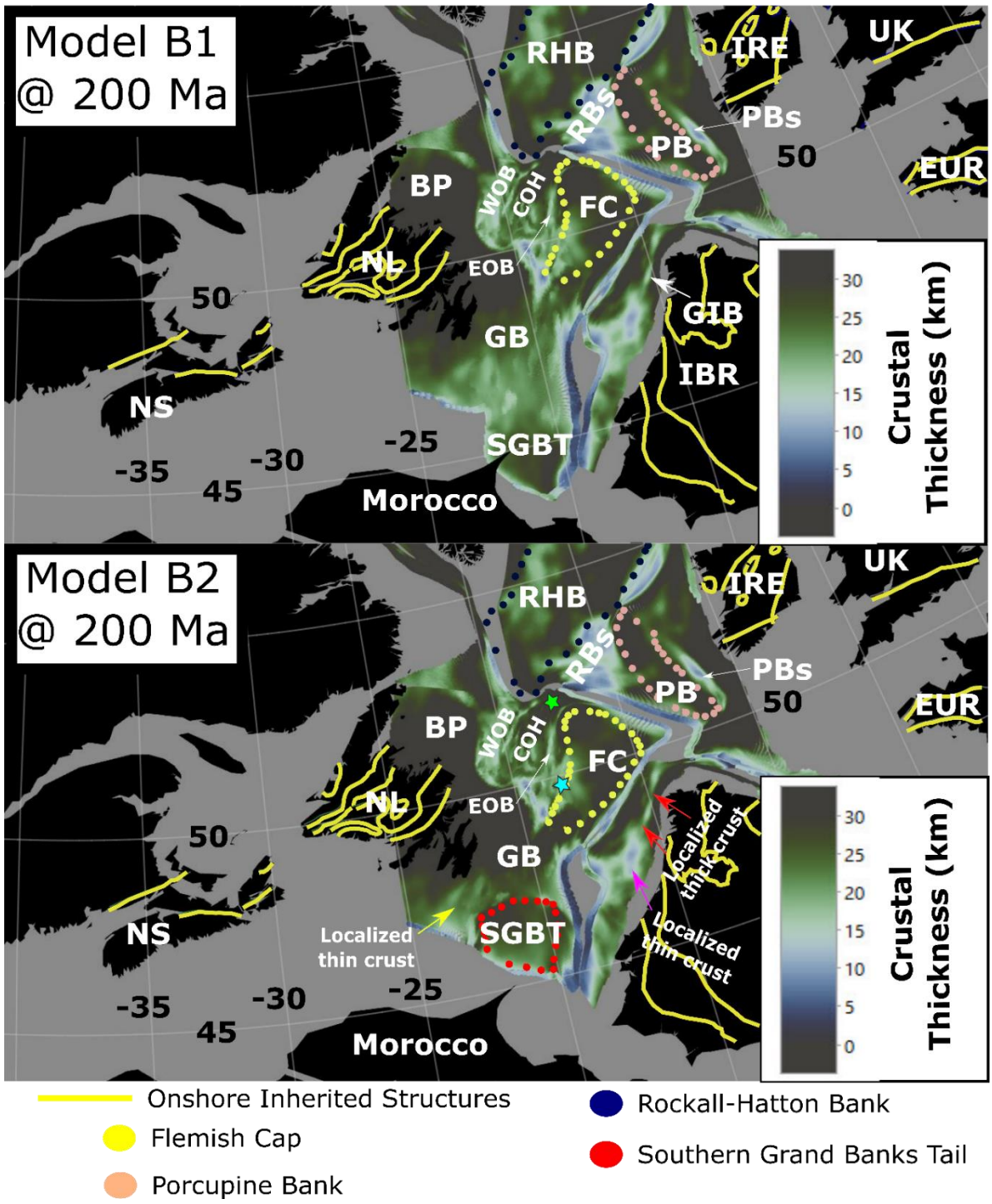

Figure 7.2 Crustal thicknesses calculated by models B1 and B2 at 200 Ma. The green and cyan stars represent the pre-Jurassic position of the Orphan Knoll and Flemish Pass, respectively.

Onshore inherited structures (yellow lines) are overlain in each model, however, these are not included within the deformable mesh. BP = Bonavista Platform, COH = Central Orphan High, EOB = East Orphan Basin, EUR = Europe, FC = Flemish Cap, GB = Grand Banks, GIB = Galicia Interior Basin, IBR = Iberia, IRE = Ireland, NL = Newfoundland, NS= Nova Scotia, PB = Porcupine Bank, PBs = Porcupine Basin, RBs = Rockall Basin, RHB = Rockall-Hatton Bank, SGBT = Southern Grand Banks Tail, UK = United Kingdom, WOB = West Orphan Basin.

7.3.2 Jurassic (200-145 Ma) crustal thickness

7.3.2.1 Newfoundland margin

Throughout the Jurassic (Figures 7.3 and 7.4), minor crustal thinning is calculated by models B1 and B2 along the Newfoundland margin. The most notable changes consist of the gradual widening and crustal thinning (crust ~ 15-20 km thick) of depocenters within the Orphan Basin and between the Grand Banks and the Southern Grand Banks Tail by 150 Ma (Figure 7.4).

7.3.2.2 Irish and West Iberian margins

Crustal thicknesses calculated by models B1 and B2 along the Irish and West Iberian margins throughout the Jurassic are identical. Along the Irish margin, crustal thinning is experienced within the central region of the Porcupine Bank by the end of the Jurassic (Figure 7.4). This leads to segmentation between the southern and northern sections of the Porcupine Bank (crust ~25-30 km thick) by a localized region of crust about 15-20 km thick. From 175 Ma (Figure 7.3) to 150 Ma (Figure 7.4), crustal thinning is experienced within the Porcupine Basin, synchronous with the progressive rotation of the Porcupine Bank. This leads to crustal thicknesses within the Porcupine Basin ranging from about 8-10 km within the basin center to about 25-30 km

along the basin edges by the end of the Jurassic (Figure 7.4). Similar to the timing of crustal thinning within the Porcupine Basin, the Rockall Basin also widens and continues to experience crustal thinning by the end of the Jurassic. This leads to crustal thicknesses ranging from about 5-10 km thick within the center of the Rockall Basin to about 20-25 km thick along the northwestern and southeastern basin edges near the Rockall-Hatton Bank and Porcupine Bank, respectively. Along the West Iberian margin, aside from minor crustal thinning experienced along the southwest Iberian margin (~ 5 km), crustal thicknesses remain very similar to those calculated at 200 Ma; most notably, in the vicinity of the Galicia Bank and Galicia Interior Basin.

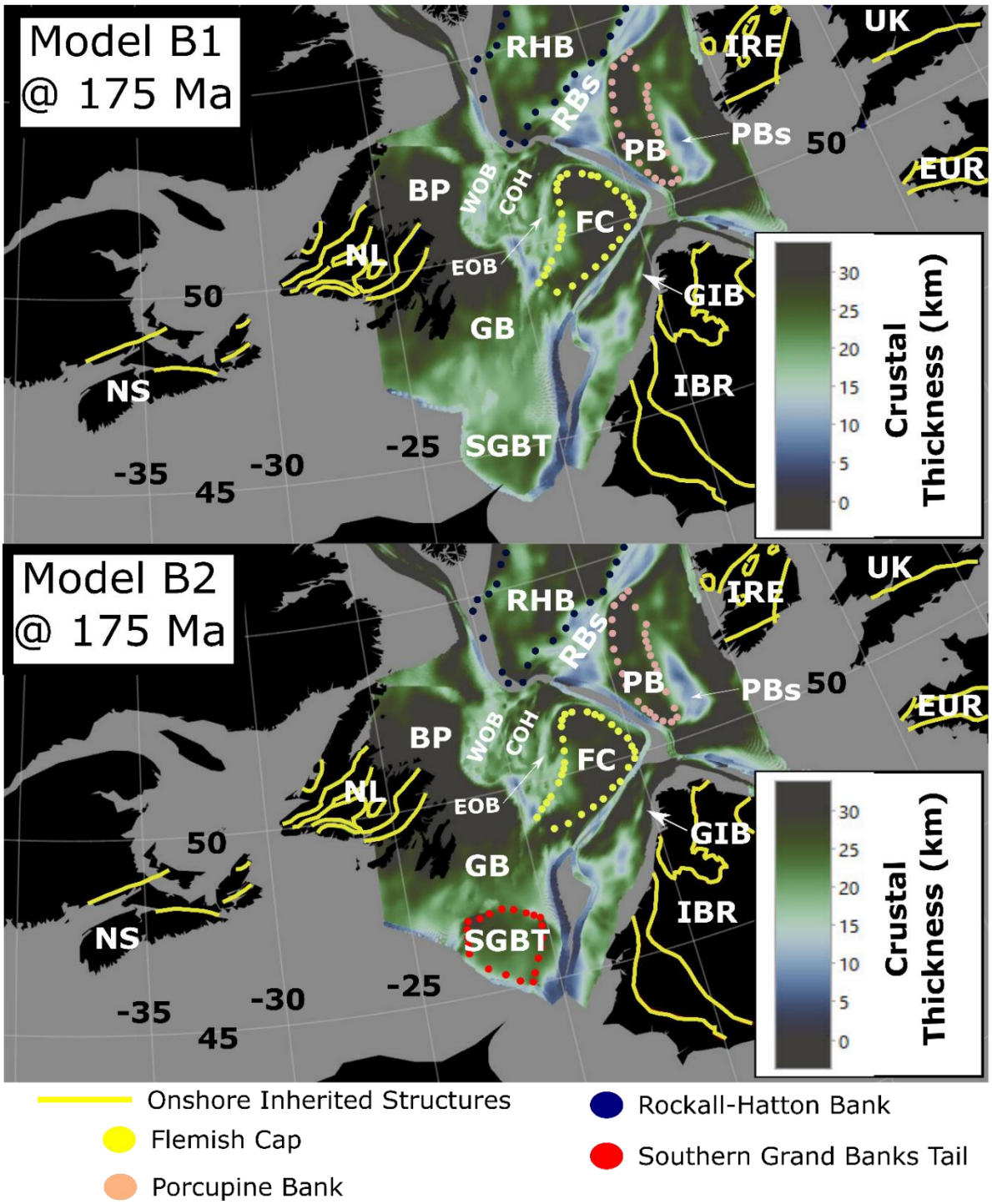

Figure 7.3 Crustal thicknesses calculated by models B1 and B2 at 175 Ma. Onshore inherited structures (yellow lines) are overlain in each model, however, these are not included within the

deformable mesh. BP = Bonavista Platform, COH = Central Orphan High, EOB = East Orphan Basin, EUR = Europe, FC = Flemish Cap, GB = Grand Banks, GIB = Galicia Interior Basin, IBR = Iberia, IRE = Ireland, NL = Newfoundland, NS= Nova Scotia, PB = Porcupine Bank, PBs = Porcupine Basin, RBs = Rockall Basin, RHB = Rockall-Hatton Bank, SGBT = Southern Grand Banks Tail, UK = United Kingdom, WOB = West Orphan Basin.

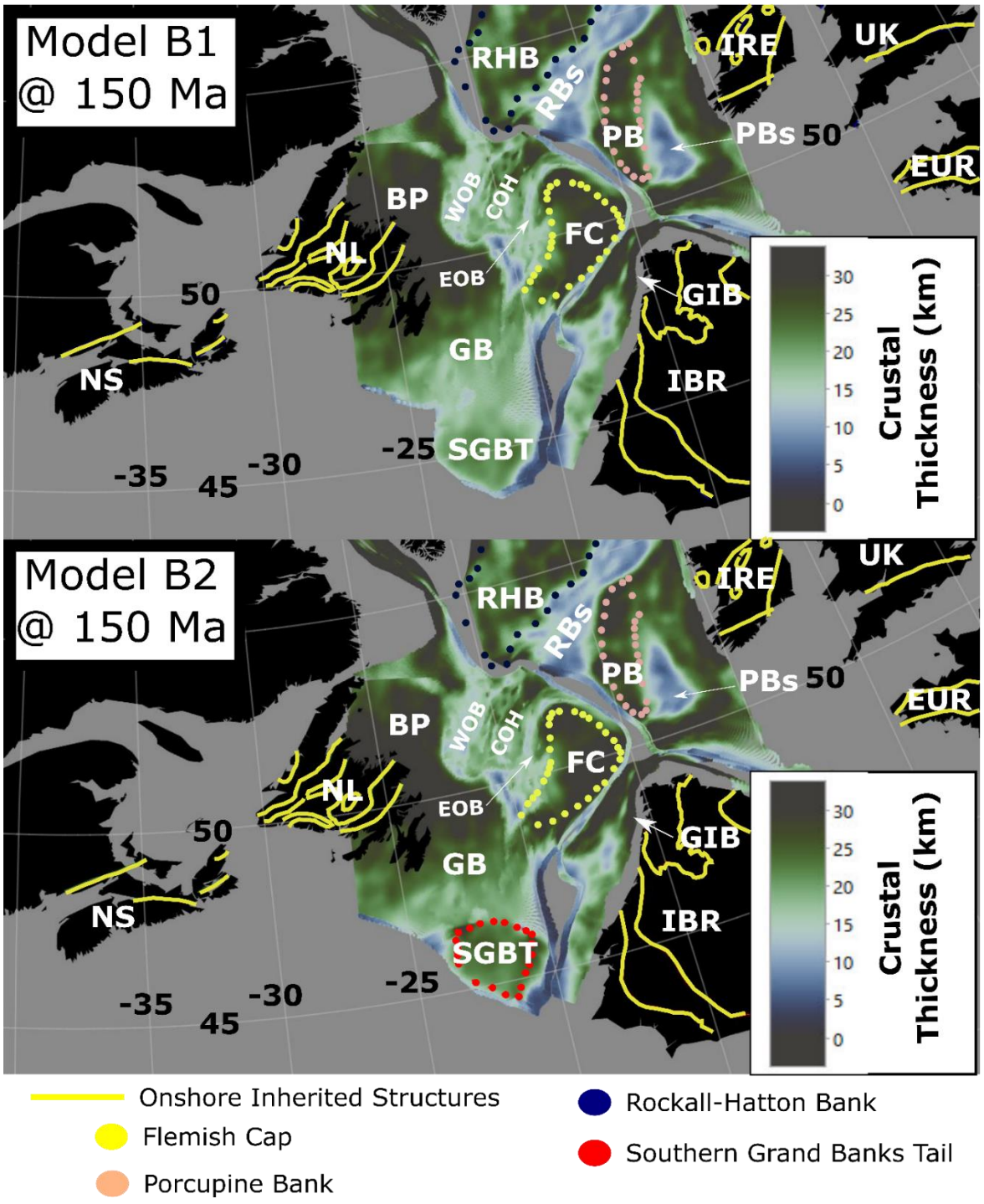

Figure 7.4 Crustal thicknesses calculated by models B1 and B2 at 150 Ma. Onshore inherited structures (yellow lines) are overlain in each model, however, these are not included within the

deformable mesh. BP = Bonavista Platform, COH = Central Orphan High, EOB = East Orphan Basin, EUR = Europe, FC = Flemish Cap, GB = Grand Banks, GIB = Galicia Interior Basin, IBR = Iberia, IRE = Ireland, NL = Newfoundland, NS= Nova Scotia, PB = Porcupine Bank, PBs = Porcupine Basin, RBs = Rockall Basin, RHB = Rockall-Hatton Bank, SGBT = Southern Grand Banks Tail, UK = United Kingdom, WOB = West Orphan Basin.

7.3.3 Cretaceous (< 145 Ma) crustal thickness

7.3.3.1 Newfoundland margin

Throughout the Early Cretaceous, crustal thicknesses indicative of significant crustal thinning (10 km or less) are calculated by models B1 and B2 within sedimentary basins along the Newfoundland margin. Within the Orphan Basin, significantly thinned crust is calculated by models B1 and B2 within the East and West Orphan basins by 125 Ma (Figure 7.5). Between the East and West Orphan basins, significantly thinned crustal zones (5-10 km thick) are partitioned by NE-SW trending blocks of relatively thicker crust (~ 15-20 km thick). In addition, internal rift-related deformation within the Flemish Cap calculated by models B1 and B2 results in crustal thicknesses ranging from 20-30 km thick within its interior, with even thinner crust in the vicinity of the Flemish Pass (crust ~ 15 km thick) (cyan star in Figure 7.5). Throughout the Bonavista Platform and Grand Banks, crustal thicknesses calculated by models B1 and B2 range from about 20-30 km thick, with localized areas of relatively thinner crust (~ 15 km thick) surrounding the Southern Grand Banks Tail.

7.3.3.2 Irish and West Iberian margins

Along the Irish margin, crustal thicknesses calculated by models B1 and B2 at 125 Ma (Figure 7.5) demonstrate continued segmentation of the Porcupine Bank by a region of localized thin crust (~ 15 km thick) within the center of the Porcupine Bank. North and south of this segmentation, crustal thicknesses within the Porcupine Bank range from about 20-30 km thick. By 125 Ma, the Porcupine and Rockall basins are significantly thinned with crust ranging from 5-10 km thick within each basin center. In addition, during the Early Cretaceous, the southeastern tip of the Porcupine Bank and the northwestern Goban Spur in models B1 and B2 begin to separate, resulting in a thinned region of crust between them (~ 10-15 km thick). Along the northwest Iberian margin, crustal thinning is observed within the Galicia Bank, resulting in crustal thicknesses ranging from 15-25 km thick within its interior. Within the Galicia Interior Basin, models B1 and B2 reveal localized regions of significantly thinned crust (10 km or less) that are segmented by NW-SE trending regions of relatively thicker crust (~ 15 km thick).

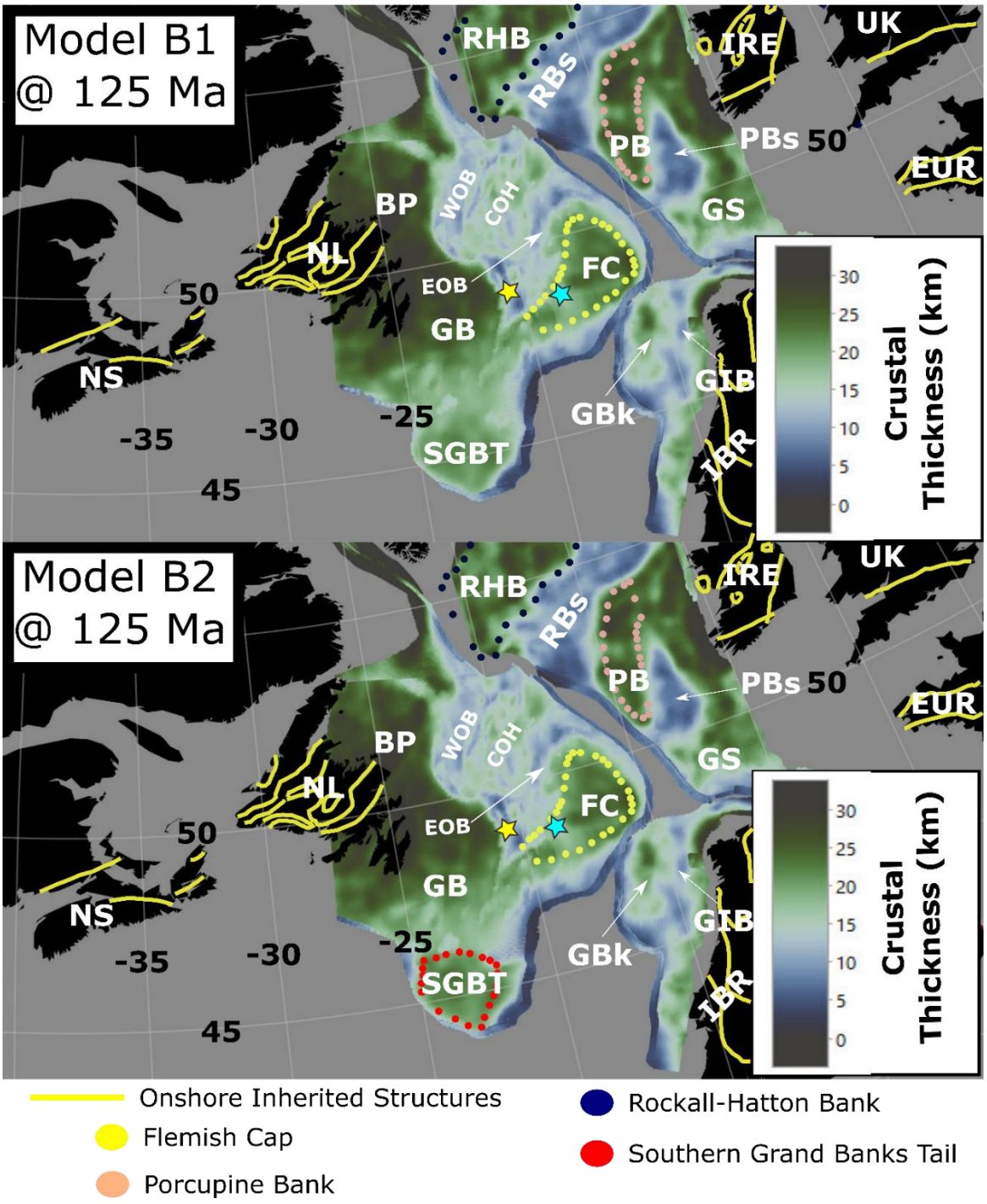

Figure 7.5 Crustal thicknesses calculated by models B1 and B2 at 125 Ma (Barremian). The cyan and yellow stars represent a localized region of thinned crust within the Flemish Pass and a region

of significantly thinned crust located southwest of the Flemish Pass, respectively. Onshore inherited structures (yellow lines) are overlain in each model, however, these are not included within the deformable mesh. BP = Bonavista Platform, COH = Central Orphan High, EOB = East Orphan Basin, EUR = Europe, FC = Flemish Cap, GB = Grand Banks, GBk = Galicia Bank, GIB = Galicia Interior Basin, GS = Goban Spur, IBR = Iberia, IRE = Ireland, NL = Newfoundland, NS= Nova Scotia, PB = Porcupine Bank, PBs = Porcupine Basin, RBs = Rockall Basin, RHB = Rockall-Hatton Bank, SGBT = Southern Grand Banks Tail, UK = United Kingdom, WOB = West Orphan Basin.

7.4 Discussion

7.4.1 Pre-Jurassic crustal thickness

In this section, the pre-Jurassic (200 Ma) crustal thickness template of model B2 (Figure 7.6) is described and compared with observations from previous studies regarding the pre-Jurassic template of the southern North Atlantic Ocean. Model B1 is excluded from this discussion due to its similarities with model B2 along the Newfoundland, Irish, and West Iberian margins aside from an improved reconstruction of the Grand Banks in model B2.

7.4.1.1 Newfoundland margin

The pre-Jurassic structure of the Newfoundland margin has been argued to be highly variable due to the interpreted onshore to offshore extension of accretionary boundaries inherited from Appalachian and Caledonian orogenic events (Ady and Whittaker, 2018; Waldron et al., 2019) and the partitioning of sedimentary basins by continental blocks (Sibuet et al., 2007; Nirrengarten et al., 2018; Peace et al., 2019b). Considering the magnitude of pre-Jurassic crustal

thicknesses proposed from previous seismic and modelling studies along the Newfoundland margin (Funck et al., 2003; Mohn et al., 2015; Brune et al., 2017; Peace et al., 2019b), it is commonly assumed that pre-Jurassic crustal thicknesses range from approximately 30-35 km thick, despite the difficulty in achieving these values in previous crustal restoration studies (Sandoval et al., 2019; MacMahon et al., 2020; Cawood et al., 2021b).

In model B2, pre-Jurassic crustal thicknesses calculated along the Newfoundland margin show significant variability (Figure 7.6), with values ranging from ~ 15-35 km thick. Within the Orphan Basin, numerous pre-Jurassic depocenters (crust ~15-20 km thick) are observed that are partitioned by regions of relatively thicker crust (~ 25-35 km thick) such as the Flemish Cap, Central Orphan High, and Bonavista Platform. However, the width of these regions of relatively thinner crust are highly variable from east to west. Within the East Orphan Basin and Central Orphan High, the widths of these depocenters range from about 10-20 km wide. In contrast, the West Orphan Basin is restored as a wider (~ 50 km wide) NE-SW trending basin with relatively thinner crust ranging from about 15-20 km thick. Interestingly, the pre-Jurassic width of the West Orphan Basin approximately aligns with the offshore extension of accretionary boundaries that divide Newfoundland into different geological zones that are associated with the collision of Laurentian and peri-Gondwanan terranes during the closure of the Iapetus Ocean (Figure 7.6B) (Waldron et al., 2019). In particular, the West Orphan Basin appears to be bounded by the offshore extension of the Dover Fault to the east, and the Mekwe'jit Line, often referred to as the Iapetus Suture, to the west. Furthermore, additional inherited boundaries such as the Ganderia Boundary and Dog Bay Line (Figure 7.6B) have also been postulated to extend offshore, suggesting a large degree of orogenic inheritance within the pre-Jurassic template of the West Orphan Basin. As a

result, the inherited structural variability within the West Orphan Basin is postulated to be the cause of its relatively thinner pre-Jurassic crustal thicknesses compared to the regions eastward. We suggest that the offshore extension of these orogenic boundaries promoted a zone of relatively weaker and mechanically unstable crust within the West Orphan Basin, leading to variable crustal thicknesses at 200 Ma as a result of older tectonic events and offshore structural trends in the same orientation as those onshore Newfoundland (NE-SW).

Considering pre-Jurassic crustal thicknesses calculated by model B2 within previously recognized continental blocks (Flemish Cap and Orphan Knoll), crustal thicknesses within these blocks vary from about 20-35 km thick. Within the Flemish Cap, crustal thicknesses mostly range from about 25-35 km thick, aside from the western edge of the Flemish Cap (Flemish Pass) where the crust is approximately 20 km thick. At 200 Ma, the Orphan Knoll (green star in Figure 7.6A) comprises the northeastern portion of the Central Orphan High, a relatively thicker NE-SW trending crustal block (~ 20-30 km thick) whose structure is partitioned by localized depocenters to the southwest. Additionally, the Orphan Knoll appears to be conjugate to the Rockall-Hatton Bank, suggesting that the two blocks may have been connected prior to the onset of rift-related deformation within the Orphan Basin.

Along the Grand Banks, pre-Jurassic crustal thicknesses range from about 20-30 km thick, aside from localized regions of relatively thinner crust (~ 15-20 km thick) (yellow arrow in Figure 7.6A) in the vicinity of the Horseshoe and Whale basins (Figure 7.1B) to the northwest of the Southern Grand Banks Tail. Inspired by the crustal thickness segmentation of the Grand Banks observed in model B1, the inclusion of the Southern Grand Banks Tail as an independent crustal block within model B2 allows for more appropriate pre-Jurassic crustal thicknesses to be

calculated along the Grand Banks and a more symmetric fit between the southeastern Newfoundland and southwest Iberian margins. The northern limit of the Southern Grand Banks Tail is interpreted to be delimited by the offshore extension of the Meguma terrane boundary (Meguma Suture in Figure 1.2), suggesting a Meguma origin for the Southern Grand Banks Tail.

7.4.1.2 Irish margin

Throughout the Irish margin, pre-Jurassic crustal thicknesses calculated by model B2 are highly variable. Within the Porcupine Bank, crustal thicknesses range from about 25-35 km thick, aside from a localized region of thinner crust (~ 20-25 km thick) near the center and western edge of the Porcupine Bank. This segmentation demonstrates interesting correlations with previous studies that suggest segmentation of the pre-Jurassic structure of the Porcupine Bank (Yang et al., 2021). In particular, the pre-Jurassic position of the Porcupine Bank appears to intersect the offshore extension of the Iapetus Suture from the Irish interior, correlating with the region of crustal thickness segmentation calculated by model B2. Thus, in support of previous studies (Yang et al., 2021), the offshore extension of the Iapetus Suture appears to segment the Porcupine Bank, leading to localized crustal thinning within its interior during rift-related deformation (Figure 7.6B). Within the Porcupine Basin, a NW-SE trending region of crust ranging from 13-15 km thick is observed within the center of the basin and is bordered by proximal areas with crust ranging from 25-30 km thick (Figure 7.6). The nature of this relatively thinner region of crust is still unclear, as to our knowledge, there are no NW-SE trending inherited structures that could provide a potential explanation for the thinner pre-Jurassic crust within this region. This region of thinner crust calculated by model B2 within the Porcupine Basin could possibly be caused by the lack of consideration for Triassic and older tectonic events in the deformable modelling. However, similar

to the pre-Jurassic crustal thickness estimates reconstructed along the Newfoundland margin, these observations emphasize that complex tectonism and accretion were experienced within these regions prior to Jurassic rifting. Thus, pre-Jurassic crustal thicknesses calculated by Model B2 demonstrate the influence of older tectonic events on the pre-Jurassic template of the southern North Atlantic and the lack of support for uniformly thick crust prior to Jurassic rifting. Within the Rockall Basin, a similar phenomenon is observed regarding the preservation of relatively thin pre-Jurassic crust within the center of the basin. Aside from the exclusion of older Permo-Triassic tectonic events from the deformable modelling and pre-Jurassic crustal thickness calculations, the presence of NE-SW trending Caledonian sutures within the Rockall Basin (Schiffer et al., 2019; Waldron et al., 2019) are also considered to have potentially contributed to the relatively thin pre-Jurassic crust calculated throughout the basin.

7.4.1.3 West Iberian margin

The pre-Jurassic crustal thickness template calculated by model B2 along the West Iberian margin demonstrates interesting variabilities from north to south. Within the northwest Iberian margin, the pre-Jurassic geometry and crustal thickness of the Galicia Bank (~ 25-30 km thick) are revealed. Considering the interpreted geometry of the Galicia Bank in model B2 (Figure 7.6), interesting correlations can be made between the results calculated by model B2 and the preferred models from a previous deformable plate modelling study focused on the Galicia Bank kinematics (King et al., 2020) (Chapter 3). In particular, the reconstructed geometry of the Galicia Bank appears similar to that suggested in model 8 of King et al., (2020), however, model B2 in this study suggests that the Galicia Bank was connected to the Flemish Cap at 200 Ma, a scenario similar to the other preferred plate model (model 9) from King et al., (2020). Thus, the results calculated by

model B2 of this study appear to be a hybrid of the preferred plate models from King et al., (2020). However, the Galicia Bank itself is not considered as an independent model input in model B2 in comparison to previously published deformable plate models of the northwest Iberian margin (King et al., 2020). Thus, similar to the Orphan Knoll, the position and reconstructed thickness of the Galicia Bank are deemed to be highly dependent on the kinematics of the Flemish Cap. Furthermore, although it is still considered a continental block, the Galicia Bank appears to be an extensional relic of the Flemish Cap during the formation of the North Atlantic Ocean. As for the cause of their separation, a possible scenario relates to the position of the Variscan Front relative to the Flemish Cap and Galicia Bank at 200 Ma (Figure 7.6B). Analysis of well data drilled into the Flemish Cap concluded that the Flemish Cap encompasses Avalonian terrane rocks (King et al., 1985). In contrast, the Galicia Bank is often assumed to be Variscan in nature, despite a lack of drilling into the Galicia Bank itself. As a result, the Variscan Front is interpreted to extend between the Galicia Bank and Flemish Cap (Figure 7.6B), suggesting that it acted as an inherited weakness that promoted the breaking apart of the two blocks following the onset of significant rift related deformation during the Early Cretaceous (Figure 7.5). Considering the pre-Jurassic template of the Galicia Interior Basin, crustal thicknesses range from about 15-25 km thick. Notably, the Galicia Interior Basin encompasses localized regions of thinner crust (~ 15-20 km thick) that appear segmented by regions of relatively thicker crust (~ 25 km thick) (Figure 7.6). In comparison with that suggested in Chapter 3, the nature of this segmentation appears to align with previously interpreted transfer zones considered to have formed via the interplay between NE-SW Variscan trends and regional extension directions. Thus, the preservation of this pre-Jurassic segmentation calculated by model B2 further suggests that the offshore extension of Variscan

boundaries also exerted a control on pre-Jurassic crustal thicknesses within the Galicia Interior Basin (Figure 7.6B).

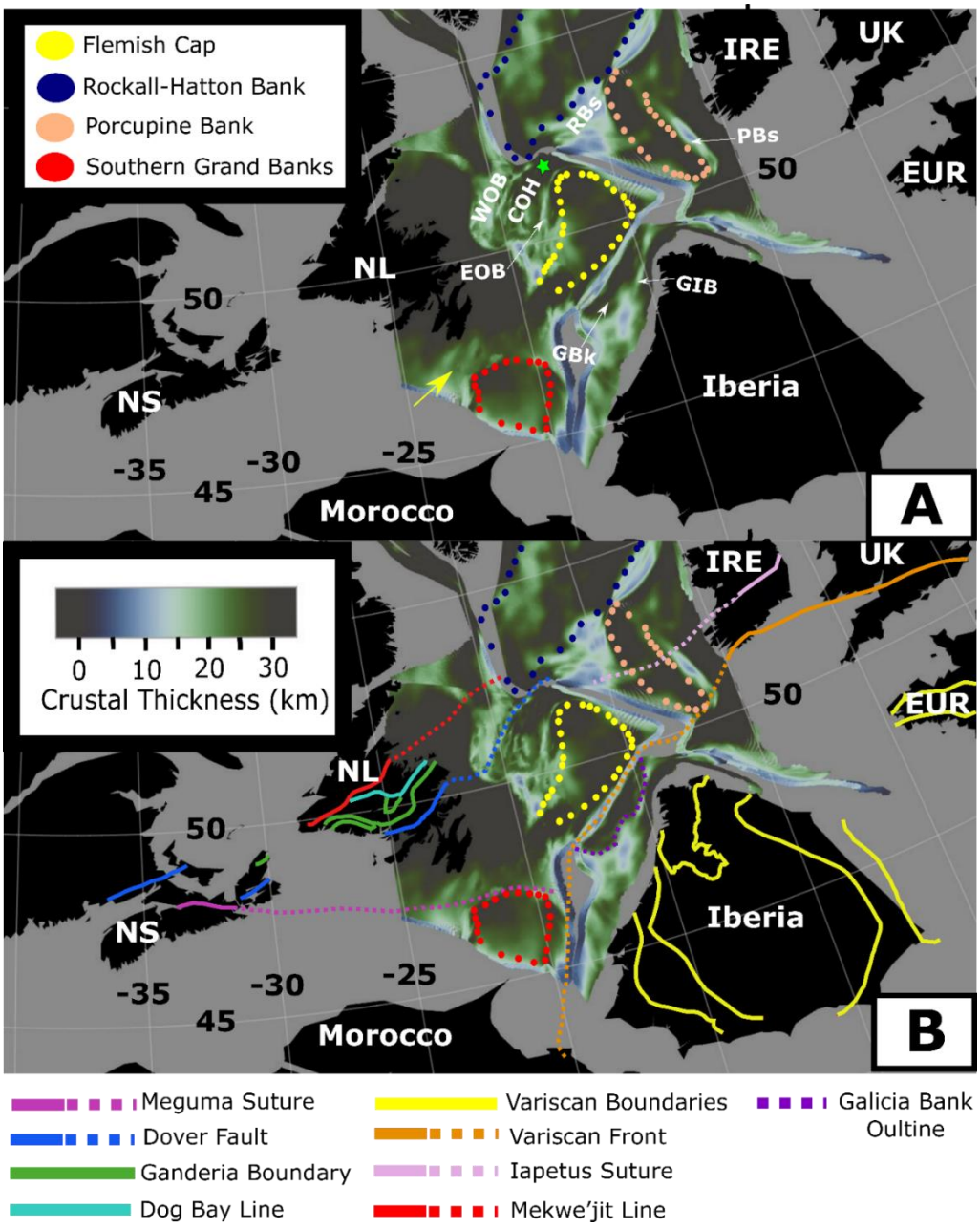

Figure 7.6 A) Crustal thicknesses calculated by model B2 at 200 Ma. The yellow arrow and green star represent a region of localized thinned crust along the southern Grand Banks and the pre-

Jurassic position of the Orphan Knoll, respectively. B) Same as (A) except with the orientation of offshore-onshore inherited boundaries modified after Waldron et al., (2019) and Nirrengarten et al., (2018) overlain on crustal thicknesses calculated by model B2. COH = Central Orphan High, EOB = East Orphan Basin, EUR = Europe, GBk = Galicia Bank, GIB = Galicia Interior Basin, IRE = Ireland, NL = Newfoundland and Labrador, NS = Nova Scotia, PBs = Porcupine Basin, RBs = Rockall Basin, UK = United Kingdom, WOB = West Orphan Basin.

7.4.2 Temporal crustal thickness evolution

In this section, the temporal crustal thickness evolution of model B2 is described. In addition, the temporal variations in crustal thickness calculated by model B2 are compared with previously published observations made from independent interpretation and modelling studies.

7.4.2.1 Newfoundland margin

Throughout the Jurassic (Figures 7.3 and 7.4), rift related deformation experienced along the Newfoundland margin in model B2 is regionally diffuse and causes minimal amounts of crustal thinning. This observation is in general agreement with the lack of Early to Mid Jurassic rifting and syn-rift sediment interpreted from seismic and well data throughout the Newfoundland margin (Sinclair, 1995; Tucholke and Sibuet, 2006; Mohn et al., 2015; Sandoval et al., 2019; MacMahon et al., 2020; Cawood et al., 2021a). However, in comparison to the Orphan Basin and Bonavista Platform, crustal thinning is more significant within regions surrounding the Southern Grand Banks Tail (crust ~ 15-20 km thick). The larger degree of crustal thinning within this region is in agreement with the Middle to Late Jurassic onset of rift-related deformation inferred from seismic and well data within the southwestern Iberia (e.g. Lusitanian and Alentejo basins) and southeastern

Newfoundland sedimentary basins (e.g. Whale and Horseshoe basins) (Alves et al., 2009; Pimentel and Pena Dos Reis, 2016; Alves and Cunha, 2018). Transitioning into the Late Jurassic and Early Cretaceous, this time frame corresponds to the onset of significant crustal thinning and widening of depocenters throughout the Orphan Basin, synchronous with the accelerated clockwise rotation of the Flemish Cap (Sibuet et al., 2007). Similar to that inferred from previous seismic and crustal restoration studies within the Orphan Basin (Sandoval et al., 2019; MacMahon et al., 2020; Cawood et al., 2021b), the most significant and widely distributed crustal thinning occurs within the East and West Orphan basins. Near the end of the Early Cretaceous (Figure 7.5), the East and West Orphan basins and the NW-SE trending region of thinned crust situated west of the Flemish Pass (yellow star in Figure 7.5) remain separated by NE-SW trending blocks of crust (~ 15-20 km thick) with localized basins in between (crust ~ 10-15 km thick) that make up the Central Orphan High. Along the Grand Banks, the most significant crustal thinning also takes place during the Late Jurassic to Early Cretaceous, synchronous with the breakup of Iberia from southeastern Newfoundland. By the end of the Albian (~ 100 Ma), rift related deformation and subsequent crustal thinning have ceased in model B2 along the Newfoundland margin.

7.4.2.2 Irish margin

Temporal variations in crustal thickness along the Irish margin are largely dependent and synchronous with the kinematics of the Porcupine and Rockall-Hatton banks. Near the end of the Jurassic (150 Ma) (Figure 7.4), significant crustal thinning (crust 10 km thick or less) is experienced within the Porcupine Basin as a result of the clockwise rotation of the Porcupine Bank. Additionally, similar to the interpretation by Yang et al., (2021), the Porcupine Bank experiences internal deformation, localized crustal thinning, and segmentation throughout the Jurassic along

its intersection with the offshore trend of the Iapetus Suture. Thus, this promotes the segmentation of the Porcupine Bank into two clearly defined crustal blocks in model B2, despite previous studies that suggest the potential segmentation of the Porcupine Bank into four blocks (Yang et al., 2021). Furthermore, near the end of the Jurassic, the Porcupine Basin appears to be isolated from conjugate basins due to a thicker region of crust (~ 25 km thick) preserved at the southern tip of the Porcupine Bank and the northwestern limit of the Goban Spur. Within the Rockall Basin, significantly thinned crust is calculated near the end of the Jurassic (Figure 7.4) as a result of the northwestward motion of the Rockall-Hatton Bank away from the Porcupine Bank. By the early Cretaceous (125 Ma) (Figure 7.5), NE-SW regional extension results in the onset of continental breakup and separation of the Newfoundland and Irish margins. In addition, rotation of the Porcupine Bank southern tip away from the Goban Spur during the Early Cretaceous causes the opening of the Porcupine Basin and potential for connectivity with the Galicia Interior Basin.

7.4.2.3 West Iberian margin

From 200 Ma until the Late Jurassic (150 Ma), crustal thinning is minimal along the West Iberian margin aside from localized thinning experienced along the southwest Iberian margin (Figure 7.4). This observation is in general agreement with interpretations made from seismic and well data that suggest pulses of Jurassic extension within basins south of the Galicia Interior Basin (Pereira and Alves, 2011; Alves and Cunha, 2018). During the Early Cretaceous, significant rift related deformation and subsequent crustal thinning is experienced within the Galicia Bank and Galicia Interior Basin as a result of the breakup between southeastern Newfoundland and Iberia. Although a Late Jurassic onset of significant crustal thinning is postulated in Chapter 3 along the Northwest Iberian margin, the timing of crustal thinning calculated by model B2 throughout the

Northwest Iberian margin is in agreement with previous seismic and well data interpretations (Reston, 2005; Alves and Cunha, 2018; Lymer et al., 2019) and the results calculated by model 9 in Chapter 3 that suggest an Early to Mid Cretaceous onset of rift related deformation within the Galicia Interior Basin. By 125 Ma (Figure 7.5), the Galicia Interior Basin is comprised of localized regions with significantly thinned crust (10 km of less) that are segmented by NW-SE trending regions of thicker crust (Murillas et al., 1990; King et al., 2020).

7.4.3 Orogenic inheritance within the southern North Atlantic

Inherited structures are demonstrated to be very influential during the formation of rifted margins and often lead to significant variability and asymmetry within their present day structure (Chenin et al., 2015; Manatschal et al., 2015; Peace et al., 2018; Heron et al., 2019; Schiffer et al., 2019). In this study, ancient orogenic terrane boundaries inherited from the formation of the supercontinent Pangaea are interpreted to play a key role in the pre-Jurassic crustal structure and subsequent development of sedimentary basins and continental blocks throughout the southern North Atlantic (Figure 7.6). In particular, a common phenomenon observed across all margins studied is the correlation between crustal thickness segmentation and the onshore to offshore extension of inherited terrane boundaries (Figure 7.6B). For the Newfoundland and Irish margins, these boundaries are typically defined on land via geological field mapping and extended offshore using potential field data (Figure 7.6B). Using the deformable plate modelling approach presented in the companion contribution of this study (Chapter 6), datasets such as offshore magnetic anomalies (e.g. EMAG3) throughout the southern North Atlantic can be reconstructed back

through time within topological networks. As a result, this can reveal their pre-Jurassic state and correlation with Appalachian and Caledonian structural trends interpreted onshore (Figure 7.7).

Within the Orphan Basin, the correlation of these magnetic boundaries (Figure 7.7) with regions of variable crustal thickness (Figure 7.6B) demonstrates the potential role of older tectonic events on pre-Jurassic templates and the possibility for thinner regions of pre-Jurassic crust than typically expected (~ 30-35 km thick). Along the Irish margin, similar to inferences from previous studies (Yang et al., 2021), segmentation and localized thinning of the Porcupine Bank correlate with its intersection with the interpreted Iapetus Suture. Similarly, along the southern Grand Banks, the correlation between the offshore extension of the Meguma terrane boundary and pre-Jurassic position of the Southern Grand Banks Tail suggests that it also played a role as a crustal weakness, causing segmentation of the SGBT away from the northern portion of the Grand Banks. Thus, the examples shown in this study highlight the importance of considering inherited structures on the pre-Jurassic and early stages of rifted margin development. The observations and ideas discussed in this work could also potentially be applied to other rifted margins elsewhere (e.g. South China Sea) where inheritance from prior orogenic events has also been considered to be highly influential (Gozzard et al., 2019; Cao et al., 2020; Nirrengarten et al., 2020; Zhao et al., 2020).

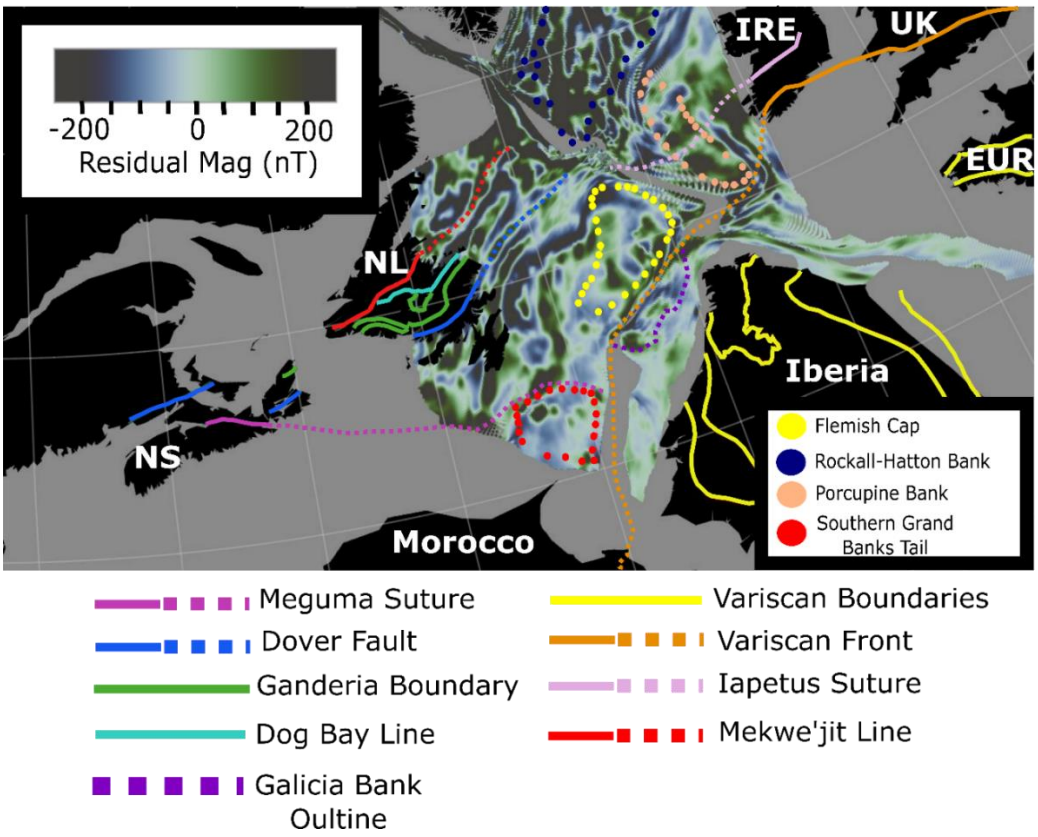

Figure 7.7 Reconstructed residual magnetic anomaly map (EMAG3) calculated by model B2 at 200 Ma with the orientation of offshore-onshore inherited boundaries modified after Waldron et al., (2019) and Nirrengarten et al., (2018) overlain. EUR = Europe, IRE = Ireland, NL = Newfoundland and Labrador, NS = Nova Scotia, UK = United Kingdom.

7.4.4 Re-appraisal of continental blocks throughout the southern North Atlantic

Based on the crustal thickness evolution of models shown in this study and its corresponding companion (Chapter 6), the need to include continental block kinematics in order to restore appropriate pre-Jurassic templates of the southern North Atlantic Ocean is demonstrated.

However, considering independent blocks that are not included within this study (e.g. Orphan Knoll and Galicia Bank) but which are implemented in Chapter 3, their evolution and structure still organically appear in the reconstructed models despite their exclusion as model inputs. In contrast, the explicit inclusion of the Flemish Cap, Porcupine Bank, and Rockall-Hatton Bank within topological networks appears to be necessary in order to achieve crustal thicknesses that are consistent with pre-Jurassic crust within surrounding sedimentary basins. These modelling observations may represent geologically-interpretable trends in how continental blocks formed and subsequently developed within the southern North Atlantic. For the Flemish Cap, Porcupine, and Rockall-Hatton banks, these continental blocks are large in size and appear to dictate the deformation experienced in their vicinities. In contrast, the Orphan Knoll and Galicia Bank are relatively smaller blocks that appear to evolve and deform according to the kinematics of larger blocks around them. Thus, the Galicia Bank and Orphan Knoll are interpreted to have a similar geological history with respect to their crustal thickness evolution and present day structure as they represent extensional relics formed via interactions between larger continental blocks and inherited structures. The architecture of the Galicia Bank appears to be largely dependent on the Flemish Cap, while the Orphan Knoll is dependent on both the Flemish Cap and Rockall-Hatton Bank. By reconstructing crustal thicknesses back through time, the evolution of smaller continental blocks can be studied in more detail, while also mitigating model edge effects that often occur in the deformable plate models presented in Chapters 3-5 when smaller blocks are explicitly included.

7.4.5 Crustal evolution of the southern North Atlantic: new insights, limitations, and future considerations

The deformable plate modelling approach originally presented in the companion contribution of this study (Chapter 6) permits the crustal evolution of the southern North Atlantic to be studied in detail. In contrast to the deformable plate models of the southern North Atlantic presented in Chapters 3-5, the models presented in Chapters 6 and 7 allow for the pre-Jurassic crustal structure, strain partitioning within continental blocks, and the evolution of proximal rift domains to be visualized and investigated. Furthermore, the results of this study demonstrate the potential role played by both inherited structures and continental blocks during rifting. Regarding inheritance, the offshore extensions of Appalachian and Caledonian terrane boundaries demonstrate strong correlations with the segmentation observed within pre-Jurassic crustal thickness templates of the North Atlantic (e.g. Orphan Basin) and the subsequent localization of crustal thinning within continental blocks (e.g. Porcupine Bank). For continental blocks, the kinematics of larger continental blocks (e.g. Flemish Cap, Porcupine Bank, and Rockall-Hatton Bank) play a key role in the distribution of rift related deformation within sedimentary basins. Additionally, their consideration also has a large impact on the reconstructed architecture and subsequent evolution of smaller continental blocks (e.g. Galicia Bank and Orphan Knoll).

However, despite the advances made in this study regarding the tectonic evolution of the southern North Atlantic, the new workflow presented also reveals several discrepancies and avenues for future work. Arguably, the most notable discrepancies in this work are the preservation of significantly thinned crust in pre-Jurassic templates and crustal thickness gaps observed within

continent-ocean transitions. Although the pre-Jurassic poles of rotation for North America, Europe, and Iberia are not altered in this study, we believe that an updated fit between the larger tectonic plates is not a direct solution to the discrepancies observed in our results. More specifically, a revised fit of the larger tectonic plates would be poorly constrained and add further uncertainty regarding the relative motions of surrounding continental blocks. In our opinion, the exclusion of phenomena such as continental allochthons within exhumed mantle domains, volcanism, and the potential for temporal and spatial variabilities in depth dependent deformation are thought to be the main contributors to the observed crustal thickness gaps and poor restoration of continent-ocean transitions. In spite of these limitations, the deformable plate models presented provide insightful results regarding the deformation experienced within sedimentary basins and continental blocks throughout the southern North Atlantic. Future improvements made to deformable plate modelling approaches may help improve the results shown in this study. These will likely involve workflows using pyGPlates and the coupling of deformable plate models with geodynamic numerical models that accommodate depth-dependent phenomena and surface processes.

7.5 Conclusions

The deformable plate models presented in this study provide insight regarding the pre-Jurassic template and subsequent crustal thickness evolution of the southern North Atlantic. The main findings of this study include:

1. The inclusion of continental block kinematics within deformable plate models is necessary in order to restore pre-Jurassic crustal thicknesses within the sedimentary basins throughout the southern North Atlantic.
2. The kinematics of the Flemish Cap, Porcupine Bank, and Rockall-Hatton Bank exert a significant control on the timing and extent of rift related deformation throughout the southern North Atlantic. In addition, their kinematics are interpreted to control the pre-Jurassic geometry and evolution of the smaller Galicia Bank and Orphan Knoll, which appear to evolve in a similar manner.
3. The segmentation of crustal thicknesses observed in each model presents strong correlations with the offshore extension of Appalachian and Caledonian terrane boundaries. These observations suggest that the offshore extension of inherited orogenic boundaries induced variable pre-Jurassic crustal thicknesses and block segmentation within Orphan Basin and Porcupine Bank, respectively.
4. Along the Newfoundland Grand Banks, models that exclude the independent kinematics of the Southern Grand Banks Tail result in unrealistic segmentation of the Grand Banks crustal structure and asymmetry with the West Iberian margin. The correlation of this segmentation with the offshore extension of the Meguma terrane boundary suggests that the Meguma terrane boundary and its interplay with regional stress directions potentially induced segmentation of the Southern Grand Banks Tail as an independent crustal block. This interpretation suggests that the Southern Grand Banks Tail is of Meguma basement affinity.

5. The pre-Jurassic crustal thickness template of each model suggests that the Galicia Bank and Flemish Cap were connected as one block 200 Ma. The offshore extension of the Variscan Front is postulated to have acted as an inherited weakness that promoted their separation into two independent continental blocks during Early Cretaceous rifting.
6. The deformable plate modelling approach used in this study is unable to reconstruct appropriate pre-Jurassic crustal thicknesses in proximity of continent-ocean transitions. Future studies should consider the coupling of deformable plate models with geodynamic numerical models as a potential avenue for addressing these discrepancies.

Chapter 8

8 Beyond 2-D: an approach for validating 2-D structural restorations using deformable plate tectonic models

The material presented in this chapter can also be found in a manuscript that is currently being prepared for submission.

8.1 Introduction

Sedimentary basins hosted within offshore rifted margins are of vital importance for the exploration for natural resources and for carbon capture targets required to meet energy needs and climate change policy goals. As a result, studies that aim to understand the present-day structure of rifted margins, their crustal evolution, and the causes and mechanisms for their formation are of utmost importance. In most cases, preliminary investigations of rifted margins involve two-dimensional (2-D) data acquisition and interpretation (e.g., seismic and potential field methods) in order to understand their regional structure and distribution of rift domains (Péron-Pinvidic et al., 2007; Péron-Pinvidic and Manatschal, 2009; Peron-Pinvidic et al., 2013; Tugend et al., 2015b). Naturally, following the acquisition and interpretation of 2-D data, 2-D modelling and structural restoration techniques using software such as MOVE (https://www.petex.com/products/move-suite/2d-kinematic-modelling/) are often used to gain insight into the temporal evolution of rifted

margins based on present-day observations and interpretations (Gouiza et al., 2017; Sandoval et al., 2019; MacMahon et al., 2020; Cawood et al., 2021b, 2021a). Furthermore, to investigate conjugate relationships and temporal variations in basin connectivity along rifted margins, as well as the consequences of plate kinematic models, a common practice involves reconstructing the present-day orientation of 2-D seismic lines back through time within rigid plate tectonic reconstructions (Causer et al., 2019; Sandoval et al., 2019; MacMahon et al., 2020; Yang et al., 2021).

Despite the value of the insights drawn from these preliminary 2-D studies, the highly variable and three-dimensional (3-D) nature of rifting processes often limit our ability to study their evolution using 2-D methods alone (Figure 8.1). Using the relatively well studied rifted margins of the southern North Atlantic Ocean as an example, recent studies have shown that crustal extension and the opening of oceans dominantly occur during oblique phases of rifting (Brune et al., 2018), and are highly influenced by the interplay of regional plate kinematics (Barnett-Moore et al., 2018; Nirrengarten et al., 2018), continental block rotations (Sibuet et al., 2007; Peace et al., 2019b; Neuharth et al., 2021; Yang et al., 2021; King and Welford, 2022a, 2022b), and the heterogeneous nature of pre-rift templates caused by ancient tectonic events (Jammes and Lavier, 2019; King and Welford, 2022a; Peron-Pinvidic et al., 2022). As a result, these factors collectively contribute to the challenges associated with reconstructing the tectonic history of rifted margins, especially when 2-D methodologies are used exclusively.

In this study, we attempt to address these shortcomings by presenting a new workflow for reconstructing 2-D seismic line interpretations back through time within deformable plate tectonic models built using the interplay of GPlates (Müller et al., 2018) and its python programming

library, pyGPlates. In particular, this workflow involves restoring present-day 2-D seismic line locations as deformable points back through time within deformable plate models that account for variable plate kinematic motions and pre-rift crustal thickness templates. To test the validity of this approach, we apply this workflow using six previously published plate tectonic reconstructions and two structurally restored 2-D seismic line interpretations within the Orphan Basin, offshore Newfoundland, Canada (Gouiza et al., 2017; Cawood et al., 2021b, 2021a) (Figure 8.2) and make comparisons between results calculated by our approach (e.g., crustal thickness and total extension estimates) versus similar calculations made based on the 2-D structural restorations. The Orphan Basin is chosen due to its exploration interest as a frontier sedimentary basin, its geological complexity as an offshore rift basin that initiated within a Paleozoic mountain belt (Waldron et al., 2019), and the abundance of recently published 2-D seismic interpretation and structural restoration studies conducted within the basin (Gouiza et al., 2017; Sandoval et al., 2019; MacMahon et al., 2020; Cawood et al., 2021b, 2021a). Comparisons between crustal thickness and total extension estimates independently calculated by GPlates in this study and previously published estimates calculated using MOVE provide detailed insight into the crustal evolution of the Orphan Basin, and reveal geologically significant discrepancies. In addition, our results emphasize the importance of accounting for variable stress directions and pre-rift templates, which are often excluded from 2-D structural restorations, when reconstructing rifted margins and their overlying sedimentary basins.

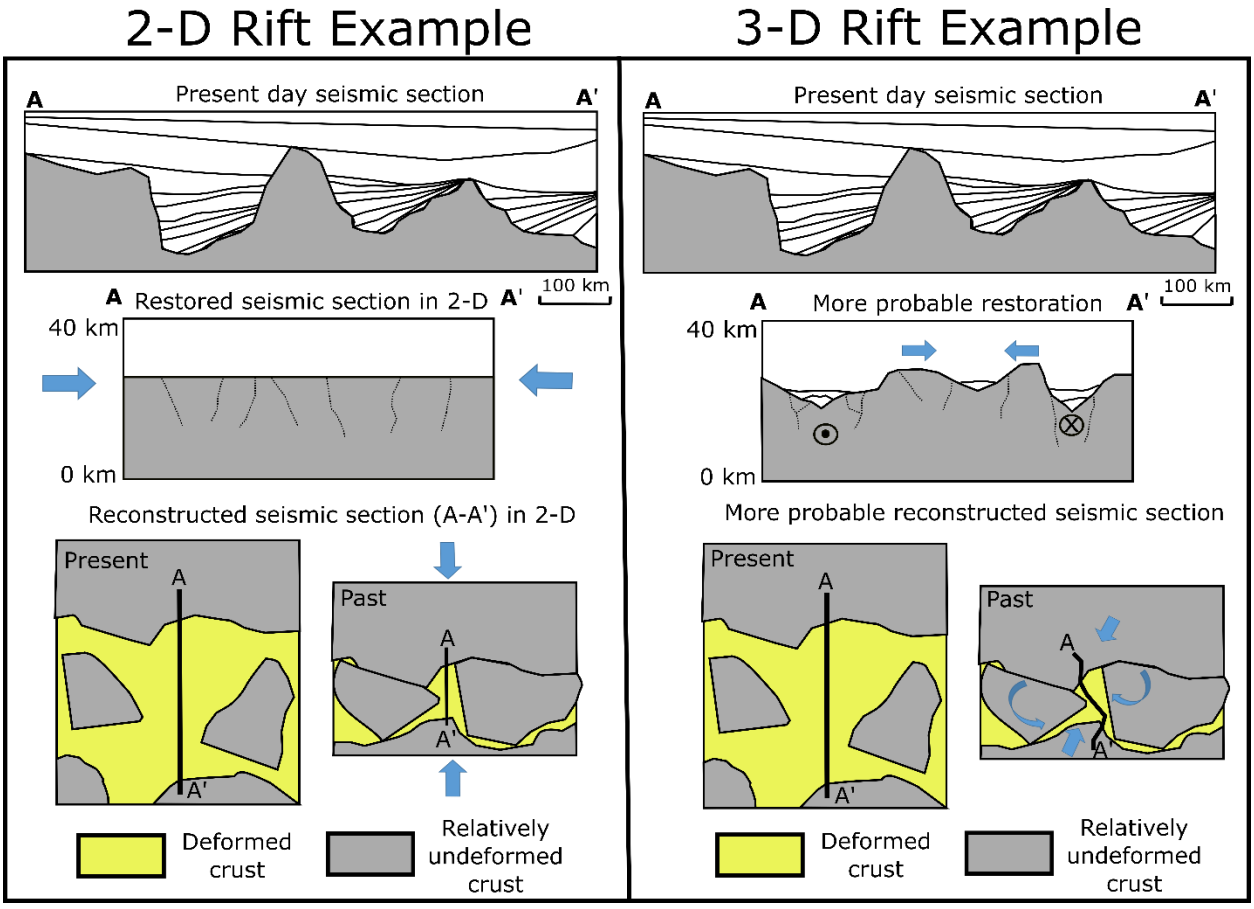

Figure 8.1 Cartoon illustration depicting some of the key differences between 2-D and 3-D seismic restorations and their reconstructed length, linearity, and orientation within plate kinematic models. The blue arrows represent regional stress directions accommodated using both approaches.

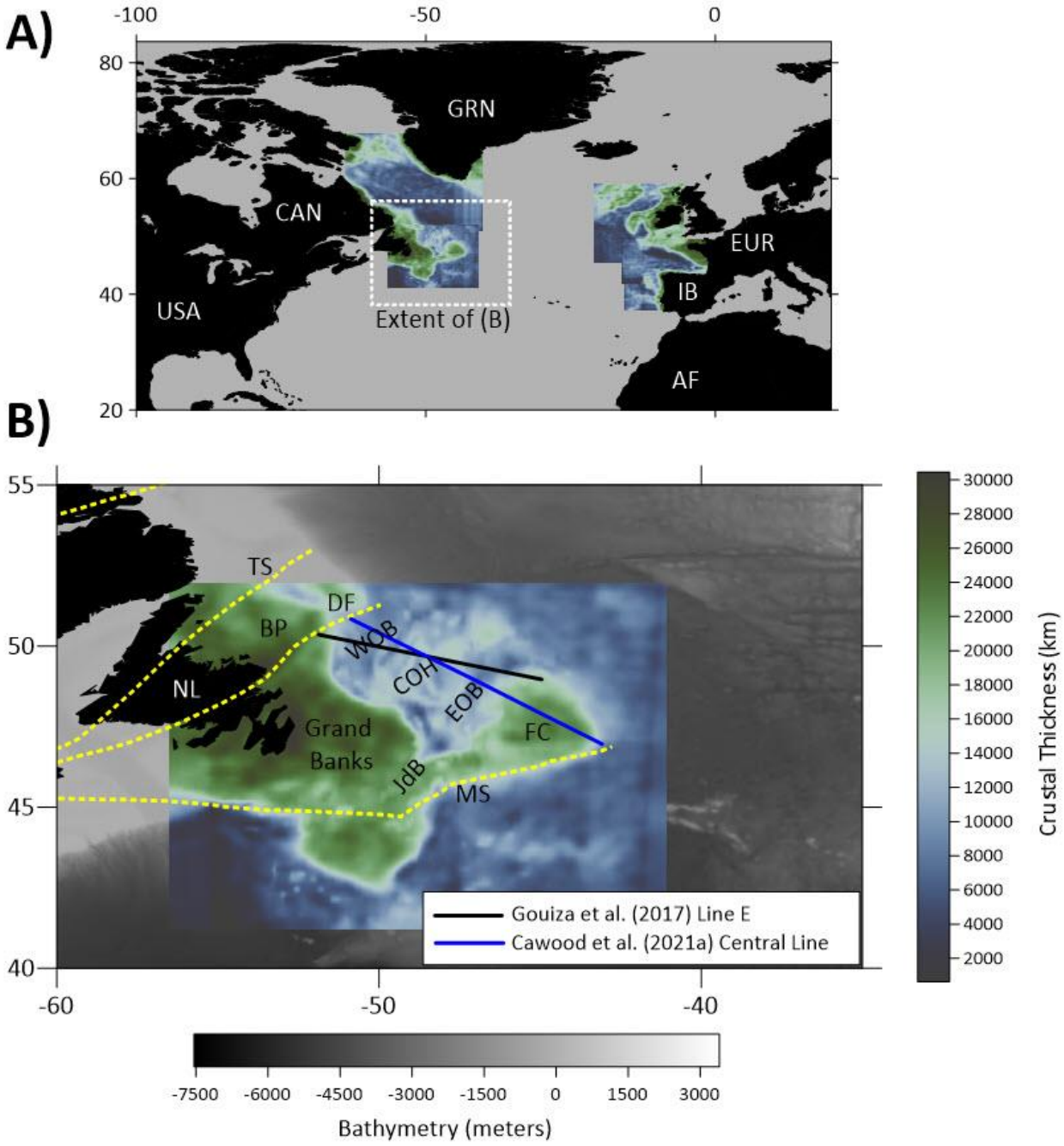

Figure 8.2 A) Crustal thickness estimates calculated from gravity inversion along the Newfoundland and Labrador, Irish, and West Iberian offshore rifted margins. Latitude and longitude values are in degrees (WGS84 coordinate reference system). B) Crustal thickness

estimates calculated from gravity inversion along the Newfoundland margin (colour plot), overlying bathymetry (greyscale). Previously published seismic lines of interest are overlain within the Orphan Basin (Gouiza et al., 2017; Cawood et al., 2021b) as are onshore to offshore Paleozoic orogenic boundaries (yellow dashed lines, extracted from Welford et al. (2012)). AF = Africa, BP = Bonavista Platform, CAN = Canada, COH = Central Orphan High, DF = Dover Fault, EOB = East Orphan Basin, EUR = Europe, FC = Flemish Cap, GRN = Greenland, IB = Iberia, JdB = Jeanne d'Arc Basin, MS = Meguma Suture, OK = Orphan Knoll, TS = Taconian Suture, USA = United States of America, WOB = West Orphan Basin.

8.2 Methodology

8.2.1 Two-dimensional structural restorations of seismic interpretations using MOVE

Seismic interpretation involves assigning geological significance (e.g., faults and horizons) to 2-D/3-D seismic reflection profiles/volumes based on changes in observed seismic character (e.g., continuity, amplitude, and phase). If well data are available within an area of interest, these can also be used by interpreters to determine time-depth relationships, changes in lithofacies, and geological ages of seismic reflectors. Following the interpretation of faults and horizons along a seismic line, structural restorations carried out using industry standard software such as MOVE by Petroleum Experts Ltd. (https://www.petex.com/products/move-suite/2d-kinematic-modelling/) are commonly used to restore faults and sedimentary columns back through time.

For 2-D seismic lines, structural restorations of seismic interpretations are usually calculated via a simple shear mode of deformation (Gouiza et al., 2017) and include additional assumptions pertaining to phenomena such as paleobathymetry, lithological compositions and

physical properties (McKenzie, 1978), compaction and thermal subsidence trends (Sclater and Christie, 1980), and the duration and timing of tectonic activity. Naturally, the results of 2-D structural restorations are highly dependent on the level of detail included in the seismic interpretation such as the depth, angle, displacement, and number of fault picks, and the interpreted age of geological horizons. Ultimately, the non-unique nature of seismic interpretation can lead to highly variable structural restoration results.

8.2.2 Crustal restoration of seismic line locations using deformable plate tectonic models

A common approach used to assess conjugate relationships in rifted margin studies consists of reconstructing rigid 2-D seismic line locations back through time according to a plate reconstruction of interest (Gerlings et al., 2012; Causer et al., 2019; Sandoval et al., 2019; MacMahon et al., 2020; Biari et al., 2021; Yang et al., 2021). Using the GPlates software, this can be done by assigning a unique plate ID to a seismic line, or by simply assigning it the same plate ID as the plate that it resides on so that the line moves relative to this plate throughout the model history (Figure 8.3). However, there are two important pitfalls associated with this approach. The first pitfall is simply that the reconstructed position of a seismic line will depend on the kinematics of a single plate/feature, ignoring the more likely scenario where multiple plates and blocks contribute to its reconstructed orientation. Second, and most importantly, reconstructed/reoriented seismic lines (and the linear margin sections that they capture) are often assumed to remain straight and rigid when in reality their length, linearity, and orientation would likely change throughout geological time according to temporal variations in deformation. As a result, this can lead to

challenges when trying to assess conjugate relationships and basin connectivity based on rigid plate reconstructions of 2-D seismic line locations alone.

In this study, we present a new workflow for warping present-day 2-D seismic line locations back through time within deformable plate tectonic models that account for plate kinematics, deformation, and variable pre-rift crustal thickness templates using the GPlates software and its python programming library, pyGPlates. Building upon concepts presented in Chapter 6, this workflow samples and represents a seismic line as a collection of points (data file containing longitude and latitude values for each of the points) that are initially created using pyGMT (https://www.pygmt.org/latest/) and subsequently converted into a scalar coverage file (.gpml file) using pyGPlates. Following these steps, the scalar coverage points are used to sample a map of crustal thickness estimates obtained from 3-D gravity inversion. The scalar coverage points (now including a value for crustal thickness) are then uploaded in GPlates and placed within a deformable plate model. They can then be used to determine the reconstructed nature of the seismic line location as a collection of deformable points (Figures 8.3 and 8.4).

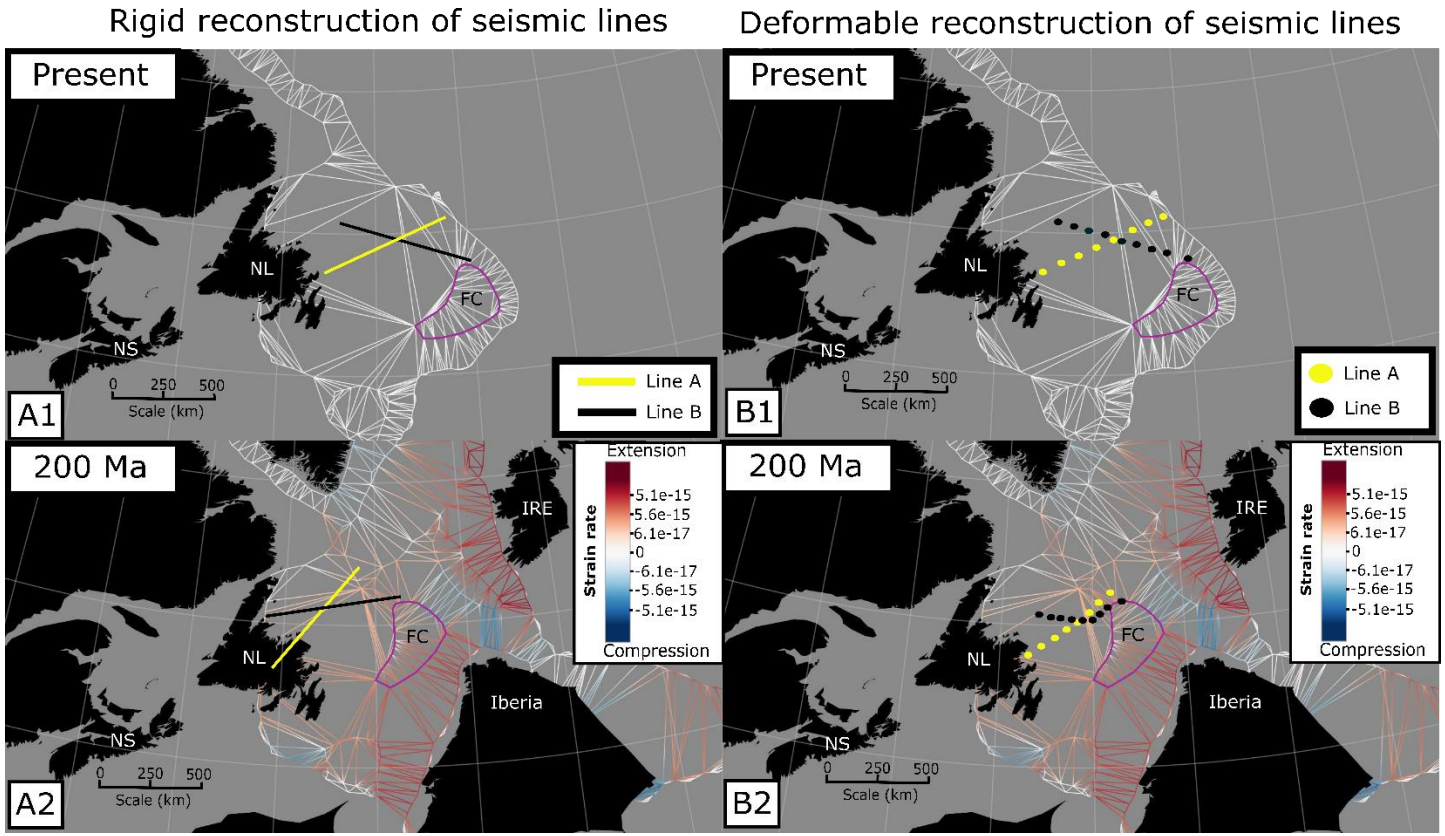

Figure 8.3 Rigid (A1 and A2) versus deformable (B1 and B2) pre-Jurassic plate reconstruction of two seismic lines from Gouiza et al. (2017) using deformable plate model B2 from Chapter 7. Note that lines A and B are sampled as points (GPlates scalar coverage points) within the deformable reconstruction (B1 and B2) as opposed to rigid lines that are reconstructed relative to the Flemish Cap (FC – outlined in purple) within the rigid plate reconstruction (A1 and A2).

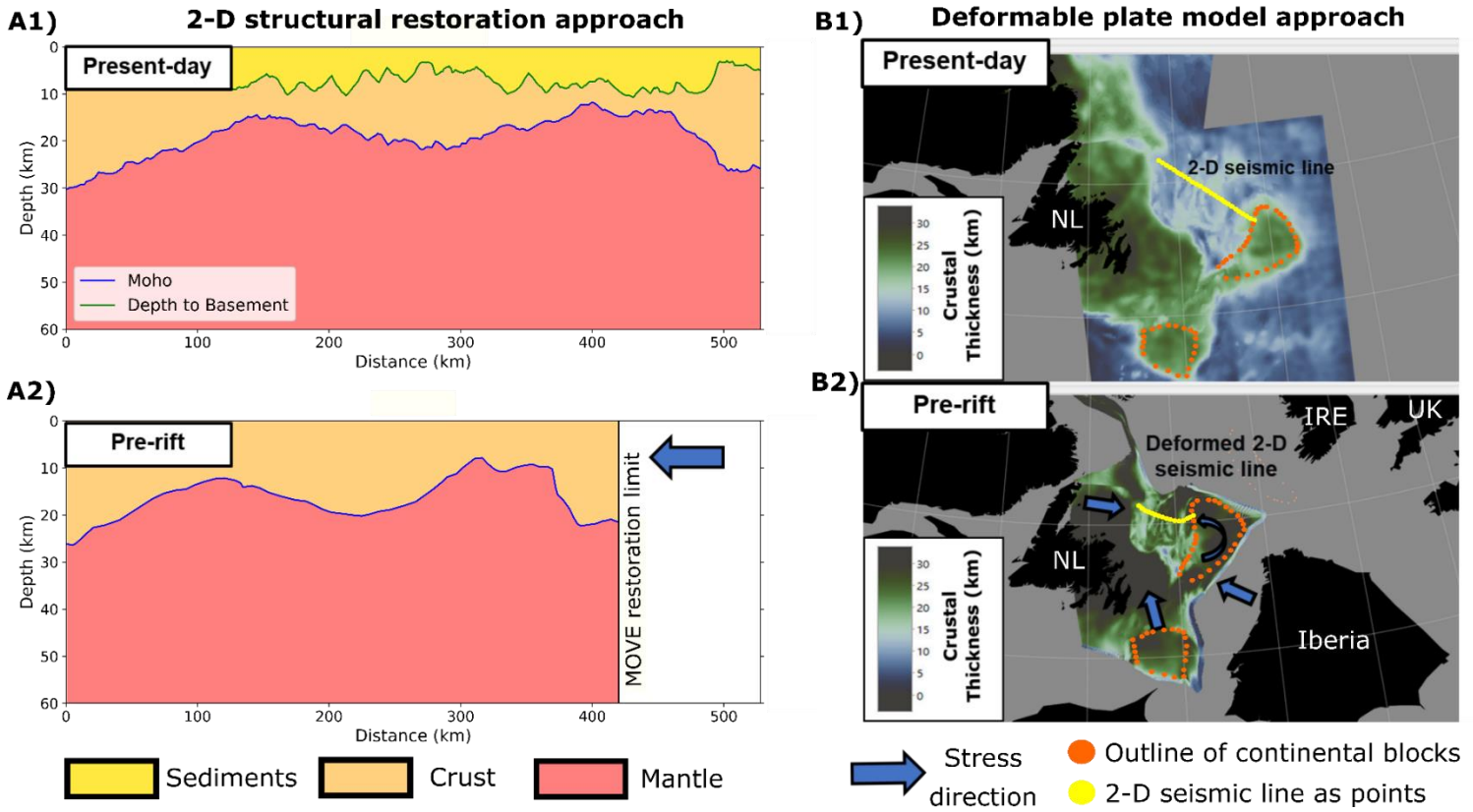

Figure 8.4 2-D structural restoration approach (A1 and A2) versus deformable plate modelling approach (B1 and B2) for restoring 2-D seismic line locations back through time. Note the variations in stress directions accounted for by using the GPlates approach versus the assumption of rift-perpendicular kinematics when using 2-D structural restorations. The 2-D structural restoration results (A1 and A2) are modified after Gouiza et al. (2017) and the deformable plate model (B1 and B2) is from Chapter 7.

8.3 Application and Results

8.3.1 Application – Orphan Basin, offshore Newfoundland, Canada

In this study, we apply our new 2-D seismic line restoration workflow using deformable plate tectonic models to investigate previously published 2-D structural restorations of seismic interpretations within the Orphan Basin, offshore Newfoundland, Canada (Figure 8.2) (Gouiza et al., 2017; Cawood et al., 2021b).

The Orphan Basin is chosen for this assessment due to its geological complexity as a poly-phased and magma-poor rift basin that initiated within an assemblage of Paleozoic terranes, and because of the abundance of 2-D seismic interpretation and structural restoration studies (Gouiza et al., 2017; Sandoval et al., 2019; MacMahon et al., 2020; Cawood et al., 2021b, 2021a), and deformable plate modelling studies (Peace et al., 2019b; Yang et al., 2021; King and Welford, 2022a). In particular, two previously published 2-D structural restorations of seismic interpretations within the Orphan Basin are chosen for this assessment, which include line E from Gouiza et al. (2017) (referred to as profile 1 in this study) and the central line from Cawood et al. 2021a (referred to as profile 2 in this study) (Figure 8.2). These two previously published 2-D seismic lines were chosen because of their close spatial proximity to one another and their across-strike coverage of the Orphan Basin. However, despite their close proximity and similar orientation, profiles 1 and 2 were also chosen due to the notable differences observed between their seismic interpretations and their implications for the timing and amount of Mesozoic extension within the Orphan Basin (summarized in Table 8.1).

To assess the validity of crustal thickness and total extension estimates calculated for profiles 1 and 2 using MOVE, we compare these results with similar estimates calculated using

six previously published plate reconstructions that are either published as deformable plate models (Müller et al., 2019; King and Welford, 2022b, 2022a) or rigid plate models that are assessed in this study by adapting them using a deformable plate modelling approach (Seton et al., 2012; van Hinsbergen et al., 2020) (details for each model are specified in Table 8.2). These six deformable plate models are chosen because they rely on variable model inputs such as the inclusion/exclusion of continental block kinematics (e.g., Flemish Cap and Porcupine Bank) and poles of rotation for larger tectonic plates (e.g., North America and Europe) and micro-plates (e.g., Iberia) (Table 8.2) that allow for a broad and comprehensive assessment of the Orphan Basin plate kinematics. Furthermore, each deformable plate model is equivalently assessed using the approach presented in Chapter 6 that allows for present-day crustal thickness estimates to be reconstructed back through time, and deformation to be experienced within continental blocks and proximal rift domains. In order to maximize the consistency between the design of model inputs for each deformable plate model considered, all deformable plate models (aside from models 2 and 4) are designed using the same boundaries and interior continental block geometries as model 1 (model B2 in Chapter 7). Note that in the original deformable plate model from Müller et al. (2019) (model 3 in this study), the Flemish Cap (and other continental blocks) is included as a rigid block and has a geometry that changes in size and shape with time. Furthermore, the model boundaries used to create the original deformable plate model of the North Atlantic Ocean from Müller et al. (2019) (originally from Barnett-Moore et al. 2018) also dynamically evolve and have specified timings of appearance and disappearance throughout the model history. Unfortunately, these assumptions and model inputs are problematic when using the deformable plate modelling approach presented in Chapter 6 because they restrict the regions that can actively deform back through time and often

lead to significant edge effects when calculating estimates such as crustal thickness. As a result, aside from the models that are also presented in Chapter 6 (models 2 and 4), the design of all model boundaries and interior continental blocks (when continental block poles of rotation are specified) are the same as model 1 in order to maximize model consistency and reduce the occurrence of edge effects caused by rigid interior blocks and model boundaries.

Using the GPlates approach, the reconstructed seismic line lengths are used to estimate total extension by adding together the cumulative distance between the reconstructed 2-D seismic line points for geological time frames of interest. Each profile tested herein is sampled in GPlates using a present-day 10 km point spacing. This sampling interval is deemed appropriate based on the sampling of the gravity inversion crustal thickness grid (5 km mesh size) and the variable sizes of triangles that make up the model 1 deformable mesh. It should be noted that unlike 2-D structural restorations calculated using MOVE, factors such as sedimentation and subsidence are not accounted for using the GPlates approach. As a result, calculations made using GPlates primarily provide insight into crustal evolution.

2-D structural restoration outputs	Profile 1	Profile 2
Jurassic total extension	50 km	158 km
Cretaceous total extension	60 km	17 km
Total extension	110 km	181 km

Table 8.1 Previously published Orphan Basin extension estimates calculated using MOVE for profiles 1 (Gouiza et al., 2017) and 2 (Cawood et al., 2021b).

Model #	Poles of rotation	Continental block kinematics included?	Previously published as a GPlates deformable plate model?	Model boundaries and continental block geometries
1	King and Welford 2022b Model B2	Yes	Yes	King and Welford 2022b Model B2
2	King and Welford 2022a Model A2	Yes	Yes	King and Welford 2022a Model A2
3	Müller et al. (2019)	Yes	Yes	King and Welford 2022b Model B2
4	King and Welford 2022a Model A1	No	Yes	King and Welford 2022a Model A1
5	Seton et al. (2012)	No	No	King and Welford 2022b Model B2
6	Van Hinsbergen et al. (2020)	No	No	King and Welford 2022b Model B2

Table 8.2 Inputs and details for all six deformable plate models used in this study.

8.3.2 Results

Herein, crustal restoration results calculated using the newly presented GPlates approach for six deformable plate models and the previously published MOVE approach along profile 1 (Figure 8.5) and profile 2 (Figure 8.6) are described. In this section, special emphasis is given to the restored line lengths and crustal thicknesses calculated at time frames of interest (pre-Jurassic, Tithonian, Aptian-Albian, and present-day) across each profile using both approaches. On all plots in figures 8.5 and 8.6, the MOVE restoration results are plotted as thick black lines.

8.3.2.1 Profile 1

Overall, the pre-Jurassic length of profile 1 calculated by MOVE (420 km) is longer than that calculated by all deformable plate models except for model 5 which has a line length that is approximately equivalent to the line length calculated by MOVE (Figure 8.5A1). In addition, the

average pre-Jurassic crustal thickness calculated by MOVE along profile 1 (16.5 km) is also less than that calculated by all plate models.

By the end of the Tithonian (Figure 8.5B1 and 8.5B2), the length of profile 1 (470 km) is longer than that calculated by the majority of deformable plate models aside from models 5 and 6 which are nearly equivalent to the line length calculated by MOVE. From the start of profile 1 (0 km) to about 280 km eastward, crustal thickness estimates calculated by all deformable models are generally similar to estimates calculated by MOVE aside from models 1 and 2 which are approximately 5 km thicker on average (Figure 8.5B2). However, eastward of 280 km in models 1, 2, and 3, crustal thickness estimates calculated by deformable plate models are greater than those calculated by MOVE (~ 10 km thicker or more) along profile 1, as these models explicitly include the Flemish Cap.

By the Aptian-Albian (Figure 8.5C1), crustal thicknesses and line lengths calculated by deformable plate models and MOVE are approximately equivalent. Apart from model 5, total extension estimates calculated by MOVE along profile 1 (110 km) are less than those calculated by all other deformable plate models, especially models that include Flemish Cap kinematics (Figure 8.5C2).

Similar to the Aptian-Albian crustal thickness estimates, present-day crustal thicknesses calculated along profile 1 by MOVE and GPlates demonstrate very similar trends and values.

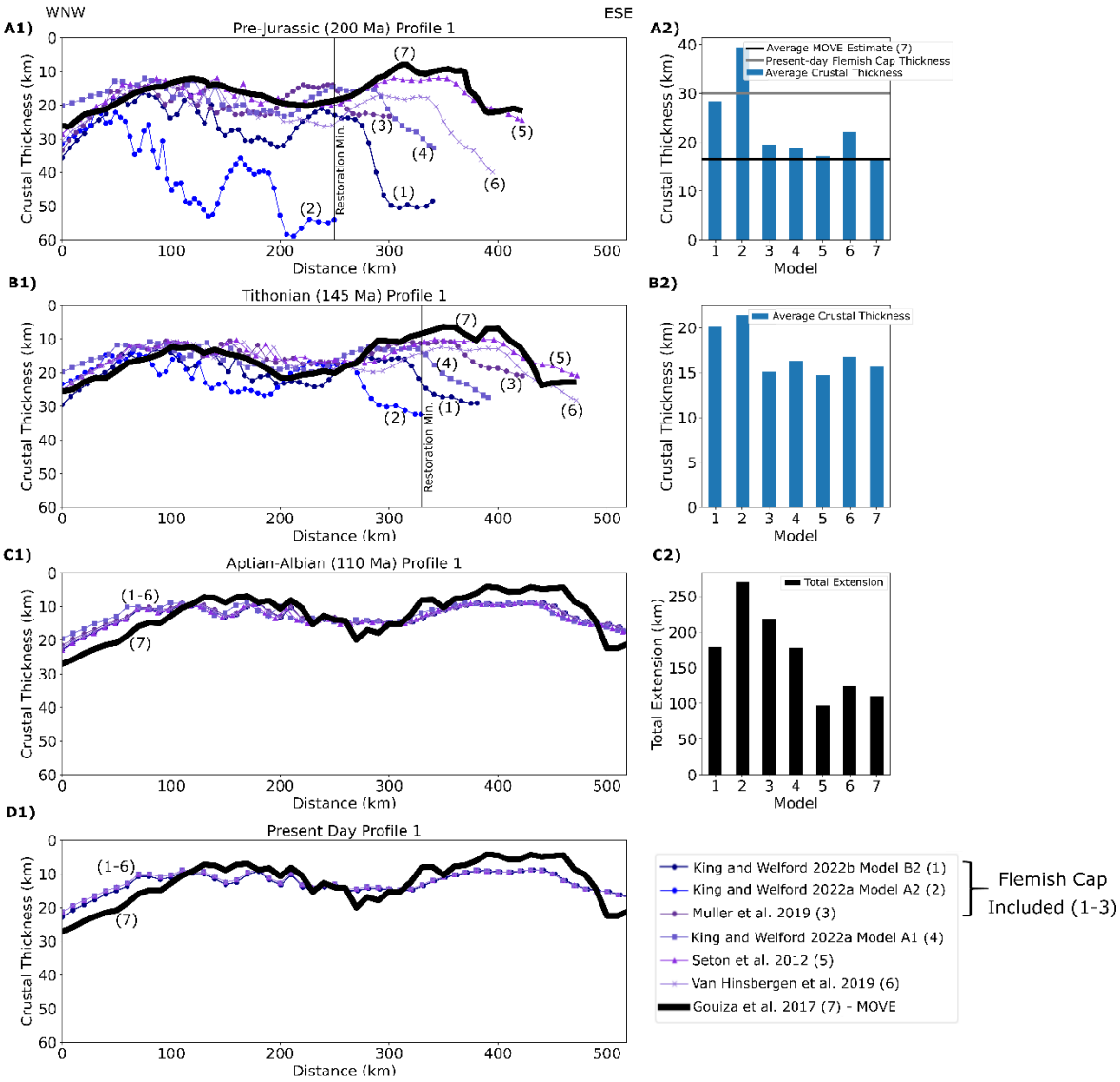

Figure 8.5 Crustal thickness estimates (A1-D1), profile lengths (A1-D1), average crustal thickness estimates (A2-B2), and total extension estimates (C2) calculated at different time frames along profile 1 by GPlates deformable plate models and 2-D structural restorations using MOVE.

8.3.2.2 Profile 2

The pre-Jurassic line length of profile 2 calculated by MOVE is 288 km, which is shorter than that calculated by deformable plate models 3-6 but longer than the line lengths calculated by

models 1 (239 km) and 2 (178 km) (Figure 8.6A1). The average pre-Jurassic crustal thickness calculated along profile 2 using MOVE is 18.5 km which is nearly identical to that calculated by models 3-6 but less thick than that calculated by model 1 (25 km) and model 2 (40 km) (Figure 8.6A2).

The length of profile 2 calculated by MOVE at the end of the Tithonian (446 km) is greater than that calculated by all deformable plate models considered, with the largest differences for line lengths calculated by model 1 (251 km long) and model 2 (293 km long) (Figure 8.6B1). Tithonian crustal thickness estimates calculated by MOVE and all deformable plate models from the start of profile 2 (0 km) until approximately 225 km eastward are generally similar (± 5 km). However, eastward of 225 km, larger differences are observed between crustal thickness estimates calculated by MOVE and all deformable plate models (~ 5-15 km thicker) except for estimates calculated by model 5 which are almost equivalent to those calculated by MOVE.

Aside from the thicker deformable plate modelling crustal thickness estimates along the western portion of the Aptian-Albian profile 2 (~ 5-10 km thicker), crustal thickness and line length estimates calculated by all deformable plate models and MOVE are nearly identical. Following the end of extension in the Orphan Basin by the Aptian-Albian, the total amount of extension calculated along profile 2 by MOVE is 181 km. This estimate is larger than that calculated by all deformable plate models except models 1 (224 km) and 2 (282 km).

At present-day, crustal thicknesses calculated by MOVE and GPlates are also nearly identical aside from the MOVE crustal thicknesses being approximately 5 km thinner within

localized regions of the Central Orphan High. This disagreement reflects a mismatch between the Moho inferred from the gravity inversion and the Moho interpreted along the seismic profile.

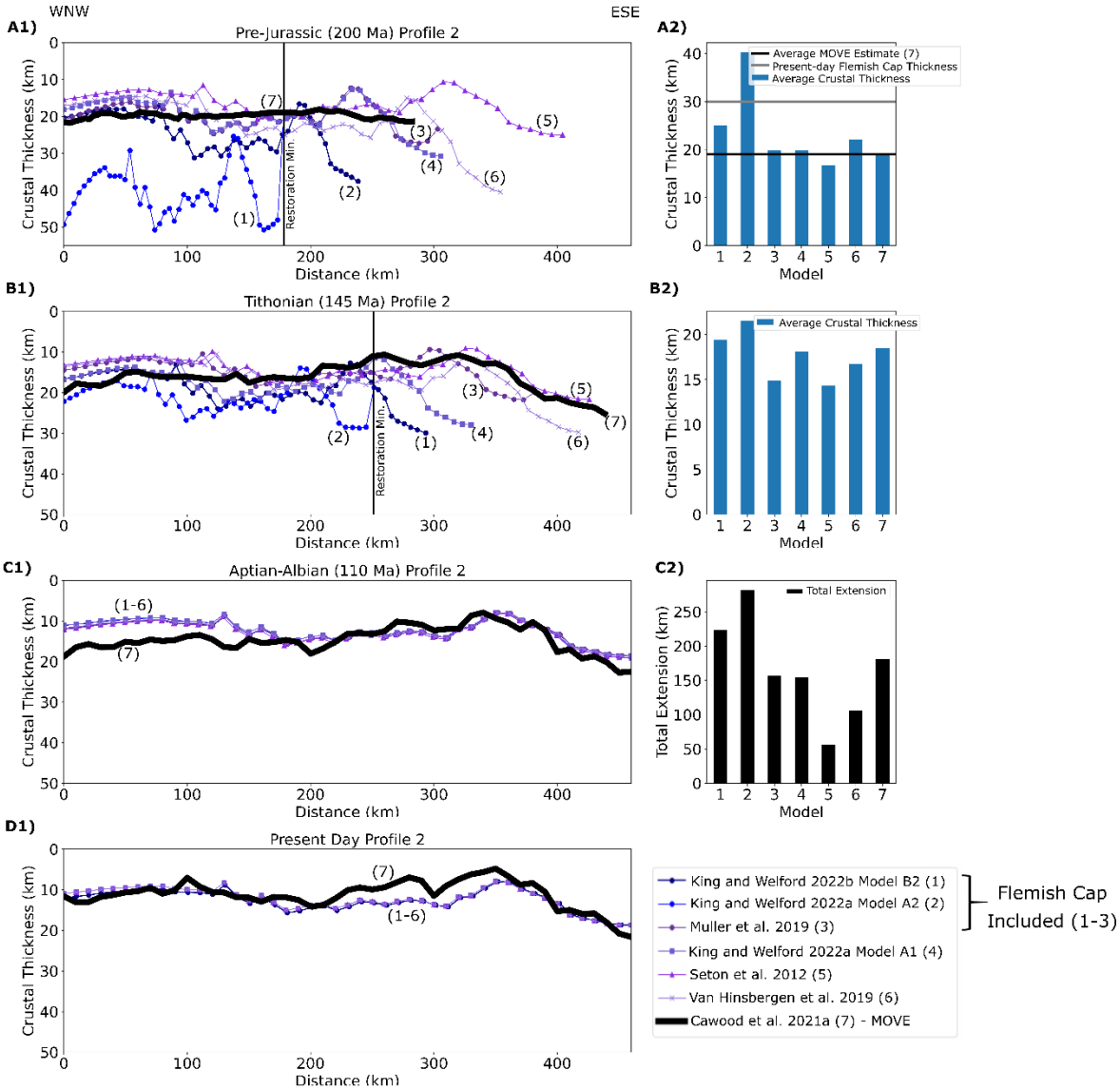

Figure 8.6 Crustal thickness estimates (A1-D1), profile lengths (A1-D1), average crustal thickness estimates (A2-B2), and total extension estimates (C2) calculated at different time frames along profile 2 by GPlates deformable plate models and 2-D structural restorations using MOVE.

8.4 Discussion

8.4.1 Crustal evolution of the Orphan Basin: comparing MOVE and GPlates results

The GPlates restoration approach defined in this chapter provides insight into the pre-Jurassic crustal architecture and subsequent crustal evolution of the Orphan Basin and reveals discrepancies when making comparisons with previously published 2-D structural restorations calculated using MOVE (Gouiza et al., 2017; Cawood et al., 2021b, 2021a).

Comparing the pre-Jurassic 2-D restoration results calculated by MOVE and GPlates along profile 1 (Figure 8.5), models that include the kinematics of the Flemish Cap (models 1-3) provide thicker average pre-Jurassic crustal thickness estimates than those calculated by MOVE. In particular, the pre-Jurassic average crustal thickness estimates calculated by models 1 and 2 are closest to the present-day 30 km average thickness of relatively undeformed crust of the Flemish Cap (Funck et al., 2003; Welford et al., 2012) in contrast to the 16.5 km pre-Jurassic average calculated by MOVE. Furthermore, within the central and eastern regions of profile 1 during the pre-Jurassic (250 km and eastward in Figure 8.5A1), crustal thicknesses calculated by all deformable plate models (except model 5) are much thicker than those calculated by MOVE with differences ranging from a minimum of 10 km (e.g., model 3) to a maximum of about 40 km (e.g., models 1 and 2). By the end of the Tithonian, similar trends are observed along profile 1 (300 km and eastward in Figure 8.5B1) indicating clear discrepancies between crustal thicknesses calculated by GPlates and MOVE in the vicinity of the East Orphan Basin and Flemish Cap during the Jurassic period (200 – 145 Ma). Based on these results, it appears that accounting for temporal variations in plate kinematics using the GPlates restoration approach is primarily responsible for

the differences between pre-Jurassic and Tithonian crustal thickness estimates calculated by GPlates and MOVE. In particular, the independent kinematics of the Flemish Cap exert a strong control on the restored pre-Jurassic and Tithonian crustal thicknesses within the Orphan Basin and this is largely the reason why the pre-Jurassic restored lengths of profile 1 calculated by GPlates are generally shorter and have higher crustal thickness estimates than those calculated by MOVE. However, as described in Chapter 7, west to east variabilities in pre-Jurassic crustal thicknesses throughout the Orphan Basin are attributed to complex accretion and tectonism experienced prior to the time frame of all models considered, which resulted in the pre-rift crust consisting of the amalgamation of various crustal terranes bordered by ancient Appalachian terrane boundaries (Hall et al., 1998; Waldron et al., 2019). Thus, the results of this study further emphasize that the pre-Jurassic and Tithonian crustal thickness templates of the Orphan Basin were strongly influenced by the kinematics of the Flemish Cap and earlier orogenic inheritance, both of which are not considered for the 2-D structural restorations.

For the 2-D structural restoration results calculated along profile 2 (Figure 8.6), little to no variations in pre-Jurassic crustal thickness are observed (consistently ~20 km thick) while crustal thickness estimates calculated using the GPlates approach for each model are highly variable from west to east. Similar to the results calculated along profile 1, pre-Jurassic crustal thickness estimates calculated within the eastern regions of profile 2 by deformable plate models are generally thicker (~ 5-30 km thicker) than the easternmost region of the MOVE profile. In contrast to profile 1, the pre-Jurassic length of profile 2 calculated by MOVE (282 km) is less than that calculated by the majority of deformable plate models aside from models 1 and 2. The shorter pre-Jurassic line lengths calculated by models 1 and 2 are caused by their pre-Jurassic position of the

Flemish Cap being further westward (within the present-day Central Orphan High) relative to its position in all other models considered. Furthermore, the pre-Jurassic average crustal thickness estimates calculated along profile 2 also demonstrate similar relationships to those seen for profile 1. In particular, models that consider the kinematics of the Flemish Cap also provide pre-Jurassic crustal thickness values that are closer in magnitude to the average present-day crustal thickness of the relatively undeformed Flemish Cap (~ 30 km thick) in contrast to that calculated by MOVE (18.5 km). As a result, these relationships further support the need to account for continental block kinematics (e.g., the Flemish Cap) when reconstructing the Orphan Basin and emphasize the potential value of our GPlates restoration approach when reconstructing other sedimentary basins globally that have complicated present-day crustal architectures.

By the end of the Jurassic (Figure 8.6B1), the length of profile 2 calculated by MOVE surpasses that calculated by all deformable plate models, demonstrating a large amount of Jurassic extension calculated by MOVE compared to that calculated by all deformable plate models considered. This stark discrepancy between both approaches regarding the amount of Orphan Basin Jurassic extension are geologically significant and are discussed more thoroughly in the subsequent section.

8.4.2 Assessing discrepancies in the timing of extension within the Orphan Basin

An abundance of seismic interpretations and structural restorations (Sibuet et al., 2007; Gouiza et al., 2017; Sandoval et al., 2019; MacMahon et al., 2020; Cawood et al., 2021b, 2021a) and deformable plate modelling studies (Peace et al., 2019b; King and Welford, 2022a, 2022b) have provided insight into the crustal evolution of the Orphan Basin. In this study, restoration of

2-D seismic line interpretations from Cawood et al. (2021a) and Gouiza et al. (2017) using MOVE and GPlates help reveal discrepancies when evaluating the timing of extension within the Orphan Basin depending on the approach used (Figure 8.7).

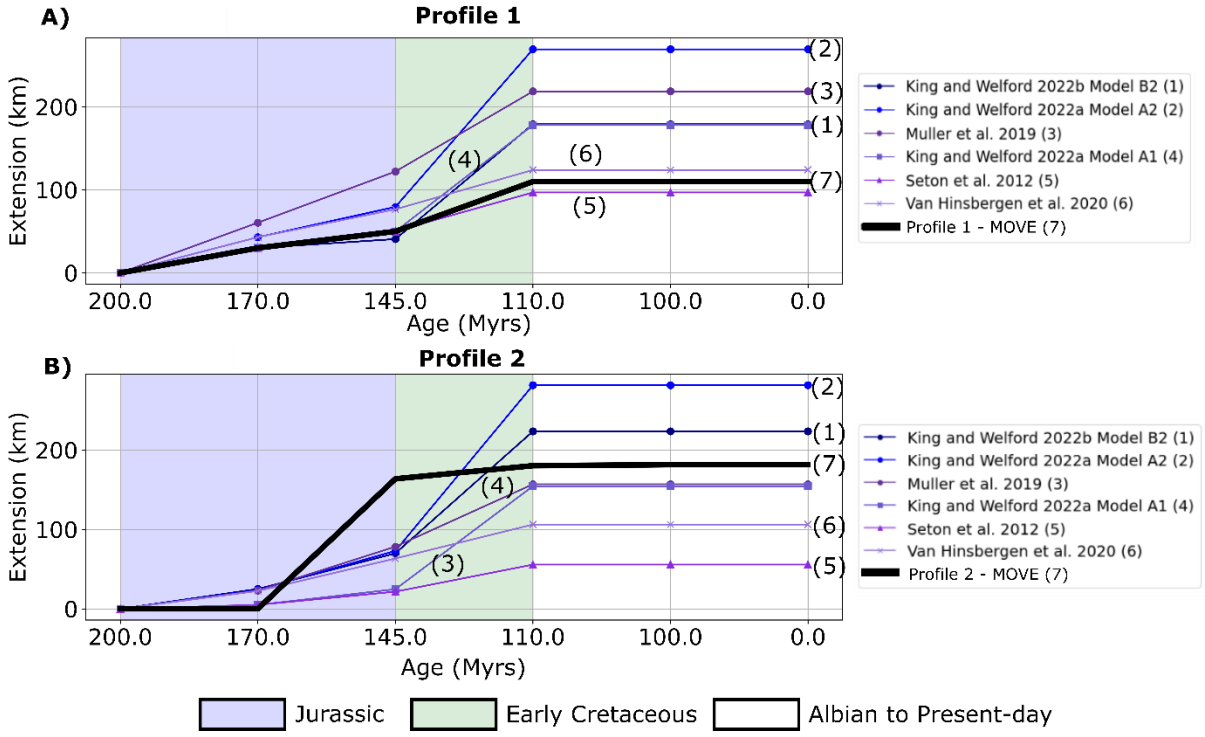

Figure 8.7 Amount and timing of Orphan Basin extension calculated using GPlates and MOVE for profiles 1 and 2.

For profile 1, the total extension calculated using MOVE (110 km) is less than that calculated by all deformable plate models (except model 5) (Figure 8.5C2) and is less than the total amount of extension calculated along profile 2 (181 km). Model 5 is a consistent outlier in our analysis because it calculates the lowest values of total extension and average crustal thickness estimates amongst all models tested within the Orphan Basin (Figures 8.5 and 8.6). This is interpreted to be caused by the lack of consideration for the Flemish Cap kinematics and the

minimal amounts of Iberian micro-plate displacement in model 5 relative to all other models considered during the Jurassic and Cretaceous periods. Throughout the Jurassic, 50 km of total extension is calculated by MOVE along profile 1, similar to the values calculated by the majority of deformable plate models aside from higher amounts of Jurassic extension calculated by model 3 (122 km) (Figure 8.7). However, a notable difference is the lack of Cretaceous extension calculated by MOVE along profile 1 (60 km) in comparison to the amounts calculated by all deformable plate models (~ 100 km or greater). Overall, temporal variations in total extension and crustal thickness estimates calculated along profile 1 are generally much lower than those calculated by GPlates and for profile 2 (Figure 8.7).

Regarding the total extension calculated for profile 2 within the Orphan Basin from 200-110 Ma, deformable plate models that include continental block kinematics (models 1-3) provide the closest total extension amounts to those calculated by MOVE (181 km) (Figure 8.6C2). However, significant discrepancies are observed when assessing the temporal evolution of extension calculated by MOVE and deformable plate models along profile 2 (Figure 8.7). In particular, the 158 km of total Jurassic extension calculated by MOVE is at least 85 km greater than the next closest deformable plate model estimates by the end of Jurassic (78 km of Jurassic extension calculated by model 3). In contrast, all deformable plate models in this study suggest larger amounts of early Cretaceous extension compared to that calculated by MOVE along profile 2 (17 km) (Figure 8.7).

To assess the geodynamic consequences of these discrepancies in timing and amounts of Jurassic extension, we revisit the plate kinematics of models 1 and 3 in Figure 8.8. Models 1 and 3 are chosen in order to provide a more comprehensive assessment of the Orphan Basin kinematics

using two different plate models of the North Atlantic that both include the Flemish Cap kinematics but provide different poles of rotation for the Flemish Cap and other highly debated micro-plates such as Iberia (Barnett-Moore et al., 2016). Therein, we observe several complications along the West Iberian and Irish margins. In particular, the Tithonian seismic line lengths calculated by 2-D structural restorations for profile 2 would result in Jurassic compressional stresses along the West Iberian margin, overlap between the Flemish Cap and Northwest Iberian interior (observed in model 1), and inter-basin connectivity between the East Orphan Basin and the Porcupine Basin, a phenomenon suggested to be unlikely based on previous seismic (Sandoval et al., 2019) and plate kinematic studies (Barnett-Moore et al., 2018; Nirrengarten et al., 2018; Yang et al., 2021). Thus, based on the need to account for Flemish Cap kinematics in order to properly restore the crustal evolution of the Orphan Basin within a regional context (Sibuet et al., 2007; Barnett-Moore et al., 2018; Nirrengarten et al., 2018; Peace et al., 2019b; King and Welford, 2022a, 2022b), we suggest that models with larger amounts of Cretaceous extension within the Orphan Basin than those suggested by Cawood et al. (2021a) seem to provide a more plausible geodynamic scenario and avoid plate kinematic conflicts with surrounding margins. We acknowledge that deformable plate models do not provide a perfect solution to all available constraints throughout the southern North Atlantic Ocean, but overall, the crustal thicknesses and timing of total extension calculated by deformable plate models (model 1 in particular) appear to provide a reasonable fit given the majority of available constraints and limitations of deformable plate models.

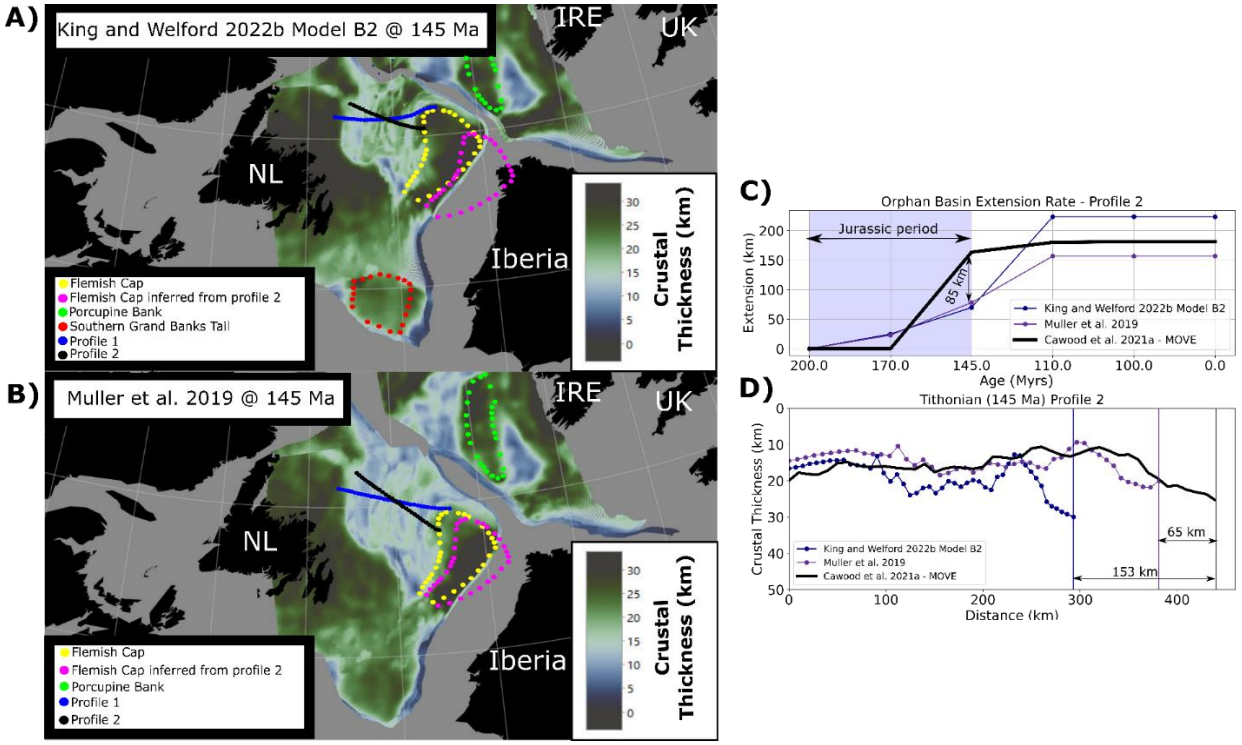

Figure 8.8 Tithonian (145 Ma) crustal restoration of profile 2 calculated by MOVE and GPlates and their relationship with the position of the Flemish Cap and crustal thicknesses calculated at 145 Ma by models 1 (A) and 3 (B). The approximate location of the Flemish Cap at 145 Ma inferred from the restoration length of profile 2 calculated by MOVE is shown by the magenta points. Also shown are the Orphan Basin extension amounts (C) and the Tithonian restoration of profile 2 (D) using deformable plate models and MOVE.

8.4.3 Evaluating uncertainties of deformable plate tectonic models

Quantifying uncertainty within deformable plate tectonic models represents a challenging task. This view is based on the fact that deformable plate models not only encompass uncertainties associated with plate kinematic constraints (e.g., paleomagnetics, identification of oceanic magnetic anomalies, etc.) but also absorb the uncertainties that are characteristic of geophysical methods (e.g., seismic and gravity methods) and modelling techniques (e.g., 3-D gravity inversion) used to calculate model inputs such as present-day crustal thickness estimates. In this chapter, we present a new approach for quantifying extension and crustal thickness estimates within deformable plate models that can be quantitatively compared with similar, yet independently obtained, estimates calculated by 2-D structural restorations of seismic interpretations. In our opinion, this approach creates an avenue for minimizing uncertainty associated with deformable plate models, or conversely, it can also be used to assess the influence of regional plate kinematics and variable pre-rift templates on 2-D structural restoration results. An application of this approach to the Orphan Basin, offshore Newfoundland, allows for discrepancies to be recognized between the timing of extension suggested by previously published plate kinematic models and 2-D structural restorations based on seismic interpretations. Although the Orphan Basin still represents a frontier hydrocarbon exploration target with sparse offshore drilling samples, the impact of 3-D kinematics, orogenic inheritance, and their relationships with surrounding conjugate margins are all factors that should be taken into consideration as part of future studies of the Orphan Basin, and rifted margins in general. In our opinion, the full consideration of these phenomena,

continued data acquisition, and the use of our newly presented workflow with future 2-D structural restorations of seismic interpretations may help address the current uncertainties regarding the amount of Jurassic extension that took place within the Orphan Basin. In addition, future improvements made to the GPlates crustal restoration approach introduced herein should focus on exploring the coupling between plate kinematic, mantle convention, and basin and landscape models as done in previous studies elsewhere (Flament et al., 2014; Harrington et al., 2019). These future steps may help improve our knowledge of rifted margin development, sedimentary basin formation, and the geodynamic consequences of plate kinematic models.

8.5 Conclusions

The newly presented workflow used to reconstruct previously published 2-D seismic line interpretations within deformable plate models back through time using the interplay of GPlates and pyGPlates provided insight into the crustal evolution of the Orphan Basin. The main conclusions of this work are:

1. The reconstruction of 2-D seismic lines as deformable points permitted their restored length, orientation, and linearity to be visualized within deformable plate tectonic models. For tectonic regimes that are interpreted to have evolved under oblique stress directions (e.g., the North Atlantic Ocean), rigid reconstructions of 2-D seismic lines and 2-D structural restorations of seismic interpretations should be exercised with caution as their lack of accountability for variations in regional stresses and deformation through time may be misleading.

2. The crustal evolution of the Orphan Basin is interpreted to have been highly influenced by the kinematics of the Flemish Cap and orogenic inheritance. This is emphasized by plate models and 2-D structural restorations that underestimate Jurassic crustal thickness and extension estimates when the Flemish Cap kinematics and variable pre-Jurassic crustal thickness templates are not considered.
3. The ability to account for variable plate kinematics and pre-Jurassic crustal thickness templates using the GPlates restoration approach revealed notable discrepancies regarding the timing of deformation within the Orphan Basin implied from 2-D structural restorations. In particular, the magnitude of Jurassic extension calculated by 2-D structural restorations is at least double the amount suggested by all deformable plate models considered.
4. Calculating Orphan Basin extension estimates also revealed a lack of Cretaceous extension calculated by 2-D structural restorations in comparison to larger amounts calculated by the majority of deformable plate models considered in this study.
5. Reconstructing 2-D seismic lines as deformable points provides an approach for quantifying uncertainties between deformable plate models and structural restorations based on seismic interpretations. Although there are many uncertainties associated with deformable plate models (as there are with seismic interpretation and 2-D structural restorations), this capability provides an additional method of comparison to assess relationships between deformable plate models and independent observations.

In addition to the usefulness of our newly presented workflow for studying the formation of rifted margins and their overlying sedimentary basins, the GPlates restoration approach described herein can also be readily applied to study other tectonic regimes.

Chapter 9

9 Summary, conclusions, and future work

9.1 Summary and conclusions

The primary motivation of this research was to investigate the role of continental block kinematics on the crustal evolution of Iberia, and the Newfoundland and Irish offshore rifted margins. Taking into consideration the deformable plate modelling workflows and applications presented, this thesis provides valuable insight into how continental block kinematics impacted the partitioning of rift-related deformation during the formation of the southern North Atlantic Ocean.

In Chapters 3-5, special emphasis was given to investigating the plate kinematics of the Iberian micro-plate using previously published and newly presented plate reconstructions. Collectively, the use of deformable plate models provides insight into how continental blocks partitioned the timing and extent of Mesozoic deformation experienced throughout Iberia's present-day offshore rifted margins (e.g., West Iberian and Bay of Biscay margins) and former rifted margins that have been re-activated by compressional deformation (e.g., Pyrenees and Iberian Ranges). More specifically, Chapters 3-5 conclude

that continental block kinematics are needed within deformable plate models of Iberia in order to calculate variations in present-day crustal thickness templates (e.g., Figure 4.4) and the temporal partitioning of rift domains that are more similar to those interpreted from independent observations (e.g., Figure 5.8). In particular, the most influential Iberian continental blocks include the Galicia Bank along the northwest Iberian margin (Chapter 3) and the Landes High and Ebro Block located within the Bay of Biscay (Chapter 4) and Pyrenean realm (Chapter 5), respectively.

Re-visiting the disputed Mesozoic plate kinematics of the Iberia-Eurasia plate boundary (Figure 2.4), the deformable plate models presented in Chapters 4 and 5 suggest that this region was unlikely to be a continuous plate boundary controlled by the motions of two rigid tectonic plates (e.g., Iberia and Eurasia). Instead, the preferred deformable plate models in Chapters 4 and 5 suggest that the kinematics of the Landes High and Ebro Block partitioned the deformation experienced between Iberia and Europe and induced transtensional phases of rifting within the Bay of Biscay and Pyrenean realm throughout the Jurassic and Cretaceous. As also suggested by geological and geophysical studies throughout Iberia (Oliva-Urcia et al., 2011; Soto et al., 2011; Tugend et al., 2015a; Aldega et al., 2019; Asti et al., 2022), these oblique rift phases led to creation of the variable rift domains and localized sedimentary depocenters that are observed present-day along strike of the Bay of Biscay and Pyrenees.

However, despite the improved correlations between crustal thickness estimates calculated by deformable plate models and independent observations such as 3-D gravity inversion when continental block kinematics are considered, discrepancies between both

approaches are still nonetheless observed. Most commonly, the largest discrepancies are observed in regions in the vicinity of major lithospheric boundaries inherited from pre-rift tectonism (e.g., Figure 4.4), or within the continental blocks themselves due to their inability to experience internal deformation (e.g., Figure 3.8). As a result, despite providing new insights into the role of continental blocks and the consequences of previously published and newly presented plate reconstructions of Iberia using a deformable plate modelling approach, improved methodologies were needed in order to more accurately validate their results.

In Chapters 6-8, new deformable plate modelling workflows using the interplay of GPlates and its python programming library, pyGPlates, were introduced and applied to study the plate kinematic evolution of the southern North Atlantic Ocean. Motivated by the deformable plate modelling assumptions and limitations used in Chapters 3-5, Chapter 6 introduces new approaches for reconstructing present-day crustal thickness estimates back through time, and simulating deformation within continental blocks and proximal rift domains. The application of these newly presented workflows in Chapters 6 and 7 permits more detailed classifications to be made regarding the potential origin and evolution of continental blocks and sedimentary basins located along the Newfoundland, Irish, and West Iberian margins that were un-identifiable in Chapters 3-5. In particular, continental blocks that are larger in size, such as the Flemish Cap, Porcupine Bank, and Rockall-Hatton Bank, are referred to as “primary blocks” because of their significant control on the deformation experienced within neighbouring sedimentary basins and smaller continental blocks referred to as “secondary blocks” (e.g., the Galicia Bank and Orphan Knoll).

Furthermore, given the larger size of these so-called primary continental blocks during the pre-Jurassic and their structural variations that are often segmented by the trends of ancient crustal sutures (e.g., the Porcupine Bank) (Figure 7.6), it is postulated that primary blocks are ancient terranes/crustal blocks inherited from Paleozoic tectonism that were subsequently re-activated during North Atlantic rifting. In contrast, secondary continental blocks (e.g., the Galicia Bank and Orphan Knoll) are considered to have formed via extensional processes during North Atlantic rifting such as the interactions between propagating rifts and inherited structures. Overall, the workflows introduced in Chapters 6 and 7 provide detailed insight into the pre-Jurassic template (Figure 7.6) and subsequent crustal evolution of continental blocks within the southern North Atlantic Ocean (Figures 7.2-7.5) that were poorly understood and assumed to be uniform and rigid by deformable plate models presented in Chapters 3-5.

However, despite the modelling improvements presented in Chapters 6 and 7, a re-occurring topic of discussion in each chapter of this thesis involves comparing deformable plate modelling outputs (e.g., temporal variations in crustal thickness) with the timing of deformation inferred from independent observations such as interpretations of regional seismic reflection profiles and well data to assess their validity. More often than not, these correlations are qualitative because there are no known workflows that can be used to quantify the uncertainties of deformable plate models and the differences between their outputs and independent observations. As a step towards addressing these unsatisfying problems, Chapter 8 presented a new workflow for making quantitative comparisons between the results calculated by deformable plate models (e.g., crustal thickness and

extension estimates) with those calculated by 2-D structural restorations of seismic interpretations. More generally, this approach can be used to assess the kinematics and crustal evolution of 2-D seismic line locations back through time within deformable plate models, regardless of whether or not they have been structurally restored using software such as MOVE. As a result, this workflow can be used by seismic interpreters to reconstruct 2-D seismic line locations back though time, which could also help constrain future deformable plate modelling studies via the integration of newly presented datasets into their design. Following an application of this workflow to the Orphan Basin, the results reveal that 3-D plate kinematics and variable pre-rift crustal thickness templates calculated by deformable plate models can significantly impact the crustal evolution of rifted margins, which are usually unaccounted for by 2-D methods. As a result, these improved workflows for building deformable plate models and making quantitative comparisons between their outputs and geophysical and geological observations has provided a more comprehensive crustal-scale reconstruction of the southern North Atlantic offshore rifted margins.

9.2 Future Work

This thesis presents the first investigation of the Iberian plate kinematics using a deformable plate modelling approach and provides new workflows that should be considered in future deformable plate modelling studies. Moreover, the work conducted in this thesis has also allowed for the identification of recommendations and avenues for future studies focussed on rifted margin formation, and deformable plate modelling strategies.

Chapters 6 and 7 present new deformable plate modelling workflows for reconstructing present-day crustal thickness estimates back through time, and for simulating deformation within proximal rift domains and continental blocks. Considering their application to the West Iberian margin, this permitted the origin and crustal thickness evolution of the Galicia Bank to be more clearly understood in contrast to that identified in Chapter 3. As a result, these workflows should also be applied to study the crustal evolution of the Bay of Biscay and Pyrenean realm using the models presented in Chapters 4 and 5 as a starting point. However, this will also require new 3-D gravity inversion studies of these regions in order to calculate more finely sampled onshore crustal thickness estimates needed to reconstruct crustal thicknesses within the Iberian interior back through time.

In addition, despite the improved deformable plate modelling workflows presented in Chapters 6-8, the lack of consideration for rheological controls and depth-dependent deformation within deformable plate models is geologically unsatisfying. As a result, future studies should investigate how deformable plate models can be coupled with other modelling techniques that account for phenomena such as depth-dependent deformation, surface processes, and rheological controls. Based on the current state of geodynamic modelling, one possible avenue for extending the capabilities of deformable plate models consists of using their plate kinematic velocities as inputs on a free-surface within 3-D mantle-convection models (Flament et al., 2014). As a result, this would allow one to investigate the consequences of deformable plate modelling outputs on phenomena such as mantle dynamics and dynamic topography, which can subsequently be used to constrain basin and landscape models (Harrington et al., 2019). Alternatively, another avenue for

addressing the geodynamic consequences of deformable plate models along rifted margins could involve using their outputs (e.g., extension velocities and spatial limits) as inputs for 2-D/3-D thermo-mechanical models that are typically used to explain causes and mechanisms for rifted margin formation (Pérez-Gussinyé et al., 2003; Brune et al., 2014; Neuharth et al., 2022). This approach would allow one to investigate the more local impacts of deformable plate modelling outputs on phenomena such as lithospheric architecture, crustal faulting, and sedimentation. Collectively, these ideas could provide improved workflows for making correlations between plate tectonic reconstructions and regional to local-scale observations along rifted margins and their overlying sedimentary basins.

Bibliography

Ady, B.E., Whittaker, R.C., 2018. Examining the influence of tectonic inheritance on the evolution of the North Atlantic using a palinspastic deformable plate reconstruction. Geol. Soc. London, Spec. Publ. SP470.9. https://doi.org/10.1144/sp470.9

Aldega, L., Viola, G., Casas-Sainz, A., Marcén, M., Román-Berdiel, T., van der Lelij, R., 2019. Unraveling Multiple Thermotectonic Events Accommodated by Crustal-Scale Faults in Northern Iberia, Spain: Insights From K-Ar Dating of Clay Gouges. Tectonics 38, 3629–3651. https://doi.org/10.1029/2019TC005585

Alvarez-Marrón, J., Pérez-Estaún, A., Dañobeitia, J.J., Pulgar, J.A., Martínez Catalán, J.R., Marcos, A., Bastida, F., Ayarza Arribas, P.A., Aller, J., Gallart, A., Gonzalez-Lodeiro, F., Banda, E., Comas, M.C., Córdoba, D., 1996. Seismic structure of the northern continental margin of Spain from ESCIN deep seismic profiles. Tectonophysics 264, 153–174. https://doi.org/10.1016/S0040-1951(96)00124-2

Alvarez-Marrón, J., Rubio, E., Torne, M., 1997. Subduction-related structures in the North Iberian Margin. J. Geophys. Res. 102, 22,497-22,511.

Alves, T., Moita, C., Pinheiro, L., Monteiro, J., 2003. Evolution of deep-margin extensional basins: the continental slope basins offshore West Iberia. AAPG Int. … 1, 1–5.

Alves, T.M., Bell, R.E., Jackson, C.A.L., Minshull, T.A., 2014. Deep-water continental margins: Geological and economic frontiers. Basin Res. 26, 3–9. https://doi.org/10.1111/bre.12053

Alves, T.M., Cunha, T.A., 2018. A phase of transient subsidence, sediment bypass and

deposition of regressive–transgressive cycles during the breakup of Iberia and Newfoundland. Earth Planet. Sci. Lett. 484, 168–183. https://doi.org/10.1016/j.epsl.2017.11.054

Alves, T.M., Moita, C., Cunha, T., Ullnaess, M., Myklebust, R., Monteiro, J.H., Manuppella, G., 2009. Diachronous evolution of late jurassic-cretaceous continental rifting in the northeast atlantic (west iberian margin). Tectonics 28, 1–32. https://doi.org/10.1029/2008TC002337

Alvey, A., Gaina, C., Kusznir, N.J., Torsvik, T.H., 2008. Integrated crustal thickness mapping and plate reconstructions for the high Arctic. Earth Planet. Sci. Lett. 274, 310–321. https://doi.org/10.1016/j.epsl.2008.07.036

Angrand, P., Mouthereau, F., 2021. Evolution of the Alpine orogenic belts in the Western Mediterranean region as resolved by the kinematics of the Europe- Africa diffuse plate boundary. Bull. la Société Géologique Fr.

Angrand, P., Mouthereau, F., Masini, E., Asti, R., 2020. A reconstruction of Iberia accounting for W-Tethys/N-Atlantic kinematics since the late Permian-Triassic. Solid Earth Discuss. 1–24. https://doi.org/10.5194/se-2020-24

Arenas, R., Díez Fernández, R., Sánchez Martínez, S., Gerdes, A., Fernández-Suárez, J., Albert, R., 2014. Two-stage collision: Exploring the birth of Pangea in the Variscan terranes. Gondwana Res. 25, 756–763. https://doi.org/10.1016/j.gr.2013.08.009

Asti, R., Saspiturry, N., Angrand, P., 2022. The Mesozoic Iberia-Eurasia diffuse plate boundary: A wide domain of distributed transtensional deformation progressively focusing along the North Pyrenean Zone. Earth-Science Rev. 230, 104040.

https://doi.org/10.1016/j.earscirev.2022.104040

Avedik, F., Camus, A.L., Ginsburg, A., Montadert, L., Roberts, D.G., Whitmarsh, R.B., 1982. A seismic refraction and reflexion study of the continent-ocean transition beneath the north Biscay margin. Philos. Trans. R. Soc. London. Ser. A, Math. Phys. Sci. 305, 5–25. https://doi.org/10.1098/rsta.1982.0023

Ayarza, P., Martínez Catalan, J.R., Gallart, J., Pulgar, J.A., Dañobeitia, J.J., 1998. Estudio Sismico de la Corteza Iberica Norte 3.3: A seismic image of the Variscan crust in the hinterland of the NW Iberian Massif. Tectonics 17, 171–186.

Barnett-Moore, N., Font, E., Neres, M., 2017. A Reply to the Comment on "Assessing Discrepancies Between Previous Plate Kinematic Models of Mesozoic Iberia and Their Constraints" by Barnett-Moore Et Al. Tectonics 36, 3286–3297. https://doi.org/10.1002/2017TC004760

Barnett-Moore, N., Hosseinpour, M., Maus, S., 2016. Assessing discrepancies between previous plate kinematic models of Mesozoic Iberia and their constraints. Tectonics 35, 1843–1862. https://doi.org/10.1002/2015TC004019

Barnett-Moore, N., Müller, D.R., Williams, S., Skogseid, J., Seton, M., 2018. A reconstruction of the North Atlantic since the earliest Jurassic. Basin Res. 30, 160–185. https://doi.org/10.1111/bre.12214

Biari, Y., Klingelhoefer, F., Franke, D., Funck, T., Loncke, L., Sibuet, J.C., Basile, C., Austin, J.A., Rigoti, C.A., Sahabi, M., Benabdellouahed, M., Roest, W.R., 2021. Structure and evolution of the Atlantic passive margins: A review of existing rifting models from wide-

angle seismic data and kinematic reconstruction. Mar. Pet. Geol. 126, 104898. https://doi.org/10.1016/j.marpetgeo.2021.104898

Biteau, J.J., Le Marrec, A., Le Vot, M., Masset, J.M., 2006. The Aquitaine Basin. Pet. Geosci. 12, 247–273. https://doi.org/10.1144/1354-079305-674

Boillot, G., Dupeuble, P.A., Malod, J., 1979. Subduction and tectonics on the continental margin off northern Spain. Mar. Geol. 32, 53–70. https://doi.org/10.1016/0025-3227(79)90146-4

Boillot, G., Winterer, E.L., 1988. Drilling on the Galicia Margin: Retrospect and Prospect. Proc. Ocean Drill. Program, 103 Sci. Results. https://doi.org/10.2973/odp.proc.sr.103.180.1988

Bois, C., Gariel, O., Lefort, J.P., Rolet, J., Brunet, M.F., Masse, P., Olivet, J.L., 1997. Geologic contribution of the Bay of Biscay deep seimic survey : a summary of the main scientific results, a discussion of the open questions and suggestions for further investigations. Mém. Soc. Géol. Fr. 171, 193–209.

Bronner, A., Sauter, D., Manatschal, G., Péron-Pinvidic, G., Munschy, M., 2011. Magmatic breakup as an explanation for magnetic anomalies at magma-poor rifted margins. Nat. Geosci. 4, 549–553. https://doi.org/10.1038/ngeo1201

Brune, S., 2018. Forces within continental and oceanic rifts: Numerical modeling elucidates the impact of asthenospheric flow on surface stress. Geology 46, 191–192. https://doi.org/10.1130/focus022018.1

Brune, S., Heine, C., Clift, P.D., Pérez-Gussinyé, M., 2017. Rifted margin architecture and crustal rheology: Reviewing Iberia-Newfoundland, Central South Atlantic, and South China

Sea. Mar. Pet. Geol. 79, 257–281. https://doi.org/10.1016/j.marpetgeo.2016.10.018

Brune, S., Heine, C., Pérez-Gussinyé, M., Sobolev, S. V., 2014. Rift migration explains continental margin asymmetry and crustal hyper-extension. Nat. Commun. 5, 1–9. https://doi.org/10.1038/ncomms5014

Brune, S., Williams, S.E., Dietmar Müller, R., 2018. Oblique rifting: The rule, not the exception. Solid Earth 9, 1187–1206. https://doi.org/10.5194/se-9-1187-2018

Brunet, M.F., 1984. Subsidence history of the Aquitaine basin determined from subsidence curves. Geol. Mag. 121, 421–428. https://doi.org/10.1017/S0016756800029952

Bullard, E., Everett, J., Smith, A., 1965. The Fit of the Continents around the Atlantic Author (s): Edward Bullard , J . E . Everett and A . Gilbert Smith Source : Philosophical Transactions of the Royal Society of London . Series A , Mathematical and Physical Sciences , Vol . 258 , No . 1088 , 258, 41–51.

Burg, J.P., Van Den Driessche, J., Brun, J.P., 1994. Syn- to post-thickening extension in the Variscan Belt of Western Europe: modes and structural consequences. Geol. la Fr. 3, 33–51.

Cadenas, P., Fernández-Viejo, G., 2017. The Asturian Basin within the North Iberian margin (Bay of Biscay): seismic characterisation of its geometry and its Mesozoic and Cenozoic cover. Basin Res. 29, 521–541. https://doi.org/10.1111/bre.12187

Cadenas, P., Fernández-Viejo, G., Pulgar, J.A., Tugend, J., Manatschal, G., Minshull, T.A., 2018. Constraints Imposed by Rift Inheritance on the Compressional Reactivation of a Hyperextended Margin: Mapping Rift Domains in the North Iberian Margin and in the

Cantabrian Mountains. Tectonics 37, 758–785. https://doi.org/10.1002/2016TC004454

Cadenas, P., Manatschal, G., Fernandez-Viejo, G., 2020. Unravelling the arcitecture and evolution of the inverted multi-stage North Iberian-Bay of Biscay rift. Gondwana Res. 88, 67–87.

Cao, X., Zahirovic, S., Li, S., Suo, Y., Wang, P., Liu, J., Müller, R.D., 2020. A deforming plate tectonic model of the South China Block since the Jurassic. Gondwana Res. https://doi.org/10.1016/j.gr.2020.11.010

Capdevila, R., Mougenot, D., 1988. Pre-Mesozoic basement of the western Iberian continental margin and its place in the Variscan belt. Proc., Sci. results, ODP, Leg 103, Galicia Margin 3–12. https://doi.org/10.2973/odp.proc.sr.103.116.1988

Casas-Sainz, A.M., Gil-Imaz, A., 1998. Extensional subsidence, contractional folding and thrust inversion of the eastern Cameros basin, northern Spain. Geol. Rundschau 86, 802–818. https://doi.org/10.1007/s005310050178

Catalán, J.R.M., Arenas, R., García, F.D., Cuadra, P.G., Gómez-Barreiro, J., Abati, J., Castiñeiras, P., Fernández-Suárez, J., Martínez, S.S., Andonaegui, P., Clavijo, E.G., Montes, A.D., Pascual, F.J.R., Aguado, B.V., 2007. Space and time in the tectonic evolution of the northwestern Iberian Massif: Implications for the Variscan belt 1200, 403–423. https://doi.org/10.1130/2007.1200(21)

Catalán, J.R.M., Pascual, F.J.R., Montes, A.D., Fernández, R., Barreiro, J.G., Da Silva, Í.D., Clavijo, E.G., Ayarza, P., Alcock, J.E., 2014. The late variscan HT/LP metamorphic event in NW and Central Iberia: Relationships to crustal thickening, extension, orocline

development and crustal evolution. Geol. Soc. Spec. Publ. 405, 225–247. https://doi.org/10.1144/SP405.1

Causer, A., Pérez-Díaz, L., Adam, J., Eagles, G., 2019. Uncertainties in breakup markers along the Iberia-Newfoundland margins illustrated by new seismic data. Solid Earth Discuss. 1–33. https://doi.org/10.5194/se-2019-141

Cawood, A.J., Ferrill, D.A., Morris, A.P., Norris, D., McCallum, D., Gillis, E., Smart, K.J., 2021a. Tectonostratigraphic evolution of the Orphan Basin and Flemish Pass region – Part 2: Regional structural development and lateral variations in rifting style. Mar. Pet. Geol. 133, 105219. https://doi.org/10.1016/j.marpetgeo.2021.105219

Cawood, A.J., Ferrill, D.A., Morris, A.P., Norris, D., McCallum, D., Gillis, E., Smart, K.J., 2021b. Tectonostratigraphic evolution of the Orphan Basin and Flemish Pass region – Part 1: Results from coupled kinematic restoration and crustal area balancing. Mar. Pet. Geol. 128, 105042. https://doi.org/10.1016/j.marpetgeo.2021.105042

Chappell, A.R., Kusznir, N.J., 2008. Three-dimensional gravity inversion for Moho depth at rifted continental margins incorporating a lithosphere thermal gravity anomaly correction. Geophys. J. Int. 174, 1–13. https://doi.org/10.1111/j.1365-246X.2008.03803.x

Chenin, P., Manatschal, G., Lavier, L.L., Erratt, D., 2015. Assessing the impact of Orogenic inheritance on the architecture, timing and magmatic budget of the North Atlantic rift system: A mapping approach. J. Geol. Soc. London. 172, 711–720. https://doi.org/10.1144/jgs2014-139

Chevrot, S., Sylvander, M., Diaz, J., Martin, R., Mouthereau, F., Manatschal, G., Masini, E.,

Calassou, S., Grimaud, F., Pauchet, H., Ruiz, M., 2018. The non-cylindrical crustal architecture of the Pyrenees. Sci. Rep. 8, 1–8. https://doi.org/10.1038/s41598-018-27889-x

Chian, D., Reid, I.D., Jackson, H.R., 2001. Crustal structure beneath Orphan Basin and implications for nonvolcanic continental rifting. J. Geophys. Res. Solid Earth 106, 10923–10940. https://doi.org/10.1029/2000jb900422

Choukroune, P., Mattauer, M., 1978. Tectonique des plaques et Pyrenees; sur le fonctionnement de la faille transformante nord-pyreneenne; comparaisons avec des modeles actuels. Bull. la Société géologique Fr. 7, 689–700.

Choukroune, P., Roure, F., Pinet, B., Ecors Pyrenees Team, 1990. Main results of the ECORS Pyrenees profile. Tectonophysics 173. https://doi.org/10.1016/0040-1951(90)90234-Y

Clark, S.A., Sawyer, D.S., Austin, J.A., Christeson, G.L., Nakamura, Y., 2007. Characterizing the Galicia Bank-Southern Iberia Abyssal Plain rifted margin segment boundary using multichannel seismic and ocean bottom seismometer data. J. Geophys. Res. Solid Earth 112, 1–17. https://doi.org/10.1029/2006JB004581

Clerc, C., Lagabrielle, Y., 2014. Thermal control on the modes of crustal thinning leading to mantle exhumation: Insights from the cretaceous pyrenean hot paleomargins. Tectonics 33, 1340–1359. https://doi.org/10.1002/2013TC003471

Clerc, C., Lagabrielle, Y., Labaume, P., Ringenbach, J.C., Vauchez, A., Nalpas, T., Bousquet, R., Ballard, J.F., Lahfid, A., Fourcade, S., 2016. Basement – Cover decoupling and progressive exhumation of metamorphic sediments at hot rifted margin. Insights from the Northeastern Pyrenean analog. Tectonophysics 686, 82–97.

https://doi.org/10.1016/j.tecto.2016.07.022

Clerc, C., Lahfid, A., Monié, P., Lagabrielle, Y., Chopin, C., Poujol, M., Boulvais, P., Ringenbach, J.C., Masini, E., De St Blanquat, M., 2015. High-temperature metamorphism during extreme thinning of the continental crust: A reappraisal of the North Pyrenean passive paleomargin. Solid Earth 6, 643–668. https://doi.org/10.5194/se-6-643-2015

Cowie, L., Kusznir, N., 2013. Mapping crustal thickness and oceanic lithosphere distribution in the eastern Mediterranean using gravity inversion. Pet. Geosci. 18, 373–380. https://doi.org/10.1144/petgeo2011-071

Cox, A., & Hart, R. B. (1991). Plate tectonics: How it works. John Wiley & Sons.

Crosby, A.G., White, N.J., Edwards, G.R.H., Thompson, M., Corfield, R., MacKay, L., 2011. Evolution of deep-water rifted margins: Testing depth-dependent extensional models. Tectonics 30, 1–36. https://doi.org/10.1029/2010TC002687

De Charpal, O., Guennoc, P., Montadert, L., Roberts, D.G., 1978. Rifting, crustal attenuation and subsidence in the Bay of Biscay. Nature 275, 706–711. https://doi.org/10.1038/275706a0

Desegaulx, P., Moretti, I., 1988. Subsidence history of the Ebro basin. J. Geodyn. 10, 9–24. https://doi.org/10.1016/0264-3707(88)90003-8

Diaz, J., Gallart, J., Carbonell, R., 2016. Moho topography beneath the Iberian-Western Mediterranean region mapped from controlled-source and natural seismicity surveys. Tectonophysics 692, 74–85. https://doi.org/10.1016/j.tecto.2016.08.023

Dietz, R.S., 1961. Continent and ocean basin evolution by spreading of the sea floor. Nature

4779, 854–857.

Druet, M., Muñoz-Martín, A., Granja-Bruña, J.L., Carbó-Gorosabel, A., Acosta, J., Llanes, P., Ercilla, G., 2018. Crustal Structure and Continent-Ocean Boundary Along the Galicia Continental Margin (NW Iberia): Insights From Combined Gravity and Seismic Interpretation. Tectonics 37, 1576–1604. https://doi.org/10.1029/2017TC004903

Ducoux, M., Jolivet, L., Masini, E., Augier, R., Lahfid, A., Bernet, M., Calassou, S., 2021. Distribution and intensity of High-Temperature Low-Pressure metamorphism across the Pyrenean-Cantabrian belt: constraints on the thermal record of the pre-orogenic hyperextension rifting. BSGF - Earth Sci. Bull. 192, 43. https://doi.org/10.1051/bsgf/2021029

Duretz, T., Asti, R., Lagabrielle, Y., Brun, J.P., Jourdon, A., Clerc, C., Corre, B., 2020. Numerical modelling of Cretaceous Pyrenean Rifting: The interaction between mantle exhumation and syn-rift salt tectonics. Basin Res. 32, 652–667. https://doi.org/10.1111/bre.12389

Enachescu, M., Hogg, J., Fowler, M.G., Brown, D.E., Atkinson, I., 2010. Late Jurassic source rock super-highway on conjugate margins of the North and Central Atlantic (offshore east coast Canada, Ireland, Portugal, Spain and Morocco), II Central and North Atlantic conjugate margins conference.

Espurt, N., Angrand, P., Teixell, A., Labaume, P., Ford, M., de Saint Blanquat, M., Chevrot, S., 2019. Crustal-scale balanced cross-section and restorations of the Central Pyrenean belt (Nestes-Cinca transect): Highlighting the structural control of Variscan belt and Permian-

Mesozoic rift systems on mountain building. Tectonophysics 764, 25–45. https://doi.org/10.1016/j.tecto.2019.04.026

Etheve, N., Mohn, G., Frizon de Lamotte, D., Roca, E., Tugend, J., Gómez-Romeu, J., 2018. Extreme Mesozoic Crustal Thinning in the Eastern Iberia Margin: The Example of the Columbrets Basin (Valencia Trough). Tectonics 37, 636–662. https://doi.org/10.1002/2017TC004613

Fernández-Viejo, G., Gallart, J., Pulgar, J.A., Gallastegui, J., Danobeitia, J.J., Cordoba, D., 1998. Crustal transition between continental and oceanic domains along the North Iberian margin from wide angle seismic and gravity data. Geophys. Res. Lett. 25, 4249–4252.

Fernández-Viejo, G., Gallastegui, J., Pulgar, J.A., Gallart, J., 2011. The MARCONI reflection seismic data: A view into the eastern part of the Bay of Biscay. Tectonophysics 508, 34–41. https://doi.org/10.1016/j.tecto.2010.06.020

Fernandez-Viejo, G., López Fernández, C., Domínguez Cuesta María, J., Cadenas, P., 2014. How much confidence can be conferred on tectonic maps of continental shelves? the Cantabrian-Fault case. Sci. Rep. 4, 1–7. https://doi.org/10.1038/srep03661

Fernández-Viejo, G., Pulgar, J.A., Gallastegui, J., Quintana, L., 2012. The fossil accretionary wedge of the Bay of Biscay: Critical wedge analysis on depth-migrated seismic sections and geodynamical implications. J. Geol. 120, 315–331. https://doi.org/10.1086/664789

Ferrer, O., Jackson, M.P.A., Roca, E., Rubinat, M., 2012. Evolution of salt structures during extension and inversion of the Offshore Parentis Basin (Eastern Bay of Biscay). Geol. Soc. Spec. Publ. 363, 361–380. https://doi.org/10.1144/SP363.16

Ferrer, O., Roca, E., Benjumea, B., Muñoz, J. A., Ellouz, N., Gallart, J., Díaz, J., Ruíz, M., Schimmel, M., Gaspà, O., Rubio, E., Pulgar, J.A., Gallastegui, J., Fernández-Viejo, G., Pedreira, D., López, C., González-Cortina, J.M., Fernández-Baniela, F., Muñoz, Josep A., Roca, Eduard, Benjumea, Beatriz, Ferrer, Oriol, Almar, Y., Falgas, E., Alonso, B., Ercilla, G., Casas, D., Estrada, F., Farran, M., Acosta, J., Herranz, P., Maestro, A., Barnolas, A., Vicente, M., Bartolomé, R., 2008. The deep seismic reflection MARCONI-3 profile: Role of extensional Mesozoic structure during the Pyrenean contractional deformation at the eastern part of the Bay of Biscay. Mar. Pet. Geol. 25, 714–730. https://doi.org/10.1016/j.marpetgeo.2008.06.002

Flament, N., Gurnis, M., Williams, S., Seton, M., Skogseid, J., Heine, C., Dietmar Müller, R., 2014. Topographic asymmetry of the South Atlantic from global models of mantle flow and lithospheric stretching. Earth Planet. Sci. Lett. 387, 107–119. https://doi.org/10.1016/j.epsl.2013.11.017

Frasca, G., Manatschal, G., Cadenas, P., Miro, J., Lescoutre, R., 2021. A kinematic reconstruction of Iberia using intracontinental strike-slip corridors. Terra Nov. https://doi.org/10.1111/ter.12549

Frizon De Lamotte, D., Fourdan, B., Leleu, S., Leparmentier, F., De Clarens, P., 2015. Style of rifting and the stages of Pangea breakup. Tectonics 34, 1009–1029. https://doi.org/10.1002/2014TC003760

Funck, T., Hopper, J.R., Larsen, H.C., Louden, K.E., Tucholke, B.E., Holbrook, W.S., 2003. Crustal structure of the ocean-continent transition at Flemish Cap: Seismic refraction results. J. Geophys. Res. 108, 1–20. https://doi.org/10.1029/2003jb002434

Gallastegui, J., Pulgar, J.A., Gallart, J., 2002. Initiation of an active margin at the North Iberian continent-ocean transition. Tectonics 21, 15-1-15–14. https://doi.org/10.1029/2001TC901046

García-Mondéjar, J., 1996. Plate reconstruction of the Bay of Biscay. Geology 24, 635–638. https://doi.org/10.1130/0091-7613(1996)024<0635:PROTBO>2.3.CO;2

Gerlings, J., Louden, K.E., Minshull, T.A., Nedimović, M.R., 2012. Flemish Cap-Goban Spur conjugate margins: New evidence of asymmetry. Geology 40, 1107–1110. https://doi.org/10.1130/G33263.1

Glerum, A., Brune, S., Stamps, D.S., Strecker, M.R., 2020. Victoria continental microplate dynamics controlled by the lithospheric strength distribution of the East African Rift. Nat. Commun. 11, 1–15. https://doi.org/10.1038/s41467-020-16176-x

Gómez-Romeu, J., Masini, E., Tugend, J., Ducoux, M., Kusznir, N., 2019. Role of rift structural inheritance in orogeny highlighted by the Western Pyrenees case-study. Tectonophysics 766, 131–150. https://doi.org/10.1016/j.tecto.2019.05.022

Gong, Z., 2008. The rotation of Iberia during the Aptian and consequences for pervasive Cretaceous remagnetization.

Gong, Z., Langereis, C.G., Mullender, T.A.T., 2008. The rotation of Iberia during the Aptian and the opening of the Bay of Biscay. Earth Planet. Sci. Lett. 273, 80–93. https://doi.org/10.1016/j.epsl.2008.06.016

Gong, Z., van Hinsbergen, D.J.J., Dekkers, M.J., 2009. Diachronous pervasive remagnetization

in northern Iberian basins during Cretaceous rotation and extension. Earth Planet. Sci. Lett. 284, 292–301. https://doi.org/10.1016/j.epsl.2009.04.039

Gouiza, M., Hall, J., Welford, J.K., 2017. Tectono-stratigraphic evolution and crustal architecture of the Orphan Basin during North Atlantic rifting. Int. J. Earth Sci. 106, 917–937. https://doi.org/10.1007/s00531-016-1341-0

Gozzard, S., Kusznir, N., Franke, D., Cullen, A., Reemst, P., Henstra, G., 2019. South China sea crustal thickness and oceanic lithosphere distribution from satellite gravity inversion. Pet. Geosci. 25, 112–128. https://doi.org/10.1144/petgeo2016-162

Greenhalgh, E.E., Kusznir, N.J., 2007. Evidence for thin oceanic crust on the extinct Aegir Ridge, Norwegian Basin, NE atlantic derived from satellite gravity inversion. Geophys. Res. Lett. 34, 1–5. https://doi.org/10.1029/2007GL029440

Grevemeyer, I., Ranero, C.R., Papenberg, C., Sallares, V., Bartolomé, R., Prada, M., Batista, L., Neres, M., 2022. The continent-to-ocean transition in the Iberia Abyssal Plain. Geology 50, 615–619. https://doi.org/10.1130/G49753.1

Gurnis, M., Yang, T., Cannon, J., Turner, M., Williams, S., Flament, N., Müller, R.D., 2018. Global tectonic reconstructions with continuously deforming and evolving rigid plates. Comput. Geosci. 116, 32–41. https://doi.org/10.1016/j.cageo.2018.04.007

Hall, J., Marillier, F., Dehler, S., 1998. Geophysical studies of the structure of the Appalachian orogen in the Atlantic borderlands of Canada. Can. J. Earth Sci. 35, 1205–1221. https://doi.org/10.1139/e98-075

Harrington, L., Zahirovic, S., Salles, T., Braz, C., Müller, R.D., 2019. Tectonic, geodynamic and surface process driving forces of Australia's paleogeography since the Jurassic. Sediment. Basins West. Aust. V Proc. Pet. Explor. Soc. Aust. 29.

Heine, C., Zoethout, J., Müller, R.D., 2013. Kinematics of the South Atlantic rift. Solid Earth 4, 215–253. https://doi.org/10.5194/se-4-215-2013

Heron, P.J., Peace, A.L., McCaffrey, K.J.W., Welford, J.K., Wilson, R., van Hunen, J., Pysklywec, R.N., 2019. Segmentation of Rifts Through Structural Inheritance: Creation of the Davis Strait. Tectonics 38, 2411–2430. https://doi.org/10.1029/2019TC005578

Jabaloy, A., Galindo-Zaldívar, J., González-Lodeiro, F., 2002. Palaeostress evolution of the Iberian Peninsula (Late Carboniferous to present-day). Tectonophysics 357, 159–186. https://doi.org/10.1016/S0040-1951(02)00367-0

Jammes, S., Huismans, R.S., Muñoz, J.A., 2014. Lateral variation in structural style of mountain building: Controls of rheological and rift inheritance. Terra Nov. 26, 201–207. https://doi.org/10.1111/ter.12087

Jammes, S., Lavier, L., Manatschal, G., 2010a. Extreme crustal thinning in the Bay of Biscay and the Western Pyrenees: From observations to modeling. Geochemistry, Geophys. Geosystems 11. https://doi.org/10.1029/2010GC003218

Jammes, S., Lavier, L.L., 2019. Effect of contrasting strength from inherited crustal fabrics on the development of rifting margins. Geosphere 15, 407–422. https://doi.org/10.1130/GES01686.1

Jammes, S., Manatschal, G., Lavier, L., 2010b. Interaction between prerift salt and detachment faulting in hyperextended rift systems: The example of the Parentis and Mauléon basins (Bay of Biscay and western Pyrenees). Am. Assoc. Pet. Geol. Bull. 94, 957–975. https://doi.org/10.1306/12090909116

Jammes, S., Manatschal, G., Lavier, L., Masini, E., 2009. Tectonosedimentary evolution related to extreme crustal thinning ahead of a propagating ocean: Example of the western Pyrenees. Tectonics 28, 1–24. https://doi.org/10.1029/2008TC002406

Jammes, S., Tiberi, C., Manatschal, G., 2010c. 3D architecture of a complex transcurrent rift system: The example of the Bay of Biscay-Western Pyrenees. Tectonophysics 489, 210–226. https://doi.org/10.1016/j.tecto.2010.04.023

King, L.H., Fader, G.B., Poole, W.H., Wanless, R.K., 1985. Geological setting and age of the Flemish Cap granodiorite, east of the Grand Banks of Newfoundland. Can. J. Earth Sci. 22, 1286–1298. https://doi.org/10.1139/e85-133

King, M.T., Welford, J.K., 2022a. Advances in Deformable Plate Tectonic Models: 2. Reconstructing the Southern North Atlantic Back Through Time. Geochemistry, Geophys. Geosystems 23, 1–23. https://doi.org/10.1029/2022gc010373

King, M.T., Welford, J.K., 2022b. Advances in Deformable Plate Tectonic Models: 1. Reconstructing Deformable Continental Blocks and Crustal Thicknesses Back Through Time. Geochemistry, Geophys. Geosystems 23. https://doi.org/10.1029/2022gc010372

King, M.T., Welford, J.K., Cadenas, P., Tugend, J., 2021. Investigating the Plate Kinematics of the Bay of Biscay Using Deformable Plate Tectonic Models. Tectonics 40, 1–27.

https://doi.org/10.1029/2020tc006467

King, M.T., Welford, J.K., Peace, A.L., 2020. Investigating the role of the Galicia Bank on the formation of the North West Iberian margin using deformable plate tectonic models. Tectonophysics 789, 228537. https://doi.org/10.1016/j.tecto.2020.228537

Kreemer, C., Blewitt, G., Klein, E.C., 2014. A geodetic plate motion and Global Strain Rate Model. Geochemistry, Geophys. Geosystems 15, 3849–3889. https://doi.org/10.1002/2014GC005407

Kusznir, N.J., Roberts, A.M., Alvey, A.D., 2020. Crustal structure of the conjugate equatorial atlantic margins, derived by gravity anomaly inversion. Geol. Soc. Spec. Publ. 476, 83–107. https://doi.org/10.1144/SP476.5

Lagabrielle, Y., Asti, R., Duretz, T., Clerc, C., Fourcade, S., Teixell, A., Labaume, P., Corre, B., Saspiturry, N., 2020. A review of cretaceous smooth-slopes extensional basins along the Iberia-Eurasia plate boundary: How pre-rift salt controls the modes of continental rifting and mantle exhumation. Earth-Science Rev. 201, 103071. https://doi.org/10.1016/j.earscirev.2019.103071

Lagabrielle, Y., Bodinier, J.L., 2008. Submarine reworking of exhumed subcontinental mantle rocks: Field evidence from the Lherz peridotites, French Pyrenees. Terra Nov. 20, 11–21. https://doi.org/10.1111/j.1365-3121.2007.00781.x

Lagabrielle, Y., Labaume, P., De Saint Blanquat, M., 2010. Mantle exhumation, crustal denudation, and gravity tectonics during Cretaceous rifting in the Pyrenean realm (SW Europe): Insights from the geological setting of the lherzolite bodies. Tectonics 29, 1–26.

https://doi.org/10.1029/2009TC002588

Larrasoana, J.C., Parés, J.M., Millán, H., del Valle, J., Pueyo, E.L., 2003. Paleomagnetic, structural, and stratigraphic constraints on transverse fault kinematics during basin inversion: The Pamplona Fault (Pyrenees, north Spain). Tectonics 22. https://doi.org/10.1029/2002tc001446

Le Breton, E., Brune, S., Ustaszewski, K., Zahirovic, S., Seton, M., Dietmar Müller, R., 2021. Kinematics and extent of the Piemont-Liguria Basin-implications for subduction processes in the Alps. Solid Earth 12, 885–913. https://doi.org/10.5194/se-12-885-2021

Le Pichon, X., Barbier, F., 1987. Passive margin formation by low-angle faulting wihtin the upper crust: the Northern Bay of Biscay. Tectonics 6, 133–150.

Leleu, S., Hartley, A.J., van Oosterhout, C., Kennan, L., Ruckwied, K., Gerdes, K., 2016. Structural, stratigraphic and sedimentological characterisation of a wide rift system: The Triassic rift system of the Central Atlantic Domain. Earth-Science Rev. 158, 89–124. https://doi.org/10.1016/j.earscirev.2016.03.008

Lescoutre, R., Manatschal, G., Muñoz, J.A., 2021. Nature, Origin, and Evolution of the Pyrenean-Cantabrian Junction. Tectonics 40, 1–40. https://doi.org/10.1029/2020TC006134

Li, Y., Oldenburg, D.W., 1998. 3-D inversion of gravity data. Geophysics 63, 109–119. https://doi.org/10.1190/1.1444302

Li, Y., Oldenburg, D.W., 1996. 3-D inversion of magnetic data. 1996 SEG Annu. Meet. 61, 400–402. https://doi.org/10.1190/1.1822498

Lundin, E., 2002. North Atlantic – Arctic : Overview of sea-floor spreading and rifting history. Mid Norw. plate Reconstr. atlas with Glob. Atl. Perspect. 41–75.

Lymer, G., Cresswell, D.J.F., Reston, T.J., Bull, J.M., Sawyer, D.S., Morgan, J.K., Stevenson, C., Causer, A., Minshull, T.A., Shillington, D.J., 2019. 3D development of detachment faulting during continental breakup. Earth Planet. Sci. Lett. 515, 90–99. https://doi.org/10.1016/j.epsl.2019.03.018

MacMahon, H., Kim Welford, J., Sandoval, L., Peace, A.L., 2020. The rockall and the orphan basins of the southern north atlantic ocean: Determining continuous basins across conjugate margins. Geosci. 10. https://doi.org/10.3390/geosciences10050178

Makris, J., Ginzburg, A., Shannon, P.M., Jacob, A.W.B., Bean, C.J., Vogt, U., 1991. A new look at the Rockall region, offshore Ireland. Mar. Pet. Geol. 8, 410–416. https://doi.org/10.1016/0264-8172(91)90063-7

Manatschal, G., Lavier, L., Chenin, P., 2015. The role of inheritance in structuring hyperextended rift systems: Some considerations based on observations and numerical modeling. Gondwana Res. 27, 140–164. https://doi.org/10.1016/j.gr.2014.08.006

Manatschal, G., Mohn, G., Masini, E., Peron-Pinvidic, G., Unternehr, P., Karner, G.D., 2009. Mapping Structures of Ancient Exposed Hyperextended Margins in the Alps: A Key to Understand the Evolution of Ultra-Deep Water Passive Continental Margins? Search Discov. 50172, 50172.

Martín-Martín, J.D., Travé, A., Gomez-Rivas, E., Salas, R., Sizun, J.P., Vergés, J., Corbella, M., Stafford, S.L., Alfonso, P., 2015. Fault-controlled and stratabound dolostones in the Late

Aptian-earliest Albian Benassal Formation (Maestrat Basin, E Spain): Petrology and geochemistry constrains. Mar. Pet. Geol. 65, 83–102. https://doi.org/10.1016/j.marpetgeo.2015.03.019

Martins, L.T., Madeira, J., Youbi, N., Munhá, J., Mata, J., Kerrich, R., 2008. Rift-related magmatism of the Central Atlantic magmatic province in Algarve, Southern Portugal. Lithos 101, 102–124. https://doi.org/10.1016/j.lithos.2007.07.010

Masini, E., Manatschal, G., Tugend, J., Mohn, G., Flament, J.M., 2014. The tectono-sedimentary evolution of a hyper-extended rift basin: The example of the Arzacq-Mauléon rift system (Western Pyrenees, SW France). Int. J. Earth Sci. 103, 1569–1596. https://doi.org/10.1007/s00531-014-1023-8

Mata, J., Alves, C.F., Martins, L., Miranda, R., Madeira, J., Pimentel, N., Martins, S., Azevedo, M.R., Youbi, N., De Min, A., Almeida, I.M., Bensalah, M.K., Terrinha, P., 2015. 40Ar/39Ar ages and petrogenesis of the West Iberian Margin onshore magmatism at the Jurassic-Cretaceous transition: Geodynamic implications and assessment of open-system processes involving saline materials. Lithos 236–237, 156–172. https://doi.org/10.1016/j.lithos.2015.09.001

Mattauer, M., Henry, J., 1974. Pyrenees. Geol. Soc. London, Spec. Publ. 4, 3–21.

Matte, P., 2001. The Variscan collage and orogeny (480-290 Ma) and the tectonic definition of the Armorica microplate: A review. Terra Nov. 13, 122–128. https://doi.org/10.1046/j.1365-3121.2001.00327.x

Matte, P., 1991. Accretionary history and crustal evolution of the Variscan belt in Western

Europe. Tectonophysics 196, 309–337. https://doi.org/10.1016/0040-1951(91)90328-P

Matthews, K.J., Maloney, K.T., Zahirovic, S., Williams, S.E., Seton, M., Müller, R.D., 2016. Global plate boundary evolution and kinematics since the late Paleozoic. Glob. Planet. Change 146, 226–250. https://doi.org/10.1016/j.gloplacha.2016.10.002

McKenzie, D., 1978. Some remarks on the development of sedimentary basins. Earth Planet. Sci. Lett. 40, 25–32. https://doi.org/10.1016/0012-821X(78)90071-7

Miranda, R., Valadares, V., Terrinha, P., Mata, J., Azevedo, M. do R., Gaspar, M., Kullberg, J.C., Ribeiro, C., 2009. Age constraints on the Late Cretaceous alkaline magmatism on the West Iberian Margin. Cretac. Res. 30, 575–586. https://doi.org/10.1016/j.cretres.2008.11.002

Mjelde, R., Kvarven, T., Faleide, J.I., Thybo, H., 2016. Lower crustal high-velocity bodies along North Atlantic passive margins, and their link to Caledonian suture zone eclogites and Early Cenozoic magmatism. Tectonophysics 670, 16–29. https://doi.org/10.1016/j.tecto.2015.11.021

Mohn, G., Karner, G.D., Manatschal, G., Johnson, C.A., 2015. Structural and stratigraphic evolution of the Iberia-Newfoundland hyper-extended rifted margin: A quantitative modelling approach. Geol. Soc. Spec. Publ. 413, 53–89. https://doi.org/10.1144/SP413.9

Montadert, L., de Charpal, O., Roberts, D., Guennoc, P., Sibuet, J.C., 1979. Northeast Atlantic Passive Continental Margins: Rifting And Subsidence. Talwani, M., Hay, W., Ryan, W.B.H. (Eds.), Deep Drill. Results Atl. Ocean Cont. Margin Paleoenviron. Am. Geophys. Union, Washingt. 154–186.

Montadert, L., Roberts, D.G., Auffret, G.A., Bock, W., DuPeuble, P.A., Hailwood, E.A., Harrison, W., Kagami, H., Lumsden, D.N., Muller, C., Schnitker, D., Thompson, R.W., Thompson, T.L., Timofeev, P.P., 1977. Rifting and subsidence on passive continental margins in the North East Atlantic. Nature 268, 305–309. https://doi.org/10.1038/268305a0

Mouthereau, F., Filleaudeau, P.Y., Vacherat, A., Pik, R., Lacombe, O., Fellin, M.G., Castelltort, S., Christophoul, F., Masini, E., 2014. Placing limits to shortening evolution in the Pyrenees: Role of margin architecture and implications for the Iberia/Europe convergence. Tectonics 33, 2283–2314. https://doi.org/10.1002/2014TC003663

Müller, R.D., Cannon, J., Qin, X., Watson, R.J., Gurnis, M., Williams, S., Pfaffelmoser, T., Seton, M., Russell, S.H.J., Zahirovic, S., 2018. GPlates: Building a Virtual Earth Through Deep Time. Geochemistry, Geophys. Geosystems 19, 2243–2261. https://doi.org/10.1029/2018GC007584

Müller, R.D., Zahirovic, S., Williams, S.E., Cannon, J., Seton, M., Bower, D.J., Tetley, M.G., Heine, C., Le Breton, E., Liu, S., Russell, S.H.J., Yang, T., Leonard, J., Gurnis, M., 2019. A Global Plate Model Including Lithospheric Deformation Along Major Rifts and Orogens Since the Triassic. Tectonics 38, 1884–1907. https://doi.org/10.1029/2018TC005462

Murillas, J., Mougenot, D., Boulot, G., Comas, M.C., Banda, E., Mauffret, A., 1990. Structure and evolution of the Galicia Interior Basin (Atlantic western Iberian continental margin). Tectonophysics 184. https://doi.org/10.1016/0040-1951(90)90445-E

Neres, M., Font, E., Miranda, J.M., Camps, P., Terrinha, P., Mirão, J., 2012. Reconciling Cretaceous paleomagnetic and marine magnetic data for Iberia: New Iberian paleomagnetic

poles. J. Geophys. Res. Solid Earth 117, 1–21. https://doi.org/10.1029/2011JB009067

Neuharth, D., Brune, S., Glerum, A., Heine, C., Welford, J.K., 2021. Formation of continental microplates through rift linkage: Numerical modelling and its application to the Flemish Cap and Sao Paulo Plateau. Geochemistry, Geophys. Geosystems.

Neuharth, D., Brune, S., Wrona, T., Glerum, A., Braun, J., Yuan, X., 2022. Evolution of Rift Systems and Their Fault Networks in Response to Surface Processes. Tectonics 41, 1–22. https://doi.org/10.1029/2021TC007166

Nirrengarten, M., Manatschal, G., Tugend, J., Kusznir, N., Sauter, D., 2018. Kinematic Evolution of the Southern North Atlantic: Implications for the Formation of Hyperextended Rift Systems. Tectonics 37, 89–118. https://doi.org/10.1002/2017TC004495

Nirrengarten, M., Manatschal, G., Tugend, J., Kusznir, N.J., Sauter, D., 2017. Nature and origin of the J-magnetic anomaly offshore Iberia–Newfoundland: implications for plate reconstructions. Terra Nov. 29, 20–28. https://doi.org/10.1111/ter.12240

Nirrengarten, M., Mohn, G., Kusznir, N.J., Sapin, F., Despinois, F., Pubellier, M., Chang, S.P., Larsen, H.C., Ringenbach, J.C., 2020. Extension modes and breakup processes of the southeast China-Northwest Palawan conjugate rifted margins. Mar. Pet. Geol. 113, 104123. https://doi.org/10.1016/j.marpetgeo.2019.104123

O'Reilly, B.M., Hauser, F., Jacob, A.W.B., Shannon, P.M., 1996. The lithosphere below the Rockall Trough: Wide-angle seismic evidence for extensive serpentinisation. Tectonophysics 255, 1–23. https://doi.org/10.1016/0040-1951(95)00149-2

O'Reilly, B.M., Hauser, F., Ravaut, C., Shannon, P.M., Readman, P.W., 2006. Crustal thinning, mantle exhumation and serpentinization in the Porcupine Basin, offshore Ireland: Evidence from wide-angle seismic data. J. Geol. Soc. London. 163, 775–787. https://doi.org/10.1144/0016-76492005-079

Oliva-Urcia, B., Casas, A.M., Soto, R., Villalaín, J.J., Kodama, K., 2011. A transtensional basin model for the Organyà basin (central southern Pyrenees) based on magnetic fabric and brittle structures. Geophys. J. Int. 184, 111–130. https://doi.org/10.1111/j.1365-246X.2010.04865.x

Olivet, J.L., 1996. La cinématique de la plaque ibérique / Kinematics of the Iberian Plate. Bull. Cent. REch. Explor. Prod. Elf Aquitaine 20, 195.

Pastouret, L., Auffret, G.A., 1976. OBSERVATIONS SUR LES MICROFACIES DES ROCHES SÉDIMENTAIRES PRÉLEVEES SUR LA MARGE ARMORICAINE (*). Rev. L'INSTITUT FRANÇAIS DU PÉTROLE XXXI, 365–389.

Peace, A., McCaffrey, K., Imber, J., van Hunen, J., Hobbs, R., Wilson, R., 2018. The role of pre-existing structures during rifting, continental breakup and transform system development, offshore West Greenland. Basin Res. 30, 373–394. https://doi.org/10.1111/bre.12257

Peace, A.L., 2021. Beyond crumple zones: Recent advances, applications and future directions in deformable plate tectonic modelling. Geol. Mag. 158, 1704–1710. https://doi.org/10.1017/S0016756821000534

Peace, A.L., Phethean, J.J.J., Franke, D., Foulger, G.R., Schiffer, C., Welford, J.K., McHone, G., Rocchi, S., Schnabel, M., Doré, A.G., 2019a. A review of Pangaea dispersal and Large

Igneous Provinces – In search of a causative mechanism. Earth-Science Rev. 102902. https://doi.org/10.1016/j.earscirev.2019.102902

Peace, A.L., Welford, J.K., Ball, P.J., Nirrengarten, M., 2019b. Deformable plate tectonic models of the southern North Atlantic. J. Geodyn. 128, 11–37. https://doi.org/10.1016/j.jog.2019.05.005

Pereira, R., Alves, T.M., 2012. Tectono-stratigraphic signature of multiphased rifting on divergent margins (deep-offshore southwest Iberia, North Atlantic). Tectonics 31, 1–21. https://doi.org/10.1029/2011TC003001

Pereira, R., Alves, T.M., 2011. Margin segmentation prior to continental break-up: A seismic-stratigraphic record of multiphased rifting in the North Atlantic (Southwest Iberia). Tectonophysics 505, 17–34. https://doi.org/10.1016/j.tecto.2011.03.011

Pérez-Gussinyé, M., Morgan, J.P., Reston, T.J., Ranero, C.R., 2006. The rift to drift transition at non-volcanic margins: Insights from numerical modelling. Earth Planet. Sci. Lett. 244, 458–473. https://doi.org/10.1016/j.epsl.2006.01.059

Pérez-Gussinyé, M., Ranero, C.R., Reston, T.J., Sawyer, D., 2003. Mechanisms of extension at nonvolcanic margins: Evidence from the Galicia interior basin, west of Iberia. J. Geophys. Res. Solid Earth 108, 1–19. https://doi.org/10.1029/2001jb000901

Perez-Gussinye, M., Reston, T., 2001. of Detachments Leading To Continental Breakup. J. Geophys. Res. 106, 3961–3975.

Peron-Pinvidic, G., Fourel, L., Buiter, S.J.H., 2022. The influence of orogenic collision

inheritance on rifted margin architecture: Insights from comparing numerical experiments to the Mid-Norwegian margin. Tectonophysics 828, 229273. https://doi.org/10.1016/j.tecto.2022.229273

Péron-Pinvidic, G., Manatschal, G., 2010. From microcontinents to extensional allochthons: Witnesses of how continents rift and break apart. Pet. Geosci. 16, 189–197. https://doi.org/10.1144/1354-079309-903

Péron-Pinvidic, G., Manatschal, G., 2009. The final rifting evolution at deep magma-poor passive margins from Iberia-Newfoundland: A new point of view. Int. J. Earth Sci. 98, 1581–1597. https://doi.org/10.1007/s00531-008-0337-9

Peron-Pinvidic, G., Manatschal, G., Alves, T., Andersen, T., Andres-Martinez, M., Autin, J., Ball, P., Brune, S., Buiter, S., Cadenas, P., Cresswell, D., Epin, M.E., Gómez-Romeu, J., Gouiza, M., Harkin, C., Heine, C., Hopper, J., Jackson, C., Jolivet, L., Katz, R., Lescoutre, R., Lymer, G., Magee, C., Masini, M., Miro, J., Molnar, N., Mouthereau, F., Muntener, O., Naliboff, J., Norcliffe, J., Osmundsen, P.T., Pérez Díaz, L., Philips, T.P., Ramos, A., Ranero, C., Reston, T., Ribes, C., Rooney, T., Rowan, M., Snidero, M., Tugend, J., Wang, L., Zwaan, F., 2019. Rifted Margins: State of the Art and Future Challenges. Front. Earth Sci. 7, 1–8. https://doi.org/10.3389/feart.2019.00218

Péron-Pinvidic, G., Manatschal, G., Minshull, T.A., Sawyer, D.S., 2007. Tectonosedimentary evolution of the deep Iberia-Newfoundland margins: Evidence for a complex breakup history. Tectonics 26, 1–19. https://doi.org/10.1029/2006TC001970

Peron-Pinvidic, G., Manatschal, G., Osmundsen, P.T., 2013. Structural comparison of archetypal

Atlantic rifted margins: A review of observations and concepts. Mar. Pet. Geol. 43, 21–47. https://doi.org/10.1016/j.marpetgeo.2013.02.002

Phillips, T.B., Fazlikhani, H., Gawthorpe, R.L., Fossen, H., Jackson, C.A.L., Bell, R.E., Faleide, J.I., Rotevatn, A., 2019. The Influence of Structural Inheritance and Multiphase Extension on Rift Development, the NorthernNorth Sea. Tectonics 4099–4126. https://doi.org/10.1029/2019TC005756

Pimentel, N., Pena Dos Reis, R., 2016. Petroleum Systems of the West Iberian Margin: a Review of the Lusitanian Basin and the Deep Offshore Peniche Basin. J. Pet. Geol. 39, 305–326. https://doi.org/10.1111/jpg.12648

Pinet, B., Montadert, L., Curnelle, R., Cazes, M., Marillier, F., Rolet, J., Tomassino, A., Galdeano, A., Patriat, P., Brunet, M.F., Olivet, J.L., Schaming, M., Lefort, J.P., Arrieta, A., Riaza, C., 1987. Crustal thinning on the Aquitaine shelf, Bay of Biscay, from deep seismic data. Nature 325, 513–516. https://doi.org/10.1038/325513a0

Ranero, C.R., Pérez-Gussinyé, M., 2010. Sequential faulting explains the asymmetry and extension discrepancy of conjugate margins. Nature 468, 294–299. https://doi.org/10.1038/nature09520

Rat, J., Mouthereau, F., Brichau, S., Crémades, A., Bernet, M., Balvay, M., Ganne, J., Lahfid, A., Gautheron, C., 2019. Tectonothermal Evolution of the Cameros Basin: Implications for Tectonics of North Iberia. Tectonics 38, 440–469. https://doi.org/10.1029/2018TC005294

Reston, T.J., 2010. The opening of the central segment of the South Atlantic: Symmetry and the extension discrepancy. Pet. Geosci. 16, 199–206. https://doi.org/10.1144/1354-079309-907

Reston, T.J., 2009. The extension discrepancy and syn-rift subsidence deficit at rifted margins. Pet. Geosci. 15, 217–237. https://doi.org/10.1144/1354-079309-845

Reston, T.J., 2005. Polyphase faulting during the development of the west Galicia rifted margin. Earth Planet. Sci. Lett. 237, 561–576. https://doi.org/10.1016/j.epsl.2005.06.019

Reston, T.J., 1996. The S reflector west of Galicia: The seismic signature of a detachment fault. Geophys. J. Int. 127, 230–244. https://doi.org/10.1111/j.1365-246X.1996.tb01547.x

Roca, E., Muñoz, J.A., Ferrer, O., Ellouz, N., 2011. The role of the Bay of Biscay Mesozoic extensional structure in the configuration of the Pyrenean orogen: Constraints from the MARCONI deep seismic reflection survey. Tectonics 30, 1–33. https://doi.org/10.1029/2010TC002735

Roest, W.R., Srivastava, S.P., 1991. Kinematics of the plate boundaries between Eurasia, Iberia, and Africa in the North Atlantic from the Late Cretaceous to the present. Geology 19, 613–616. https://doi.org/10.1130/0091-7613(1991)019<0613:KOTPBB>2.3.CO;2

Rosenbaum, G., Lister, G.S., Duboz, C., 2002. Rewlative mortiosn of Frica, Iberia and europe during Alpine orogeny. Tectonophysics 359, 117–129.

Ruffell, A., 1995. Evolution and hydrocarbon prospectivity of the Brittany Basin (Western Approaches Trough), offshore north-west France. Mar. Pet. Geol. 12, 387–407. https://doi.org/10.1016/0264-8172(95)96902-3

Ruiz, M., Díaz, J., Pedreira, D., Gallart, J., Pulgar, J.A., 2017. Crustal structure of the North Iberian continental margin from seismic refraction/wide-angle reflection profiles.

Tectonophysics 717, 65–82. https://doi.org/10.1016/j.tecto.2017.07.008

Salas, R., Casas, A., 1993. Mesozoic extensional tectonics, stratigraphy and crustal evolution during the Alpine cycle of the eastern Iberian basin. Tectonophysics 228, 33–55. https://doi.org/10.1016/0040-1951(93)90213-4

Salas, R., Guimera, J., Mas, R., Martin-Closas, C., Melendez, A., Alonso, A., 2001. Evolution of the Mesozoic Central Iberian Rift System and its Cainozoic inversion (Iberian chain), Mémoires du Muséum national d'histoire naturelle.

Salas Ramon , Guimera Joan, Mas Ramon, Carles Martin-Closas Carles, Melendez Alfonso, A.A., 2001. Evolution of the Mesozoic Central Iberian Rift System and its Cainozoic inversion (Iberian chain), Mémoires du Muséum national d'histoire naturelle.

Sandoval, L., Welford, J.K., MacMahon, H., Peace, A.L., 2019. Determining continuous basins across conjugate margins: The East Orphan, Porcupine, and Galicia Interior basins of the southern North Atlantic Ocean. Mar. Pet. Geol. 110, 138–161. https://doi.org/10.1016/j.marpetgeo.2019.06.047

Sandwell, D.T., Müller, R.D., Smith, W.H.F., Garcia, E., Francis, R., 2014. New global marine gravity model from CryoSat-2 and Jason-1 reveals buried tectonic structure. Science (80-.). 346, 65–67. https://doi.org/10.1126/science.1258213

Saspiturry, N., Allanic, C., Razin, P., Issautier, B., Baudin, T., Lasseur, E., Serrano, O., Leleu, S., 2020. Closure of a hyperextended system in an orogenic lithospheric pop-up, Western Pyrenees: The role of mantle buttressing and rift structural inheritance. Terra Nov. https://doi.org/10.1111/ter.12457

Saspiturry, N., Cochelin, B., Razin, P., Leleu, S., Lemirre, B., Bouscary, C., Issautier, B., Serrano, O., Lasseur, E., Baudin, T., Allanic, C., 2019. Tectono-sedimentary evolution of a rift system controlled by Permian post-orogenic extension and metamorphic core complex formation (Bidarray Basin and Ursuya dome, Western Pyrenees). Tectonophysics 768, 228180. https://doi.org/10.1016/j.tecto.2019.228180

Saspiturry, N., Issautier, B., Razin, P., Baudin, T., Asti, R., Lagabrielle, Y., Allanic, C., Serrano, O., Duretz, T., 2021. Review of Iberia–Eurasia plate-boundary basins: Role of sedimentary burial and salt tectonics during rifting and continental breakup. Basin Res. 33, 1626–1661. https://doi.org/10.1111/bre.12529

Schiffer, C., Doré, A.G., Foulger, G.R., Franke, D., Geoffroy, L., Gernigon, L., Holdsworth, B., Kusznir, N., Lundin, E., McCaffrey, K., Peace, A.L., Petersen, K.D., Phillips, T.B., Stephenson, R., Stoker, M.S., Welford, J.K., 2019. Structural inheritance in the North Atlantic. Earth-Science Rev. 102975. https://doi.org/10.1016/j.earscirev.2019.102975

Sclater, J.G., Christie, P.A.F., 1980. Continental stretching: An explanation of the Post-Mid-Cretaceous subsidence of the central North Sea Basin. J. Geophys. Res. Solid Earth 85, 3711–3739. https://doi.org/10.1029/jb085ib07p03711

Scrutton, R.A., Bentley, P.A.D., 1988. Major Cretaceous volcanic province in southern Rockall Trough. Earth Planet. Sci. Lett. 91, 198–204. https://doi.org/10.1016/0012-821X(88)90161-6

Seton, M., Müller, R.D., Zahirovic, S., Gaina, C., Torsvik, T., Shephard, G., Talsma, A., Gurnis, M., Turner, M., Maus, S., Chandler, M., 2012. Global continental and ocean basin

reconstructions since 200Ma. Earth-Science Rev. 113, 212–270. https://doi.org/10.1016/j.earscirev.2012.03.002

Shannon, P.M., Corcoran, D. V., Haughton, P.D.W., 2001. The petroleum exploration of Ireland's offshore basins: Introduction. Geol. Soc. Spec. Publ. 188, 1–8. https://doi.org/10.1144/GSL.SP.2001.188.01.01

Sibuet, J.C., Rouzo, S., Srivastava, S., 2012. Paleogeographic maps of the Central and North Atlantic Oceans. 3P Arct. - Polar Pet. Potential Conf. Exhib. 30196.

Sibuet, J.C., Srivastava, S.P., Enachescu, M., Karner, G.D., 2007. Early Cretaceous motion of Flemish Cap with respect to North America: Implications on the formation of Orphan Basin and SE Flemish Cap-Galicia Bank conjugate margins. Geol. Soc. Spec. Publ. 282, 63–76. https://doi.org/10.1144/SP282.4

Sibuet, J.C., Srivastava, S.P., Spakman, W., 2004. Pyrenean orogeny and plate kinematics. J. Geophys. Res. Solid Earth 109, 1–18. https://doi.org/10.1029/2003JB002514

Sinclair, I.K., 1995. Sequence stratigraphic response to Aptian-Albian rifting in conjugate margin basins: a comparison of the Jeanne d'Arc Basin, offshore Newfoundland, and the Porcupine Basin, offshore Ireland. tectonics, Sediment. palaeoceanography North Atl. Reg. 29–49.

Soto, R., Casas-Sainz, A.M., Villalaín, J.J., 2011. Widespread Cretaceous inversion event in northern Spain: Evidence from subsurface and palaeomagnetic data. J. Geol. Soc. London. 168, 899–912. https://doi.org/10.1144/0016-76492010-072

Spooner, C., Stephenson, R., Butler, R.W.H., 2019. Pooled subsidence records from numerous wells reveal variations in pre-break-up rifting along the proximal domains of the Iberia-Newfoundland continental margins. Geol. Mag. 156, 1323–1333. https://doi.org/10.1017/S0016756818000651

Srivastava, S.P., Schouten, H., Roest, W.R., Klitgord, K.D., Kovacs, L.C., Verhoef, J., Macnab, R., 1990. Iberian plate kinematics: A jumping plate boundary between Eurasia and Africa. Nature. https://doi.org/10.1038/344756a0

Srivastava, S.P., Sibuet, J.C., Cande, S., Roest, W.R., Reid, I.D., 2000. Magnetic evidence for slow seafloor spreading during the formation of the Newfoundland and Iberian margins. Earth Planet. Sci. Lett. 182, 61–76. https://doi.org/10.1016/S0012-821X(00)00231-4

Stampfli, G.M., Borel, G.D., 2002. A plate tectonic model for the Paleozoic and Mesozoic constrained by dynamic plate boundaries and restored synthetic oceanic isochrons. Earth Planet. Sci. Lett. 196, 17–33. https://doi.org/10.1016/S0012-821X(01)00588-X

Stampfli, G.M., Hochard, C., Vérard, C., Wilhem, C., vonRaumer, J., 2013. The formation of Pangea. Tectonophysics 593, 1–19. https://doi.org/10.1016/j.tecto.2013.02.037

Stanton, N., Manatschal, G., Autin, J., Sauter, D., Maia, M., Viana, A., 2016. Geophysical fingerprints of hyper-extended, exhumed and embryonic oceanic domains: the example from the Iberia–Newfoundland rifted margins. Mar. Geophys. Res. 37, 185–205. https://doi.org/10.1007/s11001-016-9277-0

Sutra, E., Manatschal, G., Mohn, G., Unternehr, P., 2013. Quantification and restoration of extensional deformation along the Western Iberia and Newfoundland rifted margins.

Geochemistry, Geophys. Geosystems 14, 2575–2597. https://doi.org/10.1002/ggge.20135

Szameitat, L.S.A., Ferreira, F.J.F., Manatschal, G., da Costa Pereira Lavalle Heilbron, M., 2018a. Evidence of mantle inheritance on the ultra-distal western iberian margin from transformed total magnetic anomaly. Rev. Bras. Geofis. 36, 307–316. https://doi.org/10.22564/RBGF.V36I3.1957

Szameitat, L.S.A., Ferreira, F.J.F., Manatschal, G., Helbron, M. da C.P.L., 2018b. Evidence of Mantle Inheritance on the Ultra-Distal Western Iberian Margin From Transformed Total Magnetic Anomaly. Rev. Bras. Geofísica 36, 1. https://doi.org/10.22564/rbgf.v36i3.1957

Szameitat, L.S.A., Manatschal, G., Nirrengarten, M., Ferreira, F.J.F., Heilbron, M., 2020. Magnetic characterization of the zigzag shaped J-anomaly: implications for kinematics and breakup processes at the Iberia-Newfoundland margins. Terra Nov. https://doi.org/10.1111/ter.12466

Tavani, S., Bertok, C., Granado, P., Piana, F., Salas, R., Vigna, B., Muñoz, J.A., 2018. The Iberia-Eurasia plate boundary east of the Pyrenees. Earth-Science Rev. 187, 314–337. https://doi.org/10.1016/j.earscirev.2018.10.008

Teixell, A., Labaume, P., Ayarza, P., Espurt, N., de Saint Blanquat, M., Lagabrielle, Y., 2018. Crustal structure and evolution of the Pyrenean-Cantabrian belt: A review and new interpretations from recent concepts and data. Tectonophysics 724–725, 146–170. https://doi.org/10.1016/j.tecto.2018.01.009

Thinon, I., 1999. Structure profonde de la Marge Nord Gascogne et du Bassin Armoricain. Ph.D. Thesis.

Thinon, I., Fidalgo-gonzalez, L., Rehault, J.P., Olivet, J.L., 2001. Pyenean defromations in the Bay of Biscay. Comptes Rendus l'Académie des Sci. 332, 561–568.

Thinon, I., Matias, L., Réhault, J.P., Hirn, A., Fidalgo-González, L., Avedik, F., 2003. Deep structure of the Armorican Basin (Bay of Biscay): A review of Norgasis seismic reflection and refraction data. J. Geol. Soc. London. 160, 99–116. https://doi.org/10.1144/0016-764901-103

Thinon, I., Réhault, J.P., Fidalgo-González, L., 2002. La couverture sédimentaire syn-rift de la marge Nord-Gascogne et du Bassin armoricain (golfe de Gascogne): à partir de nouvelles données de sismique réflexion. Bull. la Soc. Geol. Fr. 173, 515–522. https://doi.org/10.2113/173.6.515

Tucholke, B.E., Sawyer, D.S., Sibuet, J., Brest, I.C. De, 2007. Breakup of the Newfoundland – Iberia rift 3, 9–46.

Tucholke, B.E., Sibuet, J.C., 2006. Leg 210 synthesis: Tectonic, magmatic, and sedimentary evolution of the Newfoundland-Iberia rift. Proc. Ocean Drill. Progr. Sci. Results 210. https://doi.org/10.2973/odp.proc.sr.210.101.2007

Tugend, J., Manatschal, G., Kusznir, N., Masini, E., Mohn, G., Thinon, I., 2014. Formation and deformation of hyperextended rift systems: Insights from rift domain mapping in the Bay of Biscay-Pyrenees. Tectonics 33, 1239–1276. https://doi.org/10.1002/2014TC003529.Received

Tugend, J., Manatschal, G., Kusznir, N.J., 2015a. Spatial and temporal evolution of hyperextended rift systems: Implication for the nature, kinematics, and timing of the

Iberian- European plate boundary. Geology 43, 15–18. https://doi.org/10.1130/G36072.1

Tugend, J., Manatschal, G., Kusznir, N.J., Masini, E., 2015b. Characterizing and identifying structural domains at rifted continental margins: Application to the Bay of Biscay margins and its Western Pyrenean fossil remnants. Geol. Soc. Spec. Publ. 413, 171–203. https://doi.org/10.1144/SP413.3

Vacherat, A., Mouthereau, F., Pik, R., Bellahsen, N., Gautheron, C., Bernet, M., Daudet, M., Balansa, J., Tibari, B., Pinna Jamme, R., Radal, J., 2016. Rift-to-collision transition recorded by tectonothermal evolution of the northern Pyrenees. Tectonics 35, 907–933. https://doi.org/10.1002/2015TC004016

Vacherat, A., Mouthereau, F., Pik, R., Huyghe, D., Paquette, J.L., Christophoul, F., Loget, N., Tibari, B., 2017. Rift-to-collision sediment routing in the Pyrenees: A synthesis from sedimentological, geochronological and kinematic constraints. Earth-Science Rev. 172, 43–74. https://doi.org/10.1016/j.earscirev.2017.07.004

Van Avendonk, H.J.A., Lavier, L.L., Shillington, D.J., Manatschal, G., 2009. Extension of continental crust at the margin of the eastern Grand Banks, Newfoundland. Tectonophysics 468, 131–148. https://doi.org/10.1016/j.tecto.2008.05.030

van Hinsbergen, D.J.J., Spakman, W., Vissers, R.L.M., van der Meer, D.G., 2017. Comment on "Assessing Discrepancies Between Previous Plate Kinematic Models of Mesozoic Iberia and Their Constraints" by Barnett-Moore Et Al. Tectonics 36, 3277–3285. https://doi.org/10.1002/2016TC004418

van Hinsbergen, D.J.J., Torsvik, T.H., Schmid, S.M., Maţenco, L.C., Maffione, M., Vissers,

R.L.M., Gürer, D., Spakman, W., 2020. Orogenic architecture of the Mediterranean region and kinematic reconstruction of its tectonic evolution since the Triassic. Gondwana Res. 81, 79–229. https://doi.org/10.1016/j.gr.2019.07.009

Vargas, H., Gaspar-Escribano, J.M., López-Gómez, J., Van Wees, J.D., Cloetingh, S., de La Horra, R., Arche, A., 2009. A comparison of the Iberian and Ebro Basins during the Permian and Triassic, eastern Spain: A quantitative subsidence modelling approach. Tectonophysics 474, 160–183. https://doi.org/10.1016/j.tecto.2008.06.005

Vergés, J., Poprawski, Y., Almar, Y., Drzewiecki, P.A., Moragas, M., Bover-Arnal, T., Macchiavelli, C., Wright, W., Messager, G., Embry, J.C., Hunt, D., 2020. Tectono-sedimentary evolution of Jurassic–Cretaceous diapiric structures: Miravete anticline, Maestrat Basin, Spain. Basin Res. 32, 1653–1684. https://doi.org/10.1111/bre.12447

Vissers, R.L.M., Meijer, P.T., 2012. Mesozoic rotation of Iberia: Subduction in the Pyrenees? Earth-Science Rev. 110, 93–110. https://doi.org/10.1016/j.earscirev.2011.11.001

Vissers, R.L.M., van Hinsbergen, D.J.J., van der Meer, D.G., Spakman, W., 2016. Cretaceous slab break-off in the Pyrenees: Iberian plate kinematics in paleomagnetic and mantle reference frames. Gondwana Res. 34, 49–59. https://doi.org/10.1016/j.gr.2016.03.006

Vogt, U., Makris, J., O'Reilly, B.M., Hauser, F., Readman, P.W., Brian Jacob, A.W., Shannon, P.M., 1998. The Hatton Basin and continental margin: Crustal structure from wide-angle seismic and gravity data. J. Geophys. Res. Solid Earth 103, 12545–12566. https://doi.org/10.1029/98jb00604

Waldron, J.W.F., Schofield, D.I., Murphy, J.B., 2019. Diachronous paleozoic accretion of peri-

gondwanan terranes at the laurentian margin. Geol. Soc. Spec. Publ. 470, 289–310. https://doi.org/10.1144/SP470.11

Walker, O.A., Alves, T.M., Hesselbo, S.P., Pharaoh, T., Nuzzo, M., Mattos, N.H., 2021. Significance of Upper Triassic to Lower Jurassic salt in the identification of palaeo-seaways in the North Atlantic. Mar. Pet. Geol. 123, 104705. https://doi.org/10.1016/j.marpetgeo.2020.104705

Wang, Y., Chevrot, S., Monteiller, V., Komatitsch, D., Mouthereau, F., Manatschal, G., Sylvander, M., Diaz, J., Ruiz, M., Grimaud, F., Benahmed, S., Pauchet, H., Martin, R., 2016. The deep roots of the western Pyrenees revealed by full waveform inversion of teleseismic P waves. Geology 44, 475–478. https://doi.org/10.1130/G37812.1

Watremez, L., Prada, M., Minshull, T., O'Reilly, B., Chen, C., Reston, T., Shannon, P., Wagner, G., Gaw, V., Klaeschen, D., Edwards, R., Lebedev, S., 2018. Deep structure of the Porcupine Basin from wide-angle seismic data. Pet. Geol. Conf. Proc. 8, 199–209. https://doi.org/10.1144/PGC8.26

Welford, J.K., Dehler, S.A., Funck, T., 2020. Crustal velocity structure across the Orphan Basin and Orphan Knoll to the continent ocean transition, offshore Newfoundland, Canada. Geophys. J. Int. 221, 37–59. https://doi.org/10.1093/gji/ggz575

Welford, J.K., Hall, J., 2007. Crustal structure of the Newfoundland rifted continental margin from constrained 3-D gravity inversion. Geophys. J. Int. 171, 890–908. https://doi.org/10.1111/j.1365-246X.2007.03549.x

Welford, J.K., Peace, A.L., Geng, M., Dehler, S.A., Dickie, K., 2018. Crustal structure of Baffin

Bay from constrained three-dimensional gravity inversion and deformable plate tectonic models. Geophys. J. Int. 214, 1281–1300. https://doi.org/10.1093/GJI/GGY193

Welford, J.K., Shannon, P.M., O'Reilly, B.M., Hall, J., 2012. Comparison of lithosphere structure across the Orphan Basin-Flemish Cap and Irish Atlantic conjugate continental margins from constrained 3D gravity inversions. J. Geol. Soc. London. 169, 405–420. https://doi.org/10.1144/0016-76492011-114

Welford, J.K., Shannon, P.M., O'Reilly, B.M., Hall, J., 2010. Lithospheric density variations and Moho structure of the Irish Atlantic continental margin from constrained 3-D gravity inversion. Geophys. J. Int. 183, 79–95. https://doi.org/10.1111/j.1365-246X.2010.04735.x

Whitmarsh, R.B., Langford, J.J., Buckley, J.S., Bailey, R.J., Blundell, D.J., 1974. The crustal structure beneath Porcupine Ridge as determined by explosion seismology. Earth Planet. Sci. Lett. 22, 197–204.

Whitmarsh, R.B., Manatschal, G., Minshull, T.A., 2001. Evolution of magma-poor continental margins from rifting to seafloor spreading. Nature 413, 150–154. https://doi.org/10.1038/35093085

Williams, C.A., 1975. Sea-floor spreading in the Bay of Biscay and its relationship to the North Atlantic. Earth Planet. Sci. Lett. 24, 440–456. https://doi.org/10.1016/0012-821X(75)90151-X

Williams, H., 1984. Miogeoclines and suspect terranes of the Caledonian-Appalachian orogen; tectonic patterns in the North Atlantic region. Can. J. Earth Sci. 21, 887–901. https://doi.org/10.1139/e84-095

Williams, S.E., Dietmar Müller, R., Landgrebe, T.C.W., Whittaker, J.M., 2012. An open-source software environment for visualizing and refining plate tectonic reconstructions using high-resolution geological and geophysical data sets. GSA Today 22, 4–9. https://doi.org/10.1130/GSATG139A.1

Wilson, J.T., 1965. A new class of faults and their bearing on continental drift. Nature 205, 343–347.

Wilson, R.C.L., Hiscott, R.N., Willis, M.G., Gradstein, F.M., 1989. The Lusitanian Basin of west-central Portugal: Mesozoic and Tertiary tectonic, stratigraphic, and subsidence history. Extensional tectonics Stratigr. North Atl. margins 341–361.

Withjack, M.O., Jamison, W.R., 1986. Deformation produced by oblique rifting. Tectonophysics 126, 99–124. https://doi.org/10.1016/0040-1951(86)90222-2

Yang, P., Welford, J.K., King, M.T., 2021. Assessing the Rotation and Segmentation of the Porcupine Bank, Irish Atlantic Margin, During Oblique Rifting Using Deformable Plate Reconstruction. Tectonics 40, 1–27. https://doi.org/10.1029/2020tc006665

Zhao, F., Alves, T.M., Xia, S., Li, W., Wang, L., Mi, L., Wu, S., Cao, J., Fan, C., 2020. Along-strike segmentation of the South China Sea margin imposed by inherited pre-rift basement structures. Earth Planet. Sci. Lett. 530, 115862. https://doi.org/10.1016/j.epsl.2019.115862

Appendices

A Open-access supplementary data files

The majority of the work conducted for my doctoral thesis was carried out using open-source software, python programming libraries, and data files. As a result, all of the GPlates files, pyGPlates code, crustal thickness estimates, and poles of rotation used to create the deformable plate models presented in this thesis are freely available and can be downloaded from https://data.mendeley.com/datasets/3577pvv6c8/draft?a=e666048f-6c98-4fd2-a0b7-f433a96c1637.